IS NEURAL CREST CELL DELAMINATION REQUIRED FOR NORMAL CRANIAL NEURAL TUBE CLOSURE?

Julie Cooper

U.C.L.

PhD

SIGNED DECLARATION

I Julie Cooper confirm that the work presented in this thesis is my own. Where information has been derived from other sources I confirm that this has been indicated in the thesis.

SIGNED:

D a t e

ABSTRACT

Numerous correlations are described in the literature between cranial neural tube defects (NTDs) and neurocristopathies indicating that cranial neural tube closure and neural crest cell (NCC) development may be linked by more than just spatial and temporal contiguity. Detailed analysis of the morphology of the cranial neural plate identified the midbrain as a region in which several features combine that are likely to result in resistance to the apposition and subsequent closure of the neural folds. The relationship between elevation, bending and closure of the midbrain neural folds and the specification and delamination of NCC indicates that NCC may act in conjunction with other permissive processes to facilitate a) elevation of the neural folds by contributing to expansion of cranial mesenchyme and b) formation of dorsolateral hinge points (DLHP) by reducing cell density and thus enhancing flexibility of the dorsal neural folds. These two processes are requirements for the subsequent closure of the midbrain.

To address the hypothesis that NCC delamination is required for the elevation of the midbrain neural folds and their bending at the DLHP, mouse models known to harbour mutations resulting in both NTDs and neurocristopathies were studied to assess the relationship between the two defects. In support of the idea that NCC delamination facilitates midbrain elevation and DLHP formation, failure of cranial NCC delamination associates with reduced cranial elevation, absence of DLHPs and midbrain exencephaly in the *Kumba* mutant mouse model. This is in contrast to the dissociation between the trunk NCC phenotype and hindbrain exencephaly observed in the *Splotch* model. The hypothesis was tested experimentally by chemically inhibiting the delamination of NCC in cultured embryos. This adversely affected elevation of the neural folds and DLHP formation, and in some instances resulted in failure of midbrain closure. A transgenic model was developed which was predicted to provide an *in vivo* model of inhibition of delamination of NCC. The shRNA mediated knockdown of *FoxD3* expression in NCC did not, however, affect the early specification or delamination of NCC. Instead it resulted in a failure of maintenance of NCC progenitors during their migration in the cranial mesenchyme. This model displayed no incidence of midbrain exencephaly. Failure of proper NCC derived mesenchymal ‘scaffolding’ surrounding the cranial neural tube did, however, lead to a reopening of the forebrain in some instances.

Based on the evidence described above, I propose a model in which the development of NCC exerts complex multilevel mechanical regulation on the formation and maintenance of the neural tube. NCC delamination facilitates DLHP formation, while NCC migration and proliferation in the mesenchyme contributes to elevation of the cranial neural folds and also ‘scaffolds’ the neural folds to maintain closure.

ACKNOWLEDGEMENTS

I would like to thank my supervisors Prof. Andy Copp and Dr. Nick Greene for imparting their invaluable knowledge and skills and for their support and unending patience in the compiling of this thesis.

I am also grateful to the members of my lab for their support and for providing light-hearted relief in times of stress, especially Dawn Savery, Valentina Massa and Pachy Ybot-Gonzalez for all their assistance and Cynthia Andoniadou for numerous cups of tea!

Finally I would like to thank my family for their confidence, support, patience and baby sitting!

CONTENTS

PAGE

LIST OF FIGURES

LIST OF TABLES

LIST OF ABBREVIATIONS

BA	Branchial Arch
BA1	First Branchial Arch
bp	Base Pair
BBR	Boehringer's Blocking Reagent
BMP	Bone Morphogenetic Protein
CS	Carnegie Stage
°C	Degrees Centigrade
DEPC	Diethylpyrocarbonate
DIG	Dioxygenin
DLHP	Dorsolateral Hinge Points
DMEM	Dulbecco's Modified Eagle's Medium
DRG	Dorsal Root Ganglia
DTA	Dyphtherin Toxin A
E	Embryonic day
ECM	Extra Cellular Matrix
ENS	Enteric Nervous System
EMT	Epithelial to Mesenchymal Transition
ESC	Embryonic Stem Cell
FGF	Fibroblast Growth Factor
GFP	Green Fluorescing Protein
h	Hour
H & E	Hematoxylin and Eosin Stain
HFM	Hemifacial Microsomia
HPE	Holoprosencephaly
IMS	Industrial Methylated Spirits
ISH	*In Situ* Hybridisation
KD	Knockdown
KDa	Kilodalton
M	Mole
mA	Milliamp
MHP	Median Hinge Point
MHO	Mid- Hindbrain Organiser

min	Minute
µl	Microlitre
ml	Millilitre
mM	Millimole
MMP	Matrix Metalloproteinase
NCC	Neural Crest Cell
NR	Non-Recombined
NTD	Neural Tube Defect
p	p-value (probability)
PBS	Phosphate Buffered Saline
PBT	Phosphate Buffered Saline with 0.1% Tween-20
PCP	Planar Cell Polarity
PCR	Polymerase Chain Reaction
PFA	Paraformaldehyde
PNP	Posterior Neuropore
qRT-PCR	Quantitative Reverse Transcription PCR
R	Recombined
RA	Retinoic Acid
RIPA	Radioimmunoprecipitation Assay
RISC	RNA Induced Silencing Complex
RNAi	RNA interference
rpm	Revolutions Per Minute
RT	Room Temperature
SEM	Scanning Electron Microscopy
shRNA	Short Hairpin RNA
siRNA	Short Interfering RNA
TCS	Treacher Collins Syndrome
V	Voltage
Wnts	Wingless / INT-related
WT	Wild Type

CHAPTER 1

INTRODUCTION

This dissertation investigates the relationship between the processes of neural tube closure and neural crest cell (NCC) emigration. Both neurulation and NCC migration are well-studied embryonic processes but their relationship to each other is poorly understood. This project examines the hypothesis that NCC emigration in the cranial region is necessary for completion of neural tube closure during mouse development. Before addressing the relationship between neurulation and NCC migration, these processes will be described in the context of embryonic development, referring mainly to the mouse model initially before describing differing features of other models.

1.1. NEURULATION

The fertilised embryo undergoes three main processes during embryogenesis: initial cleavage results in a multicellular blastula which is then reorganised during gastrulation to form the three primary germ layers. This is followed by organogenesis which begins with neurulation. Neurulation has three main functions: it results primarily in the formation of the neural tube (precursor to the brain and spinal cord), but it also results in the specification of the neural crest (a multipotent migratory population of cells) and the formation of the epidermis covering the neural tube.

1.1.1. PRIMARY NEURULATION

Primary neurulation is the process whereby the neural plate is first induced and shaped in dorsal ectoderm, then bends to produce the neural folds, which elevate, appose and fuse to form the cranial and most of the spinal neural tube (see Figure 1.1). In the mouse embryo there are three distinct anatomical closure siteswhich are characterised by different morphology and mechanisms: Closure 1 at the hindbrain/cervical spine boundary, Closure 2 at the midbrain/forebrain boundary and Closure 3 at the rostral end of the forebrain. Closure spreadsrostrally and caudally from these sites (Figure 1.2).

1.1.2. SECONDARY NEURULATION

Secondary neurulation occurs at levels caudal to the upper sacral spine, where the neural tube is formed from the mesenchymal cells of the tail bud which undergo epithelialisation to form a central lumen continuous with that produced by primary neurulation (Schoenwolf, 1984).

Figure 1.1. The Processes of Primary Neurulation

Shaping: Specification & shaping of the neural plate (blue) flanked by non-neural ectoderm (turquoise) and lying over the notochord (yellow).

Bending: The neural plate bends around the median hinge point (purple).

Elevation: The neural plate elevates to form the neural folds and neural crest cells become specified at their dorsal tips (pink).

Apposition: The neural folds bend again around the dorsolateral hinge points (red) allowing the dorsal tips of the neural folds to converge and appose.

Fusion: The dorsal tips of the neural folds fuse to form a complete tube and the non-neural ectoderm separates. Neural crest cells begin migration before/after fusion at different axial levels.

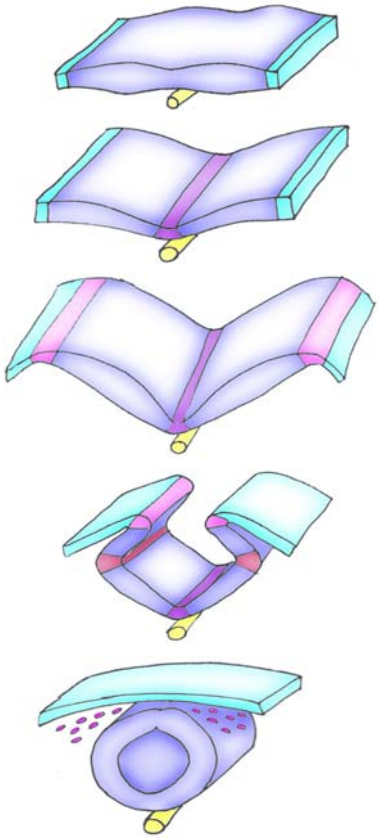

Figure 1.2. The Sites of Initiation of Closure in the Mouse Embryo

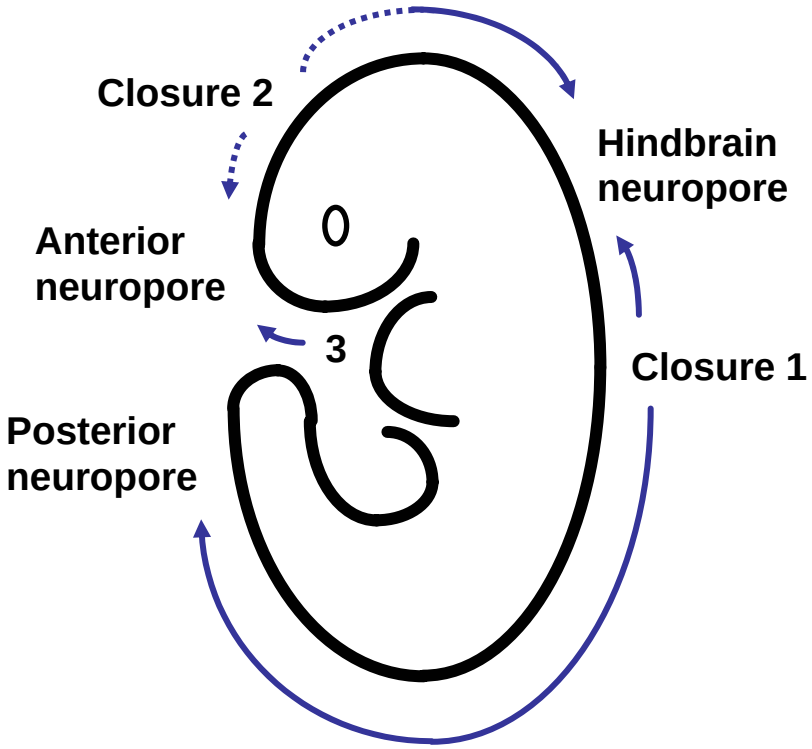

Closure 1 occurs at the hindbrain-cervical spine boundary at the 6-7 somite stage. The second site of closure at the forebrain-midbrain boundary is a polymorphic trait (varying rostrocaudally) (Juriloff et al. 1991). The final initiation of closure (3) occurs at the most anterior end of the neural tube. Diagram modified from (Copp et al., 2003b).

1.1.3. NEURAL TUBE DEFECTS

Failure of neural tube closure results in the relatively common congenital malformations known as neural tube defects (NTD) which affect around 1 in 1000 live births in Europe (EUROCAT Working Group, 1991). These may manifest at different levels of the rostrocaudal axis.Exencephaly (open brain) is a failure of closure of the cranial neural tube, which may result from a failure of initiation of Closure 2 or Closure 3, or from failure of closure of the neuropores. Later in gestation the open neural folds degenerate and the condition becomes known as anencephaly (absent brain). A failure of Closure 1 results in craniorachischisis, in which most of the brain and the entire spinal cord remain open. All of the cranial phenotypes are lethal prior to or at birth. Open spina bifida results from failure of closure of the posterior neuropore and is compatible with postnatal survival. The less severe failure of secondary neurulation is known as spinal bifida occulta or spinal dysraphism. Mouse mutants exist which model the various NTDs (Figure 1.3).

NTDs have a complex etiology, involving both environmental and genetic factors and while their molecular and cellular pathogenic mechanisms remain poorly understood, elucidation of these mechanisms gives important insights into the normal processes of neurulation. The processes of neurulation will now be discussed with reference to the studies of genetic mouse models of NTDs.

Figure 1.3. E15.5 Mouse Embryos Demonstrating NTDs

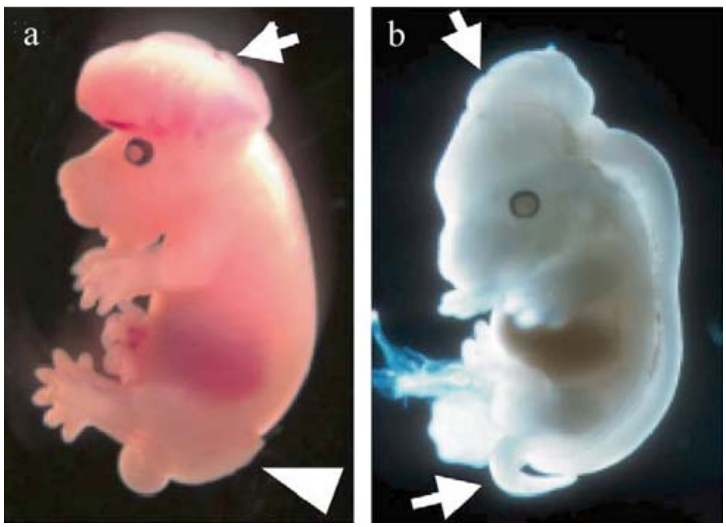

a) *Curly tail* mutant displaying both midbrain exencephaly (upper arrow) and lumbosacral spina bifida (lower arrowhead).
b) *Celsr1* mutant displaying craniorachischisis – the neural tube is open from the midbrain (upper arrow) to the lower spine (lower arrow). Reproduced from (Copp, 2005).

1.1.4. THE PROCESSES OF NEURULATION

1.1.4.1. NEURAL INDUCTION

Spemann and Mangold's (1924) classic transplantation studies in the amphibian model demonstrated the existence of an organising centre in the dorsal lip of the blastopore which was able to induce neural tissue in the neighbouring ectoderm. Subsequently equivalent regions were discovered in the other vertebrate classes –the shield of teleosts (Luther 1935) and Hensen's node of birds and mammals (Waddington, 1936).

The Default Model gave the first molecular explanation for the mechanism by which the organizing centres induce neural tissue. This states that the default fate of ectodermal cells is neural, but those which are exposed to bone morphogenetic proteins (BMPs) (specifically BMP4) form epidermis. The organising centre secretes the BMP antagonists noggin, chordin and follstatin which allow adjacent dorsal midline ectoderm tissues to realise their default neural fate producing the apicobasally thickened neural plate (Hawley et al., 1995; Wilson and Hemmati-Brivanlou, 1997; Wilson et al., 1997). Since the proposal of the Default Model, other factors have been implicated as necessary for neural induction, including fibroblast growth factors (FGFs) and Wnts (Baker et al., 1999).

Subsequent to the specification of the neural plate and in response to specific levels of the factors implicated in neural induction, a further population of cells is induced at the boundary of the neural plate and the epidermis – the neural crest cells.

The neural plate is initially induced in the dorsal midline ectoderm as a flat sheet of cells (Stern, 2002) but subsequent shaping, tissue expansion and bending events vary along the length of the neural plate causing the mechanisms and morphology of neural tube closure to vary significantly along the anterior-posterior axis of the embryo.

1.1.4.2. SHAPING OF THE NEURAL PLATE

Shaping events occur after induction, which cause the neural plate to further thicken apicobasally and to transform into an elongated keyhole shaped structure. The cranial region remains broad in contrast to the spinal region, in which the medial movement and midline intercalation of cells, known as convergent extension, results in a lengthening and narrowing of the neural plate and underlying mesoderm (Keller, 2002; Copp et al., 2003a).

The cellular mechanism of convergent extension involves the extension of polarised lamellipodia from the cells, which then exert traction between the cells (Elul and Keller, 2000). Its molecular mechanism is controlled cell-autonomously by non-canonical Wnt-frizzled-dishevelled signalling in the planar cell-polarity (PCP) pathway (Ybot-Gonzalez et al., 2007b). Mouse mutant models of craniorachischisis have all been found to harbour mutations in genes involved in this pathway, such as *vangl2, dishevelled, celsr1* and *scrb1,* indicating a requirement for convergent extension movements in the initial closure of the neural tube (Kibar et al., 2001; Hamblet et al., 2002; Curtin et al., 2003; Murdoch et al., 2003). These mutants display broad and short neural plates and it has been suggested that failure of Closure 1 is due to an inability of the wide neural folds to achieve apposition (Ueno and Greene, 2003). Similar disorders result from misexpression of these genes in *Xenopus* (Wallingford et al., 2000; Wallingford and Harland, 2001; Darken et al., 2002).

1.1.4.3. BENDING, ELEVATION AND APPOSITION OF NEURAL FOLDS

Bending of the neural plate at hinge points (furrowing) and its subsequent rotation around these hinge points (folding) allows the flat neural plate to form a tube and is achieved by the adoption of a wedge shape by neuroepithelial cells. Neural folds form in the flat plate, initially at the hindbrain/cervical boundary and subsequently more rostrally and caudally (Golden and Chernoff, 1993) as a result of bending at the midline. In general the neural plate midline anchors to the underlying axial mesoderm (the prechordal plate mesoderm at the level of the forebrain, and the notochord caudally from that) and signalling emanating from the notochord causes it to furrow and form the median hinge point (MHP). The lateral neural plate elevates on either side of the MHP to form bilateral neural folds, consisting of inner neural plate and outer surface ectoderm, which flank the neural groove (Figure 1.4).

The paired dorsolateral hinge points (DLHP) initiate at the site of attachment of the overlying surface ectoderm to the neural folds and rotation around the DLHP brings about convergence and apposition of the dorsal tips of the neural folds.

Bending of the neural plate along the anterior-posterior axis demonstrates a mechanistic heterogeneity which is reflected in the specificity of level of NTD evident in various mouse models in which bending is perturbed. The mechanisms of bending in the different anterior-posterior regions of the embryo also vary according to the animal model and will now be discussed in relation specifically to the mouse model.

Figure 1.4. Chick Neural Folds

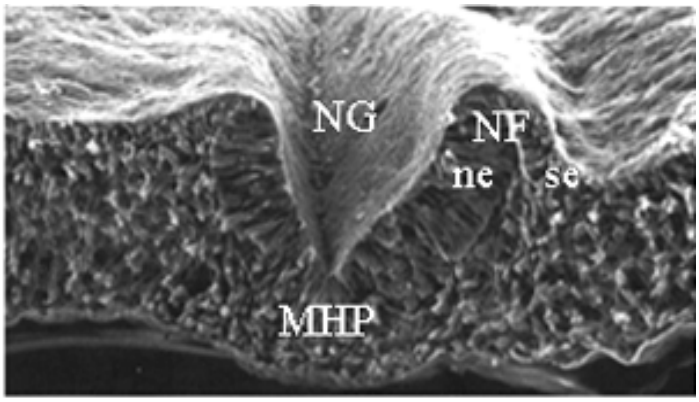

Scanning electron micrograph. Transverse section showing the median hinge point (MHP), neural groove (NG) and neural folds (NF) including the neural epithelium (ne) and the surface ectoderm (se). Reproduced from Developmental Biology. 6th edition, Gilbert 2000.

1.1.4.3.1. SPINAL BENDING

Spinal neurulation achieves a neural tube with a small lumen and the mechanisms by which the tube is formed have been subdivided into three modes, although these in fact represent a smooth continuum along the anterior-posterior axis of the embryo (Shum and Copp, 1996). Mode 1 neurulation in embryos with around 7 to 15 somites results from MHP formation alone and is the mechanism adopted at the site of Closure 1, resulting in a slit-shaped neural tube lumen. Mode 2 occurs more caudally, in embryos with between 16 and 24 somites, and involves MHP and DLHP formation producing a diamond-shaped lumen. Mode 3 begins in embryos with around 25 somites and closure results from DLHP formation alone, producing a flatter, wider lumen (Ybot-Gonzalez and Copp, 1999).

Cells of the neural plate exhibit interkinetic nuclear migration and an accumulation of cells in the S- and early G2-phases of the cell cycle, during which their nuclei are located

basally, results in basal expansion of the cells and the adoption of a wedge shape as required for bending (Schoenwolf, 1985; Smith et al., 1994). This has been observed in spinal MHP formation (Gerrelli and Copp, 1997). It is not yet clear whether a similar mechanism is responsible for DLHP formation in the spinal region.

1.1.4.3.2. CRANIAL BENDING, ELEVATION AND APPOSITION

The mechanisms adopted by the cranial region of the neural plate to achieve closure of the neural tube differ from those in the spinal region and in fact appear to be more prone to perturbation, as indicated by the more than 150 mouse genetic mutations (Harris and Juriloff, 2010) and many teratogenic influences (Copp et al., 1990) which result in cranial specific NTD – ie exencephaly.

The MHP forms in the cranial neural plate as described above and subsequently the underlying mesenchyme undergoes a process of expansion via cell proliferation and an increase in extracellular space, which causes the neural folds to elevate and adopt a biconvex morphology, especially in the midbrain region (Morriss and Solursh, 1978). This mesenchymal expansion is specific to elevation in the cranial region and appears to be necessary for cranial neurulation as inferred from the study of the *Twist* and *Cart1* mutant mice which are mesenchyme deficient and exencephalic (Chen and Behringer, 1995; Zhao et al., 1996). Analysis of *Twist* chimeras indicated that a reduction of *Twist* in the neural plate did not affect neural tube closure, but *Twist-/-* cells in the mesenchyme act in a cell-autonomous manner to produce the exencephalic phenotype implicating the mesenchymal phenotype as conducive to exencephaly.

To enable the biconvex neural folds to form a tube with a large central lumen further bending is induced in the dorsolateral neuroepithelium of the midbrain producing the DLHPs. This causes the biconvex neural folds to flip around in a medial direction to adopt a biconcave morphology, allowing the tips of the neural folds to appose at the site of Closure 2 (Morriss-Kay, 1981).

In addition to the biconvex nature of the cranial neural folds, which must be overcome in order to undergo DLHP formation, the cranial neural plate is subject to a further source of mechanical tension in the ventral cephalic flexures of the rostral body axis (Jacobson and Tam, 1982). Experimental evidence for the effect of curvature on neural tube closure was provided by analysis of the chick posterior neuropore (PNP); neural tube explants were cultured on curved substrates and a higher degree of curvature was found to predict a slower rate of PNP closure (Van Straaten et al. 1993). Furthermore

comparison of the rate of PNP closure in different species demonstrated that rate of closure was inversely proportional to angle of axial curvature (Peeters et al., 1998). This morphology's significance in the cranial region of the mouse is indicated by the effect of the position of Closure 2 (a polymorphic trait) (Juriloff et al., 1991) on the occurrence of cranial NTDs. Mouse strains which exhibit a caudally located Closure 2 are resistant to exencephaly as Closure 2 facilitates the subsequent closure of the region of high curvature in the midbrain, whereas strains in which Closure 2 is located rostrally in the forebrain are prone to exencephaly as Closure 2 is less able to support the subsequent closure of the midbrain region (Fleming and Copp, 2000).

Thus, apposition of the tips of the neural folds in the cranial region is resisted by high degrees of mechanical tension due to the morphology of the neural plate. The biconvex nature of the neural folds arises from the large neural plate being elevated around the MHP. This resists folding of the neural plate in the opposite direction at neurulation. Furthermore axial curvature at the cranial flexures impinges on neurulation, forcing closure to occur on the outside of a curve. As a result neurulation in the cranial region is prone to perturbation in both mouse mutant models and in response to teratogens. A number of processes have been implicated in assisting the neural folds to overcome this tension, including contraction of apical actin microfilaments on the luminal surface of the neuroepithelium, neuroepithelial proliferation, apoptosis and perhaps also neural crest cell delamination. Evidence linking each process to cranial closure is presented below and the processes known or postulated to be relevant to bending of the neural plate in DLHP formation are summarised in Figure 1.5.

Hinge point formation is known to require the adoption of a wedge shape by neuroepithelial cells and constriction of the apical ends of the cells is a mechanism by which this is achieved (Karfunkel, 1974; Sadler et al., 1982). Exencephaly induced upon depolymerisation of actin microfilaments with cytochalasin-D has implicated the 'purse string' contraction of apical actin microfilaments as essential for cranial hinge point formation and closure (Morriss-Kay and Tuckett, 1985; Matsuda and Keino, 1994). This finding is supported by numerous mouse models harbouring mutations for genes involved in cytoskeletal function, which display specifically cranial (but not generally spinal) NTDs such as MARKS-/-, *Vinculin*-/- and *p190RhoGAP*-/- (Stumpo et al., 1995; Xu et al., 1998; Brouns et al., 2000).

During neurulation the neuroepithelium is proliferative (only differentiating after closure of the neural tube) and mouse models of exencephaly in which proliferation is reduced,

associated with premature differentiation (such as *HesI-/-* and *Numb-/-* (Ishibashi et al., 1995; Zhong et al., 2000), may reflect an inability to maintain the correct numbers of cells required for the morphological changes associated with DLHP formation. Conversely an excess of proliferation may also disrupt the balance of cell numbers. Alternatively premature differentiation could result in the neural plate becoming mechanically inflexible preventing DLHP bending, or could interfere with the release of NCC.

Another process which has been implicated as essential for bending of the cranial neural plate is apoptosis, which occurs in the neuroepithelium at the DLHPs and the dorsal tips of the neural folds (Lawson et al., 1999). Numerous mouse mutants show exencephaly (but no spinal defect) which is attributable to a reduction of apoptosis in the neural tube- for example *Apaf-1-/-*, *p53-/-* and *Caspase-9-/-* (Oppenheim et al., 2001). This may imply that removal of cells from the neural tube at the secondary sites of bending (the DLHP and the dorsal tips of the neural folds) is necessary to confer the degree of flexibility required for these flexures – a flexibility which is not required in the spinal area, explaining the specificity of the defect observed in mouse models. On the other hand pharmacological inhibition of apoptosis does not cause NTDs (Massa et al., 2009). Again the converse model of excess apoptosis also results in exencephaly in the *AP-2-/-* and *Tcof1-/-* mutants (Zhang et al., 1996; Dixon et al., 2000).

Similarly the process of NCC delamination and migration away from the dorsal tips of the cranial neural folds prior to closure of the neural tube (Tan and Morriss-Kay, 1985) may be necessary to disrupt the epithelial layer and basal lamina and to reduce the density of cells thus increasing the flexibility of the dorsal tips of the neural folds, allowing the 'flip-around' event of DLHP formation to occur – this is the hypothesis postulated in the current research. The spatial and temporal correlation of NCC delamination and apposition of the cranial neural folds supports this idea (unlike in spinal regions where closure precedes NCC migration (Erickson and Weston, 1983) as does the plethora of mouse mutant models and the effects of teratogens which demonstrate a concurrence of exencephaly and neural crest related defects (neurocristopathies). This evidence will be discussed fully after an introduction to the processes of NCC induction, delamination, migration and differentiation.

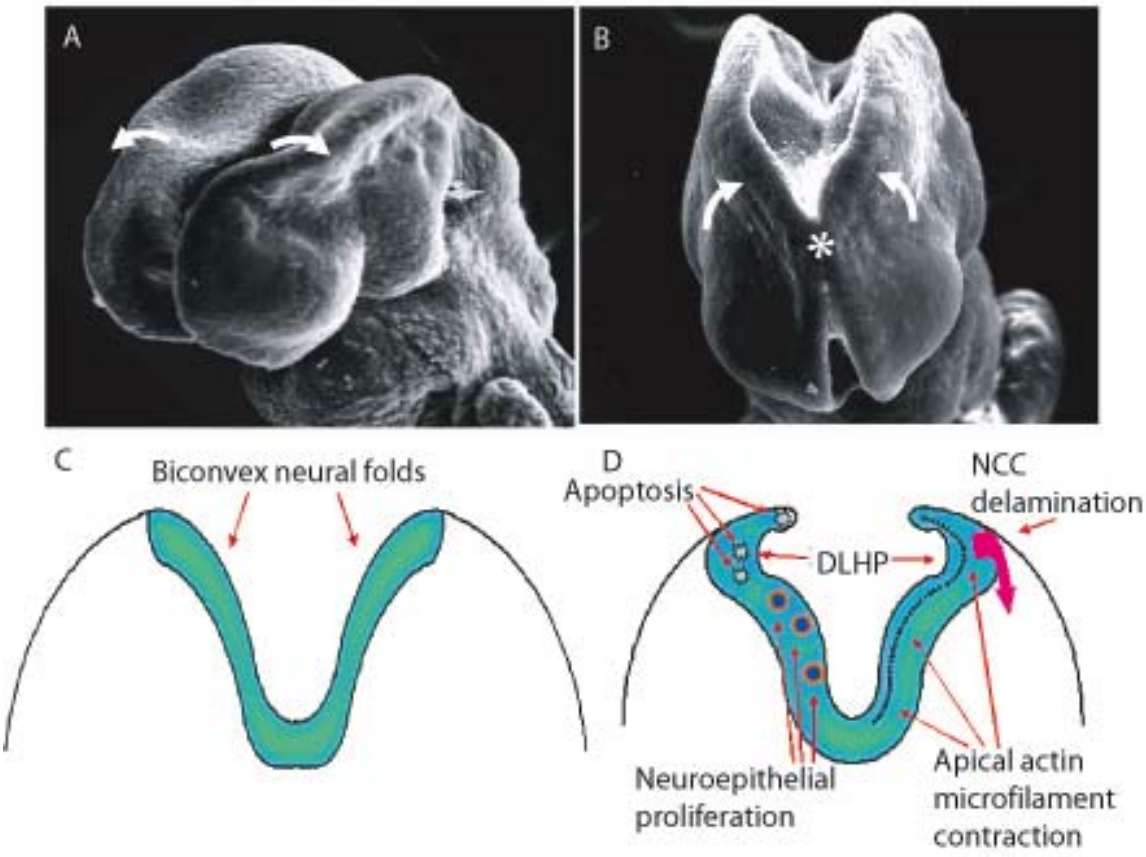

Figure 1.5. DLHP Formation in the Biconvex Neural Folds

(A,B) Scanning electron micrographs and (C,D) schematics of neural folds before and after DLHP formation.

(**A,C**) widely spaced biconvex neural folds indicated by white arrows in A. (**B**) Neural folds have flipped around at the DLHPs (white arrows) to achieve apposition and closure at the site of Closure 2 (white asterisk). (**C**) Processes implicated in DLHP formation are indicated.

A and B taken from (Fleming & Copp, 2000) and B and C modified from (Copp et al., 2003b).

1.1.4.4. FUSION OF THE NEURAL FOLDS

Elevation and bending of the neural folds brings their tips into apposition, allowing the processes of adhesion and fusion to complete the closure of the neural tube. Lamellipodial cell protrusions have been observed to emerge from the apposing neural fold apices and interdigitate upon contact, providing an initial adhesion between the cells (Geelen and Langman, 1979). Ephrins (cell surface ligands) and their interactions with Ephs (cell surface receptors) have been implicated in intercellular interactions, chemorepulsion and cell adhesion throughout the organism. Examination of mouse mutants has revealed a crucial role for these interactions in the fusion of the neural tube: mutations in the ephrin-A5 ligand and alterations in phosphorylation of the EphA7 receptor (both of which are expressed in the cranial neuroepithelium around the time of neural tube closure) result in exencephaly, apparently due to defective fusion of the neural folds (Holmberg et al., 2000). Recently, inhibition of these molecular interactions in mouse embryo culture has been shown to delay or prevent neural fold fusion (Abdul-Aziz et al., 2009).

Apoptotic remodelling events then occur at the site of fusion. These have been thought to allow the completed neural tube and the overlying surface ectoderm to separate, as evidenced by the use of an apoptosis inhibitor (Zvad-fmk) which produces spinal NTDs in chick embryos (Weil et al., 1997). The finding of spinal NTDs upon inhibition of apoptosis (in contrast to the finding of cranial NTDs associated with apoptosis mentioned above) may differentiate the effects of apoptosis in two different processes – the processes of bending and of remodelling. More recently studies using both chemical inhibitors and mutations in genes required for apoptosis have shown that absence of apoptosis in mouse embryos does not produce NTDs; therefore apoptosis does not appear necessary for neural tube closure. It was suggested that apoptosis may act to eliminate cells that lose extracellular matrix attachment (anoikis) as remodelling events proceed at the site of fusion (Massa et al., 2009).

1.2. NEURAL CREST CELLS

The NCC are a transient, multipotent, migratory cell population specific to vertebrates. They are induced at the boundary between the neural ectoderm and the epithelial ectoderm caudal to the anterior forebrain region in response to signals from the surrounding tissues. NCC then undergo an epithelial to mesenchymal transition (EMT), delaminate away from the neuroectoderm and migrate throughout the embryo in response to chemotactic signalling and local guidance cues, simultaneously proliferating and becoming progressively more lineage restricted. NCC form phenotypically diverse populations of cells upon terminal differentiation at their target organs (reviewed in Le Douarin & Kalcheim 1999, (Le Douarin, 1982) and see Figure 1.6 and Table 1.1).

1.2.1. NEUROCRISTOPATHIES

Defects in NCC derivatives are termed neurocristopathies and result in a wide range of relatively common malformations, reflecting the extensive range of derivatives of the NCC. Neurocristopathies include Hirschsprung's Disease (aganglionic hindgut) (reviewed in (Burns et al., 2009), Waardenberg syndromes (which combine craniofacial abnormalities with pigmentation defects and in some cases deafness) (reviewed in (Read and Newton, 1997), and craniofacial abnormalities such as Treacher-Collins syndrome (underdeveloped facial bones and deafness), Pierre-Robin syndrome (failure of lower jaw development and cleft palate), DiGeorge syndrome (lack of thymus and parathyroid) and Goldenhar syndrome (facial abnormalities) (reviewed in Hunt & Hobar 2002).

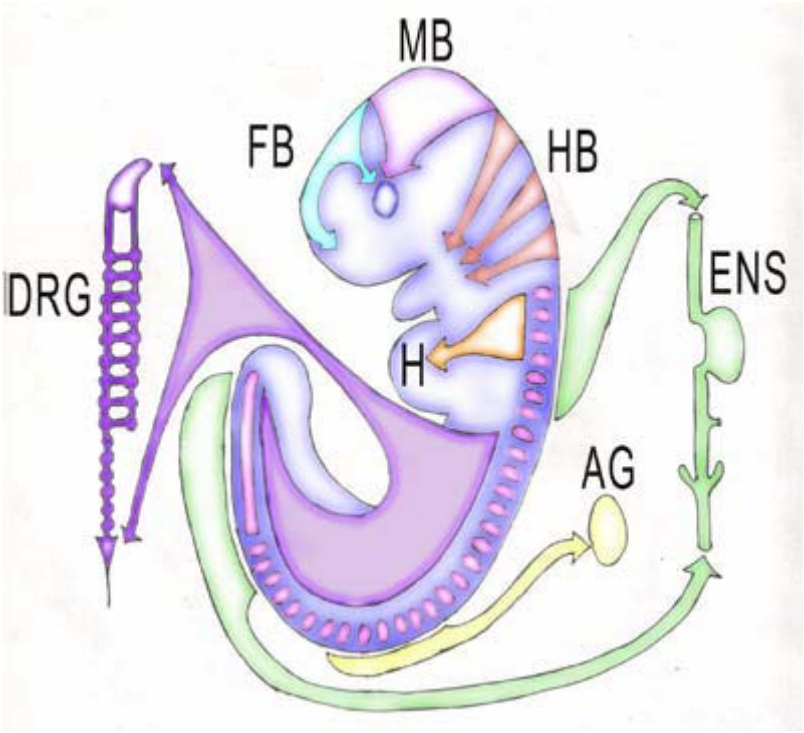

Figure 1.6. Schematic of NCC Derivatives

This demonstrates the range of both derivatives and their locations throughout the embryo.

Abbreviations: FB, forebrain; MB, midbrain; HB, hindbrain; ENS, enteric nervous system; H, heart; AG, adrenal gland; DRG, dorsal root ganglia.

Table 1.1. Derivatives of the Neural Crest

DERIVATIVE	CELL TYPE OR STRUCTURE
Peripheral nervous system	Neurons (sensory ganglia, sympathetic and parasympathetic ganglia, enteric nervous system), glia (satellite cells, Schwann cells)
Endocrine &parendocrine derivatives	Adrenal medulla, Calcitonin secreting cells, Carotid body type I cells
Pigment cells	Epidermal pigment cells, iris pigment cells
Facial cartilage & bones	Facial and anterior ventral skull cartilage and bone, including jaw and middle ear
Connective tissue	Corneal endothelium and stroma; tooth papillae; dermis, smooth muscle and adipose tissue of skin of head and neck; connective tissue of salivary, lachrymal, thymus, thyroid and pituitary glands; connective tissue and smooth muscle in arteries of aortic arch origin, septum of the outflow tract and semilunar valves of the heart

1.2.2. THE PROCESSES OF NCC COLONISATION

The colonisation of target organs by the NCC is a multi-step process which begins with the induction of NCC in the neuroepithelium, followed by an EMT, then migration, proliferation and differentiation. These processes will now be discussed in greater depth.

1.2.2.1. INDUCTION OF NEURAL CREST

NCC arise at the border between the neural and non-neural ectoderm directly following induction of the neural plate, as a result of the inductive interactions of several factors from neural and non-neural ectoderm and the underlying mesoderm.

Dorsoventral patterning gradients, which have already been implicated in neural induction, confer a competence territory for NCC induction. BMPs secreted by the ectoderm are antagonised by factors secreted ventrally from the notochord, such as chordin, noggin and follistatin. This ventral antagonism results in a dorso-ventral BMP gradient and while the lowest levels of BMP signalling induce neural plate tissue, intermediate levels present at the boundary of the neural and non-neural ectoderm are necessary for the induction of NCC (Steventon et al., 2009).

At the neural plate boundary, in the region of intermediate BMP activity posteriorising signals have been implicated as necessary to provide competence for NCC induction in regions posterior to the presumptive forebrain. These signals include FGFs (secreted by the paraxial mesoderm), retinoic acid and Wingless/INT-related (Wnts) (secreted by the paraxial mesoderm and the non-neural ectoderm) (Liem et al., 1995; Streit and Stern, 1999; Mayor and Aybar, 2001; Garcia-Castro et al., 2002; Villanueva et al., 2002; Bastidas et al., 2004) (see Figure 1.7).

Figure 1.7. Signals Defining a Competence Territory for NCC Induction

Red arrows indicate NCC competence signals. An intermediate level of BMP signalling in the epithelium, FGFs arising in the underlying mesoderm (blue) and Wnts and retinoic acid (RA) arising in the non-neural epithelium (orange) provide the competence territory for NCC (red) induction at the border of the neural (green) and non-neural ectoderm.

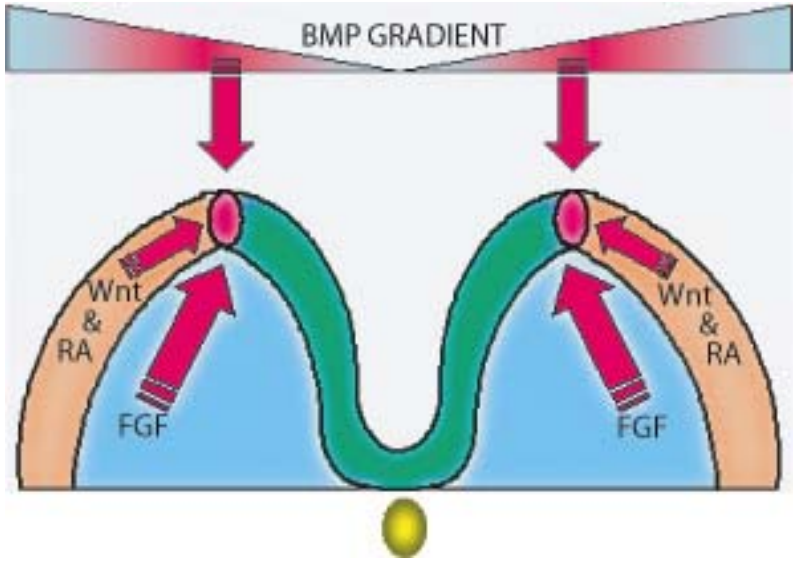

Numerous other factors forming complex regulatory networks have been implicated in the induction of NCC in the competent territory (Sauka-Spengler and Bronner-Fraser, 2008) and provide early markers for NCC. Experimental models have comprised gain and loss of function studies and mouse mutant models.

Gene gain and loss of function in the chick and *Xenopus* models have implicated *Sox10* and *Sox9*, as well as their targets *Slug* and *Snail* as being both necessary and sufficient for NCC specification (LaBonne and Bronner-Fraser, 2000; Spokony et al., 2002; Del Barrio and Nieto, 2002; Aybar et al., 2003; Cheung and Briscoe, 2003). The Wnt regulated transcription factor AP2α, the *Msx* homeobox downstream targets of BMP signalling, the paired-box transcription factors Pax3 and Pax7, members of the Zic family of zinc finger proteins and *FoxD3* have all also been implicated in NCC specification in *Xenopus* (Dottori et al., 2001; Luo et al., 2003; Inoue et al., 2004). The effects of mutations in these genes in mouse models are presented in Table 1.2.

Table 1.2. Mouse Models with Mutations in Genes Implicated in NCC Specification

GENE	NCC PHENOTYPE	REFERENCE
AP2α	Facial clefting and ganglia abnormalities	(Schorle et al., 1996)
FoxD3	Lethal in gastrulation	(Hanna et al., 2002)
Msx1	Cleft palate, craniofacial and tooth abnormalities	(Satokata and Maas, 1994)
Msx2	Craniofacial abnormalities including facial clefting	(Satokata et al., 2000)
Pax3	Cardiac, DRG, cranial ganglia, melanocyte defects	(Epstein et al., 1991)
Pax7	Defects in cranial NCC derivatives	(Mansouri et al., 1996)
Snai1	Lethal in gastrulation due to EMT involvement	(Carver et al., 2001)
Snai2	No NCC phenotype	(Jiang et al., 1998)
Sox9	Premature apoptosis of migratory NCC	(Cheung et al., 2005)
Sox10	Premature apoptosis of migratory NCC	(Southard-Smith et al., 1998)
Zic5	Craniofacial defects	(Inoue et al., 2004)

1.2.2.2. EPITHELIAL TO MESENCHYMAL TRANSITION AND DELAMINATION

The NCC are initially specified in the neuroepithelium at the dorsal tips of the elevating neural folds. Epithelial cells are tightly packed adherent cells characterised by a two dimensional layered organisation which is facilitated by a basal lamina, apical-basal cell polarity and intercellular junctions (such as tight junctions and adherens junctions). After specification, the NCC undergo epithelial to mesenchymal transition (EMT) in which they lose their epithelial features and markers such as E-cadherin, α-catenin and γ-catenin are down-regulated. The disruption of cell-cell adhesion (by transcriptional repression of genes involved in adherens and tight junctions), degradation of the basal lamina and reorganisation of the actin cytoskeleton (such as apical constriction) facilitates delamination. Concomitant with the down-regulation of epithelial characteristics, there is an up-regulation of mesenchymal characteristics. The cells become fibroblastic, up-regulating mesenchymal markers such as N-cadherin, vimentin and fibronectin as well as

matrix metalloproteases (which degrade the extracellular matrix (ECM)) and integrins (which mediate cell-ECM adhesion). These changes facilitate their migration through the ECM (this process is summarised in Table 1.3).

The EMT is characteristic of remodelling and migratory processes throughout the organism, including the movements of gastrulation, delamination of NCC and metastasis of carcinomas, and the signalling pathways which govern the EMT are similar in these different processes (reviewed in (Thiery et al., 2009). In the case of NCC the EMT allows them to delaminate away from the stratified neuroepithelium and migrate into the surrounding mesenchyme.

Table 1.3. Characteristics of the EMT

EPITHELIAL CELL CHARACTERISTICS	EMT PROCESSES	MESENCHYMAL CELL CHARACTERISTICS
Tightly packed adherent cell layer with intercellular junctions, apical-basal polarity and a basal lamina	Loss of cell-cell adhesion induces loss of cell polarity	Loosely packed migratory cells. Fibroblastic cells surrounded by ECM.
Markers include: E-cadherin (cell-cell adhesion) α- and γ-catenin (link cadherins to actin)	Breakdown of basal membrane & cytoskeletal remodellin favours delamination Delamination and migration through the ECM	Markers include: Vimentin (filament protein) Fibronectin (ECM protein) Laminin (ECM protein) Integrins (cell-ECM adhesion) Matrix metalloproteases (degrade ECM)

The *Snail* family of zinc-finger transcription factors comprises *Snai1* (or *Snail)* and *Snai2* (or *Slug)* in vertebrates. These transcription factors are expressed in NCC from their induction and evidence has already been presented which implicates them in the process of NCC specification. They are also implicated in the EMT during gastrulation, carcinoma cell metastasis and NCC development (Carver et al., 2001; Murray et al., 2007; Olmeda et al., 2008). The waters are muddied, however, by the inversion of their relative expression in different species early in development as a result of evolutionary reshuffling following genome duplication (Sefton et al., 1998; Locascio et al., 2002). In avian models, Snai2 marks premigratory NCC which are competent to undergo EMT (Carmona et al., 2000), while *Snai1* is expressed after the EMT in migratory neural crest. In *Xenopus* and mouse however, Snai1 is upstream of Snai2 (Aybar et al., 2003).

The role of *Snai1* in the EMT is demonstrated in the *Snai1*$^{-/-}$mouse, whose early embryonic lethality is attributable to a deficit in the EMT at gastrulation (Carver et al., 2001). Neither tissue specific deletion of *Snai1*, nor the *Snai2* null mouse demonstrates NCC defects (although other defects implicate them in processes such as left-right asymmetry and apoptotic protection) (Jiang et al., 1998; Murray et al., 2006). However, as with many genes involved in the development of NCC, functional redundancy is demonstrated between these two related genes and NCC specific *Snai1*deletion on a *Snai2* null genetic background results in NCC defects resembling the Pierre Robin Sequence in humans (Murray et al., 2007).

Murine Snail exerts multiple effects on the EMT, including down-regulation of epithelial markers, up-regulation of mesenchymal markers and cytoskeletal changes. One epithelial marker, the transmembrane glycoprotein E-cadherin (epithelial cadherin), mediates strong cell-cell adhesion by cadherin homophilic binding between adjacent cells which is then stabilised by linkage to the actin cytoskeleton via calcium, catenins and other molecules (Gumbiner, 2000). Snail has been shown to act as a transcriptional repressor, interacting with an element of the *E-cadherin* promoter sequence to suppress expression of *E-cadherin* and thus contributing to the destabilisation and dissociation of tightly packed epithelial cells to become a loosely organised mesenchyme (Cano et al., 2000). The basic helix-loop-helix transcription factor *Twist* has been linked to the EMT in the same way – it has been shown to interact with the same element of the E-cadherin promoter sequence as Snail, down-regulating *E-cadherin* along with *α*- and *γ-catenin*, while up-regulating *fibronectin* and *vimentin* (Yang et al., 2004).

Further studies have elucidated the roles of the Snail genes in other organisms and have highlighted the complex gene regulatory networks involved in the EMT. The dual roles of *Snai2* in both NCC specification and the EMT were dissociated by its inducible knockdown in *Xenopus* (LaBonne & Bronner-Fraser, 2000). Inactivation of *Snai2* in the chick by the use of antisense oligonucleotides impaired the EMT and interestingly resulted in a failure of neural tube closure due to failure of the tube to 'roll in' – an effect which appears to reflect a lack of DLHPs (Nieto et al., 1994).

Ectopic co-expression of *Sox9* (a NCC inducer) and either *Snai2* or *Snail* in the chick neural tube are sufficient to induce an EMT in NCC (Cheung et al., 2005). *Snai2* overexpression in the chick induces expression of *RhoB*: a small GTPase involved in actin reorganisation, whose inhibition prevents delamination of chick NCC in neural tube explants (Liu and Jessell, 1998). Overexpression of *Sox9* and *RhoB* in the chick neural tube is sufficient to induce an EMT (Cheung et al., 2005). However, *RhoB* expression in the mouse is restricted to migratory NCC (Henderson et al., 2000).

Another factor which has been implicated, independently of the Snail transcription factors, in both the specification of NCC and onset of the EMT, is the winged helix transcription factor *FoxD3*. *FoxD3* is a transcriptional repressor expressed in early embryonic stem cells, and has been described as a 'stemness' factor, being necessary for the maintenance of pluripotent progenitor cells. Later it is specifically expressed in premigratory and migratory NCC (Hanna et al., 2002) and again acts to maintain the pluripotent state of NCC by repressing melanogenesis. Attenuation of the *FoxD3* signal in *Xenopus* inhibits NCC specification, while overexpression induces ectopic NCC (Sasai et al., 2001).

Regarding the EMT, misexpression of *FoxD3* in chick neural tube induces cells to adopt a neural crest phenotype and, in some cases, delaminate and migrate from the neural tube in the trunk region, independently of Snai2 signalling (Kos et al., 2001; Dottori et al., 2001). Furthermore*FoxD3* overexpression in the chick demonstrated that *FoxD3* was not sufficient to induce the morphological features of an EMT but was able to induce changes in cell adhesion characteristic of the EMT, delamination and subsequent migration. These changes were effected via the up-regulation of cell surface proteins involved in the weak cell-ECM adhesion required for migratory behaviour (allowing rapid modification of multiple weak adhesions as mediated by integrin-β1, laminin and cadherin 7 (Cheung et al., 2005). This implies that *FoxD3* is necessary but not sufficient for the EMT of NCC.

The EMT is a critical process in the examination of the current hypothesis as it is the process which is proposed to enhance the flexibility of the dorsal neural folds, enabling the bending of the neural plate which is necessary for subsequent closure of the neural tube. The EMT of the NCC would act not only to reduce the cell density in the region of the dorsal neural folds, but also to disrupt the rigid cell adhesion in the pseudostratified neural plate. This hypothesis will be described in detail in section 1.4. Furthermore, evidence from the chick model indicates that NCC originate deeper in the neural plate than generally accepted and move gradually towards the tips of the folds before delaminating, implying that NCC development may actually affect more ventral regions of the neural plate (Krispin et al., 2010).

1.2.2.3. NEURAL CREST CELL MIGRATION, DIFFERENTIATION AND DERIVATIVES

After undergoing the EMT and delaminating away from the neuroepithelium of the tips of the neural folds, NCC begin their migration along defined migration pathways (according to their anterior-posterior location and the time of onset of their migration). They continue to proliferate and become progressively more lineage restricted, before undergoing terminal differentiation upon arrival at their target organs. NCC migration is directed by chemotactic signalling from the environment, both inhibitory and attractive, as well as requiring cell autonomous gene expression including non-canonical Wnt (planar cell polarity) signalling (De Calisto et al., 2005). NCC, although often referred to as a multipotent cell population, are in fact lineage restricted from the time of their specification according to their position along the anterior-posterior axis. For example, the Hox genes in the hindbrain provide positional identity to NCC prior to the onset of migration (Gavalas et al., 1998).

Cranial NCC contribute to the facial skeleton as well as the sensory ganglia of the twelve cranial nerves and melanocytes (Figure 1.6). Following delamination from the forebrain neuroepithelium, NCC migrate ventrally in a continuous stream through the mesenchyme between the eye and the diencephalon. In contrast, the NCC originating from the level of the midbrain migrate ventrolaterally as dispersed cells through the mesenchyme bordered by the lateral surface of the mesencephalon and ectoderm (Serbedzija et al., 1992). Derivatives include the frontonasal process and palate.

The origin of the NCC in the hindbrain is controversial. Some studies describe NCC arising equally along the length of the dorsal hindbrain, being channelled into streams upon migration leaving neural crest free zones adjacent to rhombomeres 3 and 5 in response to hindbrain patterning signals (Sechrist et al., 1993; Trainor et al., 2002). NCC which arise in rhombomeres 3 and 5 are diverted both anteriorly and posteriorly to the streams migrating from the adjacent rhombomeres. There is also evidence for enhanced levels of apoptosis in the dorsal neural ectoderm at the levels of rhombomere 3 and 5, indicating that some NCC which are specified there may be eliminated prior to delamination (Graham et al., 1996). Other studies have failed to identify NCC ever originating at the levels of rhombomeres 3 and 5 (Lumsden et al., 1991).

Thus, three subectodermal streams of NCC migrate ventrolaterally from the dorsal neural epithelium of the hindbrain into the distal portion of the adjacent branchial arch. This migration and subsequent derivatives are summarised in Figure 1.8 and Table 1.4. The first branchial arch is populated largely with NCC arising from rhombomere 2, although rhombomere 1 and the caudal midbrain region also contribute cells (primarily to the maxillary component) (Lumsden et al., 1991). Rhombomere 3 may also contribute cells. The first (mandibular) arch contains Meckel's cartilage, from which the incus and malleus of the middle ear, and the mandible derive. A maxillary component also extends from the first arch from which the upper jaw derives. The sensory ganglia of the trigeminal nerve (V) which supplies these derivatives is also derived from the NCC of the first arch (Morriss-Kay et al., 1993).

The second branchial arch or hyoid arch is populated with NCC arising in rhombomere 4 and possibly those migrating anteriorly and posteriorly from rhombomeres 5 and 3 respectively. These form the Reichert's cartilage (which develops into the hyoid bone as well as the stapes and styloid process) and the sensory ganglia of the facial nerve (VII) (Ruhin et al., 2003).

NCC from rhombomere 6, and possibly cells migrating posteriorly from rhombomere 5, populate the third branchial arch and contribute to the hyoid bone, the glossopharyngeal nerve (IX), the thymus and parathyroid gland. NCC from rhombomere 7 populate the 4thbranchial arch (although their migration stream is not so apparent) and contribute to the parathyroid and thyroid glands and the vagus nerve (X) (Jiang et al., 2000).

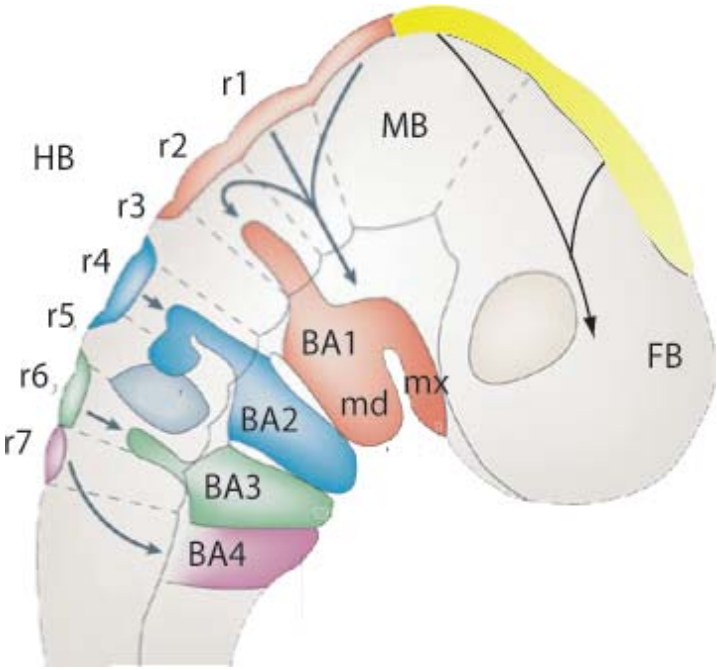

Figure 1.8. Migration Pathways of the Cranial Neural Crest

This diagram illustrates the contribution of NCC from the different rhombomeres and the midbrain and forebrain to the branchial arches and facial mesenchyme.

Abbreviations: BA, branchial arch; FB, forebrain; HB, hindbrain; MB, midbrain; md, mandibular process; mx, maxillary process; r, rhombomere.(adapted from Guthrie 2007).

Table 1.4. NCC Derivatives of the Branchial Arches

BA	Cartilage & Bone	Cranial Ganglia	Other Derivatives
1	Maxillary process → orbit, maxilla, incus Meckle's cartilage → mandible, malleus	Trigeminal (V)	
2	Reichert's cartilage → hyoid bone, stapes, styloid	Facial (VII)	
3	Hyoid bone	Glossopharyngeal (IX)	Thymus Parathyroid glands Cardiac NCC
4	Thyroid cartilage	Vagus (X)	Parathyroid glands Thyroid gland Cardiac NCC

Posterior to the hindbrain, the NCC which arise adjacent to the somites migrate along two pathways. In the avian model, a ventral pathway initially passes between the neural tube and the somite and NCC following this pathway differentiate primarily into neurons and glia of the peripheral nervous system. Later emerging NCC follow the dorsolateral pathway which passes between the dermomyotome and the epidermis and give rise primarily to the melanocytes of the skin (Reedy et al., 1998).

The mouse embryo demonstrates a different pattern of three sequential waves of NCC migration. Early migrating NCC follow a ventrolateral pathway along intersomitic blood vessels to form sympathetic neuronal progenitors and glia near the dorsal aorta (Serbedzija et al., 1990). Most NCC follow a ventromedial pathway through the anterior sclerotome of each somite, many differentiating within the somite to form the sensory neurons of the dorsal root ganglia (DRG) but some passing through the sclerotome to add to the sympathetic neurons and glia at the dorsal aorta. The late emerging NCC follow the dorsolateral pathway and give rise to melanocytes (Serbedzija et al., 1990). The derivatives of the NCC are populated in a ventral to dorsal order.

Although some NCC exiting the NT are multipotent precursors, most are fate-restricted as either glial, neuronal or later melanocytes (Henion and Weston, 1997). Entry into the different migration pathways may be governed by time of NCC specification, lineage restriction and chemotactic signalling. There is evidence to suggest that entry into the dorsolateral pathway is restricted to NCC already specified as melanoblasts(Reedy et al., 1998) and furthermore the transcriptional repressor *FoxD3* is implicated as repressing melanogenesis (via indirect repression of MITF expression) in early emigrating NCC (Thomas and Erickson, 2009). Numerous guidance cues have also been implicated in pathway selection – for example SEMA3A and its receptor neuropilin 1 guide the pathway into the anterior sclerotome (Schwarz et al., 2009).

The NCC posterior to the hindbrain can be further subdivided into overlapping functional domains. Thus, the cardiac NCC originate at the levels between the post otic hindbrain and somite 4 in the mouse and migrate in the periaortic mesenchyme, lateral to the pharynx and into the 3rd, 4th and 6thbranchial arches to colonise the aortic sac, contributing cells to the aorticopulmonary septum (Jiang et al., 2000). The vagal population of NCC arises at the level of the 1st to 7thsomites and contributes cells to the entire enteric nervous system (ENS) via the dorsolateral pathway and through the branchial arches (Reedy et al., 1998). The sacral NCC arise posterior to the level of the 28th somite and also contribute cells to the caudal ENS (Burns and Le Douarin, 2001).

1.3 NEUROCRISTOPATHIES CORRELATED WITH NTDs

Studies in rat embryos, cultured in the presence of chondroitinase ABC which digests the chondroitin sulphate side chains of proteoglycans, demonstrated an inhibition of NCC emigration correlated with retardation of neural tube closure, which was related to a delay in DLHP formation. These findings led to the suggestion that NCC emigration may be necessary for neural tube closure (Morriss-Kay and Tuckett, 1989). The current research addresses this proposal in the mouse model: that cranial NCC emigration from the dorsal neural plate may be necessary to enhance the mechanical flexibility of the neuroepithelium, allowing formation of DLHPs, apposition of the neural folds and subsequent closure. The spatial and temporal correlation of NCC delamination and cranial neural tube closure are consistent with this idea, and further lines of evidence will now be discussed which lend support to the hypothesis.

A striking number of correlations have been observed in the mouse, between defects in NCC derivatives and failure of neural tube closure, specifically between defects of the early processes (specification and delamination) of cranial NCC and exencephaly (see Table 1.5). The investigation of a possible association between human NCC-related congenital defects associated with exencephaly (or more often anencephaly) is hindered by the small sample size. The prenatal lethality of some anencephaly cases, and the ease of its detection early in gestation resulting in termination of pregnancy, mean that very few anencephalic foetuses are available for investigation. One study looked at foetal malformations associated with NTDs in South Carolina over a ten year period and detected a number of cardiac defects (which are not specified as being NCC related) and facial clefts associated with anencephaly (Stevenson et al., 2004).

Unlike in humans, there exists a plethora of mouse mutant models of exencephaly available for investigation. It is of interest that of the eleven mouse models harbouring mutations in genes reported to be involved in NCC specification (see Table 1.2), two have normal NCC specification and delamination (*Sox9*$^{-/-}$ and *Sox10*$^{-/-}$) and one shows no NCC defect (*Slug*$^{-/-}$)(perhaps due to functional redundancy). Another two are early lethal (*Snail*$^{-/-}$and *FoxD3*$^{-/-}$). Of the remaining six mutants with disrupted NCC specification, four also show exencephaly (*AP2α*$^{-/-}$, *Msx2*$^{-/-}$, *Pax3*$^{-/-}$ and *Zic5*$^{-/-}$) and the last two may show partial functional redundancy with their family members (*Msx1*$^{-/-}$ and *Pax7*$^{-/-}$).

Although the mouse harbouring a mutation of *Snail* shows early lethality due to failure of gastrulation events, antisense knockdown of the equivalent gene in the chick model (*Slug*) at the time of NCC delamination was found to disrupt the NCC EMT and also to prevent the 'rolling in' of the neural tube, thus disrupting closure (Nieto et al., 1994). While this is not a mouse mutation, it provides a conditional knockdown model of the *Snail* signalling cascade.

The transcription factor *AP2α* is prominently expressed in cranial NCC and, as described above, has been implicated in NCC specification. Its mutation results in facial clefting, defects in cranial ganglia, sensory organs and in the cardiac outflow tract (typical examples of cranial neurocristopathies) as well as a failure of the cranial neural folds to close, especially in the midbrain area (which is the site of maximum DLHP formation) (Zhang et al., 1996; Schorle et al., 1996; Kohlbecker et al., 2002; Brewer et al., 2004). The NCC defects are completely penetrant, while the NTD shows incomplete penetrance, perhaps implying that the NTD phenotype is secondary to the NCC defects.

Cited2 is known to interact with and coactivate all isoforms of *AP2α*, hence potentially implicating it in NCC specification in parallel with *AP2α.Cited2*$^{-/-}$ mice also demonstrate completely penetrant NCC defects including cardiac malformations, small and fused cranial ganglia and absence of adrenal glands, in association with an incompletely penetrant midbrain exencephaly(Bamforth et al., 2001; Martinez-Barbera et al., 2002). Sections through the neural tube defect appear to show that these mice may lack DLHPs.

Msx2 is known to be involved in NCC specification and its mutation causes defects of NCC, including complete penetrance of mandibular hypoplasia and maxillary malformations and incomplete penetrance of cleft palate. The mutation also results in an incompletely penetrant phenotype of exencephaly, thus demonstrating a correlation between NCC defects and NTD(Winograd et al., 1997). *Msx1* is also involved in NCC specification, and is 97% identical to *Msx2* in the homeodomain. Functional redundancy (although clearly not complete redundancy), could perhaps explain why no NTD is observed in *Msx1* mutant mice.

Pax3 is normally expressed in the dorsal neuroepitheliumand a subset of migrating NCC and its mutation has been well characterised in a number of *Splotch* alleles (e.g. *Sp* and *Sp*^{2H}) as well as in mice with knock-in of *Cre* into the *Pax3* locus. *Splotch* mutants have been found to display an array of trunk NCC-related anomalies, including defects in the cardiac outflow tract, DRG (especially caudally), pigmentation and enteric ganglia

(Epstein et al., 1993; Serbedzija and McMahon, 1997; Lang et al., 2000). Defects have also been observed in the cranial ganglia and nerves (Tremblay et al., 1995). These defects are coexpressed with incomplete penetrance of both spina bifida and exencephaly. However, the spinal NTD has been dissociated from the NCC defects as spina bifida may occur in the absence of obvious NCC defects (Franz, 1992). Moreover, simultaneous mutation of a *Splotch* allele in mice homozygous for the *curly tail* mutation exacerbates their pre-existing spina bifida phenotype without compromising NCC migration (Estibeiro et al., 1993).

Two members of the *Zic* gene family link NCC and neurulation defects in their mutant phenotypes.*Zic2* is expressed throughout the neural plate during neural tube closure, and loss of function (as in the Kumba mutant which harbours a point mutation in *Zic2*) leads to exencephaly, spina bifida and NCC specification defects (Elms et al, 2003). $Zic2^{Ku/Ku}$ embryos lack DLHPs in the spinal region (Ybot-Gonzalez et al., 2007a). *Zic5* expression is localised to the dorsal neural tube and limbs, and its disruption results in malformations of neural crest-derived facial bones (especially the mandible) and in delayed development of the 1stbranchial arch, and trigeminal and facial nerves. These defects are combined with failure of cranial neural tube closure. Sections through the cranial defect of $Zic5^{-/-}$ mutants demonstrate the formation of DLHPs (Inoue et al., 2004), in apparent contrast to *Zic2* mutants.

Several further models of exencephaly with associated NCC defects exist, including mutation of the actin depolymerising factor *n-cofilin* (Gurniak et al 2005), the *Twist* mutant (a factor recently implicated in EMT) (Soo et al., 2002; Yang et al., 2004), overexpression of the *connexin 43* gap junction gene in the dorsal neural tube and NCC subpopulations (Ewart et al., 1997), *lamininα5* mutations (Miner et al., 1998), the *Lrp6/Crookedtail*mutant (Barra, 1990; Carter et al., 1999) and the *Patch/PDGFRα* mutant (Sun et al., 2000; Tallquist and Soriano, 2003). These are listed in Table 1.5.

Table 1.5. Mouse Models Demonstrating a Correlation between NTDs and Neurocristopathies

GENE DISRUPTED (MOUSE MODEL)	CRANIAL NCC PHENOTYPE	NEURAL TUBE PHENOTYPE
AP2α	Facial clefting, cranial ganglia, sensory organ & heart outflow tract defects (complete penetrance)	Midbrain exencephaly (incomplete penetrance)
Cited2	Cardiac malformations, adrenal agenesis, &cranial ganglia defects (complete penetrance)	Midbrain exencephaly (incomplete penetrance); may lack DLHP.
Cx43	Cranial & spinal ganglia & cardiac defects	Exencephaly (may lack DLHP)
Laminin α5	Delayed & aberrant migration of NCC, defects of cranial & spinal ganglia	Exencephaly
Lrp6 (Crooked Tail)	Cleft palate (may be NCC-related)	Exencephaly
Msx2	Mandibular & maxillary malformations (complete penetrance) & cleft palate (incomplete penetrance)	Exencephaly (incomplete penetrance)
n-cofilin	Impaired delamination & migration into the branchial arches	Exencephaly
Patch	Craniofacial abnormalities	Exencephaly
Pax3 (Splotch)	Reduction in cranial ganglia	Exencephaly&spina bifida
Zic2 (Kumba)	Reduced NCC specification & aberrant migration	Exencephaly, holoprosencephaly&spina bifida (lack of DLHPs).
Zic5	NCC-derived bone defects	Exencephaly; DLHPs appear to form

In addition to the numerous genetic mouse models demonstrating a correlation between exencephaly and neurocristopathies, a number of teratogens also result in both defects. For example, retinoic acid (RA) is routinely used in the treatment of acne and this has been linked to a 25-fold increased risk for congenital malformations including NTDs and neurocristopathies (Lammer et al., 1985). RA over-exposure in the mouse and rat results in inhibition of cranial NCC migration and associated defects (Li et al., 2001) as well as exencephaly (Cohlan, 1954; Quemelo et al., 2007). Alcohol is another teratogen known to induce defects in both the cranial NCC and cranial neural tube in the mouse as well as in humans (Padmanabhan and Muawad, 1985; Kotch and Sulik, 1992; Ahlgren et al., 2002; Chen et al., 2005).

The above examples provide ample evidence demonstrating a correlation between the processes of neural tube closure and NCC migration. Although in most cases the NCC defects and the NTDs have previously been attributed to differing actions of the genes involved, the possibility that the two processes are in fact causally related is rarely excluded by the evidence available.

1.4. A CAUSE-AND-EFFECT RELATIONSHIP BETWEEN NEUROCRISTOPATHIES AND NTDs?

The early events of NCC development – from specification to their subsequent delamination from the neural epithelium and migration into the periphery – are both temporally and spatially contiguous with the shaping, bending and subsequent closure of the neural tube. Taken with the high frequency of associations between failure of neural tube closure and neural crest cell emigration, as reviewed above, this implies that the two processes of NCC colonisation and neural tube closure could be causally related. The nature of this relationship, however, cannot be specified without taking further evidence into consideration. The correlation may merely reflect an association between the two events, implying that they are both dependent on a common (‘upstream’) factor. Alternatively the correlation may reflect a cause-and-effect relationship: either NCC development is necessary for neural tube closure, or neural tube closure is necessary for NCC development.

The only explanation put forward for the correlation between NTDs and neurocristopathies in the literature considers the dependency of both the neural tube and the neural crest on precisely timed proliferative bursts. Folate metabolism has been found

to be of central importance for the proliferative capacity of highly mitotic cells, and the finding that several NTD and neurocristopathy models are folate responsive (including *Crooked tail, Splotch* and *Cited2*) may imply that this is the shared mechanism linking the neural crest and neural tube phenotypes in these mouse mutants (Fleming and Copp, 1998; Carter et al., 1999; Antony and Hansen, 2000; Martinez-Barbera et al., 2002; Greene and Copp, 2005). However, while this hypothesis may provide an explanation for several of the mouse models exhibiting co-existence of NCC anomalies and NTDs, there remain several convincing models which are not folate responsive.

As for the potential of a cause-and-effect relationship between NCC development and neural tube closure, the directionality of this relationship can be inferred from a number of findings. The first proposal that neural tube closure may be necessary for NCC development is precluded by the finding that, in the cranial region of the mouse, NCC migration precedes closure (so cranial closure cannot be necessary for NCC migration). Also normal NCC development is observable in the region of spina bifida in mouse mutants such as *curly tail* (Estibeiro et al., 1993), indicating that neural tube closure is not required for NCC development in the spinal region. Therefore, the converse possibility is proposed here – that normal early NCC development is necessary for neural tube closure, specifically in the cranial region. Two factors indicate that the requirement of normal NCC development for neural tube closure is specific to the cranial region: (i) spinal neural tube closure is known to precede NCC specification and migration by several hours of development (Erickson & Weston, 1983), and (ii) the NTDs noted in association with neurocristopathies are almost always exencephaly and only rarely spina bifida (Table 1.5).

Furthermore it is proposed that the mechanism by which normal NCC development may act to assist cranial neural tube closure is via EMT. Delamination of NCC from the pseudostratified neuroepithelium may act to enhance the mechanical flexibility of the dorsal neural plate, both by disrupting the epithelial layer and reducing the cell density of the region. The enhanced flexibility of the neural plate at the site of Closure 2, where there is the highest mechanical tension opposing the drawing together of the tips of the neural folds (due to both the concave nature of the neural folds and the axial curvature), allows the formation of DLHPs. Flexibility in the dorsal neuroepithelium allows the angle between the neuroepithelium and the non-neural epithelium to convert from an obtuse angle prior to DLHP formation to an acute angle upon DLHP formation. These proposals are depicted in Figure 1.9.

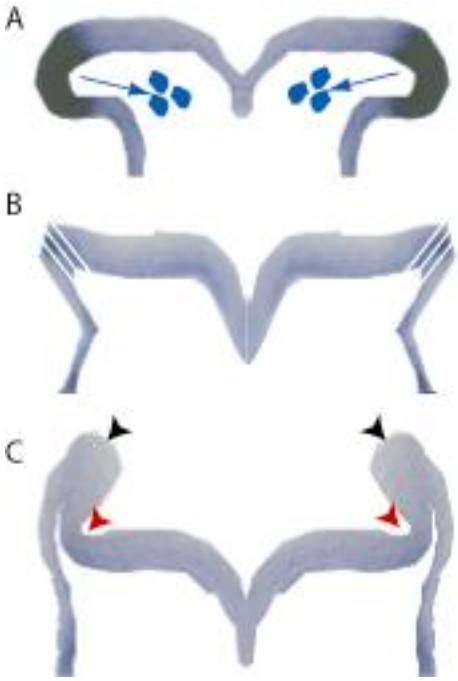

Figure 1.9. Hypothesised Mechanism for the Role of NCC in DLHP Formation.

NCC delamination from the dorsal tips of the initially biconvex neural folds (blue arrows in A) destabilises the rigid neuroepithelium at this location, increasing its mechanical flexibility (indicated by broken lines in B) and allowing the epithelial sheet to bend at an acute angle at the tips of the neural folds (black arrowheads in C) upon bending at the DLHP (red arrowheads in C).

1.5. INTERSPECIES DIFFERENCES

The processes of neurulation differ significantly between species. The human neural plate is morphologically similar to that of the mouse – large rostrally and narrow caudally. Fusion of the neural tube initiates at two sites at Carnegie stage 10 (ORahilly & Muller 2002), unlike the three closure initiation sites in the mouse. Closure of the rostral and caudal neuropores is complete by stages 11 and 12 respectively (Yoon et al 1997). The human embryo has a high degree of axial curvature in the cranial flexure (Peeters et al., 1998) and this, as in the mouse, acts to resist closure of the neural folds.

Chick neurulation occurs while the embryo is anchored relatively flat in the adjacent membranes, thus minimising the effects of axial curvature in resisting closure of the neural folds. Bending of the midline of the neural plate results in the initiation of Closure 1 in the relatively small neural folds of the midbrain. This is followed by multisite points of closure in the hindbrain and subsequent closure of the resultant neuropores (Van Straaten et al., 1996). Although DLHP have not been universally described in the chick model, the general consensus us that they are present, at least at some levels of the body axis (Smith and Schoenwolf, 1987). Xenopus neurulation also involves bending of the neural plate at the MHP and a large initial closure, followed by zipping closure of the neuropores (Shroeder., 1970). In Xenopus, as in the chick, there is minimal axial

curvature resisting closure of the neural folds. In contrast to all the other models described, zebrafish neurulation occurs by a process of canalisation whereby a solid rod of epithelial cells hollows out to form the neural tube (Nyholm et al., 2009).

Controversy exists over the temporal relationships between NCC development and neural tube closure in organisms other than the mouse. The prevailing view in the literature had been that NCC specification occurs during closure of the neural tube in *Xenopus*, zebrafish and chick models. The finding, however, of NCC specific genes such as *FoxD3, Slug* and *Snail* expressed early in prospective NCC, has led to the proposal of a general common model for NCC induction in which cranial induction precedes convergent extension movements (Mayor et al., 1995; Selleck and Bronner-Fraser, 1995; Aybar and Mayor, 2002).

In the human model spinal NCC specification is known to initiate at stage 11 (following closure in this region). The NCC migrate (as in the mouse) to form the spinal ganglia and other derivatives (O'Rahilly and Müller, 2003). The early migration of human cranial NCC, however, has not been documented.

The onset of NCC migration in the chick has been described by some as occurring after the closure of the neural tube (Schoenwolf and Smith, 1990). Others describe chick NCC migration as preceding neural tube closure and a correlation has been observed between failure of NCC delamination and neural tube 'rolling in' in the chick upon treatment with *Slug* antisense oligonucleotides (as described above) (Nieto et al., 1994). A similar controversy exists regarding NCC migration from the neural tube in *Xenopus*. Some studies describe migratory remodelling events of neural tube closure preceding NCC emigration, although homogeneity of these processes along the anterior-posterior axis is often assumed, failing to differentiate between spinal and cranial processes (Davidson and Keller, 1999). Other studies have described cephalic NCC migration initiating prior to the closure of the neural tube (Sadaghiani and Thiebaud 1987).

The evidence supports a role for the migration of NCC from the cranial neural plate in subsequent closure of the mouse neural tube. The temporal relationships of cranial NCC emigration and neural tube closure in other organisms, including chick, *Xenopus* and human may support the application of this hypothesis in these models.

1.6. AIMS OF THE PROJECT

The aim of the current research was to determine whether cranial NCC migration is necessary for subsequent dorsolateral bending of the neural plate and neural tube closure in the mouse. To achieve this, **Chapter 2** describes the processes of neurulation and NCC specification and migration in the cranial region of the normal mouse embryo. The relationship between the two processes is elucidated in greater detail than previously achieved. Further studies then investigate the relationship between neural tube closure and NCC delamination in chick and human embryos.

In **Chapter 3**, the relationship between aberrant neural tube closure and NCC specification and migration is described in a number of mouse models known to harbour mutations which affect both processes. In **Chapter** 4, the normal delamination of NCC is disrupted by use of inhibitors in both mouse whole embryo culture and in the chick embryo, in order to determine possible effects on cranial neural tube closure.

In **Chapter 5**, a new transgenic mouse is described, whose development during this PhD has enabled conditional expression of a short hairpin RNA (shRNA) targeted against *FoxD3* specifically in NCC. This *FoxD3* knockdown model is used as a tool to further dissect the role of NCC in neurulation, thereby testing the idea that inhibition of NCC delamination may disturb subsequent neural tube closure in the future brain.

CHAPTER 2

CORRELATING NEURAL CREST MIGRATION WITH NEURAL TUBE CLOSURE

2.1. INTRODUCTION

The spatial and temporal contiguity of the early processes of NCC development and neural tube closure have been discussed in Chapter 1. Numerous associations between cranial NTDs and neurocristopathies that have been noted in the literature indicate that there may be some relationship between the processes of neural tube closure and NCC emigration (Morriss-Kay and Tuckett, 1989; Zhang et al., 1996; Stevenson et al., 2004). Furthermore the association of neurocristopathies specifically with cranial NTDs, and the occurrence of normal spinal NCC development in the absence of spinal neural tube closure, both indicate that the relationship between NCC development and neural tube closure is specific to the cranial region (Franz, 1992; Estibeiro et al., 1993). Finally, the finding that cranial NCC specification and delamination precedes cranial neural tube closure (Serbedzija et al., 1992) implies the directionality of the proposed relationship – i.e. early cranial NCC development may be necessary for cranial neural tube closure.

The hypothesised mechanism by which the early processes of NCC development may act to facilitate neural tube closure in the cranial region is by the delamination of NCC from the dorsal neuroepithelium acting to increase its flexibility. It is proposed that by disrupting the tightly packed laminar structure and reducing cell density in the dorsal neuroepithelium, increased mechanical flexibility of this regionenables the bending of the neural plate at the dorsal tip of the neural folds, and consequentially at the DLHPs, and so allows apposition of the neural folds.

The aim of the current chapter is to: (i) determine the precise timing of NCC specification, delamination and migration, and (ii) correlate these events with the sequential steps of neural tube closure. While descriptions of these two events have been published previously, there has not been a detailed description in the mouse which specifically sets out to correlate the two events. Previous studies have tended to focus either on NCC development (Serbedzija et al., 1992)or on neural tube closure (Copp et al., 2000)and the most exhaustive studies of NCC development have been conducted in the chick model (Di Virgilio et al 1967;Le Douarin, 2004)

2.1.1. POSSIBLE ROLES OF TISSUE TENSION IN NEURAL TUBE CLOSURE

With regard to the analysis of neural tube closure my aim was two-fold: (i) to correlate the progression of the events of neural tube closure along the rostro-caudal axis with the events of NCC development, (ii) to draw inferences regarding the degree of mechanical tension resisting the apposition of the neural folds at the different axial levels. This was done in order to determine whether the hypothesis – that NCC emigration favours the mechanics of DLHP bending – is likely to be tenable, or not.

Many factors may contribute to tension within the closing neural folds but three specific morphogenetic events have been identified that affect closure and these are studied specifically: (i) the dorsoventral morphology of the neural folds; (ii) the morphology of adjacent tissues; (iii) axial curvature. Furthermore a high frequency of disruption of neural tube closure at the different axial levels in different mouse mutants is taken as an indication that high degrees of mechanical tension may oppose closure.

The dorso-ventral morphology of the neural folds is known to vary significantly along the anterior-posterior axis of the embryo and logic dictates that when the neural folds are widely spaced and biconvex, more effort will be required to bring the tips of the neural folds into apposition than when distance between the folds is less or the folds are pointing inwards towards each other. Regions in which the neural folds are merely being drawn together at the front of a zipping closure sequence would also intuitively require less effort to close than *de novo* sites of closure.

Tissues adjacent to the neural folds contribute to the tensions exerted on the neural folds themselves. The neural folds are continuous with the surface ectoderm prior to neural tube closure and the morphology of their relationship is predicted to exert differing degrees of tension opposing neural tube closure. Furthermore the underlying mesenchyme is likely to contribute to the tensions exerted on the neuroepithelium in differing ways according to the morphology of the embryo at different axial levels.

In correlational studies, axial curvature was found to be inversely proportional to rate of closure in both anterior and posterior neuropores of the pig embryo (Van Straaten et al., 2000) and in the posterior neuropore of chick, rabbit, mouse, rat and human embryos (Peeters et al., 1998). Experimental manipulations in both the mouse and chick models demonstrated that high degrees of axial curvature inhibit posterior neuropore closure (van Straaten et al., 1993), as in the case of the *curly tail* (*ct*) mutant which develops spina bifida (Peeters et al., 1997).

The axial curvature of the cranial flexures may also affect closure of the neural tube. Closure 2 is known to be a polymorphic trait, its anterior-posterior location varying between different inbred mouse strains, and this location has been shown to confer differing susceptibility to exencephaly. Strains with a caudally-located Closure 2 site are relatively resistant to exencephaly while those with a rostrally-located Closure 2 are more susceptible (Juriloff et al., 1991; Fleming and Copp, 2000). This may reflect the tensions opposing closure in the midbrain imposed by the midbrain flexure (Jacobson and Tam, 1982). A caudal Closure 2 may enhance closure in the midbrain region of highest axial curvature. A rostral Closure 2 conversely may not provide the support required at the site of maximum axial curvature, destabilising the elevation and apposition of the midbrain neural folds.

The relationship between the processes of NCC development and neural tube closure was further investigated in chick and human embryos to determine whether the findings in mice are generally applicable or specific to this species.

2.2. METHODS

2.2.1. PREPARING RIBOPROBES FOR IN SITU HYBRIDISATION

Digoxigenin (DIG)-labelled RNA probes were prepared by transcription from plasmids containing a cDNA insert of the gene of interest. Plasmids (listed in Table 2.1) were obtained as solutions or on filter paper. Those on filter paper were resuspended by addition of 100 µl 10 mM Tris (pH 7.6) and incubation for 5 min at room temperature. All solutions used in riboprobe preparation are listed in Table 2.2. The Hesx1 riboprobe (from J.P.Martinez-Barbera) the cSox9 and cSox10 riboprobes (from A. Barlow) and the SOX9 (human) riboprobe (from the Human Developmental Biology Resource) were received as labelled RNA probes.

Table 2.1. Antisense RNA Probes Used for ISH in the Mouse

PLASMID	INSERT SIZE (bp)	INSERT SITE	LINEAR-ISE WITH	TRANSCR-IBE WITH	SOURCE
Cdh6	460	KpnI / XbaI	BamH1	T7	P. Ybot-Gonzalez
FoxD3	558	EcoR1	BamH1	T3	P. Labosky
Krox20	750	PstI / ApaI	BamH1	T3	D. Wilkinson
Snai1	391	ApaI / NotI	SalI	T7	M.Sefton
Sox9	500	XBaI / EcoRI	EcoR1	T3	S. Lovell-Badge

2.2.1.1. TRANSFORMATION AND AMPLIFICATION

Plasmid DNA was used to transform DH5α competent cells (Gibco, BRL). Cells were gently thawed on ice then 50 µl competent cells and 1 µl plasmid DNA (10 µg/ml) were transferred to a round bottomed tube under sterile conditions. Cells were incubated for 30 min on ice followed by heat shock at 42°C for 45 sec. The transformed cells were cooled on ice for 2 min and then 500 µl LB-Broth (Gibco) was added and they were incubated for 1 h at 37°C with shaking.

Cells were pelleted by centrifugation at 1000 x g at 4°C for 3 min, the supernatant discarded and cells resuspended in 200 µl LB-Broth. 50 µl was streaked onto agar plates (LB agar, Gibco) containing 50 µg/ml ampicillin. After 5 min at room temperature the plates were inverted and incubated at 37°C overnight.

Four colonies were picked from each plate with pipette tips and transferred into universals containing 10 ml LB-Broth with 50 µg/µl ampicillin. Plates were sealed with nescofilm and stored at 4°C for up to a month. Colonies were grown up by incubation with shaking at 37°C for 8 h (these were used for small scale plasmid preparations). For large scale preparations the 10 ml colonies were transferred into 50 ml LB-Broth with 50 µg/µl ampicillin in a conical flask for incubation at 37°C overnight.

Glycerol stocks of colonies were prepared by mixing 0.5 ml glycerol and 0.5 ml cell suspension and stored at -70°C. These were grown up by adding 100 µl of glycerol stock to 10 ml LB-Brothwith 50 µg/µl ampicillin and treating as above.

2.2.1.2. ISOLATION OF PLASMID DNA & DIAGNOSTIC DIGESTS

Cell suspensions were centrifuged at 6000 xg at 4°C for 15 min to pellet the bacterial cells. Plasmid DNA was extracted using the Qiagen mini-prep kit (using 4 ml of the 10 ml colonies) or midi-prep kits (using 60 ml colonies), according to the manufacturer's instructions.The concentration of plasmid DNA was measured using a nanodrop spectrophotometer and then adjusted to 0.5 µg/µl by adding Milli-Q water.

Diagnostic digestions were conducted on the plasmid DNA to confirm the correct sizes of DNA fragments were produced. The following mix was prepared and incubated at 37°C for 2 h:

16 µl Milli-Q water

2 µl DNA

1 µl restriction enzyme buffer

1 µl restriction enzyme

DNA gel electrophoresis was used to visualise the DNA fragments. 8 µl of the mix was loaded onto one lane and a molecular weight marker (Hyperladder I or V) onto another lane of a 1% agarose gel and run out at around 80V. The size of the fragments was determined under a UV light by comparison to the ladder.

2.2.1.3. LINEARISATION OF PLASMID DNA & PURIFICATION

The plasmid DNA was linearised using the appropriate restriction enzyme (see Table 2.1) at 37°C for 2-4 h in the reaction below:

10 µg plasmid DNA
10 µl restriction enzyme buffer
5 µl restriction enzyme
made up to 100 µl with Milli-Q water,

5 µl linearised DNA was compared to 1 µl uncut plasmid DNA and a molecular weight marker on a 1% agarose gel. Linearised DNA was checked for complete linearisation (compared to the three bands of uncut plasmid) and size (compared to the ladder). Linearised DNA was purified using QIAquick PCR purification columns according to the kit protocol. 1 µl of DNA was run on a gel to estimate concentration.

2.2.1.4. RNA LABELLING & PURIFICATION

DIG- or fluorescein-labelled RNA probes were synthesised by 37°C incubation of the following mixture (Roche RNA labelling kits) for 2 h or 15 min respectively.

2 µl linearised DNA (0.5 µg/µl)
2 µl transcription buffer (10x)
2 µl DIG RNA labelling mix OR fluorescein RNA labelling mix
12 µl DEPC-H_2O
1 µl RNase inhibitor
2 µl RNA polymerase (see Table 2.1)

2 µl were run on an agarose gel enabling visualisation of the DNA band and the RNA band giving an indication of the degree of amplification (usually 10 times).

Labelled probes were purified using Chromaspin 100 purification columns (BD Biosciences) according to the kit protocol. The sample was recovered at a concentration of approximately 0.1 µg/µl and stored in the collection tube at -20°C.

Table 2.2 Solutions Used in Preparing Riboprobes

SOLUTION	PREPARATION	STORAGE
100 mM Tris (pH 7.5)	1.21 g Tris-base 80 ml with Milli-RO water, pH 7.5 with HCl then up to 100 ml	Room temperature (RT)
LB-Broth	20 g in 1 L Milli-RO water,	Autoclaved RT
LB-Agar	32 g in 1 L Milli-RO water (heated) Melted at 50°C for pouring plates.	Autoclaved RT
EDTA (0.5 M, pH 8.0)	93.05 g EDTA salt 400 ml Milli-RO. pH 8.0 with NaOH then up to 500 ml.	RT
50x TAE buffer	242 g Tris base 57.1 ml glacial acetic acid 100 ml EDTA (0.5 M pH8.0) up to 1 L with Milli-RO water	RT
1% agarose gel	1% agarose melted in 1x TAE buffer ethidium bromide (0.01 μg/ml)	Humid chamber 4°C 2 days

2.2.2 EMBRYO TECHNIQUES

2.2.2.1 OBTAINING MOUSE EMBRYOS

Matings between CD1 mice were set up overnight and female mice were checked for copulation plugs the following morning to confirm mating: if successful this was termed embryonic day (E0.5). The same techniques were used to obtain embryos from matings between ROSA26R and Wnt1-Cre mice. At E7.5-10.5, pregnant females were sacrificed by cervical dislocation. The ventral abdomen was opened and the uterus was removed to a 5ml aliquot of warm dissecting medium (Table 2.3).

The uterus was transferred to a petri dish containing 37°C dissecting medium. While observing at low magnification on the stage of a Zeiss SV6 stereomicroscope, decidual swellings were removed from the uterus using fine watchmaker's forceps. Next, the layers surrounding the embryos were removed: first the spongy deciduem, then the trophoblast and fine Reichert's membrane, then the yolk sac and finally the amnion. The number of somite pairs was counted for accurate staging of embryos.

Table 2.3. Solutions Used in Obtaining Mouse Embryos

SOLUTION	SOURCE / PREPARATION	STORAGE
Dulbecco's modified Eagle's medium (DMEM)	Gibco	45 ml aliquots 4°C
Fetal calf serum (FCS)	Heat inactivated for 30 min at 56°C before aliquotting	5 ml aliquots -20°C
Dissecting medium (DMEM/FCS)	90% DMEM 10% FCS	Made fresh

2.2.2.2. OBTAINING CHICK EMBRYOS

Fertilised chick (*Gallus gallus domesticus)* eggs were obtained from commercial sources, stored at 10-12°C until required and then incubated at 38°C in a humidified atmosphere. Embryos were removed after 24-40 h at the stages of cranial neurulation. Albumin (3 ml) was extracted from each egg using a syringe, creating an air pocket above the embryo, before cutting a window in the shell to visualise the embryo. The embryo was dissected free of the surrounding membranes and it was transferred to a watch glass containing Diethylpyrocarbonate (DEPC) treated 1% phosphate buffered saline (PBS) (Table 2.4). The vitelline membrane was removed.

2.2.2.3. FIXING & DEHYDRATING EMBRYOS

After dissection, embryos were rinsed twice in ice cold DEPC-PBS in petri dishes (Table 2.4) and then transferred to an ice cold 5 ml aliquot of 4% paraformaldehyde (PFA) in DEPC-PBS (Table 2.4). Fixation was continued at 4°C overnight.

Embryos for whole mount *in situ* hybridisation were dehydrated in methanol. All washes were in 5 ml at 4°C for 15 min for mouse embryos and 5 min for chick embryos. Embryos were first washed twice in DEPC-PBS, followed by successive washes in 25%, 50% and 75% methanol in DEPC-PBS, and finally two washes in 100% methanol. Dehydrated embryos were stored in 100% methanol for several months.

Embryos to be embedded in wax were dehydrated in ethanol. All washes were in 5 ml for 15 min for mouse and 5 min for chick at room temperature. Embryos were first washed twice in PBS, followed by successive washes in 25%, 50% and 75% industrial methylated spirit (IMS) and then two washes in 100% ethanol. Dehydrated embryos were processed for wax embedding (see section 2.2.7.2).

Table 2.4. Solutions Used in Fixing Embryos

SOLUTION	PREPARATION	STORAGE
Phosphate buffered saline (PBS)	10 g PBS tablets in 1 L Milli-Q H_2O	1 L RT
Diethylpyrocarbonate treated PBS (DEPC-PBS)	1ml DEPC in PBS overnight then autoclaved.	1 L RT
4% paraformaldehyde (PFA)	2 g PFA, 50 ml DEPC-PBS at 65°C	5ml aliq-20°C

2.2.3. WHOLE MOUNT IN SITU HYBRIDISATION ON THE MOUSE EMBRYO

Preparation of all solutions required for mouse wholemount *in situ* hybridisation (ISH) is summarised in Table 2.5. Incubations were at room temperature unless stated.

2.2.3.1. PREHYBRIDISATION TREATMENT

Embryos were transferred to clean staining nets in 12 well plates (requiring 3 ml solution per well) and rehydrated by transfer to successive washes (15 min, 4°C) in 75%, 50% and 25% methanol in DEPC-PBT (DEPC-PBS, 0.1% Tween-20) followed by 2 washes (15 min, room temperature) in DEPC-PBT. The embryos were then bleached with 6% hydrogen peroxide (600 µl H_2O_2 (30% stock) in 2400 µl DEPC-PBT freshly made) for 1 h, followed by three PBT washes (5 min).

Embryos were treated with 10 µg/ml proteinase K (1.5 µl Proteinase K (20 mg/ml stock) up to 3 ml DEPC-PBT freshly made). E7-8.5 embryos were treated for 1 min, E8.5-9 for 2 min, E9-10 for 2.5 min and E10.5 for 7 min. The reaction was stopped by washing in freshly prepared 2 mg/ml glycine (6 mg glycine up to 3 ml DEPC-PBT freshly made) followed by two washes in DEPC-PBT (5 min).

Embryos were refixed for 20 min in freshly prepared 0.2% glutaraldehyde in 4% PFA (24 µl glutaraldehyde (25% stock) up to 3 ml using 4% PFA in DEPC-PBT) and washed twice in DEPC-PBT (5 min, room temperature) before transfer to prewarmed prehybridisation (prehyb) mix (70°C). Once the embryos had sunk they were transferred to another well of prehyb mix and incubated at 70°C for 2 h.

2.2.3.2. HYBRIDISATION TREATMENT

Thirty microlitres of labelled probe (0.1 μg/μl) was added to the prehyb mix and embryos (up to a concentration of 1 μg of labelled RNA per ml of prehyb mix). If the embryos were to be labelled with two probes detected in different colours both the DIG-labelled probe and the fluorescein-labelled probe were added at the concentration described above. The embryos were incubated at 70°C overnight.

2.2.3.3. POST-HYBRIDISATION AND ANTIBODY TREATMENT

Embryos were removed from hybridisation mix which was stored at -20°C for subsequent use. Embryos were washed twice with Solution 1 for 30 min at 70°C and then twice with Solution 2 for 30 min at 65°C. They were then washed three times in TBST for 5 min at room temperature before being preblocked with 10% sheep serum in TBST for 90 min, also at room temperature.

Meanwhile the antibody solution was prepared. 1 ml per sample of TBST was added to 1 g embryo powder and incubated at 70°C for 30 min. It was then cooled on ice and 10 μl sheep serum and 2 μl anti-DIG-alkaline phosphatase antibody were added before incubation for 1 h at 4°C with gentle rocking. The embryo powder was allowed to settle as sediment and the supernatant was pipetted to a new tube. The supernatant was diluted up to 4 ml with 1% sheep serum in TBST and then filtered through a syringe driven 0.2 μm filter.

The blocking solution was replaced with the antibody solution and embryos were incubated overnight at 4°C with gentle rocking.

2.2.3.4. POST-ANTIBODY WASHES

Embryos were washed with TBST at room temperature with rocking, first three times for 5 min and then 5 times for 1 h. The were left TBST overnight rocking at 4°C.

2.2.3.5. COLOUR DEVELOPMENT

Embryos were washed three times in NTMT for 30 min at room temperature. They were then transferred to a glass bijoux containing NTMT and 16 µl/ml developing mix (NBT & BCIP for a purple colour on single *in situs* and BCIP alone for a blue colour in double *in situs*). They were developed in the dark with rocking for the first 20 min. The embryos were checked regularly for colour development and, when sufficient, the development reaction was stopped by three 5 min PBT washes. All embryos for comparison were processed identically for colour development. If only one probe was to be used, the embryos were photographed and stored or mounted as described in sections 2.2.7.1 and 2.2.9.1. If they were to be labelled with two different probes with different detection they were processed for double wholemount *in situ* hybridisation.

2.2.3.6. DOUBLE WHOLE MOUNT IN SITU HYBRIDISATION

The embryos were incubated in 2xSSC (pH 7.5) with 0.1% Tween-20 for 1 h at 65°C to denature the alkaline phosphatase. They were then returned to the TBST washes in the post-hybridisation step (see section 2.2.3.3) and treated in exactly the same manner apart from two exceptions. Instead of incubating with the anti-DIG antibody they were incubated with the anti-Flu antibody. Also instead of developing with BCIP they were developed with INT/BCIP.

2.2.3.7. STORAGE OF EMBRYOS AND PHOTOGRAPHY

Embryos were stored at 4°C in PBT with thimerosol to prevent fungal growth. Embryos were photographed as described in section 2.2.9.1. and then processed for sectioning (see section 2.2.7.1).

Table 2.5 Solutions Required for Wholemount ISH in the Mouse Embryo

SOLUTION	PREPARATION	STORAGE
20x SSC (stock)	3M sodium chloride 0.3M sodium citrate DEPC-H_2O to 900 ml pH 4.5 with citric acid (then make up to 1 L)	1L autoclaved then stored at RT
10x TBS (stock)	8 g sodium chloride 0.2 g potassium chloride 25 ml 1M Tris pH 7.5 up to 100 ml with DEPC- H_2O	100 ml autoclaved then stored at RT
Prehyb mix	50% formamide 5x SSC pH 4.5 1% DEPC-SDS 50 µg/ml yeast RNA 50 µg/ml heparin up to 6 ml with DEPC-H_2O	6 ml/probe Fresh or -20°C
Solution 1	50% formamide 5x SSC pH 4.5 1% DEPC-SDS up to 6 ml with DEPC-H_2O	6 m/probe fresh
Solution 2	50% formamide 5x SSC pH 4.5 up to 6 ml with DEPC-H_2O	6 ml/probe fresh
1x TBST	5 ml 10x TBS stock 0.1% Tween-20 0.5 mg/ml levamisole up to 50 ml with Milli-Q	50 ml/probe fresh
1x NTMT	100mM NaCl (300 µl of 5M stock) 100mM Tris pH 9.5 (750µl of 2M stock) 50mM $MgCl_2$ (375 µl of 2M stock) 1% Tween-20 0.5 mg/ml Levamisole (7.5 mg) up to 15 ml with Milli-Q	15 ml/probe fresh

2.2.4. WHOLE MOUNT IN SITU HYBRIDISATION IN THE CHICK EMBRYO

Preparation of all solutions required for whole mount ISH in the chick embryo are summarised in Table 2.6 apart from those previously described in Table 2.5.

2.2.4.1. PRE-HYBRIDISATION

Chick embryos were rehydrated in the same manner as mouse embryos (except they were incubated for 5 min each step instead of 15 min). They were then bleached in the same manner as mouse embryos. Following bleaching they were washed twice in DEPC-PBT for 5 min each at room temperature.

They were then transferred to the Detergent mix for three 20 min room temperature incubations, followed by refixing in 4% PFA/PBT for 20 min. After three 5 min PBT washes the embryos were rinsed in once in 50% Prehyb mix/PBT at 70°C and once in Prehyb mix at 70°C until they sank to the bottom. They were then transferred to another Prehyb mix and incubated at 70°C for 2 h.

2.2.4.2. HYBRIDISATION TREATMENT

Thirty microlitres of labelled probe (0.1 μg/μl) was added to the prehyb mix and embryos (up to a concentration of 1 μg of labelled RNA per ml of prehyb mix). The embryos were incubated at 70°C overnight.

2.2.4.3. POST-HYBRIDISATION AND ANTIBODY TREATMENT

Embryos were removed from hybridisation mix which was stored at -20°C for subsequent use. Embryos were rinsed once then washed four times with prewarmed Solution X for 30 min each at 70°C. They were then incubated for 10 min with prewarmed Solution X/MABT (50:50) at 70°C, before rinsing three times and incubating twice for 30 min each in MABT at room temperature. Embryos were then preblocked with 2% Boehringers Blocking Reagent (BBR) in MABT for 1 h, then with 20% goat serum and 2% BBR in MABT for 1-2 h. This was then replaced with anti-DIG antibody, 20% goat serum and 2% BBR in MABT rocking overnight at 4°C.

2.2.4.4. POST-ANTIBODY WASHES

Embryos were rinsed three times then washed seven times in MABT for 1 h each at room temperature and then left in MABT overnight rocking at 4°C.

2.2.4.5. COLOUR DEVELOPMENT

Embryos were washed four times in NTMT for 10 min at room temperature. They were then transferred to a glass bijoux containing NTMT and developing fixture (NBT & BCIP for a purple colour on single *in situs* and BCIP alone for a blue colour in double *in situs*). They were developed in the dark with rocking for the first 20 min, then without rocking. The embryos were checked regularly for colour development and when it had developed sufficiently the development reaction was stopped by one 10 min NTMT wash and then three 5 min PBT washes. Embryos were stored in the same manner as the mouse embryos described in section 2.2.3.6.

Table 2.6. Solutions Required for Wholemount ISH in the Chick Embryo.

SOLUTION	PREPARATION	STORAGE
Detergent Mix	1% IGEPAL (or NP-40) 1% DEPC-SDS 0.5% Deoxycholate 50 mM Tris pH8 1 mM EDTA 150 mM Sodium Chloride up to 500 ml with DEPC-H_2O	500 ml fresh
Prehyb mix	50% formamide 5x SSC pH 4.5 2% DEPC-SDS 2% Boehringer Blocking Reagent 250 µg/ml tRNA 100 µg/ml heparin up to 50 ml with DEPC-H_2O	50 ml stored at -20°C
Solution X	50% formamide 2x SSC pH 4.5 1% DEPC-SDS up to 50 ml with DEPC-H_2O	50 ml stored at 4°C
MAB Ph7.5	100mM Maleic Acid 150mM NaCl to pH 7.5 with NaOH Up to 1 L with Milli-RO	1 L autoclaved thenstored at RT
MABT	MAB with 0.1% Tween-20	70 ml/probe fresh

2.2.5. IN SITU HYBRIDISATION ON SECTIONS OF THE HUMAN EMBRYO

Preparation of all solutions required for whole mount ISH in the human embryo are summarised in Table 2.7 apart from those described above. Samples of human embryo tissue were obtained in wax sections from the Human Developmental Biology Resource (www.hdbr.org) or from H. Escovitch (Paris). In all cases, human embryonic material was obtained after full informed consent by the donors.

2.2.5.1. PRE-HYBRIDISATION

Slides containing wax sections were placed in Histoclear for two 10 min washes then rehydrated through 100% ethanol (twice for 2 min each), 75%, 50% and 25% ethanol in DEPC-PBS (2 min each) and then DEPC-PBS (twice for 2 min each). They were then refixed for 20 min in 4% PFA in DEPC-PBS and washed twice in PBS (2 min each).

The sections were then treated with 20 μg/ml proteinase K (0.8 ml of 10 mg/ml stock in 400 ml DEPC-PBS) for 8 min and then refixed in 4% PFA in DEPC-PBS for 20 min before two 2 min PBS washes. Slides were placed in 0.1 M triethaloamine (7.5 g in 400 ml DEPC-H_2O) with a stirrer and 1 ml acetic anhydride was drizzled over them before stirring for 10 min. They were washed twice for 2 min each in DEPC-PBS. The sections were then dehydrated with the same alcohol series as above but using fresh 100% ethanol followed by air drying.

2.2.5.2. HYBRIDISATION

Fresh RNAse inhibitor (1 μl/ml), tRNA (0.5 mg/ml) and riboprobe (0.1 μg/μl) was added to stock hybridisation (hyb) mix. Slides were laid out on foil and 80 μl of the hyb mix was added to each one. Slides were then covered with a cover slip and incubated in a rack in a humid chamber (moistened with 50% formamide, 50% 2x SSC) inside a sealed plastic bag at 60°C overnight.

2.2.5.3. POST-HYBRIDISATION AND ANTIBODY TREATMENT

The rack of slides was placed in a glass staining trough containing 2x SSC at 60°C for two 20 min washes and their cover slips were removed at this stage. They were transferred into Washing mix also at 60°C for two twenty min washes followed by two 30 min washes in 2x SSC and two 30 min washes in 0.2x SSC at 60°C. Finally the rack in 0.2x SSC was cooled to room temperature.

The slides were washed for 2 min in Buffer 1 and then blocked with 10% FCS in Buffer 1 applied to the slides (1 ml per slide). After draining the slides, 0.5 ml of antibody solution (anti-DIG-fab antibody diluted 1:1000 in Buffer 1 containing 2% FCS) was applied to each slide and they were incubated in a humid chamber at 4°C overnight.

2.2.5.4. POST-ANTIBODY WASHES

Slides were washed three times in Buffer 1 then twice in 1x Buffer 2 for 5 min each.

2.2.5.5. COLOUR DEVELOPMENT

A 50:50 mix of 2x Buffer 2 and 10% PVA was made and developing solutions were added to this (NBT separate solution (Roche) 4.5 µl/ml and BCIP separate solution (Roche) 3.5 µl/ml). The developing mix was stored in the dark. Developing mix (0.5 ml) was added to each slide and they were incubated in a light proof humid chamber at room temperature until the colour had developed sufficiently.

Slides were placed in a rack and washed under running tap water for 10 min to remove the developer. They were then placed at 50°C for 15 min to remove any residual PVA.The slides were dehydrated through a fresh alcohol series, then two 10 min incuation with Histoclear before mounting in Vector mount.

Table 2.7 Solutions Required for ISH in Sections of Human Tissue

SOLUTION	PREPARATION	STORAGE
Hyb mix	50% formamide 0.3 M sodium chloride 20 mM Tris HCL 5 mM EDTA 10% Dextran sulphate 1x Denhardt's solution	Aliquots 4°C
Washing mix	175 ml formamide 35 ml 20x SSC 140 ml H_2O	350 ml fresh
Buffer 1	0.1 M Tris pH 7.6 0.15 M sodium chloride	250 ml fresh
2x Buffer 2	0.2 M Tris-HCl pH 9.5 0.3 M sodium chloride 0.4 0.1M magnesium chloride	250 ml fresh

2.2.6. X-GAL STAINING OF Wnt1-Cre;ROSA26R EMBRYOS

The gene product of the LacZ gene, β-galactosidase, is expressed in cells after Cre mediated DNA excision of the ROSA26R stop sequence. X-gal staining reveals sites of β-galactosidase expression in Cre expressing embryos.

The embryos resulting from crosses of Wnt1-Cre and Rosa26R mice were dissected out and quickly fixed in 0.2% glutaraldehyde in PBS for 20 min (E8.5 embryos) and 30 min (E9.5 embryos) at 4°C. They were then washed twice in PBS for 5 min at room temperature before very gently rocking in the staining solution (Table 2.8) overnight at 37°C. The embryos were refixed in 4% PFA in PBS for 1 h, washed twice in PBS for 15 min and photographed as described in section 2.2.9.1. Embryos were then dehydrated (described in section 2.2.2.3) for wax embedding and sectioning (described in section 2.2.7.2).

Table 2.8. X-GalStaining Solution

SOLUTION	PREPARATION	STORAGE
Staining solution	5mM $K_3Fe^{3+}(CN)_6$ (250 µl of 200mM stock) 5mM $K_4Fe^{3+}(CN)_6$ (250 µl of 200mM stock) 2 mM $MgCl_2$ (20 µl of 1 M stock) PBS up to 10 ml 1 mg/ml X-Gal in DMSO (100 µl of 100mg/ml stock)	RT in dark for 1 week.

2.2.7. EMBEDDING, SECTIONING & MOUNTING EMBRYOS

Mouse and chick embryos which had been processed for wholemount *in situ* hybridisation were embedded in albumin and sectioned using a vibratome. Embryos which had been processed for X-Gal staining and which were to be processed for H&E staining were embedded in wax and sectioned using a microtome.

2.2.7.1 ALBUMIN EMBEDDING, VIBRATOME SECTIONING & MOUNTING

Embryos were soaked in albumin for between 1 h and overnight, then put into blocks under a stereomicroscope in a fume hood. 300 µl albumin was added to a small plastic well. The embryo was placed on the edge of the well and 30 µl glutaraldehyde was added to the albumin, and quickly stirred. The embryo was oriented in the mix beneath the surface and it was left to set for 1 h. The block was removed from the well and stored in PBS at 4°C.

Blocks to be sectioned were cut to shape, leaving a large surface area at the base and this was superglued to the plate of the vibratome. The block was immersed in PBS and sections were cut at 50 µm thickness and transferred to a superfrost slide. The slide was dried, then a 50:50 mix of PBS and glycerol was applied before covering with a coverslip secured with nail varnish at the corners. Slides were stored at 4°C.

2.2.7.2. WAX EMBEDDING, MICROTOME SECTIONING & MOUNTING

Embryos were dehydrated to 100% ethanol as described in section 2.2.2.3. They were then soaked in Histoclear for 30 min, then a 50:50 mix of Histoclear and wax at 65°C for a further 30 min, then 100% wax three times for 30 min each.

For embedding, embryos were oriented in hot wax in a plastic well placed on an ice pack under a stereomicroscope and then cooled to room temperature. Sections were cut at 8-10 μm thickness using a microtome and placed in PBS on a superfrost plus slide. Slides were dried overnight at 37°C. Immediately before further use, the wax was removed by two 10 min washes in Histoclear. The slides were then ready for treatment (such as H&E staining) or mounting with DPX mounting agent and a coverslip.

2.2.8. H&E HISTOLOGICAL STAINING

After Histoclear washing of slides (as in section 2.1.5.2) the sections were placed in 100% ethanol for 5 sec then rehydrated through 5 sec dips in 95% and 70% ethanol, and then left in Milli-RO water for 2 min. The nuclei of cells were then stained with an approximate 5 min wash in filtered haematoxylin (checking for staining under the microscope), followed by a 10 sec dip in Milli-RO water and then washing under a running tap for 5 min. They were dipped in acid alcohol (1% HCl in 70% ethanol) for 10 sec and put under the running tap for a further 2 min.

Cell cytoplasm was stained by placing slides for 3 min in filtered 1% eosin (checking for staining under the microscope), followed by 2 min under the running tap. Sections were then dehydrated through 5 sec dips in 95%, and two in 100% ethanol before two 1 min washes in Histoclear. The slides were then mounted with DPX mounting agent.

2.2.9. MICROSCOPY

2.2.9.1. LIGHT MICROSCOPY

Whole embryos were visualised using a Zeiss Sv11 or Leica MZFLIII stereomicroscope, and photographed using a Leica DC500 camera. Images were captured using IrfanView or IM50 Leica Image Analyser software.

Embryo sections on slides were visualised using a Zeiss Axiophot 2 compound light microscope and were photographed using a Leice DC500 camera as above.

2.2.9.2. ELECTRON MICROSCOPY

Embryos were fixed in 2% PFA, 2.5% glutaraldehyde and 0.1 M phosphate pH 7.4 and then prepared for scanning electron microscopy by critical point drying and gold coating (performed by Mark Turmaine, UCL Biosciences EM Facility). A Jeol 5410LV medium resolution tungsten variable vacuum scanning electron microscope was used to visualise embryos and images were captured digitally.

2.3. RESULTS

2.3.1: IDENTIFYING SUITABLE NCC MARKERS

In order to investigate the relationship between the morphological events of neural tube closure and the early development of NCC in the mouse, a suitable NCC marker was necessary. The marker was required to label the NCC from their specification in the neuroepithelium through their delamination and initial migration into the periphery. The expression of a number of potential candidates was examined in normal CD1 mouse embryos, using probes against the NCC genes: *Snai1, Cdh 6, Sox9 and FoxD3.*

Snai1 (Snail homologue 1) is a transcriptional repressor known to be involved in the EMT of gastrulation and metastasis of epithelial tumours (Nieto et al., 1994; Cano et al., 2000). Its expression has also been described in the early development of NCC, being implicated in their specification. This expression is maintained in migrating NCC (Sefton et al., 1998).In the current studies, the *Snai1* probe did not efficiently label the pre-migratory NCC and only weakly labelled the migratory NCC at later stages (Figure 2.1 B,G). Taken together with its staining of the presomitic mesoderm (red arrowhead in Figure 2.1 G), this precluded its use as a NCC marker.

Cdh6 (cadherin 6) is a type II classic cell adhesion molecule which is known to mark NCC, and confer specific cell adhesion properties that facilitate NCC migration. As well as its expression in pre-migratory and migratory NCC,*Cdh6* expression also delineates specific rhombomeres during early mouse development (Inoue et al., 2009). These findings were confirmed in the current studies and while the *Cdh6* probe was found to be a reliable marker of pre-migratory and migratory NCC in the mouse (Figure 2.1 D,I), its non-NCC specific labelling of regions within the hindbrain at early stages (red arrowhead in Figure 2.1 I) also eliminated it from further.

Sox9 (SRY - sex determining region Y-box 9) is a member of the SoxE subgroup of HMG-containing transcription factors which has been identified as functioning upstream of the Snail family of transcription factors in the induction of NCC (Spokony et al., 2002; Cheung and Briscoe, 2003). *Sox9* has also been implicated in fate determination of the NCC. *Sox9* expression biases NCC away from a neuronal

fate and towards a glial or melanocytic fate (Cheung & Briscoe, 2003). The embryonic expression of *Sox9* is restricted to the pre-migratory and migratory NCC.

FoxD3 (forkhead box D3) is a transcriptional repressor first expressed during gastrulation, where it acts to maintain pluripotent stem cells in the epiblast (Sutton et al., 1996; Pohl and Knöchel, 2001; Hanna et al., 2002). Later in embryogenesis, *FoxD3* is expressed in pre-migratory NCC in the dorsal neural tube and in the first wave of migratory NCC (the neuronal and glial precursors) (Kos et al., 2001). Its subsequent down-regulation in melanoblasts is attributable to its function in repressing melanogenesis in the NCC (Kos et al., 2001; Thomas and Erickson, 2009).

Both the *FoxD3* and the *Sox9* probes revealed patterns of expression consistent with NCC from their early specification and into their migration (Figure 2.1 A,F and C,H respectively). The down-regulation of *FoxD3* in later migrating NCC (evident in Figure 2.1 A) did not hamper its use in the current studies as visualisation of the NCC was mainly required up to the time of the onset of EMT and delamination from theneuroepithelium. Of these two probes the *FoxD3*probe proved the more reliable at efficiently labelling the NCC without background, thus *FoxD3* was used as a suitable marker of premigratory and early migratory NCC in this research.

Figure 2.1. Expression Analysis of NCC Markers

Mouse embryos at 20-28 somites (A-D) and 8-12 somites (F-I) hybridised as whole mounts with probes against a range of prospective NCC markers: *FoxD3* (A,F), *Snai1* (B,G), *Sox9* (C,H) and *Cdh6* (D,I). LacZ staining of a Wnt1-Cre/Rosa26R conditional reporter mouse embryo at around 22 somites (E) to illustratethe expected pattern of NCC migration and colonisation of target organs.

(**A-D; F-I**) Early migratory NCC are indicated with arrows and pre-migratory NCC with black arrowheads. The *Snai1* probe (B,G) gave a non-NCC-specific signal in the presomitic mesoderm (red arrowheads in G) and the *Cdh6* probe (D,I) gave a non-NCC-specific signal throughout the neuroepithelium in the posterior hindbrain and spinal region of the 8-12 somite embryo (caudal to the red arrowhead in I).

(**E**) LacZ staining (blue) of all cells deriving from the Wnt1 expression domain in the dorsal neural tube along the length of the embryo (black arrowhead) reveals NCC colonisation of facial structures (top white arrow) and branchial arches 1-3 (lower white arrows). In the trunk, segmented migratory neural crest can be seen in the rostral half of each somite (black arrow). Staining in the midbrain region reflects a combination of mesenchymal migratory NCC and the derivatives of the Wnt1 expression domain in the prospective midbrain at presomitic stages (red arrowhead).

Scale bars in A-I represent 100 μm.

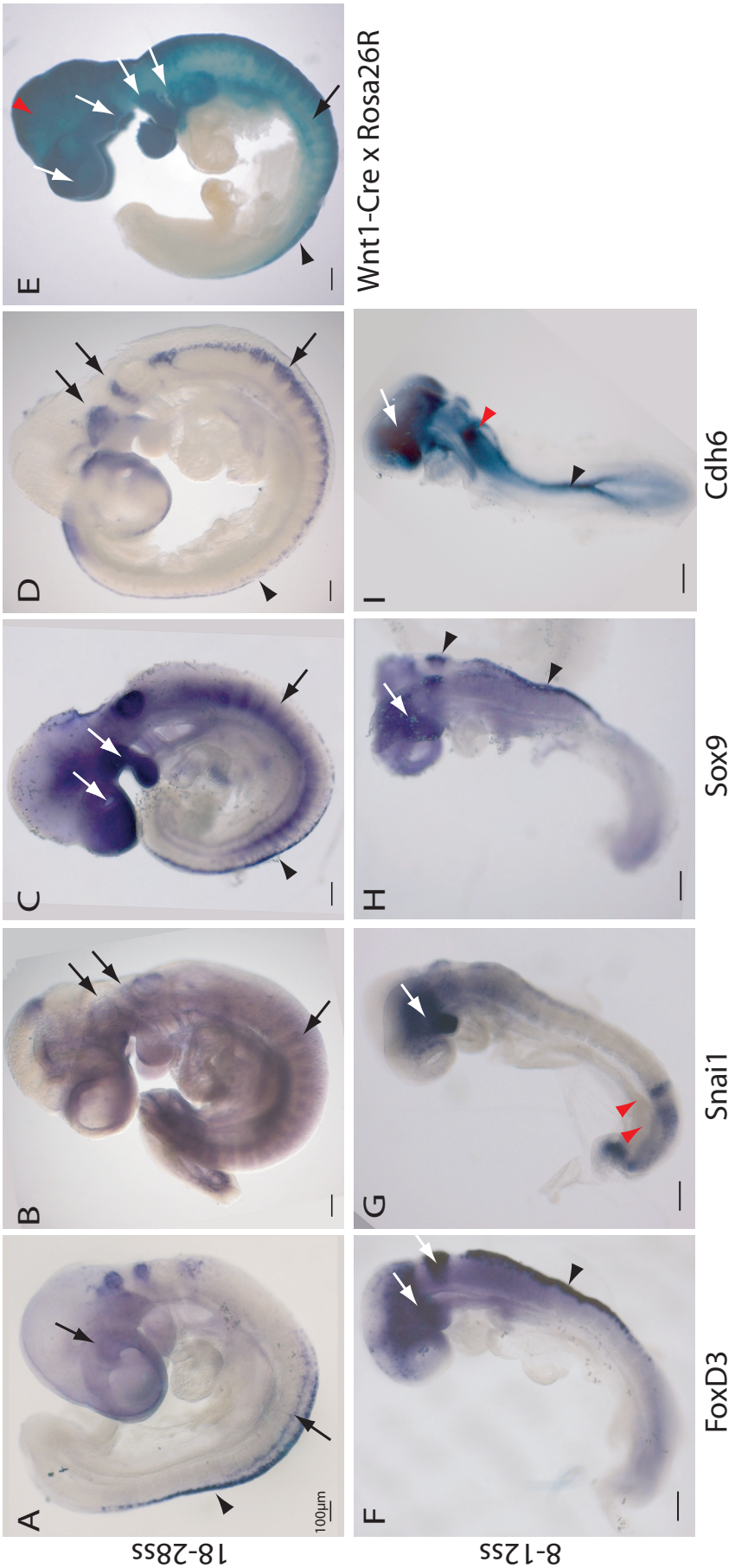
Wnt1-Cre x Rosa26R
Cdh6
Sox9
Snai1
FoxD3
18-28ss
8-12ss
A
B
C
D
E
F
G
H
I
100µm

2.3.2. MORPHOLOGICAL ANALYSIS OF MOUSE NEURAL TUBE CLOSURE

The events of neural tube closure in the mouse have been described extensively (Copp et al., 2003; Copp, 2005). The current research aimed to determine the precise morphology of the neural folds both dorsoventrally (in transverse sections) and rostrocaudally (in lateral views) and the timing of the morphogenetic events.

2.3.2.1. CLOSURE 1

In the mouse embryo, the first site of initiation of neural tube closure occurs at around the 6 somite stage at the level of the hindbrain/cervical boundary. Early shaping of the neural plate by convergent extension movements results in an elongated keyhole shaped structure. The hindbrain/cervical boundary is at the anterior limit of the narrow (future spinal) region of the neural plate. Bending at the MHP prior to closure produces neural folds which are small, 'V'-shaped and embedded in the adjacent mesenchyme (Figure 2.2 A8). They fuse to form a neural tube with a slit-shaped lumen (Figure 2.2 B8).

Closure 1 precedes embryonic axial rotation (i.e. turning). Thus a lateral view of the site of Closure 1 shows concave curvature dorsally such that the dorsal neural folds of the hindbrain and caudal spine face one another (Figure 2.2 A,B). This contrasts with the situation following axial rotation, when the body axis becomes curved in the opposite direction and closure occurs on the outside of a convex bend (Figure 2.2 D,E).

2.3.2.2. CLOSURE 2

The second *de novo* site of neural tube closure occurs in the vicinity of the forebrain-midbrain boundary at around the 11-12 somite stage. The morphology of the neural folds in this region differs dramatically from that described at the site of Closure 1, as it arises in the widest region of the keyhole shaped neural plate. The dorso-ventral morphology of the forebrain and anterior midbrain of the 4 somite embryo is evident in transverse sections and comprises two widely spaced, biconvex neural folds. In the forebrain, these are anchored to the rest of the embryo at the midline (Figure 2.2 A1) as in the midbrain where they are also supported by the underlying mesenchyme (Figure 2.2 A2). Closure 2 occurs at around the site of the cephalic flexure, so in contrast to the site of Closure 1, the dorsal aspects of the neural folds lie on the outer edge of a region of convex axial curvature (black arrowhead in Figure 2.2 D).

Figure 2.2.Anterior Neural Tube Closure in the Mouse Embryo

Whole mount double *in situ* hybridisation was performed on embryos ranging from the 4 to 17 somite stages with the NCC marker *FoxD3* (blue staining) and the anterior forebrain marker *Hesx1* (red staining) (A-E). Transverse sections from these embryos (A1-8,B1-8,C1-8,D1-8,E1-8) were cut along the lines indicated in A-E. The level of the sections are indicated on the embryo images and staining of the embryos served only as an indicator of these levels.Absence of blue staining in the hindbrain region indicates the NCC-free zones of rhombomeres 3 and 5, while red staining indicates the Hesx1-positive anterior forebrain region.

Abbreviations: a, anterior; p, posterior; hbnp, hindbrain neuropore. Scale bars represent 50 μm (apart from 200μm in D and E).

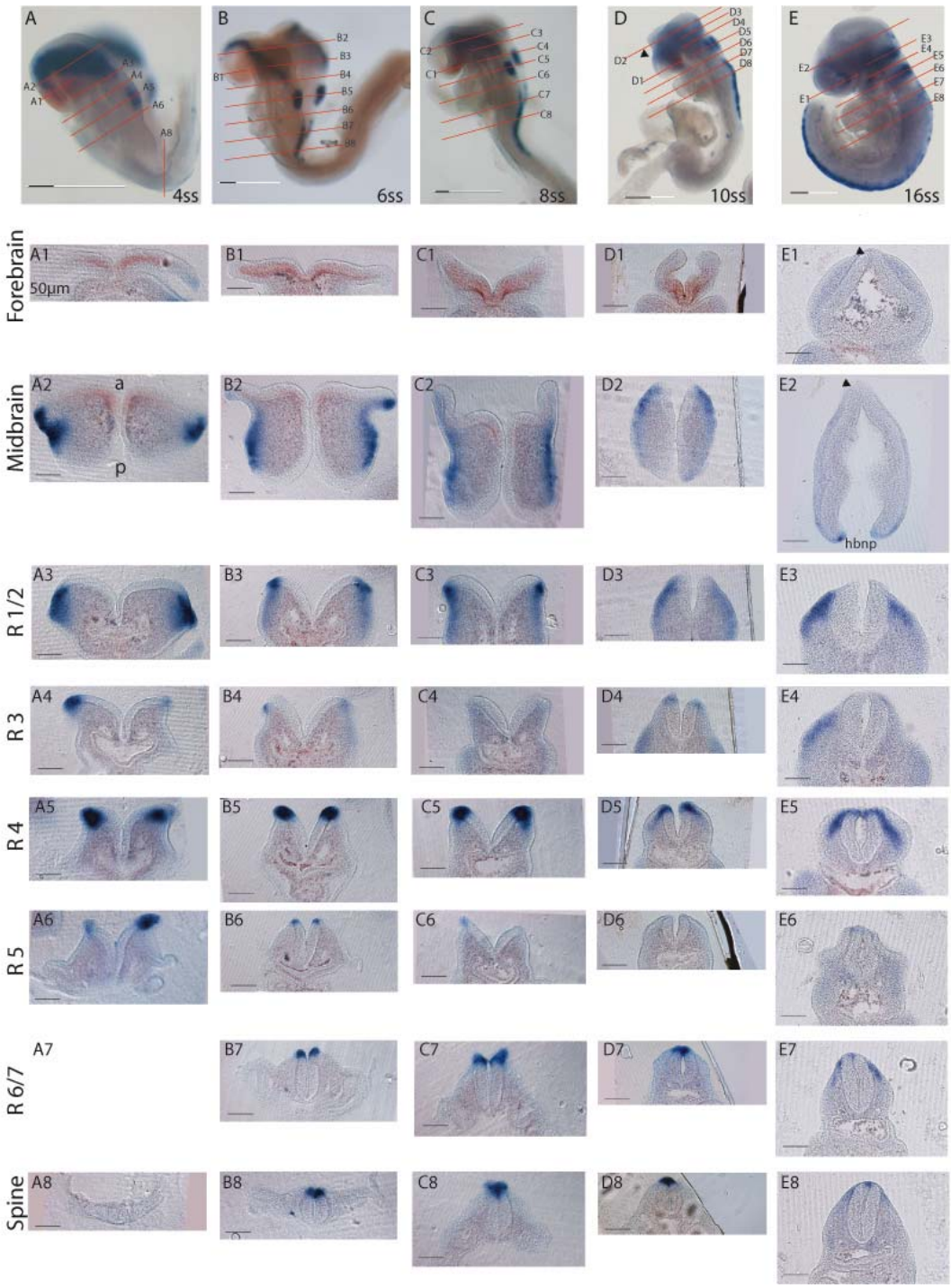
A
B
C
D
E
4ss
6ss
8ss
10ss
16ss
Forebrain
Midbrain
R 1/2
R 3
R 4
R 5
R 6/7
Spine
50µm
a
p
hbnp

Two morphogenetic processes are visible in the anterior cranial region during the development of the embryo leading up to Closure 2. First, the mesenchyme underlying the neuroepithelium of the midbrain expands, so that the midbrain neural folds are converted from a wide, flat 'M'-shaped morphology in the 4 somite embryo (Figure 2.2 A), to an elevated,biconvex 'V'-shaped morphology at 6-8 somites (Figure 2.2 B,C). This process of elevation is clearly visible in the posterior midbrain and anterior hindbrain region (Figure 2.2A2, A3, B2, B3, C2, C3), although it has greater impact in the midbrain region where it can be seen in the whole mounts (Figure 2.2 A-C).

Concomitantly the initially biconvex neural folds of the forebrain and anterior midbrain (Figure 2.2 A1,A2) kink in the middle of the neural fold at the site of the DLHP, beginning at the 6 somite stage (Figure 2.2 B1,B2) and reaching a 90^{o} angle in the anterior midbrain by the 8 somite stage (Figure 2.2 C2). The angle becomes progressively more acute bringing the tips of the neural folds closer until they appose and fuse (Figure 2.2 E1 and 2.3 B; red arrowhead). The combined effects of elevation of the neural folds and bending at the DLHPs result in the dorsal tips of the neural folds being brought into apposition at the 10 somite stage. Fusionat the site of Closure 2produces a closed neural tube with a wide lumen (red arrowhead in Figure 2.3 A,B).

2.3.2.3.CLOSURE 3

What is generally described as the third site of *de novo* neural tube closure initiation occurs at the most rostral end of the neural plate at the ventral midline at a location where the tips of the neural folds are effectively already in contact at the time of initiation of closure (blue arrowhead in Figure 2.3 A,B). Closure spreads in a caudal direction from the rostral neural plate to close the forebrain neural tube, prior to the 13 somite stage (Figure 2.3 A-D).

2.3.2.4.ZIPPING CLOSURE

During development closure spreads bidirectionally from the sites of Closure 1 (Figure 2.2 B8,C7,D7,E7-4) and Closure 2 (black arrowheads in Figure 2.2 E1,E2, red arrows in Figure 2.3 C,D), and posteriorly from Closure 3 (blue arrows in Figure 2.3 C,D) by a processlikened to zipping. This is illustrated in sections through the posterior hindbrain of an embryo in which zipping closure progresses from the site of Closure 1 (Figure 2.4 G,N) anteriorly (Figure 2.4 C-F & J-M). Although these sections illustrate the morphological process of zipping closure along the A-P axis of an embryo as a snapshot in time, they also represent the temporal sequence of events during development.

Figure 2.3. Closures 2 and 3, and the Anterior and Hindbrain Neuropores of the Mouse Embryo

(**A**) A 13 somite stage mouse embryo in which Closures 2 and 3 are indicated by red and blue arrowheads respectively. Spreading closure from Closures 2 and 3 is indicated by red and blue arrows respectively and the resultant hindbrain neuruopore (hbnp) and anterior neuropore (anp) are indicated by green lines. The levels of sections (B-F) are indicated by black lines.

(**B-F**) Sections taken from a 13 somite stage embryo and stained with H&E. The sites of Closure 2 and 3 are again represented by red and blue arrowheads respectively (B) and spreading closure from these sites by red and blue arrows respectively. The anterior and posterior limits of the anteriorneuropore are indicated with blue and red asterisks respectively. The anterior neuropore itself is demonstrated by the lack of contact betweenthe tips of the neural folds in the most rostral sections.

(**G-I**) Scanning EM images of dorsal views of 13, 14 and 15 somite embryos. The hindbrain neuropore is indicated with an asterisk in G and the anteriorlimit of the hindbrain neuropore and its spreading closure from Closure 2 is indicated by red arrows. The posterior limit of the hindbrain neuropore and its spreading closure from CLousre 1 is indicated by white arrows.

Abbreviations: hbnp, hindbrain neuropore; anp, anterior neuropore.
Scale bars represent 75μm in A and G-I and 50μm in B-F.

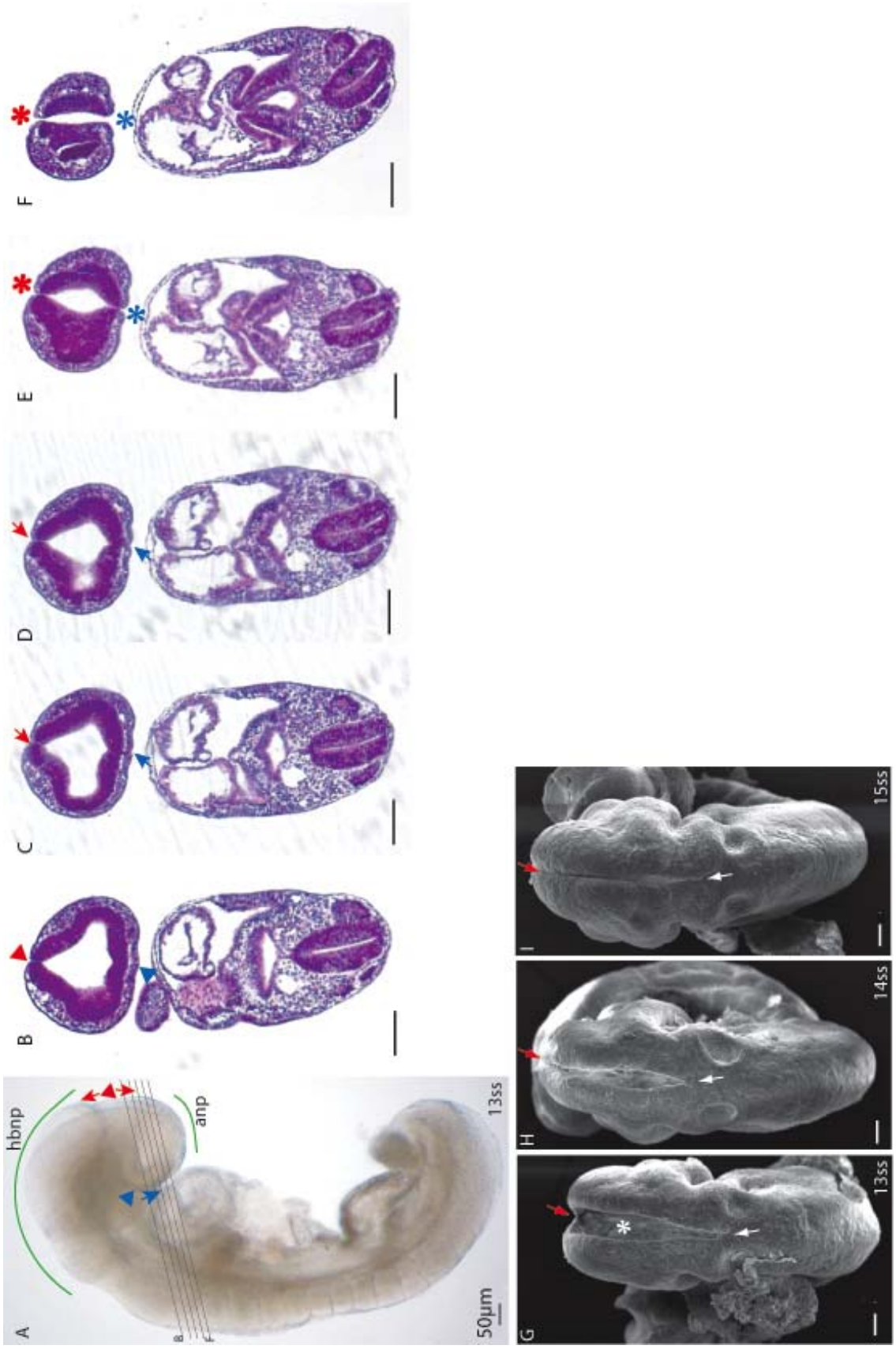
A
hbnp
anp
13ss
50µm
B
C
D
E
F
G
13ss
H
14ss
I
15ss

Figure 2.4. Zipping Closure in the Posterior Hindbrain of the Mouse

Serial sections taken through the posterior hindbrain of a 10 somite embryoafter *in situ* hybridisation for *FoxD3*(blue staining) (A-G) and with coloured overlays (H-N) to indicate the neuroepithelium (blue), surface ectoderm (red) and remodelling neuroepithelium (green). The direction of progression of zipping closure from the site of Closure 1 is indicated by the black arrow. The MHP is indicated by a black arrowhead (A). The black lines in K indicate the perpendicular orientation of the pseudostratified columnar epithelium of the two apposing neural folds.Note that *FoxD3* expression spreads in the opposite direction to the zipping closure in the hindbrain region and is absent from rhombomere 5.

Scale bars represent 50 μm.

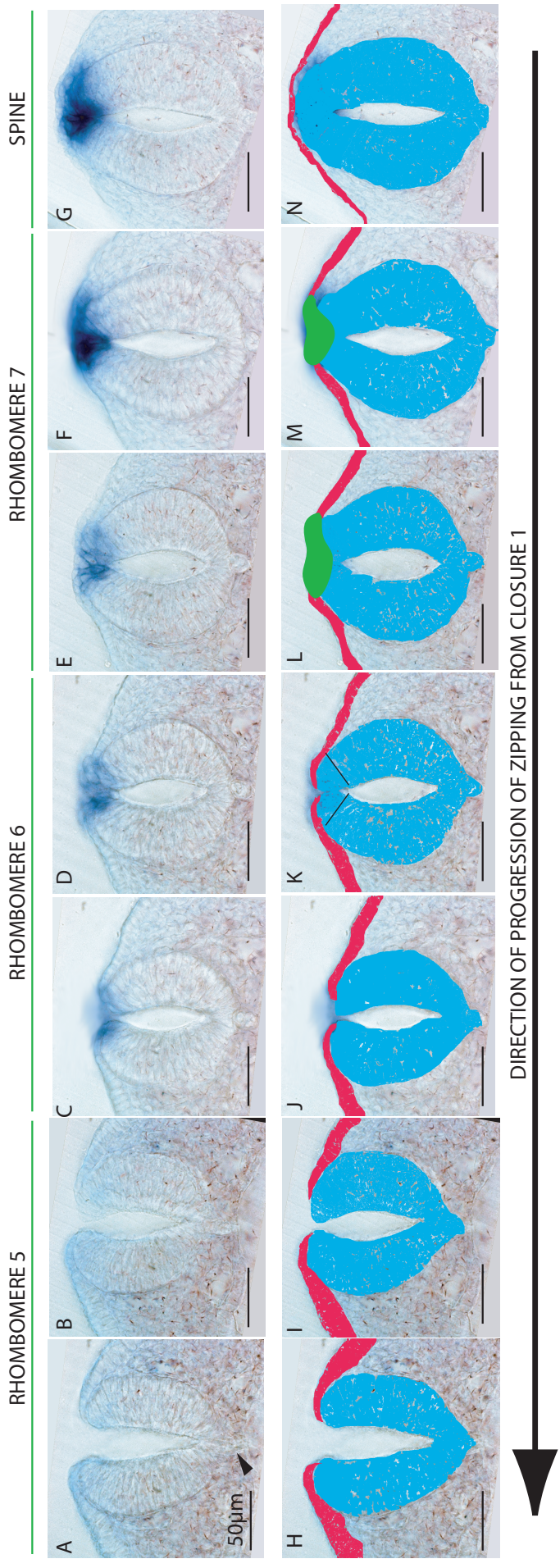
RHOMBOMERE 5
RHOMBOMERE 6
RHOMBOMERE 7
SPINE
A
B
C
D
E
F
G
H
I
J
K
L
M
N
50µm
DIRECTION OF PROGRESSION OF ZIPPING FROM CLOSURE 1

The neural folds are initially 'V'-shaped, bending around the MHP (black arrowhead in Figure 2.4 A) and the dorsal tips are separate (Figure 2.4 A-B & blue colouring in H-I). The neuroepithelium is continuous dorsolaterally with the non-neural ectoderm (red colouring in Figure 2.4 H,I). The neural folds are drawn together (by the closure of the neural tube in the preceding region) until their dorsal tips appose and contact (Figure 2.4 C-D & J-K). The cells of the dorsal tips of the neural folds then undergo remodelling which realigns the pseudostratified neuroepithelium to form the roof plate of the neural tube and the squamous ectoderm (Figure 2.4 E-F &green colouring in L-M), resulting in the separation of the overlying surface ectoderm from the completed neural tube (Figure 2.4 G & red colouring in N).

2.3.2.5. BUTTONING CLOSURE

The literature regarding mouse neurulation often describes the spreading of closure from the initial sites of fusion as one continuous process analogous to drawing closed a zip (Copp, 2005). This is in contrast to descriptions of closure in avian models in which multi-site contacts of the neural folds have been observed in association with the somites at the rhombocervical level. In contrast to the continuous process analogous to zipping, this multi-site process has been described as being analogous to "buttoning" (Van Straaten et al 1996). Detailed examination of closure in the mouse embryo identified a similar buttoning effect in the anterior hindbrain which is again illustrated by serial sections through an embryo (Figure 2.5). These sections appear to show that the neural tube becomes buttoned at rhombomeres 6, 5 and 3, while rhombomeres 4 and 2 remain temporarily open.

The zipping process described previously (Figure 2.4) progresses anteriorly during development from Closure 1, passing through the hindbrain rhombomere 6 at the 10 somite stage (Figure 2.4 C-D & J-K and Figure 2.5 E,J,O) and rhombomere 5 adjacent to the otic pits (Figure 2.5 D,I,N) before encountering rhombomere 4. In the 15 somite embryo the preceding regions (rhombomeres 6 and 5) are characterised by a completed neural tube with a narrow, slit shaped lumen (black asterisk in Figure 2.5 J) and separation of the overlying surface ectoderm (Figure 2.5 D-E, I-J & N-O).

The morphology of rhombomere 4 (Figure 2.5 C,H,M) resembles that of the neural tube at the crest of zipping closure in rhombomere 6 of the 10 somite embryo (Figure 2.4 C,J). The neural folds have contacted, but not fused, nor has the surface ectoderm separated from the underlying neuroepithelium – a morphology implying

incomplete closure (Figure 2.5 C,H). Furthermore the lumen of the neural tube is wider than the slit produced at rhombomere 6 (red asterisk in Figure 2.5 H) and the adjacent mesenchyme is expanded laterally. Very strikingly, however, even more anteriorly in rhombomere 3, the morphology reflects complete closure with separation of the overlying ectoderm to produce a neural tube with a slit-shaped lumen (Figure 2.5 B,Gblack asterisk in G indicates the narrow lumen). Hence, closure of rhombomere 4 appears to have been 'skipped', at this stage. Moe rostrally still, the neuralfolds in rhombomere 2 have not yet come into contact (Figure 2.5 A,F,K).

Further evidence in support of buttoning at this level, comes from observations on the 6 somite embryo (prior to zipping closure in the hindbrain). Here, the neural folds are closer together at rhombomeres 3 and 5 than at rhombomere 4 (green asterisk in Figure 2.5 R) which can be seen to protrude dorsally (Figure 2.5 P,Q). This indicates a buttoning process whereby the neural tube is buttoned closed at the levels of rhombomeres 5 and 3 prior to completing closure at rhombomere 4.

The patterning of NCC in the rhombomeres may be relevant to the buttoning phenomenon. Premigratory NCC are evident in rhombomeres 2, 4 and 6, and absent from rhombomeres 3 and 5 in the 6 somite embryo (Figure 2.5 P,Q,R; black arrow indicates rhombomere 4). Streams of NCC are evident migrating adjacent to rhombomeres 2, 4 and 6 in the 15 somite embryo (Figure 2.4 K,M,O respectively), with especially large numbers adjacent to rhombomere 4.

2.3.2.6. CLOSURE OF THE NEUROPORES

Closure of the neural tube culminates with the closure of the three neuropores: anterior, hindbrain and posterior (not shown here). Zipping closure spreading anteriorly from Closure 2 meets that spreading posteriorly from Closure 3 at the anterior neuropore (anp and green line in Figure 2.3 A) which can be visualised in transverse sections as gaps between the two lateral neural folds both anteriorly and posteriorly (Figure 2.3 E,F; blue asterisks and red asterisks respectively). The complete closure of the ANP is not shown here, but occurs shortly after the 13 somite stage.

The hindbrain neuropore is formed where the anteriorly spreading closure from Closure 1 meets the posteriorly spreading closure from Closure 2. The gradual drawing together of the neural folds and shortening of the neuropore is evident in Figure 2.3 G,H,I and final closure occurs shortly thereafter, at around the 17 somite stage.

Figure 2.5. Buttoning Closure in the Anterior Hindbrain of the Mouse

(A-O) Serial sections through the anterior hindbrain of a 17 somite embryo after *in situ* hybridisation for *FoxD3* (high magnification in A-E and low magnification in K-O). Coloured overlays (F-J) indicate the neuroepithelium (blue) and surface ectoderm (red). Narrow slit-shaped lumens are indicated by black asterisks in G and J, while a wide lumen is indicated by a red asterisk in H. The black arrowhead in M indicates lateral expansion of mesenchyme adjacent to the neural tube.

(**P**) Whole mount 4 somite embryo after *insitu* hybridisation for *FoxD3* (P) and sections taken at the levels indicated by lines in P, (Q,R). Black arrows indicate the dorsal protrusion of *FoxD3* positive rhombomere 4. Green asterisk in R indicates the wide lumen at the same level.

Abbreviations: ba1, 1st branchial arch; ba2, 2nd branchial arch; ov, otic vesicle.
Scale bars in A-E represent 10 μm (also in F-J) and in K-R represent 100 μm.

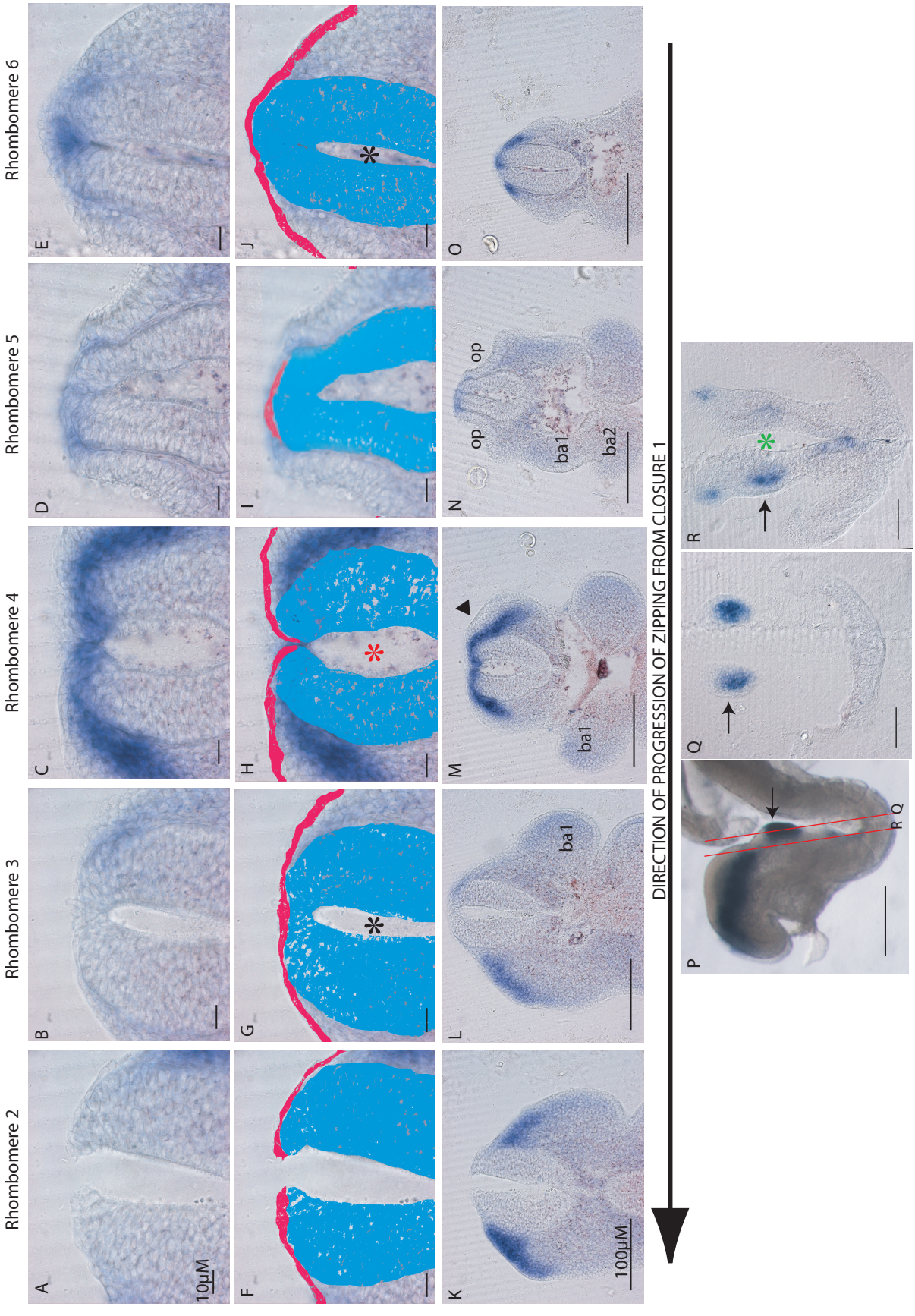
Rhombomere 2
Rhombomere 3
Rhombomere 4
Rhombomere 5
Rhombomere 6
A
B
C
D
E
F
G
H
I
J
K
L
M
N
O
P
Q
R
10μM
100μM
ba1
ba2
op
DIRECTION OF PROGRESSION OF ZIPPING FROM CLOSURE 1

2.3.3. EARLY NCC DEVELOPMENT IN THE MOUSE EMBRYO

2.3.3.1. NCC SPECIFICATION IN THE MOUSE

The early development of NCC has been most extensively reported in the chick model (for example Baker et al., 1997). Studies in which NCCs have been described in the mouse model have not set out to correlate the early events of NCC development with the morphological processes of cranial neurulation (Serbedzija et al., 1992). The aims of the current experiments were thus to determine the spatial and temporal relationship between the processes of cranial neurulation and early cranial NCC development. This aim was addressed using *FoxD3* as an early marker of NCC *to* visualise their location within the mouse embryo during development.

FoxD3 expression indicates thatNCC are initially specified, virtually simultaneously, in the dorsal tips of the neuroepithelium in the posterior forebrain, midbrain and rhombomere 1, at the 2 somite stage (Figure 2.6 A). NCC are not specified in the region immediately rostral to rhombomere 3 (i.e. the caudal part of rhombomere 2) until after the 7 somite stage (Figure 2.6 H-M & L-N; black arrowhead). The absence of NCC specification at the tips of the neural folds in the anterior forebrain is demonstrated by a lack of co-expression of the anterior forebrain marker *Hesx1* and the NCC marker *FoxD3* (Figure 2.6 F,G). Following the initiation of NCC specification in the neuroepithelium, their numbers gradually increase further (compare Figure 2.6 H,L to I,M).

A rostrocaudal wave of initiation of NCC specification then spreads along the dorsal neuroepithelium of the hindbrain and spinal region, apart from rhombomeres 3 and 5 where no FoxD3 positive NCC are ever visible. The wave reaches rhombomere 4 by the 4 somite stage, the level of the third somite by the 6 somite stage, the level of the fifth somite by the 8 somite stage and progresses along the anterior spinal region at around the same rate as somite production in the 8 and 10 somite stage embryos (black arrowheads indicate posterior limit of NCC specification in Figure 2.6 B-E). There is a delay in the onset of NCC specification in the anterior portion of rhombomere 6 adjacent to rhombomere 5 where it does not initiate until the 7 somite stage (Figure 2.6 M,N; red arrowheads). The progression of zipping closure in the spinal region precedes the front of the wave of NCC specification (Figure 2.6 C-E).

Figure 2.6. Neural Crest Specification in the Mouse Embryo

(**A-E**) Whole mount *in situ* hybridisation for *FoxD3*(blue staining) in 2-10 somite stage embryos. Black arrowheads indicate the posterior limit of *FoxD3* expression. Red arrowhead in B indicates the *FoxD3* free zone at the level of rhombomere 3.

(**F,G**) Double *in situ* hybridisation with the NCC marker *FoxD3* (blue staining) and the anterior forebrain marker *Hesx1* (red staining) in a 6 somite stage embryo. The section in G is taken from the embryo in F along the black line indicated. The *Hesx1* positive, *FoxD3* negative anterior forebrain is highlighted with a red line, while the *FoxD3* positive, *Hesx1* negative region is highlighted with a blue line.

(**H-O**) Double *in situ* hybridisation in 3-9 somite stage embryos with the NCC marker *FoxD3* and *Krox20*, a marker of rhombomeres 3 and 5. Gaps between the *FoxD3* expression domain anterior to rhombomere 3 (blue staining throughout the neuroepithelium) are indicated with black arrowheads. Red arrows in H and L indicate *FoxD3* expression at the level of rhombomere 4.

Abbreviations: ant fb, anterior forebrain: hb, hindbrain.
Scale bars in A-F and H-O represent 100 μm and in G represents 50 μm.

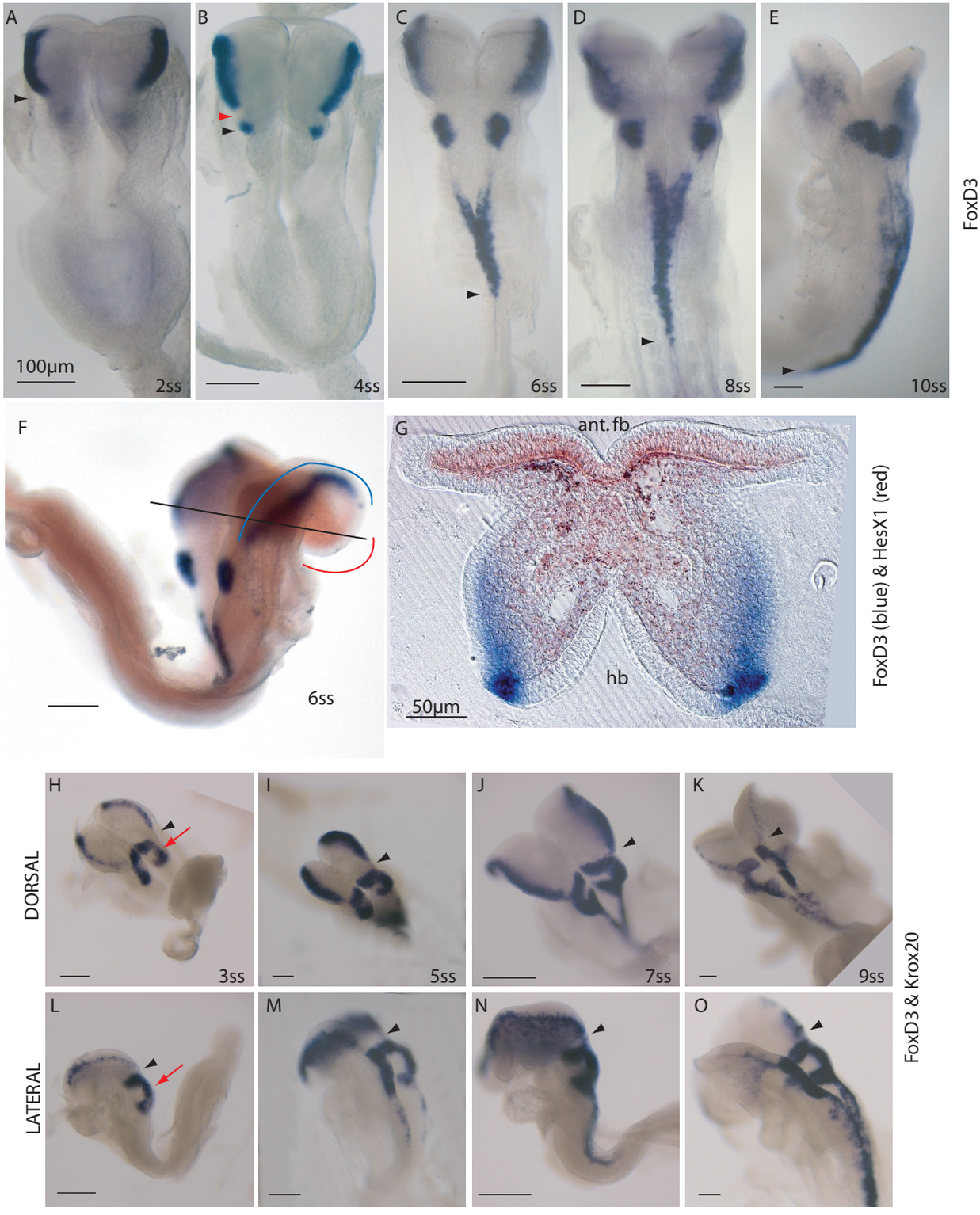
A
B
C
D
E
100µm
2ss
4ss
6ss
8ss
10ss
FoxD3
F
G
ant. fb
hb
6ss
50µm
FoxD3 (blue) & HesX1 (red)
H
I
J
K
DORSAL
3ss
5ss
7ss
9ss
L
M
N
O
LATERAL
FoxD3 & Krox20

2.3.3.2. NCC DELAMINATION IN THE MOUSE

The initiation of NCC delamination from the neuroepithelium (Figure 2.7; green background) follows the initiation of specification (Figure 2.7; yellow background) by around 4 somite stages (about 8 h assuming that a somite is generated every 2 hours). Thus, at the 3 somite stage NCC are specified in the tips of the neuroepithelium but are not evident migrating in the underlying mesenchyme (Figure 2.7 Fi). Delamination and migration of NCC has initiated in the cranial region (from the posterior forebrain to rhombomere 1) of the 6 somite embryo (Figure 2.7 B,G). Delamination from the posterior part of rhombomere 2 commences after a short delay (Figure 2.6 N). Subsequently, a rostrocaudal wave of delamination progresses along the axis of the embryo, reaching rhombomere 4 by the 8 somite stage (Figure 2.7 C,M), somite 3 by the 10 somite stage (Figure 2.7 D,S) and somite 8 by the 15 somite stage (Figure 2.7 E).

The onset of NCC delamination precedes neural tube closure in the cranial region as far posterior as rhombomere 4 (Figure 2.7 G,H,I,J,N). At the level of Closure 1 and posteriorly into the spinal region the situation is reversed, with the onset of NCC delamination following neural tube closure. Hence, the caudally directed wave of neural tube closure ‘overtakes’ the caudally directed wave of NCC delamination in the low hindbrain.

Furthermore NCC delamination precedes cranial DLHP formation. The NCC are specified in the biconvex midbrain neural folds (Figure 2.7 Fi). Their delamination and migration into the mesenchyme initiates prior to the kinking of DLHP formation in the midbrain (Figure 2.2.B2 and Figure 2.7 G lower (anterior) region). There are no NCC remaining in the midbrain neuroepithelium by the time the DLHPs have reached a 90° angle (Figure 2.2 C2) and subsequently the DLHPs progress to more acute angles (Figure 2.7 H,I lower (anterior) regions).

Figure 2.7. NCC Delamination in the Mouse Embryo

Whole mount *in situ* hybridisation for *FoxD3*in 3-15 somite stage embryos (blue staining in A-E) and sections taken from these embryos (F-X), at the levels indicated by red lines in A-E. The shallow transverse section in F shows *FoxD3* expression along the edges of the neuroepithelium.

Background colouring links sections at different rostro-caudal levels where NCC are not yet specified (blue background), where NCC specification has occurred but migration has not yet begun (yellow background), and where NCC delamination is underway (green background). This highlights the rostro-caudal waves of NCC specification and delamination that occur in the mouse embryo. Scale bars represent 100 μm.

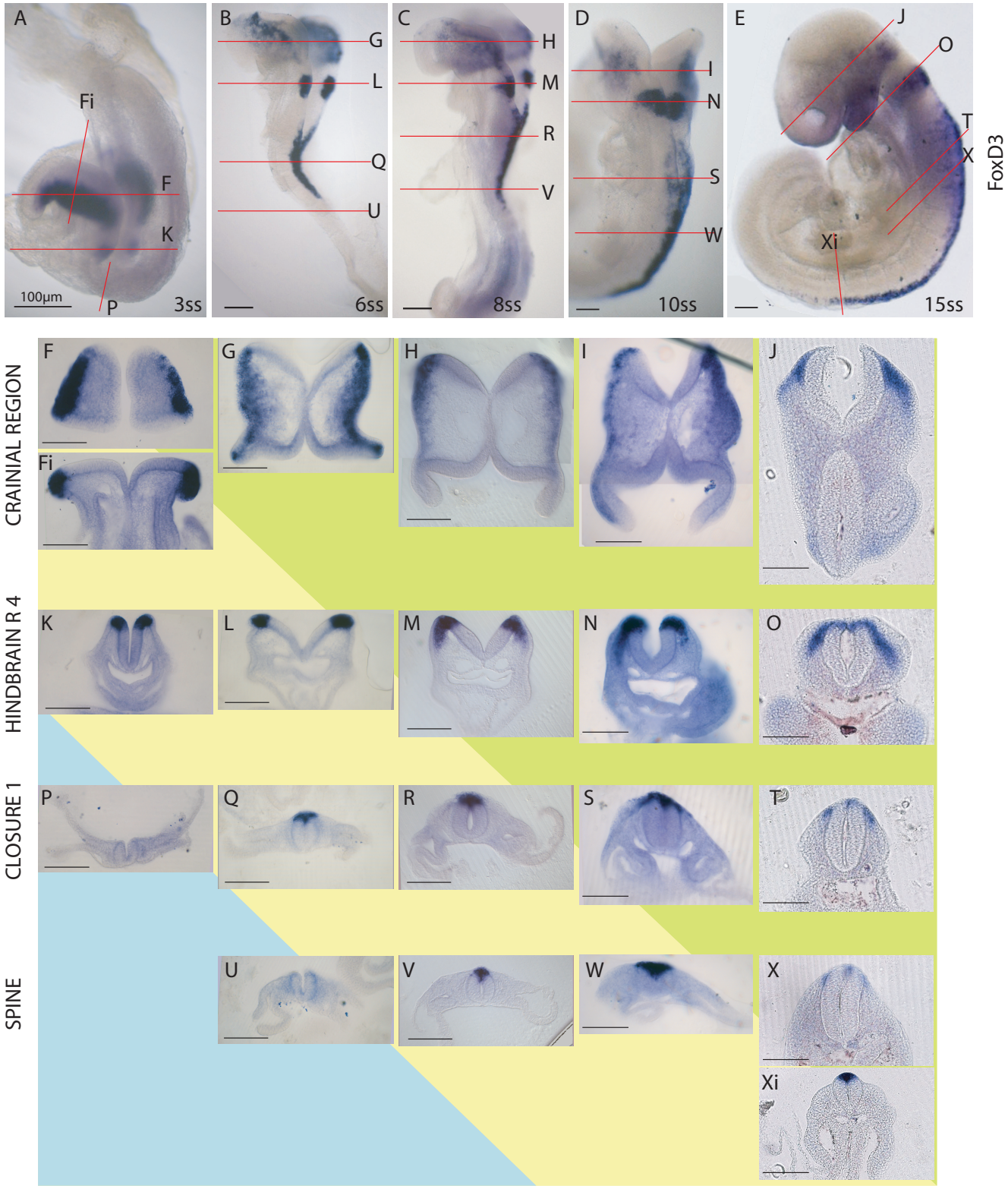
A
Fi
F
K
P
100µm
3ss
B
G
L
Q
U
6ss
C
H
M
R
V
8ss
D
I
N
S
W
10ss
E
J
O
T
X
Xi
15ss
FoxD3
CRAINIAL REGION
HINDBRAIN R 4
CLOSURE 1
SPINE
F
Fi
G
H
I
J
K
L
M
N
O
P
Q
R
S
T
U
V
W
X
Xi

2.3.4. *NEURULATION AND NCC DEVELOPMENT IN THE CHICK*

To extend the findings of previous work regarding the morphological events of neural tube closure in the chick (Van Straaten et al., 1996) these events were related to NCC development. The neural folds initially elevate around the median hinge point (especially in the cranial region; Figure 2.8 A). Initial contact occurs shortly after in the midbrain region and zipping closure progresses bidirectionally in the 6 somite embryo, resulting in an anterior neuropore (Figure 2.8 B). The rhombocervical multi-site contacts described previously and resultant rhombencephalic neuropore were also noted at this stage (Figure 2.8 B and data not shown). By the 9 somite stage the anterior neural tube is closed (Figure 2.8 C).

The morphology of transverse sections through the closed neural tube of a 10 somite chick embryo imply that the mechanism of closure differs significantly from that in the mouse. In contrast to the wide lumen shaped by the bending at the MHP and DLHPs observable in the midbrain of the mouse (Figure 2.3 B), the closed midbrain of the chick is characterised by a round neural tube (Figure 2.8 G). Caudally in the closing neural tube of rhombomeres 4 to 7, the MHP and DLHPs are evident (Figure 2.8 J-M).

The overall morphology of the chick embryo at the time of cranial neural tube closure also differs from that of the mouse. Mouse neurulation is characterised by initially large, biconvex, widely spaced cranial neural folds located on the outer curve of the cranial flexure (Figure 2.2 A). In contrast the chick cranial neural folds are relatively small and narrow (their expansion occurring largely after closure). There is also no axial curvature (Figure 2.8 A-E), the chick embryo being anchored flat under the vitelline membrane overlying the yolk sac, until after cranial neurulation when a turning event occurs.

NCC positive for *cSox10* expression are first evident in the already closed midbrain of the 6 somite chick embryo (Figure 2.8 B), and the numbers increase in the cranial region up to rhombomere 3 by the 9 somite stage (Figure 2.8 C). There appears to be sparse labelling of cSox10- and cSox9-positive NCC in the regions of rhombomeres 3 and 5 (Figure 2.8 D,E,I,K), but many NCC are visible in rhombomere 4 (Figure 2.8 J). Specification continues in a rostrocaudal wave along the axis of the embryo as in the mouse (Figure 2.8 D,E). Delamination of NCC away from the neuroepithelium initiates in the anterior region at the 10 somite stage, following the completion of cranial neural tube closure (Figure 2.8 F,G), and progresses rostrocaudally along the embryo (Figure 2.8 D,E).

Figure 2.8. Neural Tube Closure and NCC Specification and Migration in the Chick Embryo

Whole mount 3-13 somite stage chick embryos after *insitu* hybridisation for *cSox10* (A-E) and *cSox9* (N). White arrow in A indicates bending of the neural plate at the MHP. White arrowhead in B indicates the ANP and red arrowhead indicates *cSox10* positive premigratory NCC in the dorsal neuroepithelium. White arrowhead in D indicates *cSox10* positive NCC migrating in the cranial region and red arrowheads indicate NCC free zones at rhombomeres 3 and 5. Sections (F-M) are taken from the 10 somite stage embryo in N at the levels indicated by the red lines. Rhombomeres 3 and 5 are apparent from the lack of *cSox9* expression (I&K).

Abbreviations: fb, forebrain; ov, optic vesicle; rh 3, rhombomere 3; rh 5 rhombomere 5. Scale bars represent: 500 μm in A-E; 100 μm in F-G; 300 μm in N.

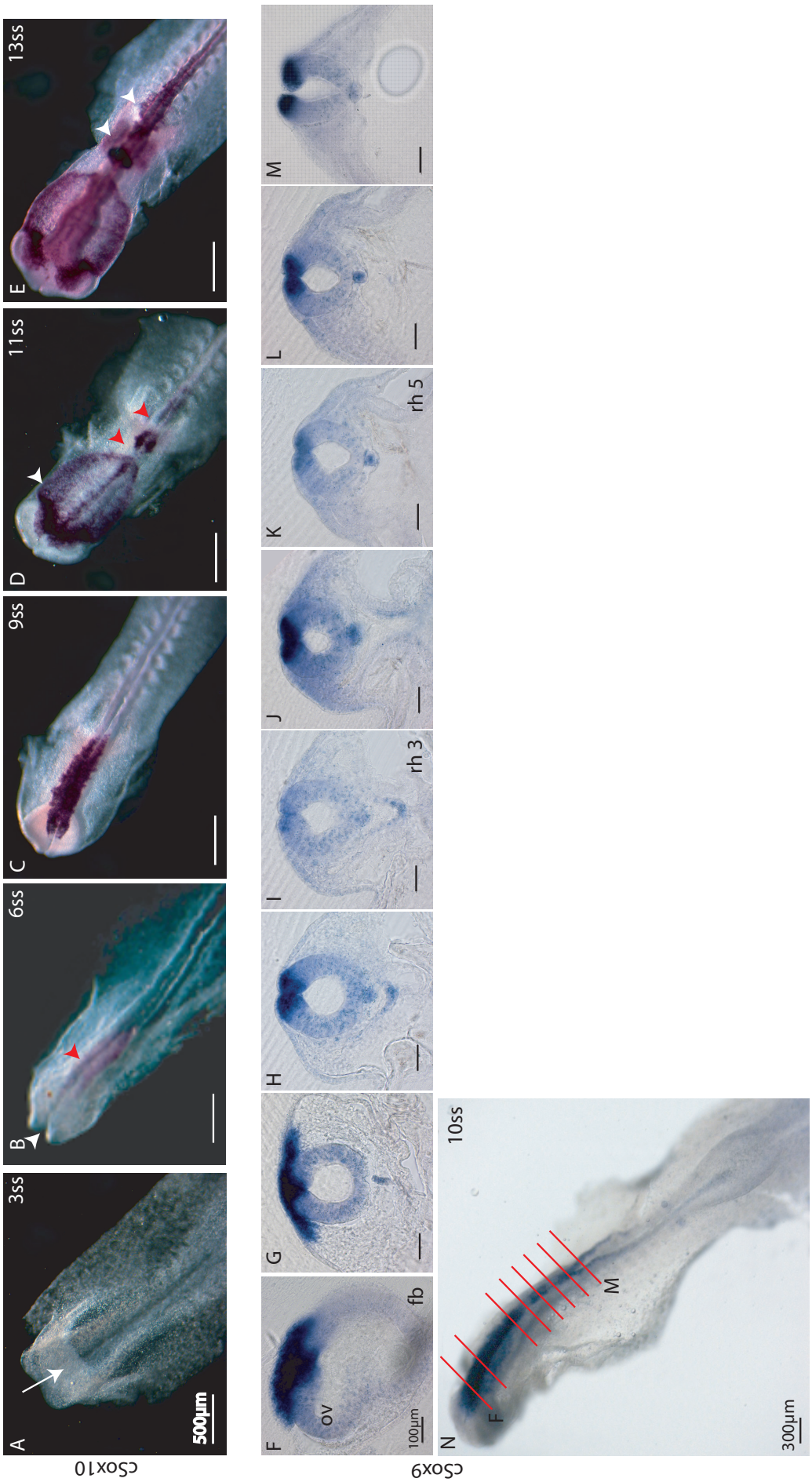
cSox10
cSox9
A
3ss
500µm
B
6ss
C
9ss
D
11ss
E
13ss
F
ov
fb
100µm
G
H
I
rh 3
J
K
rh 5
L
M
N
10ss
F
M
300µm

2.3.5. *NEURULATION AND NCC DEVELOPMENT IN THE HUMAN*

A section of the Carnegie stage (CS) 11 human neural tube taken at the level of the heart reveals neural folds which are becoming apposed with a keyhole shaped morphology (Figure 2.9 C), produced by some bending of the neuroepithelium (black arrowhead in Figure 2.9 C). This differs from the neural folds at the rhombocervical level of the mouse which are small and 'V'-shaped prior to their closure (Figure 2.2 A8). *Sox9* positive NCC are visible emigrating from the neuroepithelium into the underlying mesenchyme (arrows in 2.9 C).

Sections through a CS 12 embryo reveal what appears to be an open anterior neuropore in the forebrain (anp in Figure 2.9 D,F), although this may be an artefactual reopening (as the anterior neuropore should be closed during Carnegie stage 11). *Sox9* positive NCC are revealed in the dorsal neuroepithelium and migrating away into the mesenchyme (black arrow in Figure 2.9 D). The heart shaped morphology of the hindbrain region of the same section is an artefact of the processing of the embryo. *Sox9* positive NCC are not evident at this level – perhaps this is equivalent to the NCC free zone at rhombomere 3 in the mouse and chick (red arrowheads in Figure 2.6 B and 2.8 D).

A more caudal section of the CS 12 embryo demonstrates the typical 'V'-shaped morphology of spinal neural folds, and NCC are visible migrating into the DRG and mesenchyme (drg and black arrow in Figure 2.9 E). The neural folds at this level would also be expected to be closed by CS 12 and this may indicate that the embryo was at very early CS 12 or in fact late CS 11. Although some of the *FoxD3* staining visible in Figure 2.9 F,G correlates to the *Sox9* positive NCC, there is not complete overlap and this probably represents edge effect staining. For example the dermomyotome (d in Figure 2.9 F,G) would not be expected to contain NCC.

Figure 2.9: Neural Tube Closure and NCC Specification and Migration in the Human Embryo

(**A,B**) Whole mount human embryos at Carnegie stages 11 (A) and 12 (B) to indicate the levels of sections (C) and (D-G). were reproduced with permission from the Electronic Atlas of the Developing Human Brain (EADHB) project's website http://www.ncl.ac.uk/ihg/EADHB/.

(**C-G**) In situ hybridisation for *Sox9* (C-E) and *FoxD3* (F,G) (blue stain).(C-E) black arrows indicate *Sox9*-positive NCC (blue).Black arrowhead in C indicates neuroepithelial bending. (F,G) black arrows indicate *FoxD3*-positive NCC (blue).

Abbreviations: anp, anterior neuropore; d, dermomyotome; drg, dorsal root ganglion; ov, optic vesicle. Scale bars in C-G represent 100 μm. No scales were available for A and B.

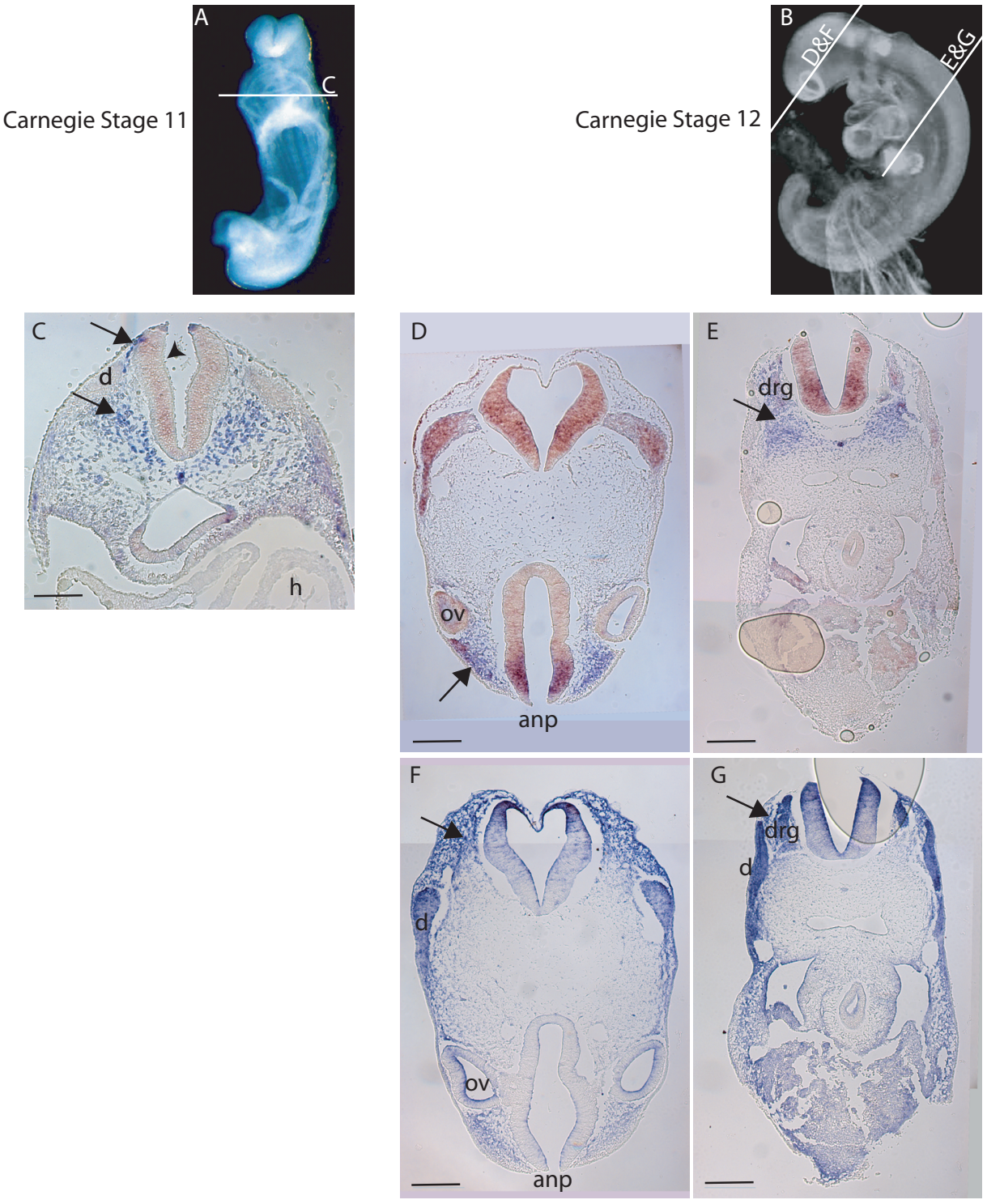
Carnegie Stage 11
A
C
Carnegie Stage 12
B
D&F
E&G
C
d
h
D
ov
anp
E
drg
Sox9
F
d
ov
anp
G
drg
d
FoxD3

2.4. DISCUSSION

The large number of mouse strains in which defects of neurulation and NCC development are present raises the possibility that a relationship exists between the two processes. Neural tube closure is, however, a highly heterogeneous event varying both morphologically and mechanistically along the axis of the embryo. This heterogeneity is indicated by the specificity of axial level of NTDs observed in different mouse mutants (Harris and Juriloff, 2010), which implies that different processes are in play in the different regions.

There are several lines of evidence that point to spatial specificity in the relationship between neural tube closure and NCC emigration: (i) mouse models demonstrate an association that appears specific for exencephaly and neurocristopathies; (ii) spinal neural tube closure cannot be necessary for spinal NCC development as normal NCC emigration is observed in regions of spina bifida in a number of mouse mutants including *splotch* (*Pax3*) and *curlytail* (*Grhl3*) (Epstein et al., 1991; Ting et al., 2003); (iii) conversely spinal NCC development cannot be necessary for neural tube closure because neural tube closure precedes NCC specification and delamination as demonstrated in the current research. Furthermore the current evidence suggests that cranial NCC development could be necessary for neural tube closure (and not vice versa) as cranial NCC specification and delamination precede neural tube closure.

Of the mouse mutants described in the literature, those with exencephaly are four times more common than those with spina bifida (Harris & Juriloff, 2010). This finding implies that closure in the cranial region may be more difficult to complete than spinal closure, therefore making it more susceptible to genetic disturbance. It is proposed here that this is because the morphology of closure in the cranial region results in a high degree of mechanical tension resisting the bringing together of the neural folds. As a result, the mechanisms required to overcome this tension may be more complex than in the spinal region and thus more prone to perturbation. It is further proposed that NCC delamination from the neuroepithelium may be one of the mechanisms employed to overcome this mechanical tension.

This hypothesis was first examined by inferring the degrees of mechanical tension opposing neural tube closure from morphological analysis at different axial levels (summarised in Table 2.9). These forces were then related to NCC development in each region.

2.4.1. MECHANICAL TENSION RELATED TO NCC DEVELOPMENT IN THE MOUSE

2.4.1.1. CLOSURE 1

The mechanical tension opposing closure of the neural tube at each axial level is inferred from the analysis of three morphological traits: (i) the morphology of the neural folds themselves, (ii) the morphology of the tissues surrounding the neuroepithelium (the surface ectoderm and mesenchyme) and (iii) axial curvature.

Convergent extension movements in the early embryo result in the shaping of the initially flat neural plate into an elongated keyhole-shaped structure (Keller et al., 2008). The anterior neural plate is wide and narrows caudally around the future site of Closure 1 at the boundary of the hindbrain and cervical spine. After bending of the neural plate at the MHP, the hindbrain/cervical boundary is thus characterised by small 'V'-shaped neural folds whose tips are close together. Closure 1 is located on the surface of a dorsally concave body axis, prior to the stage of axial rotation. This results in a transverse section through the embryo at this level resembling a 'u' shape, with the neural ectoderm being at right angles to the adjoining surface ectoderm and embedded in the adjacent mesenchyme.

Based on this morphological evidence the forces opposing the initiation of neural tube closure at Closure 1 appear to be very low (see Table 2.9),therefore being achieved with the intervention only of a midline bend of the neural plate and no dorsolateral bending. This theory is further supported by the findings that, of the few mouse mutants which display a failure of Closure 1 (resulting in craniorachischisis), all harbour mutations in genes involved in the planar cell polarity pathway known to govern convergent extension movements (Kibar et al., 2001; Hamblet et al., 2002; Curtin et al., 2003; Murdoch et al., 2003). This affects early shaping events, producing a short, broad neural plate whose neural folds are too widely spaced to close. The lack of mutants in which later events of Closure 1 are perturbed demonstrates the robustness of this closure which may reflect the simplicity of the mechanisms required and further may imply a minimal level of mechanical tension opposing the closure.

Regions in which the mechanical forces opposing closure are low are not hypothesised to require NCC delamination to facilitate closure. This is borne out in the region of Closure 1 as NCC at this level are specified around the time of closure and delaminate after closure, and so cannot be causally involved in closure.

2.4.1.2. ZIPPING CLOSURE IN THE SPINE

Zipping closure spreads bidirectionally from the site of Closure 1. Caudally it progresses through the spine via Mode 1 closure (MHP bending alone, to form a slit shaped lumen), then Mode 2 closure (MHP and DLHP bending together, to form a diamond shaped lumen), and finally Mode 3 closure (DLHP bending alone, to form a wide flat lumen) until final closure at the PNP at around the 30 somite stage (Shum and Copp, 1996; Ybot-Gonzalez and Copp, 1999). The forces opposing the zipping closure of neural folds which are not widely spaced can be assumed to be low as the tips of the neural folds will be drawn together by the closure of the preceding region.

The spinal region is characterised by a narrow neural plate due to the movements of convergent extension. Bending at the MHP in Modes 1 and 2 results in neural folds which are both small dorsoventrally and not widely spaced laterally. Furthermore Modes 1 and 2 occur in a region of relatively low axial curvature (in contrast to the high axial curvature of the cranial flexure and of the most caudal region). This implies that the forces opposing closure by Modes 1 and 2 are low (see Table 2.9). This assumption is supported by the lack of mutants in which closure by Modes 1 or 2 is disturbed.

In contrast to Modes 1 and 2, closure of the caudal spine by Mode 3 which leads to final closure of the PNP is prone to perturbation in mouse mutants, resulting in spina bifida (Juriloff and Harris, 2000). This indicates that it is mechanistically harder to complete than the preceding phases of neurulation, due in part to the complexity of mechanisms required for completion of the PNP itself, but perhaps also reflecting increased levels of force opposing closure. The lack of midline bending in Mode 3 closure means that it is reliant on bending at the DLHP to bring the small but widely spaced neural folds into apposition and contact (Ybot-Gonzalez & Copp, 1999). Failure of the DLHPs to bring the neural folds into contact has been implicated in the spina bifida defect of the *Zic2* (*Kumba*)mutant (Ybot-Gonzalez et al., 2007), indicating that DLHP formation is an essential mechanism for low spinal closure. This mechanism may be necessary to overcome the extra forces opposing closure in this region due to the increased axial curvature of the caudal spine. PNP closure rate has been shown to be inversely proportional to the angle of axial curvature in a number of animal models, demonstrating the effect of curvature in opposing closure (van Straaten et al., 1993; Peeters et al., 1998; Van Straaten et al., 2000). Thus the wide neural folds, located in a region of high axial curvature can be assumed to have an increased degree of

mechanical tension opposing their closure in relation to the rostral spine, an assumption which is supported by the frequency of failure of this closure (see Table 2.9).

There can be no role for the delamination of NCC in overcoming the forces opposing closure in the spinal region as NCC are known to be specified and delaminate after closure is complete. Moreover, neurocristopathies are not frequently associated with spina bifida. Furthermore the two defects were dissociated in the *splotch* mutant by crossing with the *curly tail* mutant, exacerbating the spina bifida defect while minimising the NCC defects (Estibeiro et al., 1993). The evidence presented regarding zipping closure in the spine does, however, provide valuable support for the use of morphology in assessing mechanical tensions opposing closure, where perturbation of closure in mutants is assumed to be indicative of levels of mechanical tension.

2.4.1.3. ZIPPING CLOSURE IN THE POSTERIOR HINDBRAIN

Zipping closure also spreads rostrally from Closure 1 into the posterior hindbrain region. The hindbrain originates from the wider anterior neural plate, so the neural folds are larger dorsoventrally than those of the spine. However, closure resembles Mode 1 in the spine in that the neural plate bends exclusively at the MHP to form 'V'-shaped neural folds which bring their tips into contact to form a tube with a slit shaped lumen. Hindbrain closure occurs on the outer edge of a region of minimal axial curvature. Overall the morphology of this region and the process of zipping closed neural folds which are not widely spaced imply low mechanical tensions opposing closure (see Table 2.9). Mutations in which closure of this region is specifically hindered are few (Juriloff & Harris, 2000).

The rostrocaudal wave of NCC specification has already passed through the posterior hindbrain by the time of its zipping closure such that specification precedes closure. The subsequent rostro-caudal wave of NCC delamination intercepts at around the level of rhombomere 7 with the caudo-rostral wave of zipping closure spreading from Closure 1. Hence, NCC delamination occurs around the same time as closure. This is in accordance with the hypothesis that NCC delamination is unnecessary for the subsequent closure of the neural tube in areas in which the mechanical tensions opposing closure are minimal.

2.4.1.4. BUTTONING CLOSURE IN THE ANTERIOR HINDBRAIN

Closure spreads through the posterior hindbrain of the mouse by a process analogous to zipping and into the anterior hindbrain where the mechanism differs, being more analogous to buttoning closure. Fusion of the neural folds and the subsequent remodelling which allows the neural tube to separate from the surface ectoderm is complete in rhombomeres 6, 5 and 3 prior to its completion in rhombomere 4. This is not the generally accepted view of cranial neurulation – a fourth site of initiation of closure has been described previously (Golden and Chernoff, 1993) but not confirmed by other authors (Copp et al., 2003).

An explanation for this buttoning phenomenon may lie in the patterning of NCC in this region. There is controversy in the literature regarding the specification and subsequent fate of NCC arising in the dorsal neuroepithelium of rhombomeres 3 and 5 in different species (see section 1.2.2.3). Some studies found that NCC are either not specified or undergo apoptosis in rhombomeres 3 and 5 (Lumsden et al., 1991). The prevailing view, however, is that NCC originate at all levels throughout the hindbrain and those at the levels of rhombomere 3 and 5 are channelled into adjacent migrating streams – largely into that of rhombomere 4 (which receives contributions from both rhombomeres 3 and 5) (Sechrist et al., 1994; Trainor et al., 2002). The current research does not support this view, finding no evidence of *FoxD3*-positive NCC in the dorsal neuroepithelium of rhombomeres 3 and 5 at any stage. Furthermore it was noted that NCC specification is delayed (relative to the rostrocaudal wave of specification) in the posterior section of rhombomere 2 which is immediately rostral to rhombomere 3 and in the anterior section of rhombomere 6 which is immediately caudal to rhombomere 5, perhaps implying some kind of inhibitory signal prevents NCC specification in these regions.

While no NCC emerge from the neuroepithelium adjacent to rhombomeres 3 and 5 (whether due to lack of specification or channelling away from these regions), an abundance of NCC emerge at the level of rhombomere 4, contributing large numbers of cells to the adjacent mesenchyme. This contribution is evident as an early dorsal protrusion and later lateral expansion as the NCC migrate along the ventrolateral pathway towards the second branchial arch.

The neural folds in this region are already elevated when NCC emigration occurs, such that their dorsal tips are above the ventral midline. The migrating NCC add to the tissue expansion of the mesenchyme underlying and adjacent to the neural folds which, may act to increase the mechanical tension opposing closure of the neural tube as depicted in Figure 2.10.

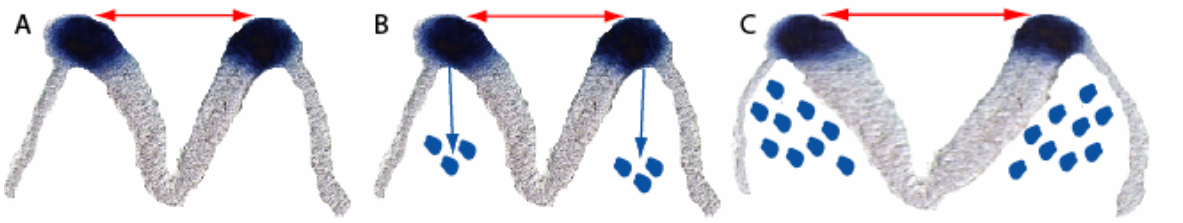

Figure 2.10. Effects of NCC Migration on Hindbrain Neural Fold Morphology.
The 'M'-shaped epithelium of the 'V'-shaped neural folds and adjacent non-neural ectoderm at the level of rhombomere 4 are represented in A and the NCC migrating into the mesenchyme in B (blue arrows). The expansion of mesenchymal tissue, aided by entry of NCC, appears to 'separate' the neural and non-neural epithelia, and may cause the stretched non-neural ectoderm to exert traction on the neural fold tips. This results in a widening of the gap between the neural folds (indicated by the red arrows in C). This effect cannot be illustrated in sections of embryos at different developmental stages as it cannot be distinguished from the other morphological effects occurring simultaneously (such as zipping closure which opposes this effect).

Thus, increased mesenchymal expansion due to abundant NCC emigration may increase the mechanical tension opposing neural tube closure at the level of rhombomere 4 in the hindbrain (in contrast to the levels of rhombomeres 3 and 5). This may delay closure at this level, resulting in the buttoning phenomenon. This finding lends credence to the concept of varied levels of mechanical tension opposing closure of the neural tube along the anterior-posterior axis of the embryo, resulting from differences in the morphology of adjacent tissues.

Despite the elevation in mechanical tension opposing closure in rhombomere 4, it remains low throughout the hindbrain in comparison to other regions of the neural tube (see Table 2.9). Morphologically the neural folds are relatively small and 'V'-shaped, and are located at a site of low axial curvature. Furthermore this is not an entirely *de novo* site of closure – the neural folds are drawn together by zipping closure

in the adjacent (more caudal) region. This relatively low force would not be predicted to require the delamination of NCC to overcome it. This is emphasised by the fact that isolated failure of hindbrain closure (i.e. not as a result of failure of Closure 2) is rare and is not generally associated with neurocristopathies(Gunn et al., 1996).

The hypothesis of the current studies states that NCC delamination facilitates neural tube closure in regions where the forces opposing closure are high. The opposite effect has been observed at the level of rhombomere 4 – NCC delamination may act to oppose closure rather than facilitate it. This apparent conflict between the hypothesis and the findings will be addressed further after describing the relationship between the mechanical tensions opposing neural tube closure and NCC delamination in the more anterior cranial region at Closure 2.

2.4.1.5. CLOSURE 2

There are a number of notable morphological traits in the midbrain region of the neurulation stage mouse embryo. The neural folds themselves are initially convex and very widely spaced, resembling a flattened 'M'-shape at the 4 somite stage. This is in contrast to the 'V'-shaped neural folds of the spinal and hindbrain regions. Moreover, the axial curvature of the midbrain region is high (Jacobson & Tam, 1982), it being the site of the cranial flexure, a further contrast to the spinal and hindbrain regions.

These factors taken together indicate that the mechanical tensions opposing the zipping closure of this region are high (see Table 2.9) – analogous to a zip being forced closed over a bulging paunch! When the zipping edges are everted (as are the dorsal tips of the neural folds in the midbrain, owing to their location on the outer extremities of the 'M'-shape) the zip will not close. Furthermore when the edges being zipped are on the outer edge of a curve (as in the cranial flexure) the zip is even harder to close – as at the corners of a overfull suitcase.

Further evidence for the forces opposing closure in the midbrain is provided by the plethora of mutations which result in failure of its closure (Copp et al., 2003). Mouse mutations resulting in exencephaly are four times more frequent than those resulting in spina bifida and these most frequently result from failure of midbrain closure specifically (Harris & Juriloff, 2010). The frequency of perturbation of midbrain closure gives an indication of the complexity of the processes involved and in turn the high degree of mechanical tension opposing closure in this region.

These high levels of mechanical tension opposing closure in the midbrain are overcome by a complex set of mechanisms which combine to allow the occurrence of a second *de novo* site of initiation of closure – Closure 2 – and the subsequent spread of closure over the apex of the midbrain cranial flexure. Closure 2 is known to be a polymorphic trait and comparisons made between mouse strains in which Closure 2 varies in location demonstrate its importance in neural tube closure (Juriloff et al., 1991; Fleming & Copp, 2000). Strains in which Closure 2 is located caudally, high in the midbrain, just rostral to the site of cranial flexure and at a location where the neural folds are highly biconvex are relatively resistant to exencephaly. In these strains, Closure 2 serves to overcome the mechanical tensions opposing closure in the midbrain. This is in contrast to the SELH/Bc strain, at the opposite end of the spectrum, which completely lacks Closure 2 and is highly prone to exencephaly (MacDonald et al., 1989). Here, there is no mechanism other than zipping caudally from Closure 3 to overcome the high degrees of mechanical tension opposing closure in the midbrain. Intermediate strains also exist in which Closure 2 is located in a rostral position and these strains exhibit moderate susceptibility to exencephaly. The rostral site of *de novo* closure provides little support for the closing neural folds in the vicinity of the cranial flexure, which has the highest mechanical tension opposing closure.

2.4.1.6. MORPHOGENETIC EVENTS THAT ENHANCE MIDBRAIN CLOSURE

Two morphogenetic events are known to help overcome the forces opposing closure, thereby facilitating Closure 2 and closure of the midbrain: (i) the elevation of the midbrain neural folds due to expansion of the underlying mesenchyme and (ii) the formation of DLHP in the forebrain and midbrain neural folds. Furthermore, each of these processes is known to be facilitated by a number of permissive mechanisms.

The first process known to facilitate Closure 2 is elevation of the neural folds. Initially the cranial neural folds (from the forebrain to the anterior hindbrain) have a flattened ‘M’-shaped morphology in which their tips are in line with the ventral midline. Subsequently the midbrain neural folds elevate relative to the ventral midline such that the tips of the neural folds are pushed dorsally, forming a biconvex ‘V’-shape and bringing the initially everted neural folds closer to apposition..

Elevation of the neural folds has been attributed to expansion of the underlying mesenchyme due to cell proliferation and an increase in extracellular space (see section 1.1.4.3.2 and (Morriss and Solursh, 1978)). Analysis of the *Twist* and *Cart1* null mice

initially attributed their exencephalic phenotypes to this failure of mesenchymal expansion (Chen and Behringer, 1995; Zhao et al., 1996). However, expansion of the cranial mesenchyme is contributed to by both the mesoderm and also the invasion of NCC delaminating from the neuroepithelium and migrating into the cranial mesenchyme around this time. Further studies of *Twist* and *Cart1* null mice have identified aberrant cranial NCC delamination, migration and colonisation of target organs, including the cranial cartilage and bone, as well as the heart (Qu et al., 1999; Vincentz et al., 2008; Bildsoe et al., 2009). This provides support for the theory that NCC migration into the mesenchyme contributes to the mesenchymal expansion required for an effective Closure 2.

The mesenchymal expansion in the midbrain region facilitates closure by elevating the flattened neural folds, thus bringing their tips closer to apposition. This is in contrast to the mesenchymal expansion at the level of rhombomere 4 (see section 2.4.1.4), where the neural folds had already elevated relative to the median hinge point. Under these circumstances, the mesenchyme expands laterally, which is hypothesised to pull the neural folds apart and thus hinder closure (contrast Figure 2.10 and 2.11).

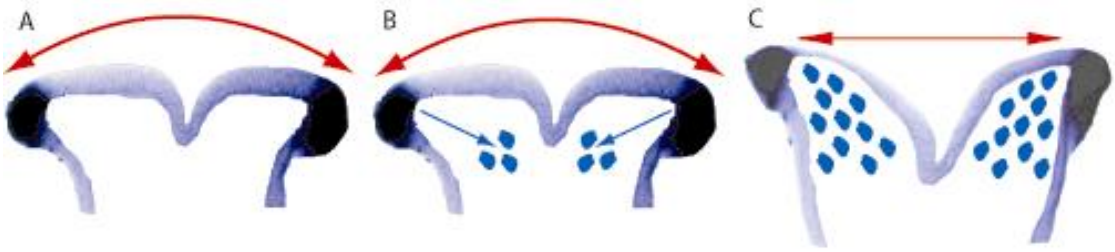

Figure 2.11. Effects of NCC Migration on Midbrain Neural Fold Morphology.
The 'M'-shaped neuroepithelium of the midbrain are represented in A and the NCC migrating into the mesenchyme in B (blue arrows). The expansion of mesenchymal tissue, aided by entry of NCC, appears to elevate the neural folds relative to the midline, resulting in the tips of the neural folds becoming closer to apposition (indicated by the red arrows in C).

The second morphogenetic mechanism that assists midbrain closure is the formation of DLHPs. These form in the elevated neural folds of the posterior forebrain and anterior midbrain. Several factors have been implicated in this process including apical actin microfilament contraction, and a balance between apoptosis and proliferation of the neuroepithelium (see section 1.4.3.2). When these factors are disrupted in mouse mutants, or by teratogens, the resultant failure of DLHP formation reliably causes exencephaly (Morriss-Kay and Tuckett, 1985; Sah et al., 1995; Ishibashi et al., 1995; Hildebrand and Soriano, 1999).

The current research proposes that NCC delamination from the neural epithelium facilitates DLHP formation thus promoting the apposition of Closure 2 and subsequent closure of the midbrain region. The proposed mechanism is that NCC delamination enhances the mechanical flexibility of the tips of the neural folds. The angle at the junction of the neural and non-neural epithelium in the biconvex anterior midbrain neural folds of the 3 somite embryo is close to a right angle. Enhancing the flexibility at this site would enable the bending of the epithelial layer to an acute angle upon the 'flip around' event of DLHP formation.

The timing of NCC delamination from the dorsal neuroepithelium is in keeping with this hypothesis. The NCC are initially specified in the dorsal neuroepithelium of the biconvex anterior midbrain neural folds and their migration is initiated prior to the kinking of the DLHPs.

NCC delamination may, therefore, be added to the list of factors that are mechanically permissive for DLHP formation. The molecular mechanism driving DLHP formation has been identified in the spinal region. Whereas midline bending is induced by signals emanating from the notochord, DLHPs are induced in the lower spine by antagonism of BMP2 as mediated by dorsal secretion of noggin. Notochordal secretion of sonic hedgehog in the upper spine inhibits noggin production, and thus DLHP formation is prevented (Smith and Schoenwolf, 1989; Ybot-Gonzalez et al., 2007). This molecular mechanism which controls the gradient of DLHP formation in the spinal region during development may also be linked to the control of the rostrocaudal wave of NCC specification and migration which is known to be dependent on specific levels of BMP signalling (Anderson et al., 2006; Correia et al., 2007). The molecular mechanism driving DLHP formation in the cranial region, however, remains to be studied in detail.

2.4.1.7. CLOSURE 3

Closure 2 brings the tips of the forebrain neural folds into apposition and is followed rapidly by the initiation of closure of the neural tube at the most rostral end of the neural plate: termed Closure 3. This is perhaps a misnomer as it does not in fact represent a *de novo* site of closure, of the type seen in Closures 1 and 2. Rather, it represents the initiation of zipping closure of the edges of the most anterior neural plate – a location at which the neural folds are already joined at the ventral midline. As such the timing of Closure 3 is difficult to pinpoint.

It can be assumed that, after Closure 2 draws the forebrain neural folds into apposition their subsequent zipping closure is opposed by low levels of mechanical tension (see Table 2.9). The persistence of Closure 3 in mutants in which Closure 2 is absent demonstrates that Closure 3 is a robust process and is in fact independent of Closure 2. On the other hand, a number of mouse mutants exhibit a split face defect in which Closure 3 (or at least progression of caudal zipping from this site) fails (Schorle et al., 1996).

The development of NCC can have no role in the anterior forebrain as this region lacks NCC. Wnt signalling is known to be essential for NCC specification and also acts as a posteriorising signal in the neural plate. Repression of *Wnt*/β-*catenin* signalling by genes including *Hesx1* and *Six3* in the anterior neural plate is necessary for normal anterior forebrain development and also prevents NCC specification in this region (Lagutin et al., 2003; Andoniadou et al., 2007).

2.4.1.8. CLOSURE OF THE CRANIAL NEUROPORES

Subsequent to the *de novo* closures, and zipping from these sites, final closure of the cranial region occurs at the anterior and hindbrain neuropores. The mechanical tension opposing closure of these neuropores can be assumed to be very low as the neural folds are drawn into apposition by bidirectional zipping closure from the *de novo* closure sites. This is further supported by the paucity of perturbations of these processes in contrast to those of Closure 2 and midbrain closure. While some mouse mutants do exist which exhibit failure of hindbrain neuropore closure, these are thought to reflect a failure of the late stages of closure, neural fold adhesion, rather than the earlier mechanical apposition of the neural folds (Camerer et al., 2010).

Table 2.9. Factors affecting the mechanical feasibility of neural tube closure in the mouse *

	Factors hampering closure				**Factors aiding closure**	
	De novo closure site?	Widely spaced neural folds?	High axial curvature?	Overall mechanical feasibility	NCC emigrate before closure	DLHPs formed
Forebrain	**YES**	No	No	High	-	-
Closure 2	**YES**	**YES**	**YES**	Very low	+	+
Midbrain	No	**YES**	**YES**	Low	+	+
Hindbrain	No	**YES**	No	High	-	-
Closure 1	**YES**	No	No	High	-	-
Upper spine	No	No	No	Very High	-	-
Lower spine	No	No	**YES**	Medium	-	+

* Unfavourable factors are indicated in bold, capitalised typeface. High axial curvature is 'weighted' more heavily than other hampering factors when determining overall mechanical feasibility of closure.

2.4.2. NEURAL TUBE CLOSURE AND NCC MIGRATION IN THE CHICK

The current study confirms previous findings which demonstrated that chick neurulation differs significantly from that in the mouse (Van Straaten et al., 1996). The cranial neural folds are initially small, undergoing expansion after closure has occurred. Their initial site of closure is located in the midbrain and is facilitated by the formation of the median hinge point only. Further closure is mediated by zipping and buttoning mechanisms.

During these processes axial curvature in the cranial region of the chick is low, becoming higher with a turning event which follows cranial neural tube closure (Peeters et al., 1998). Taken together these findings regarding cranial neurulation lead to the inference that mechanical tension opposing closure in the cranial region of the chick embryo is low. According to the hypothesis regions with low levels of opposing forces will not require DLHPs to facilitate closure – as is the case in the chick.

Cranial NCC in the chick embryo have been shown to be specified around the time of cranial neural tube closure. The onset of their delamination, however, follows completion of closure in the region, confirming previous findings (Tosney, 1982). This is in accordance with the current hypothesis; NCC delamination is not required to facilitate the formation of DLHP and closure.

2.4.3. NEURAL TUBE CLOSURE AND NCC MIGRATION IN THE HUMAN

The findings regarding neural tube closure and neural crest cell migration in the human are limited by the scarcity of tissue samples available. Furthermore the lack of whole mount images of the embryo from which sections were taken made accurate staging difficult.

De novo sites of closure of the human neural tube have been described previously, the first in the rhombocephalic region (analogous to Closure 1 in the mouse) and the second in the prosencephalon (analogous to Closure 3 in the mouse) (O'Rahilly and Muller, 1989). The human embryo does not exhibit such high degrees of axial curvature as seen in the mouse and perhaps the lack of a *de novo* site of closure in the midbrain region reflects this. The associations demonstrated between neurocristopathies and exencephaly in the human indicate that NCC delamination may still play a role in overcoming the tensions opposing cranial closure (Stevenson et al., 2004).

It is of interest to note that the current findings appears to provide evidence for initiation of DLHP correlating with migration of NCC in the closing rhombencephlic neural tube of the human CS 11 embryo. Furthermore NCC migration appears to precede closure both in the rhombencephalon of the CS 11 and in the forebrain region of the CS 12 embryo. This is in accordance with a previous study (O'Rahilly and Muller, 2007). Thus the current findings cannot exclude a role for NCC in facilitating closure of the human neural tube.

2.5. CONCLUSIONS

Morphological analysis of the neural folds and axial curvature of the mouse embryo allowed inferences to be drawn regarding the degrees of mechanical tension opposing closure in the different regions of the neural tube. These imply that the forces opposing closure are particularly high in the midbrain region of the mouse. The current work hypothesises that NCC delamination may facilitate closure in this region by enhancing the mechanical flexibility of the neural folds, allowing their bending at the DLHP. This is borne out by the finding that NCC delamination precedes the formation of DLHPs in the midbrain region of the mouse embryo. This is in contrast to the situation in the chick embryo, in whom closure of the neural folds is not predicted to be subject to tensions opposing closure, and NCC migration follows closure in the cranial region. Data from the human embryo is not conclusive, but does not exclude a role for NCC delamination in neural tube closure.

CHAPTER 3

NEURAL CREST MIGRATION AND NEURAL TUBE CLOSURE IN MUTANT MOUSE MODELS

3.1. INTRODUCTION

A review of the literature in Chapter 1 has identified numerous correlations between the processes of neural tube closure and early NCC development. The two processes are correlated both spatially and temporally (Serbedzija et al., 1990; Serbedzija et al., 1992). Furthermore, failure of the two processes correlates in a number of mouse models and in response to several teratogens (Auerbach, 1954; Morriss-Kay and Tuckett, 1989; Elms et al., 2003). These findings imply that the two processes may have a causal relationship, one being dependent upon the other.

The specificity of this relationship for the cranial region is implied by the association of cranial NTDs with neurocristopathies, while spinal NTDs have been dissociated from neurocristopathies(Franz, 1992; Estibeiro et al., 1993). Furthermore, the directionality of the causal relationship is implied by the timing of the two events in the cranial region: NCC delamination precedes neural tube closure consistent with delamination being necessary for closure (Serbedzija et al., 1992).

It was proposed in Chapter 2 that NCC delamination from the cranial neuroepitheliummay act to enhance the mechanical flexibility of the dorsal neural plate, thus facilitating apposition and closure of the neural folds. Detailed analysis of the morphology of the cranial neural plate has identified the midbrain as a region in which there is a high degree of mechanical tension resisting the apposition and closure of the neural tube. The relationship between the elevation, bending and closure of the midbrain neural folds and the specification and delamination of NCC in the midbrain indicates that NCC delamination may act in conjunction with a number of other permissive processes to facilitate the formation of DLHPs and subsequent closure of the midbrain neural tube.

The aim of the current chapter is to determine whether the hypothesis that NCC delamination facilitates midbrain DLHP formation and subsequent neural tube closure is borne out in some of the mouse strains known to exhibit neurocristopathies in conjunction with exencephaly, namely the *splotch* (*Pax3*) and *kumba*(*Zic2*) mutant mice. Further comparisons were made with a genetic ablation model: *Wnt1-Cre;ROSA26*$^{eGFP\text{-}DTA}$.

3.1.1. ZIC2-KUMBA

The *Zic* family of genes, comprising *Zic 1*to*5* in the mouse, are zinc finger-containing transcription factors implicated in neural development. They are initially expressed early in gastrulation and later in the neuroepithelium, being implicated in mediolateral segmentation of the neural plate (Nagai et al., 1997). Over-expression studies in *Xenopus* have implicated Zic proteins in early NCC induction (Brewster et al., 1998)(Nakata et al., 1997; Mizuseki et al., 1998; Nakata et al., 2000).

Disruption of genes in the *Zic* family has further implicated them in NCC development and also in neural tube closure. Mice harbouring *Zic3* mutations exhibit exencephaly in association with facial clefting (indicative of neurocristopathies) (Klootwijk et al., 2000). Disruption of *Zic5* in the mouse results in exencephaly in association with NCC defects especially of the first branchial arch and its derivatives (Inoue et al., 2004). A hypomorphic allele of *Zic2* produces exencephaly, spina bifida and holoprosencephaly (HPE) in association with an incomplete defect in DRG development (Nagai et al., 2000). Mutations in the human *ZIC2* gene have also been associated with the HPE phenotype (Brown et al., 1998).

The *Zic2-Kumba* mouse studied here harbours an ENU-induced missense mutation in the fourth zinc finger which results in a loss of function *Zic2* allele (Nolan et al., 2000; Elms et al., 2003). Embryos homozygous for this mutation have been described as displaying delayed and reduced NCC production in association with exencephaly and spina bifida, as well as HPE in some individuals (Elms et al., 2003).

HPE is a failure of the forebrain to develop into two hemispheres. In humans, HPE has also been associated with mutations in s*onichedgehog* (*SHH*), *SIX3* and *ZIC2* (Paulussen et al., 2010). The mechanism underlying the HPE phenotype caused by mutations in *Zic2* is the subject of debate. Studies in the mouse have indicated that it is caused by an early transient defect in the organiser at mid-gastrulation which results in defective prechordal plate and subsequent forebrain midline development and which is independent of *Six3* and *Shh* signalling (Warr et al., 2008). Zebrafish studies, however, have demonstrated that *zic2a* interacts with *shh*and *six3* signalling in the later formation of the prethalamus (Sanek et al., 2009).

The spina bifida defect observed in the *Zic2*$^{ku/ku}$ mutant has been attributed to a lack of DLHP bending in the regions of Modes 2 and 3 closure, resulting from a reduction in BMP antagonism (Ybot-Gonzalez et al., 2007). The basis of exencephaly observed in the*Zic2*$^{ku/ku}$ mutant has not been explained. Zic2 has, however, been linked to the formation of midbrain DLHPs in the zebrafish (Nyholm et al., 2009), although this association appears to be via a different mechanism than in the mouse spinal region, as here *zic2* is required for the organisation of apical actin microfilaments.

The Zic genes, including *Zic2*, are expressed in a broad domain spanning the prospective premigratory neural crest in response to NCC inducing signals including BMPs and Wnts. In turn, Zic genes activate the NCC specification genes *Snail*, *FoxD3* and *Sox9* (Nagai et al., 1997; Mayor and Aybar, 2001; Gaston-Massuet et al., 2005). This gene expression dependence may underlie the delay and reduction in NCC specification observed in the *Zic2*$^{ku/ku}$ mutant (Elms et al., 2003).

The association between neurocristopathies and NTDs in the *Zic2*$^{ku/ku}$ mouse has never been addressed, and research thus far has failed to identify the underlying cause of the exencephalic phenotype.

3.1.2. SPLOTCH (Sp^{2H})

Splotch mice carry a mutation in the *Pax3* gene of which there are several mutant alleles (Epstein et al., 1993; Goulding et al., 1993). Homozygous *Sp*^{2H} embryos harbour an intragenic deletion of Pax3, resulting in a truncated version of the Pax3 protein and exhibit a phenotype in which folate-responsive exencephaly and spina bifida are associated with NCC defects as well as abnormalities of limb musculature (Beechey and Searle, 1986; Epstein et al., 1991; Fleming and Copp, 1998). Mutations in the human *PAX3* gene are also associated with the neurocristopathies Waardenburg syndrome type I and III (Tassabehji et al., 1992; Wollnik et al., 2003) and there is limited evidence of an association with NTDs, which may reflect the requirement for other risk factors (genetic or environmental) in generation of this phenotype (Chatkupt and Johnson, 1993; Hol et al., 1995; Nye et al., 1998).

Pax3 is expressed in the dorsal neural tube, early migrating NCC and dermomyotomal cells entering the limb bud (Goulding et al., 1993) and like *Zic2* is involved in the signalling cascades governing NCC induction. It is induced in a domain spanning the prospective neural crest territory in response to NCC inducers including BMPs and Wnts, and is involved in activating NCC-specific genes such as *Sox9* (Taneyhill and Bronner-Fraser, 2005). *Pax3* has further been implicated in the later regulation of differentiation of peripheral neuron progenitors, maintenance and survival of cardiac neural crest progenitors and proliferation of melanoblasts (Koblar et al., 1999; Hornyak et al., 2001). The NCC defects observed in the Sp^{2H} homozygous embryos reflect the roles which have been identified for *Pax3* and include defects of pigmentation, cardiac defects and DRG defects (Asher, Jr. and Friedman, 1990).

The mechanisms underlying neural tube and NCC defects in *splotch* mice remain to be fully elucidated. Construction of chimeric embryos containing both wild type and *splotch* homozygous cells indicates that failure of neural tube closure reflects a cell autonomous requirement for *Pax3* in the dorsal neural folds (Mansouri et al., 2001). On the other hand, faulty cardiac NCC migration occurs only if *Pax3* expression is diminished in both the neural crest and their migratory environment (Chan et al., 2004). It is yet to be determined precisely which downstream genes are affected by loss of function of *Pax3* in the dorsal neural folds (Greene et al., 2009).

The NTD and neurocristopathies observed in the *splotch* mouse have never been related to each another causally. They are more generally regarded as being independent sequelae of a common upstream factor that results directly or indirectly from loss of *Pax3* function (Greene et al., 2009).

3.1.3. Wnt1-Cre;ROSA26$^{eGFP\text{-}DTA}$

In addition to the analysis of mouse lines in which neurocristopathies and NTDs are associated, a further transgenic mouse was studied in which the entire neural crest, as well as the midbrain, are genetically ablated. This conditional ablation model utilises the Cre/loxP system in which Cre recombinase is expressed under the promoter of genes of interest, such as Wnt1 (Danielian et al., 1998). Cre recombinase recognises the 34 base pair loxP sequence and mediates excision of floxed DNA (flanked by two loxP sites). Thus crossing the *Wnt1-Cre* mouse line with a transgenic mouse in which floxed

DNA has been inserted into the genome will result in the excision of the floxed region in Wnt1 expressing cells and this recombined region will persist in their progeny.

In the ROSA26 reporter mouse line, a floxed stop sequence ubiquitously inhibits expression of β-galactosidase (encoded by the *LacZ* gene) (Soriano, 1999). Crossing with *Wnt1-Cre* results in the excision of the stop sequence in Wnt1-expressing cells and expression of *LacZ*. Staining of β-galactosidase by X-gal can then be used to map all Wnt1 expressing cells and their progeny during subsequent development (Jiang et al., 2000). *Wnt1* is expressed in the presumptive midbrain as well as in the dorsal neuroepithelium, including the premigratory NCC (Wilkinson et al., 1987; McMahon et al., 1992).

Diphtheria toxin A (DTA) is a potent toxin which induces death of cells in which it is expressed. The *Wnt1-Cre;ROSA26*$^{eGFP\text{-}DTA}$ mouse line was generated to conditionally express DTA in cells of interest by utilising the Cre/loxP system (Ivanova et al., 2005). A cassette was inserted into the ROSA26 locus, containing the coding sequence for DTA preceded by a floxed enhanced green fluorescent protein (eGFP) and stop sequence. This resulted in the ubiquitous expression of eGFP but prevention of the expression of DTA in the absence of the Cre recombinase protein. Crossing this mouse with *Wnt1-Cre* results in the excision of the floxedeGFP and stop sequence in all Wnt1 expressing cells, leading to DTA production and subsequent cell death.

Study of this transgenic ablation model was intended to provide insight into the effects of removing the presumptive NCC from the dorsal neural tube. It was reasoned that this might produce an experimental situation equivalent to normal emigration of neural crest during delamination. The model proved to be complicated, however, as the neural crest, the midbrain, and other cells of the dorsal neural tube are all ablated simultaneously.

3.2. METHODS

Riboprobe preparation, mouse embryo dissection, whole mount *in situ* hybridisation, X-gal staining, H&E staining, embedding, sectioning, mounting, light microscopy and photography were conducted according to the methods described in Chapter 2.

3.2.1. CROSSING MUTANT MOUSE STRAINS

Kumba and *Splotch* embryos were generated by crosses between heterozygous mice (*Zic2*$^{ku/+}$ or *Sp*$^{2H/+}$). *Wnt1-Cre:ROSA26R* and *Wnt1-Cre:ROSA26 eGFP DTA* embryos were generated by crossing heterozygous *Wnt1-Cre*$^{+/-}$ mice with homozygous *ROSA26R*$^{+/+}$ or *ROSA26 eGFP DTA*$^{+/+}$ mice. The numbers of each resultant genotype reflected the ratio of expected genotypes and are listed in Table 3.1.

Table 3.1. Genotype Ratios of Mutant Embryos

ZIC2-KUMBA	***Ku*/+**	***Ku/Ku***	**+/+**	**TOTAL**
EXPECTED	50%	25%	25%	100%
ACTUAL	55%	24%	21%	100%
N	118	51	45	214
SPLOTCH	***Sp2H*/+**	***Sp2H/Sp2H***	**+/+**	**TOTAL**
EXPECTED	50%	25%	25%	100%
ACTUAL	52%	23%	25%	100%
N	86	37	41	164
Wnt1-Cre:ROSA26R	***Cre* +/-**		***Cre*-/-**	**TOTAL**
EXPECTED	50%		50%	100%
ACTUAL	41%		59%	100%
N	9		13	22
Wnt1-Cre: eGFP DTA	***Cre* +/-**		***Cre* -/-**	**TOTAL**
EXPECTED	50%		50%	100%
ACTUAL	43%		57%	100%
N	24		32	56

3.2.2. DNA EXTRACTION

DNA was usually extracted from the yolk sacs of embryos removed upon dissection and stored in 50 µl PBS at 4°C. Sometimes DNA was extracted from embryo samples which had already been processed for *in situ* hybridisation which were also stored in 50 µl PBS. Occasionally DNA was extracted from embryo samples stored in methanol. The samples were washed twice in PBS for 30 min with shaking, then most of the PBS was removed (leaving around 50 µl).

200 µllysis buffer (see Table 3.2)and 10 µl proteinase K (from 10 µg/µl stock) was added to the PBS. This was incubated at 55°C overnight and then centrifuged at 8000 xg and 4°C for 5 min. 90 µl of saturated sodium chloride was added and the mixture was vortexed before incubating on ice for 20 min. It was then centrifuged at 8000 xg and 4°C for 20 min. The supernatant was transferred to a new tube and precipitated with 1 ml of ethanol, vortexed and centrifuged for a further 20 min at 8000xg and 4°C. The supernatant was removed and the remaining pellet was air dried for 20 min before resuspending in 30 µl TE buffer (see Table 3.2).

Table 3.2. Solutions Required for DNA Extraction

SOLUTION	PREPARATION	STORAGE
Lysis Buffer	50 mMTris Ph8 (2.5 ml from 1 M stock) 5 mM EDTA (0.5 ml from 0.5 M stock) 100 mMNaCl (1 ml from 5 M stock) 0.5% SDS (2.5 ml from 10% stock) up to 50 ml Milli-Q	50 ml RT
TE buffer	10 mMTris pH 8.0 (100 µl from 1 M stock) 1 mM EDTA (20 µl from 0.5 M stock) up to 10 ml Milli-Q	10 ml RT

3.2.3. GENOTYPING OF MUTANT EMBRYOS

Splotch and *Kumba* embryos were genotyped by polymerase chain reaction (PCR) using the primers described in Table 3.4. The genotype of *Wnt1-Cre:ROSA26R* and *Wnt1-Cre:ROSA26 eGFP DTA* embryos was determined based on *Lac-Z* expression and morphological phenotypes.

The mixture for each reaction (set out below) was made on ice, scaled up to the number of reactions required then vortexed and aliquotted into 0.5 ml eppendorf tubes.

2.5 µl Taq polymerase buffer
2.5 µl nucleotides mix (10 0mM stock)
0.75 µl magnesium chloride (25 mM stock)
2.5 µl forwards primer (10 µM stock)
2.5 µl reverse primer (10 µM stock)
12.05 µlMilli-Q water
0.2 µl TAQ polymerase 5 u/µl

2 µl of DNA was added to each eppendorf (including one positive control and one water blank negative control) and they were inserted into a preprogrammed (as in Table 3.3) and prewarmed PCR machine. After completing the program, 12 µl of each reaction was loaded onto a 2% agarose gel and compared to a molecular weight marker to confirm the size of DNA amplified. The Sp^{2H} allele produced a 95 bp band while the *Pax3* wild type allele produced a 127 bp band. The $Zic2^{Ku}$allele produced a 176 bp product while the *Zic2* wild type allele produced a 150 bp product.

Table 3.3. PCR Program

PCR STEP	TEMPERATURE	TIME
Denaturation	94°C	2 min
Denaturation	94°C	1 min
Annealing	60°C	1 min
Extension	72°C	1 min
Number of cycles	29x	
Extension	72°C	10 min

Table 3.4. Primers used in Genotyping of Mutants

PRIMER	SEQUENCE	PRODUCT
Kumba forward	aaatggtcatccctgaaaaga	150 bp WT
Kumba reverse	caggcctctccaaagtacca	176 bp mutant
Sp2H forward	cctcggtaagcttcgccctctg	127 bp WT
Sp2H reverse	cagcgcaggagcagaaccaccttc	95 bp mutant

3.3. RESULTS

3.3.1. ZIC2-KUMBA

Labelling of the *FoxD3* positive NCC revealed no difference between the wild type and the *Zic2*$^{ku/ku}$ mouse in the specification of premigratory NCC in the cranial region at the 5 somite stage (red lines in Figure 3.1 A, B) (or any 3 to 5somite *Zic2*$^{ku/ku}$ embryos, see Table 3.5). The numbers of migratory NCC are, however, significantly reduced in the cranial region of homozygous mutants at later stages (8-22 somites), being all but absent from the midbrain, but with faint streams persisting from the hindbrain region (arrows in Figure 3.1 E, H-J, L, M and see Table 3.5). Furthermore, although the cranial NCC do not migrate into the periphery, they are not evident remaining in the neuroepithelium. In contrast, intense FoxD3 expression adjacent to the midbrain and hindbrain regions indicates progression of NCC migration in wild type embryos (arrows in Figure 3.1 C, G, K and see Table 3.5).

Resultant defects are observable in the morphology of the first branchial arch (BA1) at the 18-22 somite stage. In wild type embryos, BA1 is in close contact with the ventral anterior forebrain (Figure 3.1 G, K) and develops into a boot like shape, with the posterior edge being straight and the anterior edge being curved towards the forebrain (like the toe of a boot) (Figure 3.1 K). In contrast, an abnormal degree of separation between BA1 and the ventral forebrain is observable in some of the *Zic2*$^{ku/ku}$ mutants either distally, resulting from a downwards angling of the entire branchial arch (black asterisk in Figure 3.1 I) or in the proximal portion of BA1, the maxillary process (white asterisk in Figure 3.1 L). In the most severe *Zic2*$^{ku/ku}$ phenotype, BA1 is dramatically reduced in size and often can be hardly discerned as a distinct structure (Figure 3.1 J, M; see Table 3.5 for numbers of branchial arch defects observed).

The rostrocaudal wave of NCC specification is visible as a line of *FoxD3* expression along the trunk region of *Zic2*$^{ku/ku}$ mutant embryos (Figure 3.1 E, H, I). However, as development proceeds, *FoxD3*-positive premigratory NCC at increasingly more rostral locations become markedly reduced in *Zic2*$^{ku/ku}$embryos (red lines in Figure 3.1 E, H, I, L and absent in J, M) compared with wild type (red lines in Figure 3.1 C, G, K). This may reflect either a reduction in specification at later stages (and more rostral levels) or disappearance of those cells already specified. Migratory NCC are reduced or absent in the trunk of *Zic2*$^{ku/ku}$ mutants (Figure 4.1 E, H-J, L, M) whereas they are visible in wild type litter mates (e.g. arrow in Figure 4.1 K).

Figure 3.1. Neural Tube Closure and NCC Development in the *Zic2* (*Kumba*) Mutant

Wild type and *Zic2*$^{Ku/Ku}$ mouse embryos at 5 somites (A,B), 11 somites (C-F), 18 somites (G-J) and 22 somites (K-M) processed for *in situ* hybridisation as whole mounts for *FoxD3*. Regions of pre-migratory NCC are indicated with red lines, migratory NCC with white arrows, and post-migratory NCC in the cranial ganglia with black arrows.

(**A,B**) Dorsal views of wild type and *Zic2*$^{Ku/Ku}$ mutant embryos at 5 somites. No difference in specification of the NCC (labelled blue) in the region anterior to rhombomere 3, nor in the morphology of the neural tube, is evident at this stage.

(**C-F**) Lateral views of wild type and *Zic2*$^{Ku/Ku}$ mutant embryos at 10 somites (C,E) and sections taken at the level indicated by black lines in C and E (D,F). A reduction in NCC both in the neuroepithelium and in the migratory pathways is evident in the mutant embryo (E,F) in contrast to the wild type (C,D). There is also a dramatic difference in the morphology of the cranial neural tube. The lateral views reveal a reduction in size of the cranial region and a reduced angle of midbrain flexure in the mutant (E) compared with the wild type (C). Furthermore sections reveal that the cranial neural folds of the wild type embryo (D) are large and demonstrate dorsolateral bending (arrowheads) producing a structure with a wide lumen. In contrast the cranial neural folds of the mutant (F) are smaller with no dorsolateral bending (arrowheads).

(**G-J**) Lateral views of a wild type embryo and three *Zic2*$^{Ku/Ku}$ mutant embryos at 18 somites to illustrate the range of phenotypic severity. (G) There is normal NCC patterning in the wild type embryo and closure of the anterior neural tube is complete, while the PNP remains open. (H) A mild mutant phenotype in which morphologically the anterior neural tube is closed with normal proportions. This is associated with a minor reduction in both migratory and post-migratory NCC in the cranial region and a slight reduction in the expression domain of the pre-migratory spinal NCC. (I) A more severe mutant phenotype in which HPE (note the long tubular forebrain) is associated with a further reduction in migratory and post-migratory NCC in the cranial region, and a more severe reduction in spinal pre-migratory NCC. The morphology of the anterior neural tube and BA1 produces a gap between these two regions which is not evident in the wild type (asterisk in I). (J) The most severe mutant phenotype in which

exencephaly (the extent of which is indicated by red arrowheads) is associated with a lack of *FoxD3* labelling (except a small region of*FoxD3*-positive NCC adjacent to rhombomere 4 of the hindbrain). The morphology of BA1 in relation to the anterior neural tube cannot be discerned.

(**K-M**) Lateral views of a wild type embryo and two$Zic2^{Ku/Ku}$ mutant embryos at 22 somites, demonstrating the range of phenotypic severity. (K) The wild type embryo displays normal neural tube morphology associated with normal premigratory NCC in the spinal region and migrating NCC in the rostral spinal region and cranial region. (L) A mild mutant neural tube phenotype with a small midbrain exencephaly (between the red arrowheads) associated with a mild NCC phenotype (reduced spinal premigratory NCC and cranial and spinal migratory NCC). The maxillary process appears hypoplastic (white asterisk). (M) A more severe mutant phenotype in which a large exencephaly (between the red arrowheads) is associated with an almost complete absence of NCC (except a small region of *FoxD3*-positive NCC adjacent to rhombomere 4 of the hindbrain). The morphology of BA1 in relation to the anterior neural tube cannot be discerned.

Abbreviations: hbnp, hindbrain neuropore. Scale bars represent 100 μm.

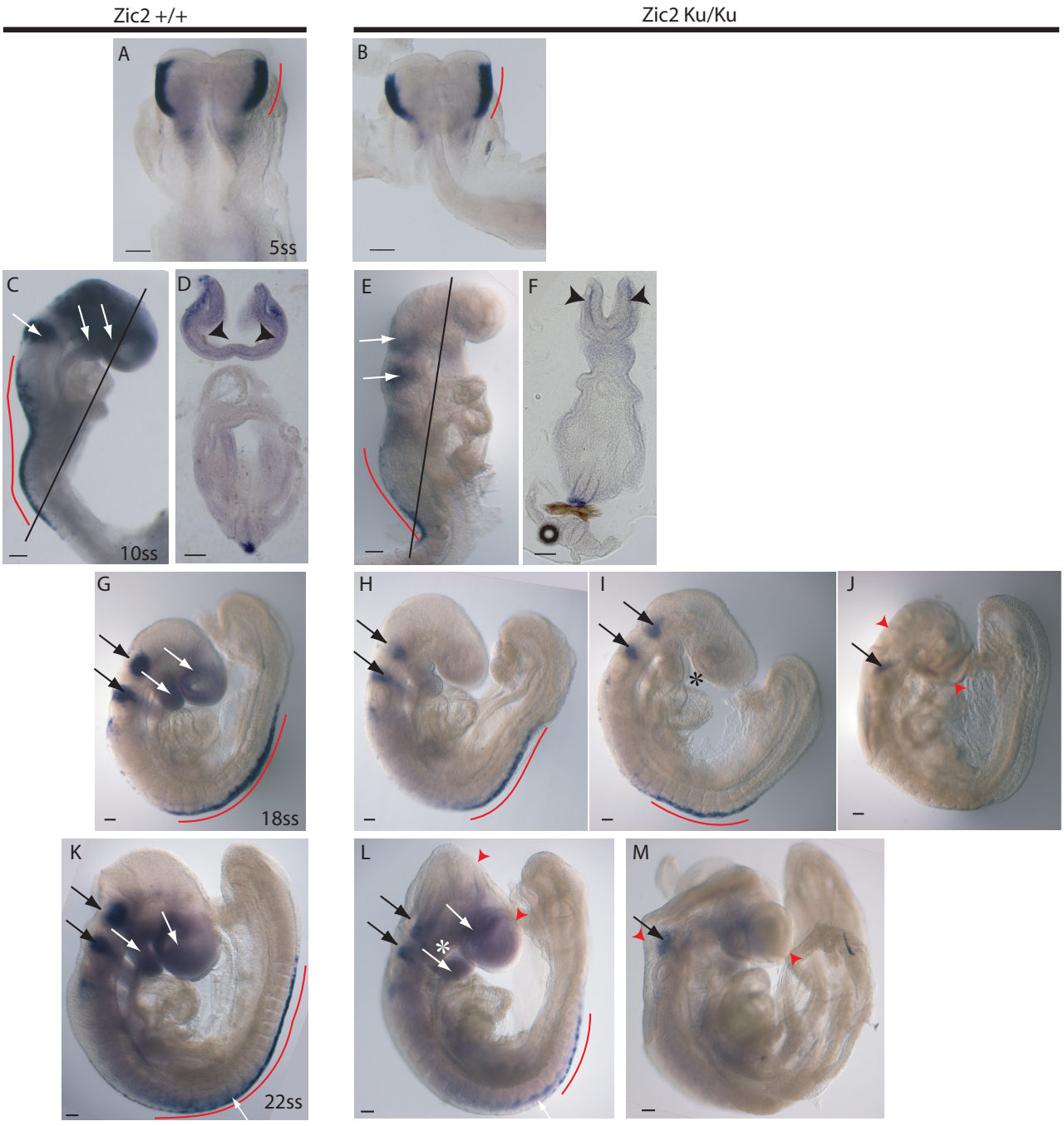
Zic2 +/+
Zic2 Ku/Ku
A
5ss
B
C
10ss
D
E
F
G
18ss
H
I
J
K
22ss
L
M

Table 3.5.Phenotypes of *Zic2*$^{ku/ku}$and wild type embryos.

PHENOTYPE	SOMITE RANGE	*Zic2*$^{ku/ku}$	Wild Type
Abnormal cranial NCC specification	3-5	0/8 (0%)	0/4 (0%)
Abnormal cranial NCC migration	8-11;18-22	29/43 (67%)	0/28 (0%)
Branchial arch defects	18-22	7/27 (26%)	0/13 (0%)
Reduced angle of cranial flexure	8-11	9/16 (56%)	0/15 (0%)
Reduced DLHP bending	8-11	9/16 (56%)	0/15 (0%)
Normal closure	18-22	4/27 (15%)	13/13 (100%)
HPE	18-22	6/27 (22%)	0/13 (0%)
Exencephaly	18-22	17/27 (63%)	0/13 (0%)
NT & NC defects proportional in severity	18-22	27/27 (100%)	N/A

Abnormalities of the cranial neural tube in *Zic2*$^{ku/ku}$ become morphologically apparent around the time of cranial neural fold elevation. A reduced angle of cranial flexure is visible in the whole mount embryo (compare Figure 3.1 C and E and see Table 3.5). Furthermore sections through the cranial region of these embryos reveal a failure of DLHP formation and a reduction in cranial tissue in the mutant (compare Figure 3.1 D and F and see Table 3.5). Black arrowheads in Figure 3.1 D indicate lateral bending of the neural plate in the wild type producing a wide lumen, while in Figure 3.1 F they indicate a lack of lateral bending and reduction in cranial tissue.

At later stages, the severity of the cranial neural tube phenotype in *Zic2*$^{ku/ku}$ mutants ranges from mild in which the cranial neural tube closes apparently normally (Figure 3.1 H), through moderate in which the neural tube closes but with HPE (Figure 3.1 I), to severe in which the neural tube fails to close producing exencephaly (Figure 3.1 J, L, M) (see Table 3.5). Importantly, the severity of the cranial neural tube phenotype correlates with the severity of the NCC phenotype (Figure 3.1 H-J, L, M) as well as the severity of associated enlarged PNP which is indicative of spina bifida development (black lines in Figure 3.1 H-J) (see Table 3.5).

3.3.2. SPLOTCH (Sp^{2H})

The cranial NCC of the homozygous Sp^{2H}mutant are specified normally as judged by *FoxD3* expression (Figure 3.2 A, B). Furthermore they appear to migrate normally both from the midbrain (Figure 3.2 C, D) and rhombomeres 1, 2 and 4 (Figure 3.2 E-H) (see Table 3.6).

As the rostrocaudal wave of NCC specification passes along the body axis of the developing wild type embryo (red line in Figure 3.2 C, E, G) a defect becomes apparent in the $Sp^{2H/2H}$ mouse. There is a severe reduction in NCC specification (and hence migratory NCC) in the post otic hindbrain and cervical region of mutant embryos (Figure 3.2 D, F). However, as the wave of specification progresses more caudally, to thoracic and lumbar regions, there is less difference visible between $Sp^{2H/2H}$and wild type in specification and migration of NCC (Figure 3.2 H). Hence, homozygous Sp^{2H}mutants exhibit a NCC defect that is most severe in the caudal hindbrain and upper spine (see Table 3.6).The cranial neural tube phenotype is evident in the 16 somiteSp^{2H} mutant as everted midbrain neural folds (Figure 3.2 F) and in the 21 somite mutant as exencephaly (Figure 3.2 H) (see Table 3.6).

Table 3.6. Phenotypes of $Sp^{2H/2H}$and wild type embryos

PHENOTYPE	SOMITE RANGE	$Sp^{2H/2H}$	Wild Type
Abnormal cranial NCC specification	3-5	0/7 (0%)	0/6 (0%)
Abnormal cranial NCC migration	8-22	0/37 (0%)	0/29 (0%)
Abnormal trunk NCC specification	8-22	11/37 (30%)	0/29 (0%)
Reduced angle of cranial flexure	8-11	0/17 (0%)	0/15 (0%)
Reduced DLHP bending	8-11	0/17 (0%)	0/15 (0%)
Normal closure	18-22	6/13 (46%)	12/12 (100%)
Exencephaly	18-22	7/13 (54%)	0/12 (0%)

Figure 3.2. Neural Tube Closure and NCC Development in the *Splotch*(Sp^{2H}) Mutant

Wild type and Splotch(Sp^{2H}) homozygous mutants at 4 somites (A,B), 9 somites (C,D), 16 somites (E,F) and 21 somites (G,H), processed for *in situ* hybridisation for *FoxD3*.

(**A,B**) Dorsal views of wild type and Sp^{2H}mutant embryos at 4 somites reveal no differences in specification of the NCC (labelled blue) in the region anterior to rhombomere 5, nor in the morphology of the neural tube, at this stage.

(**C,D**)Lateral views of wild type and Sp^{2H}mutant embryos at 9 somites. While the NCC migrating in the cranial region do not differ significantly at this stage, there is a complete absence of pre-migratory NCC in the cervical region of the mutant (D) in contrast to the wild type (red line in C).

(**E,F**)Lateral views of wild type and Sp^{2H} (exencephalic) mutant embryos at 16 somites. The cranial NCC patterning does not differ significantly between the wild type and mutant embryo, whereas pre-migratory and migratory NCC in the cervical and anterior thoracic region are severely reduced in the mutant (red line in E in contrast to dashed red line in F).

(**G,H**)Lateral views of wild type and Sp^{2H} (exencephalic) mutant embryos at 21 somites. Neither cranial nor spinal NCC patterning differ significantly between the wild type and mutant embryos. There are no *FoxD3* positive NCC in the cervical and anterior thoracic region of either embryo (due to the down regulation of *FoxD3* expression after NCC migration in the wild type).

Scale bars represent 100 μm.

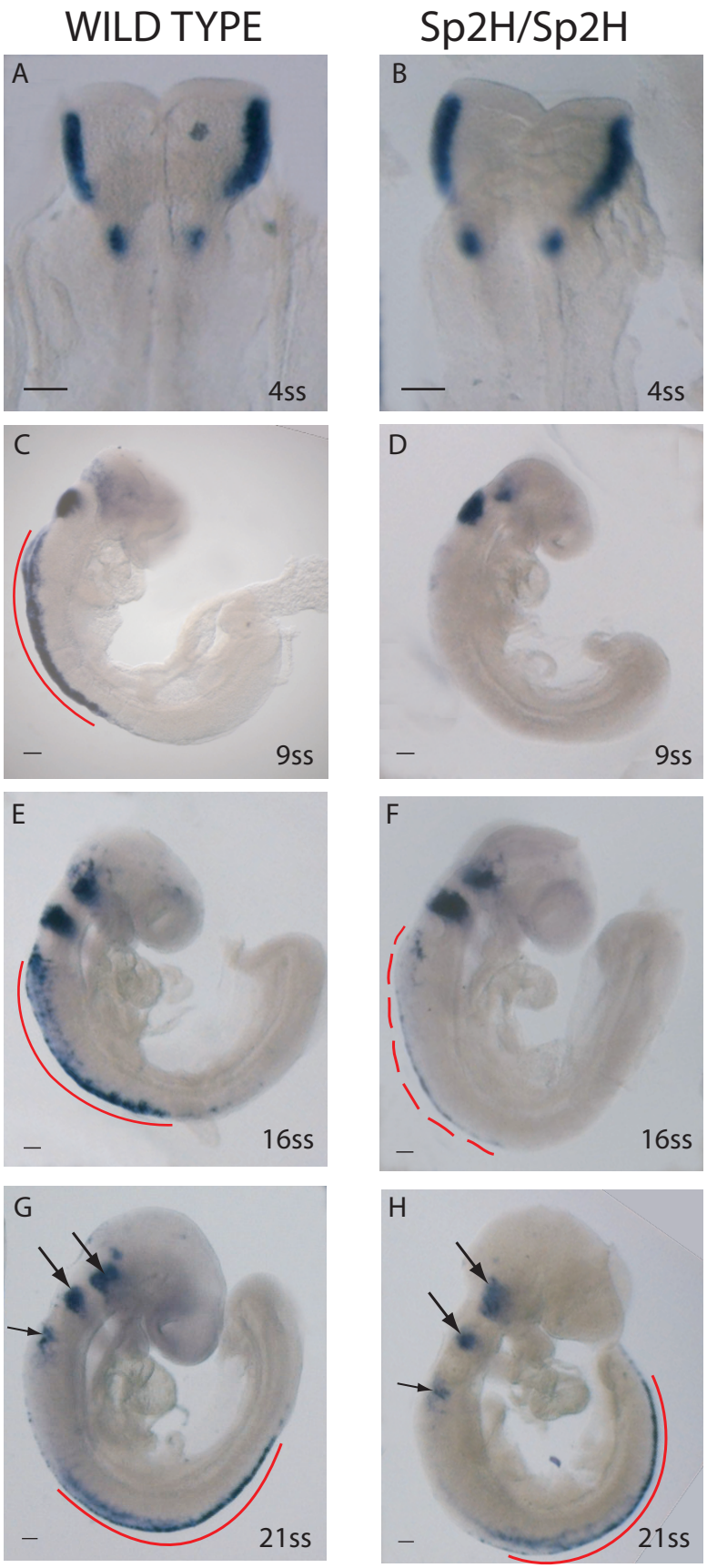
WILD TYPE
Sp2H/Sp2H
A
4ss
B
4ss
C
9ss
D
9ss
E
16ss
F
16ss
G
21ss
H
21ss

3.2.3. Wnt1-Cre;ROSA26$^{eGFP\text{-}DTA+}$

Initially all Wnt1-expressing cells and their progeny were identified by X-gal staining of the product of the *lacZ* gene (β-galactosidase) in *Wnt1-Cre;ROSA26R* embryos. These observations replicate previous findings that β-galactosidase expression (reflecting *Wnt1-Cre* expression) is limited to three locations: (i) the dorsal neuroepithelium spreading from the posterior forebrain caudally during development; (ii) the NCC which emanate from the dorsal neuroepithelium plus their derivatives; and (iii) the entire neuroepithelium of the midbrain (Figure 3.3 A-F).

Having identified the Wnt1-expressing cells and their progeny in the *Wnt1-Cre;ROSA26R* line, these mice were subsequently crossed with the conditional genetic ablation model in which DTA is expressed in all Cre expressing cells, specifically ablating them. All phenotypes described in this model were observed with 100% penetrance. *In situ* hybridisation for *FoxD3* indicated that the cranial NCC precursors of the midbrain and rhombomeres 1 and 2 are ablated before onset of *FoxD3* expression in the *Wnt1-Cre;ROSA26*$^{eGFP\text{-}DTA+}$ mouse (Figure 3.4 A,B). At more caudal levels, however, the normal rostrocaudal wave of *FoxD3*-positive NCC specification is evident in both embryos not expressing DTA (Figure 3.4 A,C,G,M) and in those expressing DTA conditionally (Figure 3.4 B,D,H,N). This is followed by a rostrocaudal wave of ablation of *FoxD3*-positive NCC in the DTA expressing embryos which precedes the rostrocaudal wave of NCC delamination and migration in the wild type embryos. Hence the rostral cranial NCC precursors are ablated prior to their specification and those more caudally are ablated before the onset of delamination in this genetic ablation model.

Further morphological phenotypes result from the ablation of the Wnt1 expressing cells. Early ablated embryos display a similar morphological phenotype to the *Zic2-Kumba* mutant in which there is a reduction in tissue around the midbrain region and reduction in cranial flexure (Figure 3.4 B,D) in contrast to the non-ablated embryos (Figure 3.4 A,C). This is in conjunction with a lack of DLHPs and failure of apposition of the neural folds at the site of Closure 2 in the ablated embryos (Figure 3.4 F), leading directly to a persistently open neural tube at the site of Closure 2 (Figure 3.4 K, L). This presumably reflects the ablation of the Wnt1 expressing tissue of the midbrain precursors. In contrast, non-DTA expressing embryos exhibit normal Closure 2 apposition (Figure 3.4 E) and subsequent closure (black arrowheads in Figure 3.4 I,J).

Figure 3.3. Wnt1 Expressing Cells and their Progeny

(A,B) Lateral views of *Wnt1-Cre* x *Rosa26R*wholemount embryos at 4 and 20 somites in which β-gal staining of the *LacZ* gene product reveals all Wnt1 expressing cells and their progeny. (C-F) Sections taken from the embryo in B at the levels indicated by white lines.

(**A**) In the 8 somite embryo, Wnt1 expressing cells and their progeny (stained blue) are located along the dorsal neural tube from the posterior forebrain to the site of Closure 1. Presumptive NCC can be seen migrating away from the neuroepithelium (white arrow). The dense blue staining indicated by the black line reflects expression of Wnt1 in the precursor of the midbrain, which begins at presomitic stages. This embryo shows the resultant pattern of the progeny of these Wnt1 expressing cells which are distributed throughout the midbrain by the 8 somite stage.

(**B**) Wnt1 expressing cells and their progeny in the 20 somite stage reveal the migration patterns of NCC exiting the dorsal neuroepithelium and migrating throughout the embryo. Cranial NCC migrate into the cranial mesenchyme and colonise the branchial arches, forming the cranial nerves *en route* (labelled: V, trigeminal nerve; VII, facial nerve; IX, glossopharyngeal nerve; X, vagus nerve). Posterior to this, the NCC enter the heart and also migrate through the rostral half of each somite to form the dorsal root ganglia along the length of the embryo.

(**C-F**) Some of these NCC migration pathways are illustrated in sections. The Wnt1 expression domain in the dorsal neural tube (black arrowheads in D,E,F) gives rise to NCC which colonise the mesenchyme of the frontonasal mass (C) and outer mesenchyme of branchial arches 1 and 2 (D and E). Note that neither the arch ectoderm nor core mesenchyme of the branchial arches are labelled; the latter is derived from cranial mesoderm. A stream of NCC is evident colonising the outflow tract(also called truncusarteriosus) of the heart (E and F). NCC are also evident surrounding the foregut (E and F), although the endoderm of the foregut remains unlabelled.

Abbreviations: as, aortic sac; ba1, branchial arch 1; ba2, branchial arch 2; fg, foregut; h, heart; ta, truncusarteriosus. Scale bars represent 100 μm.

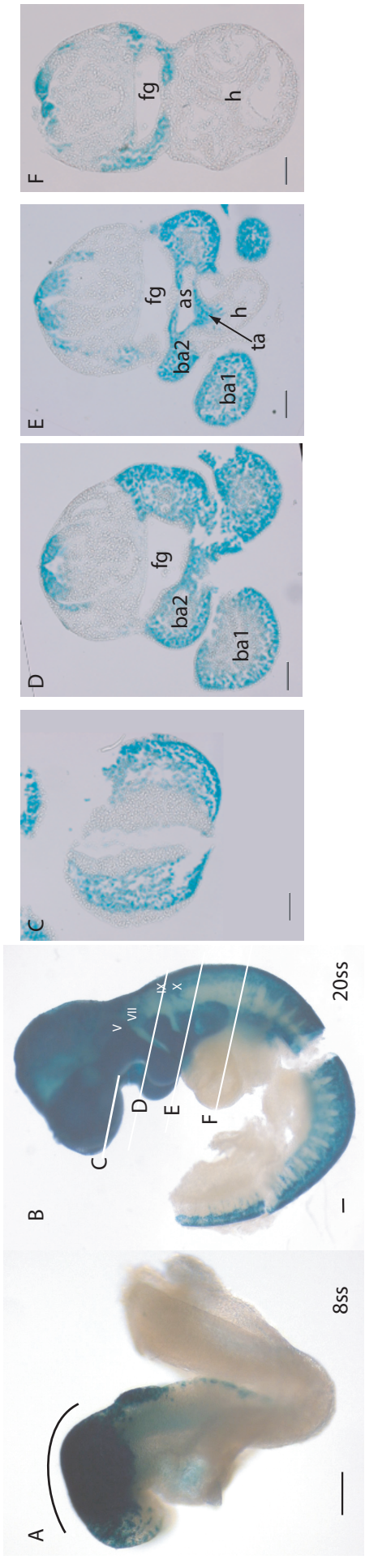
8ss
20ss
A
B
C
D
E
F
V
VII
IX
X
fg
h
as
ta
ba1
ba2

Figure 3.4: Genetic ablation of Wnt1 Expressing Cells and their Progeny

Wnt1-Cre embryos (A,C,E,G,I,J,M) and *Wnt1-Cre;ROSA26*$^{eGFP\text{-}DTA+}$ (B,D,F,H,K,L,N) at 6 somites (A,B), 8 somites (C-F), 13 somites (G-L) and 22 somites (M,N). Embryos were either photographed live (E,F), processed as whole mounts for *FoxD3in situ* hybridisation (A-D,G,H,M,N) or stained as H&E sections (I-L)at the levels indicated in G and H respectively.

(**A,B**) Lateral views of 6 somite embryos reveal a normal distribution of *FoxD3* positive NCC (stained blue) in the *Wnt1-Cre* embryo (A), which itself has a normal morphology. This is in contrast to the *Wnt1-Cre;ROSA26*$^{eGFP\text{-}DTA+}$ embryo (B), in which the pattern of *FoxD3* expression indicates that conditional DTA expression has ablated the anterior cranial premigratory and migratory NCC, although the later specified hindbrain rhombomere 4 and spinal premigratory NCC have not yet been ablated. The morphology of the neural tube in (B) has been altered by the ablation of the midbrain precursor cells so that the more posterior structures, such as rhombomere 4 in the hindbrain (highlighted by the expression of *FoxD3* and a black arrowhead), are displaced anteriorly.

(**C,D**) Lateral views of 8 somite embryos reveal that the wave of ablation of Wnt1 expressing cells and their progeny has progressed further caudally along the embryo, to include the NCC in rhombomere 4 and upper spinal region. Morphologically, the cranial region of the ablated embryo is reduced in size and appears dorso-ventrally 'flattened'.

(**E,F**) Frontal views of 8 somite *Wnt1-Cre* and *Wnt1-Cre;ROSA26*$^{eGFP\text{-}DTA+}$ embryos further illustrate differences in the morphology of the cranial neural tube. The normal apposition of the tips of the neural folds at the site of Closure 2 (white arrows in E) is not evident in the ablated embryo in which the neural folds in this region remain widely spaced (white arrow in F).

(**G,H**) Lateral views of 13 somite embryos reveal further progression of the wave of DTA ablation. Morphologically the forebrain and optic vesicles are evident in the most anterior neural tube of the ablated embryo (white arrowheads in G,H), whereas there is

no midbrain flexure (black arrowhead in G) (reflecting a lack of midbrain tissue in the ablated embryo).

(**I-L**) Sections taken through the site of Closure 2 in a *Wnt1-Cre* embryo (I,J) reveal apposition and contact of the neural folds (black arrowheads in I and J) and the optic vesicles (ov in J and L). This is in contrast to the unapposed neural folds of the *Wnt1-Cre;ROSA26*$^{eGFP\text{-}DTA+}$ ablated embryo (K,L). Closure is, however, progressing from the site of Closure 3 in the ablated embryo as in the non-ablated control (red arrowheads in I-L)

(**M,N**) By the 22 somite stage the wave of ablation has progressed more posteriorly in the ablated embryo (N). Morphologically cranial closure is complete in the *Wnt1-Cre* embryo (M), in contrast to the *Wnt1-Cre;ROSA26*$^{eGFP\text{-}DTA+}$ ablated embryo (N) in which closure has spread from Closure 3 in the most anterior region around the forebrain (a site where ablation has not occurred) and from Closure 1 (which preceded ablation) caudally along the spine. The region between these sites (presumptive hindbrain) remains open (indicated by a black line in N). The straightening of the forebrain (i.e. loss of cranial flexure) in the ablated embryo results in a gap between the first branchial arch and the anterior forebrain (asterisk in N) which is not evident in M. Note *FoxD3* expression in the low spinal region where NCC specification continues, in advance of the caudal wave of Wnt1-Cre mediated ablation.

Abbreviations: b, branchial arch 1; ov, optic vesicle. Scale bars represent 100 μm.

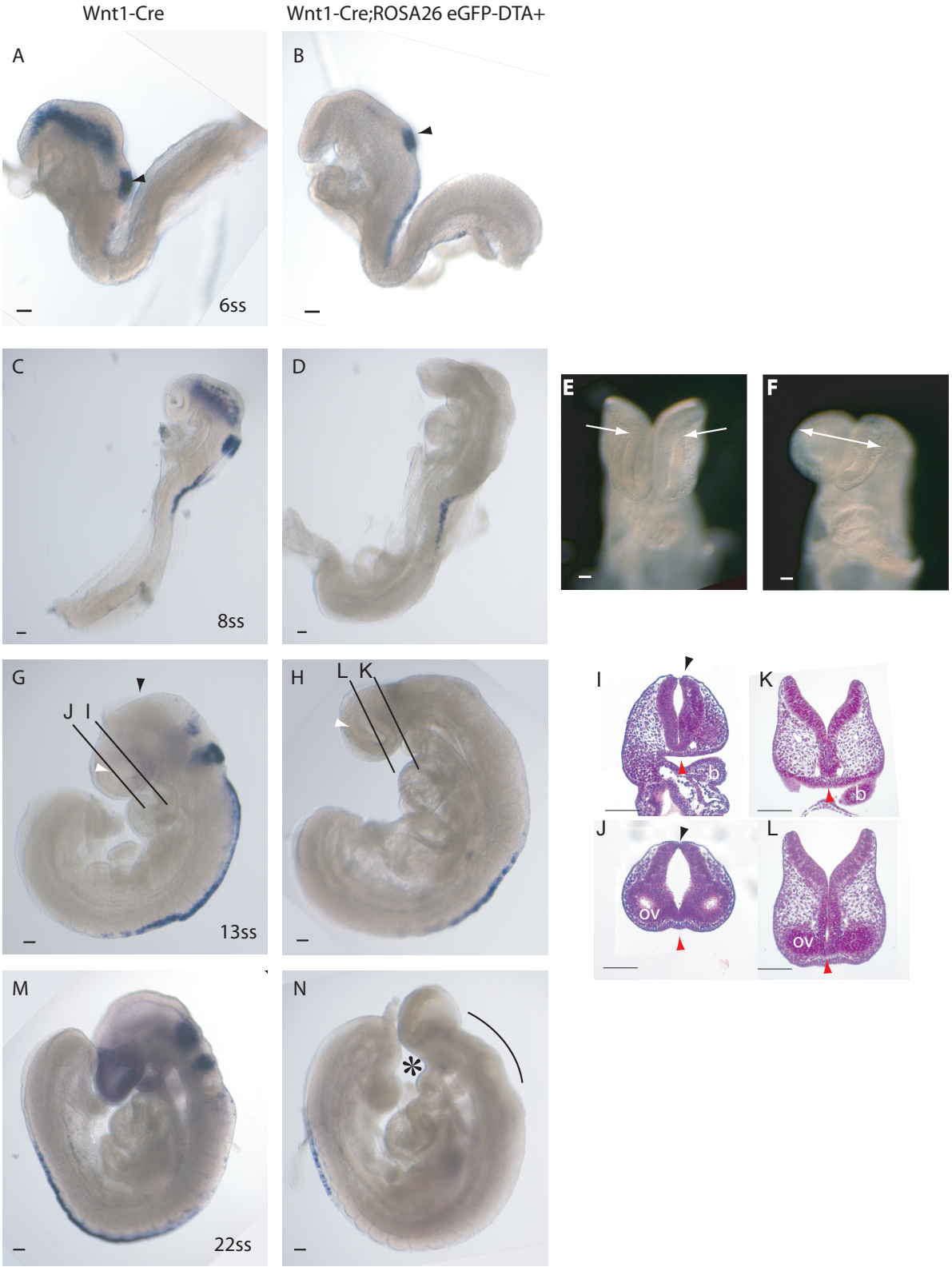
Wnt1-Cre
Wnt1-Cre;ROSA26 eGFP-DTA+
A
B
6ss
C
D
8ss
E
F
G
J I
H
L K
13ss
I
K
b
b
J
L
ov
ov
M
N
22ss

Unlike Closure 2, normal Closure 3 is evident in both ablated and non ablated embryos (red arrowheads in Figure 3.4 I-L). At the latest stages depicted when the cranial and much of the spinal neural tube is closed in the normal, non-ablated embryo (Figure 3.4 M) the neural tube of ablated embryos is open in the presumptive hindbrain region (indicated by a black line in Figure 3.4 N), although zipping closure from Closure 3 has progressed around the forebrain. The NCC defects obvious from the overall morphology of the embryos are visible in BA1. That of the non-ablated embryo is shaped like a boot, angled upwards towards the ventral anterior forebrain (Figure 3.4 M). The NCC deficient BA1 of the ablated embryo, however, although not significantly reduced in size, protrudes perpendicularly from the ventral aspect of the embryo (asterisk in Figure 3.4 N).

3.4. DISCUSSION

Numerous mouse mutants have been described in the literature in which neurocristopathies are associated with cranial NTDs. In these descriptions, however, the mechanism by which defects of NCC and neural tube closure are associated has rarely been addressed, and the idea of a cause-effect relationship existing between the two processes has been neither proposed nor studied in the mutant models.

The aim of the current chapter was to investigate whether the proposal that NCC delamination is necessary for neural tube closure and specifically DLHP formation in the cranial region is borne out in the mouse models harbouring mutations in *Zic2* (*Kumba*) and *Pax3* (*Splotch*), both of which are known to demonstrate exencephaly (as well as spina bifida) in combination with NCC defects. Furthermore, the *Wnt1-Cre;ROSA26*$^{eGFP\text{-}DTA+}$ strain was studied to examine the effects on neural tube closure of ablating the NCC and midbrain.

3.4.1. ZIC2-KUMBA

The *Kumba*mouse harbours a mutation in *Zic2* which acts as a loss of function allele (Elms et al., 2003). This produces a NCC phenotype which has been attributed to a delay and reduction in NCC specification (Elms et al., 2003). The findings of the current study, however, are not in accordance with this conclusion, as normal levels of NCC specification were observed in the cranial region at early stages, followed by the loss of these NCC such that they are neither present in the neuroepithelium nor migrating in the periphery of the cranial region at later stages (or migrating in greatly reduced numbers).

This apparent conflict between the findings of previous studies and the current work may reflect the embryonic stages studied. The previous research looked at the presence or absence of NCC in 12 somite embryos, finding delayed and reduced specification of NCC in the caudal trunk region at this time. A reduction was also noted in the NCC migrating in the cranial region and this was assumed to reflect a delay and reduction in the specification of NCC in the cranial region.

The finding that early cranial NCC are specified normally in the absence of functional Zic2, but that subsequent NCC migration is defective, raises the question of what role Zic2 may play in cranial NCC development? The defect could reflect a failure

of NCC maintenance, proliferation or EMT. Zic proteins are known to be cell cycle regulators that maintain cells in a proliferative state and prevent differentiation (Brewster et al., 1998; Aruga et al., 2002; Ebert et al., 2003; Nyholm et al., 2007). This may imply that loss of Zic2 results in lack of proliferation and premature differentiation of NCC, inhibiting the expansion of this stem cell population.

The current findings in the trunk region are more consistent with the previous work which found a delay and reduction in NCC specification (Elms et al., 2003). An alternative explanation, however, could be that the trunk NCC are specified normally and then undergo the same fate as those in the cranial region. Elms et al identified no alterations in cell death or proliferation to explain the loss of trunk NCC, which was taken as further evidence in support of a failure of initial specification.

Around the time of cranial neural tube closure, the reduction in migratory NCC in this region associates with a failure of DLHP formation, which has been described previously in the *Kumba* mutant, although only in the caudal region (Ybot-Gonzalez et al., 2007). Thus, not only does the *Kumba* mutant provide a model in which exencephaly associates with NCC defects but, in accordance with the hypothesis of the current research, these two defects are associated with a failure of DLHP formation in the cranial region. Furthermore the NCC defects are associated with a reduction in cranial axial curvature, which may reflect a lack of expansion of the neural crest stem cell population in the cranial mesenchyme

The NCC phenotype in $Zic2^{ku/ku}$embryos is variable in expression and the correlation between the severity of the NCC phenotype and the cranial neurulation phenotype – ranging from apparently normal closure, through closure with HPE (occasionally compatible with postnatal survival in humans), to exencephaly (not compatible with post natal survival in humans) – is consistent with a cause-effect relationship between the two processes. The reduction in NCC in the spinal region at a level at which there is no NTD demonstrates that the NCC phenotype is not secondary to the neurulation defect. The inverse could still be true, however: the neurulation defect may result from the NCC defect, as is proposed in the hypothesis of the current research. A third possible explanation is that both the NCC and neurulation are dependent on some other factor.

It may not actually be appropriate to place the HPE and exencephalic phenotypes on a spectrum of cranial neurulation defects as the two defects are not commonly associated in the literature and may represent separate unrelated defects. HPE results from failure

or incomplete separation of the forebrain and is a midline defect. Evidence has been mentioned previously providing explanations for the HPE phenotype independent of the NCC phenotype (described in Chapter 3.1.1.) (Warr et al., 2008; Sanek et al., 2009).

The cause of the exencephalic defect in the *Kumba* mutant has not been addressed in the literature. The current hypothesis proposes that the defect of early NCC development results in the failure of cranial DLHP formation and this in turn results in the failure of cranial neural tube closure. Studies in the zebrafish have demonstrated an involvement of Zic2 in the formation of cranial DLHPs, which actually form following neural tube formation in the zebrafish, but perhaps via conserved mechanisms (Nyholm et al., 2009). However the failure of DLHP formation in that study was attributed to defects in canonical Wnt signalling affecting actin and myosin.

3.4.2. SPLOTCH (Sp^{2H})

Numerous NCC defects have been described in *splotch* mutants including defects of the cardiac outflow tract, melanocytes (a white belly spot characterises heterozygotes), vagal NCC derived enteric ganglia, thymus, thyroid and parathyroid glands and the glossopharyngeal (IX) and vagus (X) nerves (Franz, 1989; Tremblay et al., 1995; Conway et al., 1997; Lang et al., 2000; Hornyak et al., 2001). It is immediately apparent that as described in the literature, there are no anterior cranial NCC defects: cranial NCC appear to be normally specified at early stages and subsequently migrate normally.

A lack of *FoxD3*-positive cells was observed in the neuroepithelium of the post-otic hindbrain and cervical region (to somite 7) and NCC were not observed migrating from these axial levels in the Sp^{2H} homozygous mutant. The axial level at which defects were observed in the current research coincides precisely with the levels of origin of the defective NCC derivatives described in the literature which are listed above (Le Douarin and Teillet, 1973; Bockman and Kirby, 1984; Chan et al., 2004). These NCC defects described in the literature have been attributed to a range of causes, including reduced proliferation, abnormal migration pathways and defective signalling at the target organs (Henderson et al., 1997; Conway et al., 2000; Lang et al., 2000). However, the current findings imply that the reduction in NCC specification may be an underlying cause for the range of defects of NCC derivatives arising in this specific region of the neural tube.

DRG defects are described frequently in the literature regarding the *splotch* model and the defects are usually described as being more severe caudally, with the most caudal DRG being completely absent (Auerbach, 1954; Franz, 1992; Tremblay et al., 1995; Serbedzija and McMahon, 1997). Defects are also described in other NCC derivatives in the caudal trunk region, including Schwann cells and NCC derivatives in the kidney (Grim et al., 1992; Itaranta et al., 2009). The cause of these NCC defects cannot lie in their abnormal specification, as posterior to the cervical region, the specification and early migration of NCC appeared normal in the current study of *splotch* embryos.

The finding that cranial NCC are specified and migrate normally in Sp^{2H}homozygous mutants indicates that, while expressed throughout the dorsal neural folds at all levels of the body axis, Pax3 is not required for NCC specification, proliferation or delamination in all NCC. Rather, Pax3 may play a role in proliferation of a specific subset of NCC, restricted perhaps by their location in the trunk region or alternatively by the time of their specification. This provides evidence supporting very early lineage restriction in the NCC population. Furthermore, the finding that NCC of the post-otic hindbrain and cervical spine appear unspecified (as judged by *FoxD3* expression) in the absence of functional *Pax3*, unlike those of the more caudal spine, indicates a further subdivision in the NCC population.

It is interesting to note that while in the mouse no cranial NCC defects are ever noted in *Pax3* mutants, human Waardenburg syndrome types I and III, which is associated with disruption of the *PAX3* gene, is associated with specifically cranial phenotypes. These include craniofacial abnormalities (such as a short maxillary process), pigmentation defects and sensori-neural deafness (resulting from defective melanocytes) (Tassabehji et al., 1992; Da-Silva et al., 1993; Hoth et al., 1993; Wollnik et al., 2003). These abnormalities are attributable to defects in the development of the NCC arising anterior to the otic vesicle in rhombomeres 1 to 4 and the midbrain. This marks a distinction between the roles of mouse and human *Pax3/PAX3* in cranial NCC development.

The aim of the current research was to determine whether defective cranial NCC delamination might cause exencephaly by preventing the formation of DLHPs. In the Sp^{2H}homozygous mutant, the two defects can be dissociated. The neurocristopathies are limited to derivatives of the trunk neural crest, while NCC in the cranial region, at the site of DLHP formation, are specified and migrate normally. Under these circumstances DLHPs are formed and Closure 2 occurs normally. The exencephaly in

Sp^{2H}homozygotes results from failure of the posterior midbrain or anterior hindbrain to close. This dissociation replicates previous findings in *splotch* in which the severity of both exencephaly and spina bifida were shown to be unrelated to the presence or severity of NCC defects (Franz, 1992; Tremblay et al., 1995; Conway et al., 1997). Moreover, it has been possible to dissociate the NTD and neurocristopathy defects by rescue of one without affecting the other (Fleming and Copp, 2000; Kwang et al., 2002). Furthermore, the NCC and neural tube phenotypes are dissociated in humans as, despite the presence of cranial NCC defects, anencephaly has only rarely been reported in Waardenburg syndrome (Aymé and Philip, 1995).

3.4.3. Wnt1-Cre;ROSA26$^{eGFP\text{-}DTA+}$

Crossing together the *Wnt1-Cre* and *Rosa26R* mouse lines allowed lineage labelling of Wnt1 expressing cells and their progeny. These cell populations were identified as the isthmus or mid-hindbrain organiser (MHO) at early stages, followed by the dorsal neural tube (in which *Wnt1* and *Cre* expression was upregulated in a rostrocaudal wave) and the derivatives of these cells including the NCC. This confirmed previous findings (Rowitch et al., 1997; Chai et al., 2000; Jiang et al., 2000).

Crossing together the *Wnt1-Cre* and *ROSA26*$^{eGFP\text{-}DTA+}$ mouse lines caused the specific ablation of *Wnt1* expressing cells. In keeping with the dynamic expression pattern of *Wnt1* in the developing embryo, the cell ablation began in the cranial region with the MHO. Signals emanating from this organising centre (such as FGF8) are known to be responsible for development of the entire midbrain as well defining the identity of rhombomere 1 and the posterior forebrain (Joyner et al., 2000; Simeone, 2000; Chi et al., 2003). Thus, ablation of the MHO (and signals emanating from it) results in a loss of posterior forebrain, midbrain and hindbrain rhombomere 1 tissue, replicating previous findings (Ivanova et al., 2005) and the phenotype of mutants conditionally lacking FGF8 expression in the MHO (Chi et al., 2003). Concomitant to this early loss of cranial tissue there are never any *FoxD3* positive NCC specified in the cranial region.

In the trunk of the normal embryo, the BMP inhibitor noggin is down-regulated in a rostrocaudal wave controlled by the developing somites, and the subsequent up-regulation of BMP4 signalling induces a rostrocaudal wave of Wnt1 expression (Burstyn-Cohen and Kalcheim, 2002; Burstyn-Cohen et al., 2004). The up-regulation of

Wnt1 signalling is involved in the rostrocaudal wave of NCC specification and delamination in the normal embryo (Deardorff et al., 2001). However, in the DTA ablated embryos Wnt1 expression results in a rostrocaudal wave of NCC ablation which follows specification, but precedes migration.

Morphologically, the result of the ablation of Wnt1 expressing cells is a loss of DLHPs and lack of Closure 2, a reduction in cranial tissue, reduced cranial flexure and exencephaly. Although these phenotypes are similar to those noted in association with reduced numbers of migrating NCC in the *Kumba* model, they are most simply explained by the loss of the midbrain structures of ablated embryos, which are the site of all these features. Hypoplasia of the 1stbranchial arch of ablated embryos also resembles that noted in the *Kumba* mutant, and in this instance the defect is attributable to a loss of NCC.

According to the current hypothesis, the delamination of NCC facilitates DLHP formation and subsequent closure of the neural tube at Closure 2, overcoming the high degrees of mechanical tension opposing closure in this region. The ablation of NCC by the transgenic expression of DTA may have mimicked the hypothesised effect of NCC delamination in enhancing the mechanical flexibility of the dorsal neural tube. However study of this effect is precluded by the earlier ablation of the entire midbrain region.

3.5. CONCLUSIONS

The question posed in the current research was whether NCC delamination from the midbrain dorsal neural tube acts to enhance the mechanical flexibility of this region and thus facilitate DLHP formation and subsequently Closure 2 and completion of cranial closure. Three mouse mutants were studied in which NCC defects are known to associate with exencephaly in order to determine whether the NCC defects could be causative for the exencephalic phenotype in these models.

In the *Zic2-Kumba* mutant, an association exists between early cranial NCC defects, failure of DLHP formation and exencephaly. Furthermore these embryos demonstrate a reduction in cranial tissue and cranial flexure. The effects observed in the *Kumba* mutant are, however, confused by the presence (in some embryos only) of an additional defect of HPE which also alters the morphology of the cranial region.

The *Splotch* mutant, in contrast, demonstrates a dissociation between NCC defects (which were observed only in the trunk region) and failure of cranial neural tube

closure. There was no evidence of disruption of DLHPs and the exencephalic phenotype was usually evident in the hindbrain region, unrelated to DLHP formation or Closure 2. It remains to be determined what is the cellular and morphogenetic basis of exencephaly in *Splotch* mutants.

The *Wnt1-Cre;ROSA26*$^{eGFP\text{-}DTA+}$ genetic ablation model lacked NCC and this was also associated with a lack of DLHPs and Closure 2, reduction in cranial tissue and flexure and exencephaly. However all the aspects of this phenotype are attributable to a lack of midbrain tissue, rather than a lack of NCC or DLHPs themselves.

The findings regarding the study of mouse mutants are therefore inconclusive. They neither prove nor disprove the hypothesis that NCC delamination is necessary for DLHP formation and cranial closure. They do, however provide some support for this hypothesis in the correlation of the failure of NCC development in *Kumba* with lack of DLHPs, in contrast to the normal NCC development and normal DLHP formation observed in *Splotch.*

CHAPTER 4

INHIBITION OF NCC DELAMINATION IN THE MOUSE AND CHICK

4.1. INTRODUCTION

The evidence from the previous chapter on the study of mouse mutants indicated that defective NCC development is associated with a failure of DLHP formation (as well as a reduced angle of axial curvature and reduction in cranial tissue) in the *Kumba* mutant. However, these findings do not provide conclusive evidence to confirm or refute the hypothesis that NCC delamination is necessary for DLHP formation and cranial neural tube closure. The aim of this chapter, and the following chapter, is to test this hypothesis experimentally by directly manipulating the development of NCC in embryos during the pertinent window of development. In the present chapter, chemical inhibitors of NCC delamination were applied to cultured mouse embryos, and to chick embryos *in ovo*. In Chapter 5, a transgenic gene knockdown approach was used, with the aim of inhibiting NCC delamination *in vivo*.

4.1.1. SELECTING AN INHIBITOR OF NCC DELAMINATION IN THE MOUSE

The findings of Chapter 2 indicate that the midbrain region of the mouse may be subject to high degrees of mechanical tension opposing closure and that the formation of DLHPs in this region may act to compensate for these forces and allow closure. To test experimentally whether delamination of NCC from the dorsal neural tube is required for DLHP formation and subsequent closure, a specific inhibitor of NCC delamination was required. It was decided that inhibition of NCC specification, proliferation or survival would not be an appropriate goal, as such effects might have implications for the structure of the dorsal neural folds, unrelated to delamination. Conversely inhibition of migration was not expected to affect the structure of the neural folds, and so was also not considered a suitable target of inhibition.

In order to delaminate from the pseudostratified neuroepithelium and migrate into the adjacent mesenchyme NCC must undergo an epithelial-to-mesenchymal transition (EMT). Epithelial markers are down regulated, epithelial characteristics such as cell-cell adhesion are lost and the cells acquire the characteristics of migratory mesenchymal cells, penetrating the basement membrane and invading the extracellular matrix (ECM); see section 1.2.2.2. EMT is characteristic of several developmental and pathogenic remodelling and migratory processes, including gastrulation and carcinoma metastasis (reviewed in (Thiery, 2003).

The matrix metalloproteinases (MMPs) are a family of zinc proteolytic enzymes involved in degradation of the ECM, thus facilitating cell-ECM interaction, remodelling and cell migration (Sternlicht and Werb, 2001). A review of the literature identified MMP-2 and -9 as molecules whose upregulation is intimately associated with EMT in both normal and metastatic cells. In cancer research, both MMP-2 and -9 are widely used as markers of EMT in malignant cells and their inhibition reduces metastasis both *in vitro* and *in vivo* (Chambers and Matrisian, 1997; Hofmann et al., 2000; Kosaka et al., 2010).

There is also evidence that MMP-2 is necessary for EMT during NCC development. In the chick and the mouse, MMP-2 is expressed in epithelial tissues at the onset of EMT and inhibition of MMP-2 by chemical inhibitors or morpholinos prevents the dispersal of NCC *in vivo* and *in vitro* (Erickson and Isseroff, 1989; Robbins et al., 1999; Cai and Brauer, 2002; Duong and Erickson, 2004). The murine *Patch* mutation harbours a deletion of the alpha subunit of the platelet-derived growth factor receptor and embryos homozygous for this mutation exhibit multiple NCC related defects in association with a reduction in MMP-2 expression (Stephenson et al., 1991; Morrison-Graham et al., 1992; Schatteman et al., 1992).

A number of commercially available synthetic MMP inhibitors have been used to block EMT and subsequent migration of NCC in chick embryos, both *in vivo* and *in vitro*. These include the broad spectrum hydroxamate based MMP inhibitors KB8301 (which is no longer available) and GM6001, which block the enzymatic activity of MMP-2, 3, -8, and -9 (Cai & Brauer, 2002; Anderson et al., 2006). Recently, the effects of GM6001 on the invasive capacities of the NCC have been replicated with a new MMP-2/-9 specific inhibitor, SB-3CT, and expression studies implicated MMP-2 specifically as being responsible for the effects observed (Anderson, 2010). Since, SB-3CT only became commercially available after the start of the studies in this chapter, GM6001 was used as a tool to inhibit NCC delamination in the mouse.

4.1.2. SELECTING AN INHIBITOR OF NCC DELAMINATION IN THE CHICK

The processes of chick neurulation were studied in section 2.3.4. and 2.4.2 and were shown to differ significantly from neurulation in the mouse. The predicted levels of mechanical tension opposing closure of the cranial neural folds are low as there is little axial curvature and the neural folds are small, inverted and narrow. The hypothesis of the current research predicts, therefore, that NCC delamination would not be required to assist in the closure of this region. This is in accordance with the finding that the delamination of NCC from this region occurs after closure of the neural tube. Thus inhibition of NCC delamination would be predicted to have no effect on cranial closure in the chick model.

Inhibition of NCC delamination in chick neural tube explants has been demonstrated previously by the use of *Clostridium botulinum* exotoxin C3, an inhibitor of *RhoB* activity (Liu and Jessell, 1998). Rho proteins are small GTP-binding proteins of the ras superfamily. *RhoB* is induced by BMP activity and is expressed in the chick dorsal neural tube soon after NCC specification. Expression persists until shortly after delamination (Liu & Jessell, 1998; Del Barrio and Nieto, 2004). This is in contrast to the expression of *RhoB* in the mouse embryo in which it is not detectable in NCC before emigration, but is expressed in the migratory NCC (Henderson et al., 2000).

Rho proteins have been implicated in many cell functions including adhesion and motility as well as signal transduction, especially through regulation of the actin cytoskeleton (Hall, 1998; Hall and Nobes, 2000). These are all characteristics of EMT, and inhibition of *Rhob* using C3 in chick NCC disrupts the organisation of the cytoskeleton and impairs their ability to undergo EMT (Liu & Jessell, 1998). Thus C3 was identified as a suitable inhibitor of NCC delamination in the chick embryo.

4.2. METHODS

Riboprobe preparation, whole mount ISH, embedding, sectioning, mounting, light microscopy and photography were conducted as described in section 2.2.

4.2.1. INHIBITOR TREATMENT IN MOUSE WHOLE EMBRYO CULTURE

E8 mouse embryos of the CD1 random bred strain were dissected in a similar manner to that described in Chapter 2, except that the yolk sac and amnion were maintained intact.

The GM6001 MMP inhibitor (Chemicon) was reconstituted in a minimum quantity of DMSO solvent and then made up to 100 mM stock concentrations with PBS and aliquotted before freezing. Working concentrations of 100 μM were prepared, containing 1% Fast Green to aid in visualisation.

The inhibitor (or a vehicle control at the same DMSO concentration) was microinjected into the amniotic cavity. For this procedure, embryos were placed in culture medium in a petri dish on the stage of a stereomicroscope and inhibitor solution was injected into the amniotic cavity using a mouth controlled, hand-held, fine glass micropipette, which had been pulled on an electromagnetic pipette puller and broken to a tip diameter of approximately 10-20 μm. Injection was continued until the amnion was seen to bulge and/or injected solution leaked back from the injection site. Injection volume was approximately calibrated by measuring similar amounts of inhibitor solution expelled onto a dry petri dish and measured using a P2 Gilson pipette.

Whole embryo culture was by the method described previously (Copp et al., 2000). Embryos were transferred to culture tubes (50 ml plastic universals) containing 1 ml rat serum per embryo (up to a maximum of 3 embryos per tube). A gas mixture of 5% CO_2, 5% O_2 and 90% N_2 was gently blown in and the tubes were sealed. The gas atmosphere was replenished every 12 h. The tubes were maintained at 37°C in the dark in a rolling culture system (approximately 30 rpm). Embryos were removed after 24 or 36 h and viability was measured by yolk sac circulation. Only embryos with clearly visible blood circulation in the yolk sac vessels were analysed further. Somite number was also counted and did not differ significantly between groups after 24 h (mean $\pm$ SEM somite number: 9.3 $\pm$ 0.47 in treated group N=12; 9.57 $\pm$ 0.37 in control group N=14; $p = 0.688$) nor after 36 h. (mean $\pm$ SEM somite number: 16.6 $\pm$ 0.81 in treated group N=5; 15.78 $\pm$ 0.86 in control group N=9; $p = 0.544$).

4.2.2. INHIBITOR TREATMENT IN CHICK WHOLE EMBRYO CULTURE

The exoenzyme C3 RhoB inhibitor (Calbiochem) was reconstituted in 50 µl Milli-Q water to a stock concentration of 1 µg/µl. A working concentration of 50 µg/ml was established by dilution with 1% Fast Green in PBS. Chick embryos were accessed after 30 h of incubation as described in Chapter 2, except that they were not removed from the egg. Filtered Indian ink was mouth pipetted beneath the surface of the embryo to aid in visualisation. The C3 inhibitor (or a 1% Fast Green and PBS control) was microinjected into the neural groove beneath the vitelline membrane and the eggs were incubated for up to a further 24 h before removal of the embryos for analysis.

4.3. RESULTS

4.3.1. INHIBITION OF NCC DELAMINATION IN THE MOUSE

Labelling of *FoxD3*-positive NCC revealed the normal rostrocaudal wave of NCC specification in the dorsal neuroepithelium, and subsequent NCC delamination and migration into the periphery during normal development. This was true of both untreated cultured embryos and those treated with the DMSO vehicle (Table 4.1, Figure 4.1 A, E and I, and data not shown). This is in contrast to those treated with 100 μM GM6001, which displayed NCC specification in the dorsal neuroepithelium but a significant reduction in *FoxD3* positive NCC migrating into the periphery. Defects of the 1st branchial arch were evident in some of the oldest treated embryos whereby the branchial arch was hypoplastic and separated from the ventral forebrain reflecting reduced NCC colonisation (black arrowhead in Figure 4.1 J). The MMP inhibitor caused a massive reduction in NCC delamination and migratory NCC although embryos displayed normal NCC specification posterior to the NCC free region of rhombomere 3 (at the developmental stages tested) (Figure 4.1 C, G and J). A few NCC were evident in the dorsal neural folds of the cranial region of the early embryo (Figure 4.1 C) however, after their failure to migrate, the NCC became undetectable in the neuroepithelium.

A reduction in NCC delamination and migration causes morphological alterations in the neural tube. The untreated and DMSO control embryos demonstrated normal cranial morphology, in contrast to the abnormal appearance of the treated embryos (Table 4.1). DLHPs failed to form at the fore-/midbrain boundary (white arrows in Figure 4.1 D and H), preventing the normal apposition and fusion at the site of Closure 2 (white arrows in Figure 4.1 B and F). This was despite normal closure at the site of Closure 3 (white arrowhead in Figure 4.1 H). Treated embryos also demonstrated a reduction in the angle of the cranial flexure which emerged after turning (Figure 4.1 G and J in contrast to the acute angle observed in E and I). After 36 h in culture, the somite stage of the embryos ranged from 15 to 19 and neural tube closure was completed in all control and untreated embryos which had reached beyond the 17 somite stage. Exencephaly was observed in 2 of the 3 embryos treated with MMP inhibitor that reached this stage (Table 4.1).

Figure 4.1. NCC Development in Embryos Cultured with MMP Inhibitor
Embryos at the 8 somite (A-D), 10 somite (E-H) and 18 somite (I,J) stage, following 24 h (A-H) and 36 h (I,J) culture in the presence of DMSO (A,B,E,F,I; vehicle control) or 100 mM MMP inhibitor (C,D,G,H,J). Embryos were fixed and prepared as whole mounts for *FoxD3 in situ* hybridisation.

(**A-D**) At the 8 somite stage, the MMP inhibitor treated embryo (C) displays a marked reduction in migratory NCC compared with the control treated embryo (A) (blue staining in the cranial mesenchyme). There is, however, no build up of non-migrating NCC in the neuroepithelium, as would be indicated by enhanced *FoxD3* expression at the neural fold edge. The NCC in the neuroepithelium of rhombomere 4 and the spinal region are specified as normal in the inhibitor treated embryo. Frontal views of the embryos reveal that apposition of closure 2 (white arrows in B) is perturbed in the treated embryo (D) in which the forebrain/midbrain neural folds remain widely spaced (white arrow in D).

(**E-H**) The same reduction in migratory but not in pre-migratory NCC is evident in the 10 somite inhibitor treated embryo (G,H), compared with the control treated embryo (E,F). The apposition of Closure 2 as seen in the control embryo (white arrows in F) is severely perturbed in the inhibitor treated embryo (white arrows in H) . Initiation of Closure 3 is evident in both control and inhibitor treated embryos (white arrowheads in F and H). There is a reduction in cranial size and in the angle of midbrain flexure in the inhibitor treated embryo (G) compared with DMSO-treated control (E).
(**I,J**) By the 18 somite stage, migratory NCC are largely absent from the cranial and upper spinal regions of the inhibitor treated embryo (J), apart from some expression at the site of the cranial ganglia. By contrast, the control treated embryo exhibits extensive migrating NCC (I). Note the normal specification of NCC in the lower spinal region of both control and inhibitor treated embryos (I,J). While closure of the cranial neural tube is complete in this inhibitor treated embryo, it is with an abnormal morphology. The cranial region is reduced in size, there is a reduction in the angle of midbrain flexure, an indentation in the hindbrain, at rhombomere 4 (red arrowhead), and an increased distance between the anterior forebrain and the first branchial arch (black arrowhead).

Scale bars represent 100 μm.

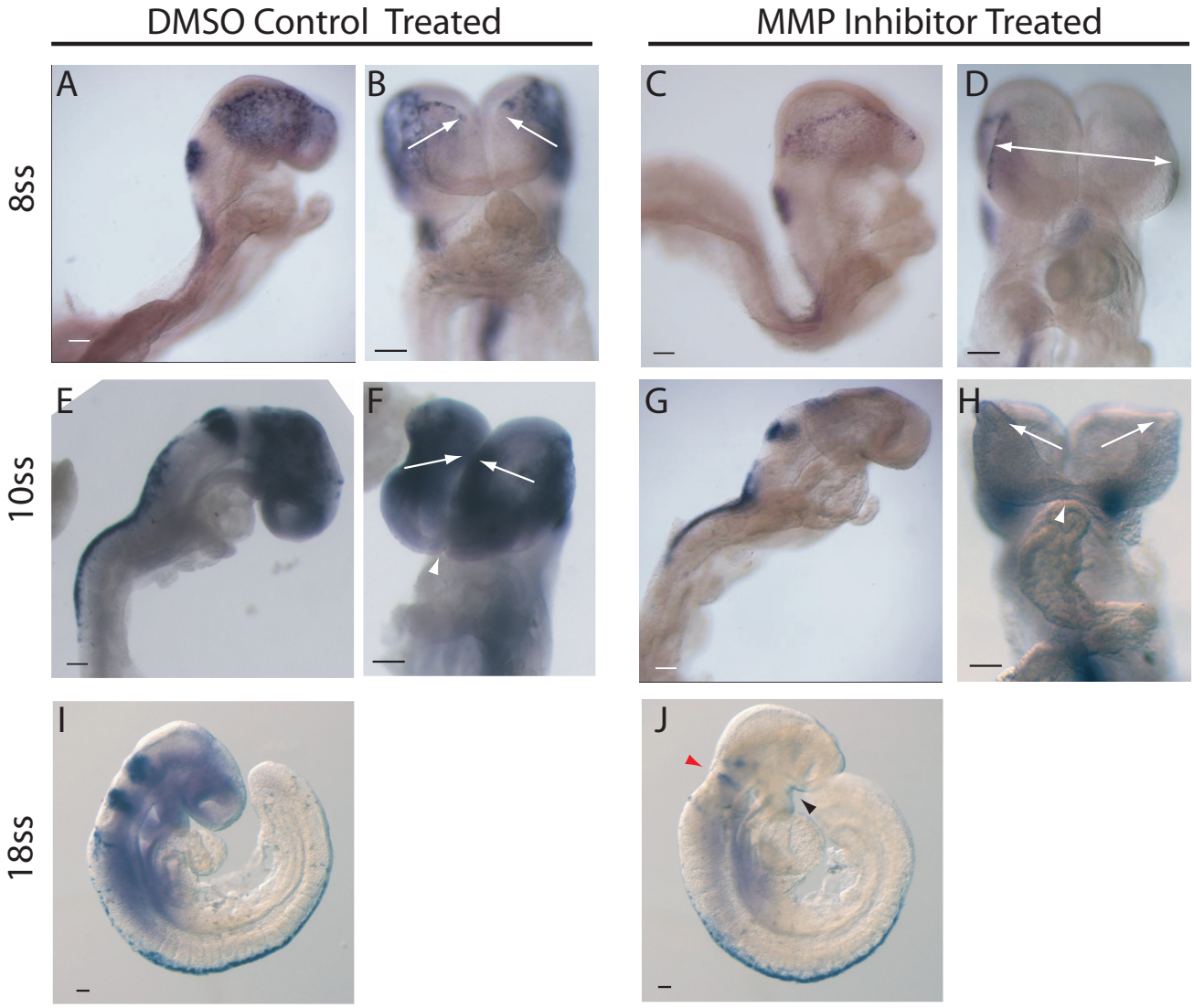
DMSO Control Treated
MMP Inhibitor Treated
8ss
10ss
18ss
A
B
C
D
E
F
G
H
I
J

Table 4.1. Mouse embryos exposed to MMP inhibitor in culture

	UNTREATED		DMSO CONTROL		GM6001 (100 μM)	
Embryos retrieved after:	24 h	36 h	24 h	36 h	24 h	36 h
Number of embryos	16	14	14	9	12	5
Mean number of somites	10	17	10	16	9	17
Standard Error	0.896	1.165	0.902	1.424	0.988	1.962
Abnormal NCC patterning	0 (0%)	0 (0%)	0 (0%)	0 (0%)	9 (75%)	4 (80%)
Failure of DLHPs and reduced axial curvature.	0 (0%)	0 (0%)	0 (0%)	0 (0%)	6 (50%)	2 (67%)
Exencephaly *	N/A	0/9 (0%)	N/A	0/4 (0%)	N/A	2/3 (67%)

* Only assessed in embryos with 17 somites or more (when cranial closure is normally complete). N/A indicates groups in which all embryos had less than 17 somites.

4.3.2. INHIBITON OF NCC DELAMINATION IN THE CHICK

In situ hybridization for cSox10 revealed a reduction (although not absence) of migratory NCC in the C3-treated chick embryos (Figure 5.2 D-F) in contrast to the PBS-treated control embryos (Figure 5.2 A-C). A reduction in NCC delamination and migration does not appear to have altered the morphology or closure of the neural tube.

Figure 4.2. RhoB Inhibition Reduces Delamination of NCC in the Chick Embryo
Chick embryos cultured for 24 h in the presence of PBS, as control (A-C), or RhoB inhibitor (D-F) were processed as whole mounts for *in situ* hybridisation with *cSox10* as a marker of premigratory and early migratory NCC. White arrowheads indicate the caudal extent of NCC specification and red arrowheads indicate migratory NCC throughout (A-F).

(**A,D**) The control embryo at 11 somites (A) demonstrates normal NCC patterning in which the wave of NCC specification has progressed into the anterior spinal region, adjacent to the first somite, and the delamination and migration of NCC is underway in the cranial region, as far as the NCC free region at rhombomere 3. The inhibitor treated embryo (D) displays a reduction in the intensity of staining in the migratory population as well as in the premigratory NCC of the cranial region, rhombomere 4 and into the spinal region. Morphologically the treated embryo looks unaltered compared with the control embryo.

(**B,E**) At 13 somites, the normal anterior-posterior spread of NCC specification (as far as the seventh somite) and migration (as far as the first somite) is observable in the control treated embryo (B). In contrast there is a reduction in migrating NCC (especially in the cranial region) in the inhibitor treated embryo (E). As with the 11 somite stage, the neural tube appears normal in the inhibitor treated 13 somite embryo.

(**C,F**) NCC specification has reached the level of the eleventh somite and migration has begun up to the sixth somite in the 15 somite control embryo (C). The levels of NCC specification and migration are both much reduced in the inhibitor treated embryo (F). This does not, however, appear to have affected the neural tube's morphology or closure.

Scale bars represent 500 μm.

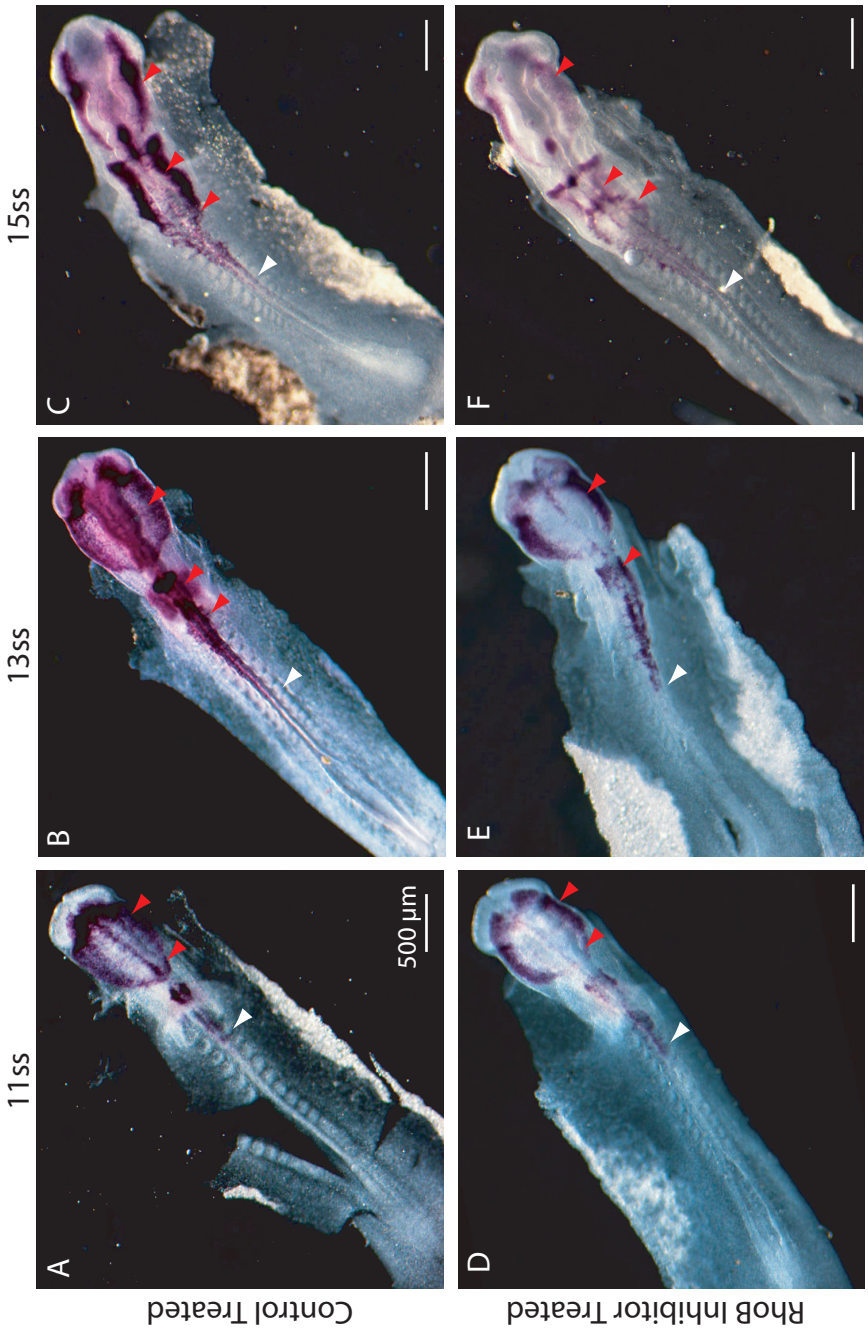
11ss
13ss
15ss
A
B
C
D
E
F
500 µm
Control Treated
Rhob Inhibitor Treated

4.4. DISCUSSION

The association of neurocristopathies and cranial NTDs in the mouse and in human pathology led to the proposal that NCC emigration and neural tube closure in the cranial region may be causally related. A detailed study of these two processes in Chapter 2 raises the possibility that NCC delamination may assist in the formation of DLHPs and subsequent closure of the midbrain neural tube in the mouse. Apposition of the midbrain neural folds appears to be resisted by high degrees of mechanical tension, as indicated by the degree of axial curvature and the biconvex morphology of the neural folds. The findings from the *Zic2-Kumba* mutant mouse strain (Chapter 3) in which NCC defects are associated with failure of DLHP formation and exencephaly provide support for this hypothesis.

The current chapter aimed to test this hypothesis experimentally by inhibiting NCC delamination in two species in which the results are predicted to differ. In the mouse, since the midbrain is predicted to be subject to high degrees of mechanical tension resisting neural fold apposition, it was hypothesised that delamination of the NCC would be necessary to facilitate DLHP formation and midbrain closure. Hence, chemical inhibition of NCC delamination in cultured mouse embryos should inhibit DLHPs and midbrain closure. In contrast to the mouse, the chick shows little axial curvature during cranial neurulation and has small inverted midbrain neural folds. Hence, mechanical tension resisting closure is inferred to be low and it was hypothesised that delamination of the NCC would not be necessary for midbrain closure in the chick.

4.4.1. INHIBITION OF NCC DELAMINATION IN THE MOUSE

The MMP inhibitor GM6001 has been used previously to inhibit the delamination of NCC in chick neural tube explants and further studies demonstrated that this effect was attributable to its inhibition of MMP-2 (Cai & Brauer, 2002; Anderson, 2010). The current studies demonstrated that GM6001 also inhibits the delamination of NCC in cultured mouse embryos, evident both as a lack of NCC migrating in the cranial mesenchyme and subsequent morphological defects of the 1st branchial arch.

NCC appear to be normally specified in the presence of the MMP inhibitor but, following their failure to delaminate, surprisingly, they do not accumulate in large numbers in the

neuroepithelium. In contrast they seem to disappear. Cell intrinsic and extrinsic cues govern the survival and proliferation of NCC and proper timing and direction of migration is required for them to encounter the cell extrinsic cues necessary for survival and differentiation (Tapadia et al., 2005; Knight and Schilling, 2006). Thus by remaining in the neuroepithelium the NCC do not encounter the necessary signals for maintenance, proliferation and survival and may dedifferentiate, fail to expand or undergo apoptosis. Further studies would be required to determine the fate of these cells whose emigration has been blocked.

Importantly, embryos in which NCC delamination was inhibited show a high frequency of failure of DLHP formation in association with reduced cranial flexure. This reduction in cranial flexure is presumed to be attributable to a lack of NCC entering into, and proliferating within, the cranial mesenchyme. At later stages, delay or total failure of midbrain neural tube closure was observed, an event that is highly dependent on DLHP formation (Jacobson and Tam, 1982). However, the number of embryos studied at this later stage was small, owing to the technical difficulty of maintaining mouse embryos in culture for periods exceeding 24 h. Hence, the relatively small time window during which the effects of inhibition of NCC delamination could be observed limited the usefulness of these culture experiments.

4.4.2. INHIBITION OF NCC DELAMINATION IN THE CHICK

Clostridium botulinum exotoxin C3 has been shown previously to inhibit *RhoB* activity and subsequently NCC EMT in chick neural tube explants (Liu & Jessell, 1998). The current studies were consistent with these findings *in vivo*, demonstrating a reduction in delaminating NCC after treatment with C3 exotoxin. The incomplete reduction in NCC delamination may be a reflection of the techniques used: previously, neural tube explants were bathed in the C3 toxin, allowing all NCC to become exposed to the inhibitor and resulting in a greater reduction in NCC delamination. This technique was not appropriate for the current research as it would have affected the morphology of neurulation. Instead the C3 toxin was microinjected beneath the vitelline membrane, into the neural groove region during a specific developmental window (just prior to NCC delamination). This method of application probably did not expose all NCC along the length of the neural tube throughout the duration of NCC specification to the toxin as a specific area was targeted and the toxin would disperse from this region over time. Nevertheless, C3

application in this study resulted in a reduction in NCC delamination affecting the NCC population which was exposed to the exotoxin.

Despite the considerable reduction in NCC delamination, closure of the chick cranial neural tube did not appear to be hampered in any way. This is in accordance with the predictions based on observations of chick neurulation in Chapter 2. The mechanical forces resisting cranial closure of the chick neural tube appear to be low, due to the lack of cranial flexure and the small, narrow, inverted neural folds, and there is no dorsolateral bending in the cranial region. Moreover, delamination of cranial NCC follows closure in the chick midbrain, in contrast to the pre-closure emigration of midbrain NCC in mouse embryos. These disparate findings in the mouse and chick models of neurulation demonstrate the importance of detailed comparisons between species before extrapolating data from one species to another.

4.5. CONCLUSIONS

The findings of the current chapter are in accordance with the hypothesis under test in this thesis. Inhibition of NCC delamination affected the morphology of the closing neural tube in the midbrain region, but not in other regions, of the mouse embryo. There was no apparent effect on the cranial morphology of the chick embryo. The mouse midbrain morphology resulting from inhibition of NCC delamination included a failure of DLHP formation and reduction in the angle of cranial curvature, as was also noted in association with defective NCC development in the *Kumba* mutant. Most importantly, when cultures reached the stage at which cranial closure should be completed (as confirmed in untreated controls), the majority of embryos with inhibition of NCC delamination showed persistently open cranial neural tubes (i.e. exencephaly).

Although these findings provide experimental evidence for a causal link between NCC delamination and midbrain closure, they are limited by the relatively short window of development which could be accessed using the whole embryo culture technique. In order to demonstrate that inhibition of NCC delamination increases the likelihood of exencephaly, a mouse mutant would be required in which NCC delamination is specifically targeted whilst leaving other aspects of midbrain development intact. In such a model neural tube closure could be observed *in vivo* at later stages than are accessible in embryo culture *in vitro*. One such approach involves transgenic gene knockdown of *Fox3*, as described in Chapter 5.

CHAPTER 5

CONDITIONAL KNOCKDOWN OF *FOXD3* IN A TRANSGENIC MOUSE

5.1. INTRODUCTION

The studies of Chapters 3 and 4 presented correlative evidence for a role for NCC delamination in the formation of DLHPs during cranial neurulation in the mouse. Furthermore the use of an inhibitor of NCC delamination in mouse whole embryo culture (Chapter 5) provided experimental evidence to support a role for NCC in DLHP formation, although the limited time for which cultures could be maintained precluded a detailed examination of the later resultant neural tube phenotype. For this reason, I decided to attempt an *in vivo* perturbation of NCC delamination using conditional transgenic technology, which would allow outcomes to be evaluated at later developmental stages. Genes were identified which have been proposed to be necessary for EMT of mouse NCC. Transgenic mice were then developed in which the expression of these genes was knocked down by the conditional expression of shRNAs specifically in the NCC.

5.1.1. IDENTIFYING GENES INVOLVED IN THE EPITHELIAL-TO-MESENCHYMAL TRANSITION OF MOUSE NEURAL CREST CELLS

The processes of EMT have been described in section 1.2.2.2 and a number of genes have been implicated as being important in the EMT of delaminating NCC in the mouse embryo. An obvious candidate whose targeted disruption was initially predicted to affect EMT in the NCC is *Snai1*. TheSnail gene superfamily encodes zinc finger transcriptional repressors which are known to be involved in the regulation of vertebrate EMT during gastrulation, carcinoma metastasis and NCC development (Carver et al., 2001; Murray et al., 2007; Olmeda et al., 2008).

Snai1 mediates the onset of EMT via repression of *E-cadherin* expression, which causes the destabilisation of epithelial structure. The tightly packed epithelial cells dissociate to become loosely organised mesenchymal cells (Cano et al., 2000). Knockout of the murine *Snai1* gene results in early embryonic lethality attributable to its role in the EMT at gastrulation: newly formed mesodermal cells fail to down-regulate *E-cadherin* and are incapable of migration, retaining epithelial characteristics (Carver et al., 2001). Hence, *Snai1* appeared a promising target for knockdown in order to perturb EMT in NCC in the present studies.

Another candidate gene which, based on studies in the chick, has been implicated in the EMT of NCC is the winged helix transcription factor *FoxD3*. One study found that *FoxD3*misexpression was sufficient to induce NCC specification and delamination from the neural tube, while others found that overexpression induced some of the features of EMT, but was not sufficient to disrupt the basement membrane (Xu et al., 1998; Dottori et al., 2001; Cheung et al., 2005). The studies were in agreement that *FoxD3*upregulates the expression of several cell adhesion molecules characteristic of migratory NCC, including HNK1, Cad-7, Integrin-β1 and Laminin. However, none proved that *FoxD3* is necessary for EMT in the NCC. Furthermore, these studies were conducted in the chick and some differences between the gene regulatory networks of chick and mouse embryos have already been described (section 1.2.2.2).

FoxD3 has been implicated in the maintenance of several pluripotent cell types, including cell lines and NCC in the chick studies (Dottori et al., 2001; Kos et al., 2001). The study of *FoxD3*'s role in the mouse NCC EMT has been limited by the early embryonic lethality (at E6.5) of the knockout mouse. This has been attributed to a requirement for *FoxD3* in the maintenance of pluripotent cells in the early embryo by the promotion of self-renewal and survival and the inhibition of differentiation (Hanna et al., 2002; Liu and Labosky, 2008). Indeed, the role of *FoxD3* in maintenance of multipotent progenitor cells could apply both in the early embryo prior to gastrulation, and in the neural crest population prior to delamination. Perhaps *FoxD3* is necessary for cells in both contexts to undergo the EMT without prematurely differentiating.

5.1.2. DEVELOPING A TARGETING STRATEGY

Having identified *Snai1* and *FoxD3* as genes that are likely to be involved in the EMT of mouse NCC, a strategy for investigating their effects on this process was developed, to inhibit EMT and determine its effect on neurulation. The early embryonic lethality of *Snai1* and *FoxD3* knockouts precluded their use for the analysis, as stages following the time of lethality needed to be studied. Thus, a conditional approach was required.

The development of a conditional knockout is a technically complex, expensive and time consuming process, and so an alternative transgenic approach was adopted utilising a relatively novel strategy of transgenic conditional RNA interference (RNAi). Short interfering (siRNA) sequences were identified which efficiently targeted *Snai1* and *FoxD3* mRNAs for degradation, resulting in protein knockdown. These sequences,

preceded by an RNA polymerase promoter and a floxed stop cassette, were randomly inserted into the genome of mice, via embryonic stem (ES) cells, to produce transgenic models in which *Snai1* and *FoxD3* could be conditionally knocked down upon crossing with a *Cre* expressing mouse line. The steps involved in the transgenic procedure are described in more detail in the following section.

Divergent roles have been identified for *Snai1* and *FoxD3* in regulation of the EMT; *Snai1* is associated with transcriptional repression of the epithelial cell adhesion molecule E-cadherin, while *FoxD3* is associated with upregulation of mesenchymal adhesion molecules such as Integrin-β1, Laminin and Cad-7. Furthermore the induction of NCC delamination by ectopic *FoxD3* expression in chick was shown to be independent of the Snail family member *Snai2* (which is upstream of *Snai1* in the chick model) (Dottori et al., 2001). Thus crossing of transgenic lines expressing shRNAs against *Snai1* and *FoxD3* might,in principle, be expected to have a compound effect on the NCC EMT, affecting both the downregulation of epithelial characteristics and the upregulation of mesenchymal characteristics.

5.1.3. TRANSGENIC shRNA TECHNOLOGY

RNAi is an endogenous system which acts to control the activity of genes via post-transcriptional regulation. RNAi is mediated by siRNA strands which are cleaved from double stranded RNA sequences by the enzyme Dicer and combine with the RNA induced silencing complex (RISC). This then targets complementary RNA sequences within the cell for degradation, thus knocking down expression of the coded gene (Hammond et al., 2000).

The RNAi pathway has been exploited to study the effects of knocking down genes of interest both *in vitro* and *in vivo* using a number of techniques. siRNAs can be generated and injected into individual cells or electroporated directly into cell cultures or regions of the developing embryo, followed by embryo culture (Calegari et al., 2002). Alternatively, DNA sequences can be generated which encode mirror image self-complementary sequences of RNA which are designed to bind to the RNA of interest. Upon transcription, short hairpin RNAs (shRNA) are produced which are subsequently processed into siRNAs by Dicer (Mikuma et al., 2004). Such DNA sequences may be inserted into expression vectors and electroporated into cells or introduced into the cell's genome via lentiviral infection. Although both these methods result in the stable

expression of shRNAs in cells and their progeny, both require the subsequent culture of the cells or whole embryos.

In the present study, it was necessary to circumvent the requirement for embryo culture, which limits the time window during which embryos can be examined (see Chapter 4). Therefore, in order to examine the effects of knocking down a gene *in vivo* using RNAi, a transgenic strategy was employed. In this procedure, shRNA coding sequences are designed and inserted into a vector under the control of the H1 RNA polymerase III promoter. This construct can then be randomly inserted into the genome of ES cells to produce transgenic mice which express the shRNA ubiquitously. This technique has been shown to produce transgenic mice which mimic the phenotype of traditional knockout mice (Kunath et al., 2003; Hemann et al., 2003), and also offers the potential to produce graded hypomorphic models with different degrees of knockdown.

The transgenic RNAi strategy has been further developed to utilise the Cre/loxP system described previously (Chapter 4.1.3.) in order to produce transgenic mice in which shRNAs against a specific RNA sequence are expressed conditionally in a subset of embryonic cells. A floxed stop cassette inserted into the shRNA expression construct between the RNA polymerase promoter and the shRNA coding sequence is excised only in cells which express Cre recombinase. This relatively novel technique, as utilised in the current research, has been validated previously (Smart et al., 2007).

5.2. METHODS

5.2.1. PREPARATION OF THE TRANSGENIC CONSTRUCT

5.2.1.1. shRNA SEQUENCE DESIGN

siRNA sequences predicted to knockdown the FoxD3 and Snai1 mRNA sequences were designed using an online tool (Ambion's siRNA Target Finder) according to the guidelines proposed by Elbashir et al, 2001. These were inserted into sequences to produce hairpin RNA as depicted in Figure 5.1.

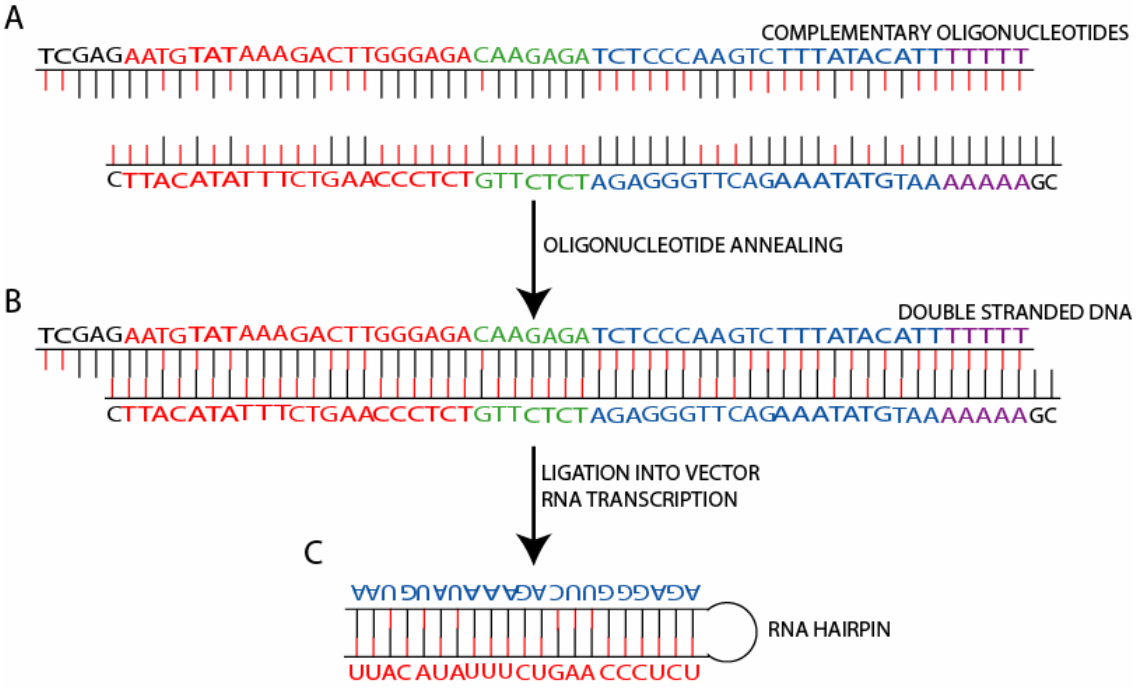

Figure 5.1. Sequence of the F5 RNA Hairpin Construct

(**A**) Oligonucleotide sequence containing a 21 base pair sequence complementary to *FoxD3* mRNA (red letters on upper strand) and the mirror image of this sequence (blue letters on upper strand), separated by a hairpin loop sequence (green letters on upper strand) and followed by a polyadenylation stop sequence (purple letters on upper strand). The lower strand depicts the complementary oligonucleotide and both strands have sticky ends complementary to the ClaI and XhoI restriction sites (black letters).

(**B**) Double stranded DNA produced after annealing

(**C**) After RNA transcription the self complementary sequence anneals to form an RNA hairpin loop.

5.2.1.2. OLIGONUCLEOTIDE ANNEALING

Forwards and reverse oligonucleotides (oligos) were obtained (Sigma Genosys) and were resuspended in Milli-Q water at 100 µM stock concentration. 1.8 µl of forward (approximately 2 µg) and reverse oligo stock was combined in 8 µl of Annealing Buffer (10 mMTris pH 7.5; 50 mMNaCl; 1 mM EDTA). This mixture was put in a PCR machine set to heat to 95°C for 2 min then gradually cool to 25°C over 45 min and then cool to a storage temperature of 4°C. The annealed double stranded DNA samples were then diluted with 72 µlMilli-Q water making a final concentration of 50 ng/µl.

5.2.1.3. VECTOR LINEARISATION

1 µg of the modified pcDNA3.1(+) vector (Smart et al., 2007) was incubated for 2 h at 37°C with 5 µlClaI buffer, 2 µlClaI restriction enzyme and made up to 50 µl with Milli-Q water. Complete linearisation was confirmed on an agarose gel and then the reaction was stopped by a 10 min incubation at 65°C.

Linearised DNA was purified using QIAquick PCR purification columns according to the kit protocol and resuspended in 40 µl Milli-Q water. This linearised vector was then incubated for 2 h at 37°C with 5 µl XhoI buffer, 2 µl XhoI restriction enzyme and 3 µl Milli-Q water.

Linearised DNA was again purified using QIAquick PCR purification columns and then resuspended in 50 µl of the kit elution buffer. 1 µl was run on an agarose gel to estimate the concentration.

5.2.1.4. LIGATION OF shRNA CONSTRUCTS INTO THE VECTOR

40 ng linearised vector (4 µl), 0.2 µg annealed shRNA insert (1 µl), 1.5 µl T4 buffer, 1 µl T4 DNA ligase and 7.5 µl Milli-Q water were mixed and incubated for 2 h at 15°C to ligate the DNA. A sample was then relinearised with ClaI (as described above) and the resultant products checked for the insert (when compared to linearised empty vector) on an agarose gel. The resultant construct is displayed in Figure 5.2.

5.2.1.5. AMPLIFICATION OF PLASMID DNA

The vector containing the *shRNAflox* transgene was transformed into bacteria, amplified and purified using the techniques described in Chapter 2. Plasmid DNA was checked by diagnostic restriction enzyme digestions, PCR (see section 5.2.7.1) and sequencing (see section 5.2.1.6).

Non-recombined (NR) plasmid DNA was used to transform Cre-expressing competent cells. After Cre mediated recombination of floxed DNA the recombined plasmid was detected using PCR. Recombined (R) DNA was transformed into standard bacterial cells, amplified and purified as above.

5.2.1.6. SEQUENCING OF CONSTRUCT

PCRs using the H1 forwards primer and the BGH reverse primer (Table 5.4) were conducted under the conditions listed in section 5.2.7.1, but the cycle number was reduced to 24 to reduce the potential for generating mutations. The PCR products were run on a gel and then purified from the gel using the Quiagen gel extraction kit.

The sequencing primers were designed running between the end of the EGFP sequence and the beginning of the pcDNA3.1(+) backbone (across the inserted shRNA sequences) using an online sequencing primer design program (GenScript Sequencing Primer Design) (Table 5.4). 2.5 µl of the PCR product (100 ng), 1 µl primer solution (from 5 µM stock), 2 µl ET-terminator, 6 µl better buffer (Gelcompany) and 8.5 µlMilli-Q were mixed. The sequencing PCR mixture was put in a PCR machine and cycled 25 times through 20 min at 95°C, 10 at 50°C and 1 min at 60°C.

2 µl ammonium acetate and 55 µl 100% ethanol were added to the products and vortexed then centrifuged for 15 min at 13000 rpm. The supernatant was removed and the pellet washed in 100 µl 70% ethanol, lightly vortexed and centrifuged for 5 min at 13000 rpm. The supernatant was removed and the pellet air dried and stored at -20°C before loading onto the capillary sequencing machine. Sequences were analysed using the FinchTV program from Geospiza.

5.2.1.7. ISOLATION OF THE shRNAflox TRANSGENE

After sequencing and testing the efficiency of the shRNA sequences in knocking down FoxD3 and Snai1 mRNA and protein in cell lines (see sections 5.2.5 and 5.2.6), the S2 and F5 sequences were selected to make transgenic mice. NR plasmid DNA was digested by the SalI restriction enzyme to release the 3774 bp *shRNAflox* transgene. This fragment was separated from the vector backbone on an agarose gel and purified using the Qiagen gel extraction kit. 30 µl of the purified *shRNAflox* transgene was sent to the ICH Embryonic Stem Cell/Chimera Production Facility where the following procedures were conducted by the Facility staff for generation of the transgenic mouse lines.

5.2.2. GENERATION OF THE FoxD3shRNAflox TRANSGENIC MOUSE LINE

5.2.2.1. SELECTION & AMPLIFICATION OF ES CELL CLONES

The transgene was transfected into ES cells by elecroporation and 70 neomycin resistant clones were isolated and amplified. The presence of the transgene in these clones was confirmed by PCR and the transgene was amplified from 12 clones and confirmed by sequencing by myself.

5.2.2.2. BLASTOCYST INJECTIONS & CHIMERA PRODUCTION

Recombinant ES cells were injected into recipient blastocysts before implantation into pseudo-pregnant female mice. Two highly chimeric mice with a high proportion of white coat colour were produced for the S1 molecule and, for the F5 molecule, 5 highly chimeric and 1 less chimeric animals were produced.

5.2.2.3. GERMLINE TRANSMISSION AND ESTABLISHING A COLONY

There was no germline transmission of the S1 *shRNAflox*transgene upon crossing with C57BL/6 mice, however germline transmission was successful in 2 of the highly chimeric mice containing the F5 *shRNAflox*transgene. One founder was used to generate a colony.

$Tg^{FoxD3shRNAflox}$hemizygous mice were backcrossed to the C57BL/6 strain to produce mice assumed to be homozygous for the transgene. Genotyping of the embryos resulting from crosses of these mice confirmed the presence of the transgene in all embryos, consistent with homozygosity.

5.2.3. GENERATING THE CONDITIONAL KNOCKDOWN MODEL

$Tg^{FoxD3shRNAflox/FoxD3shRNAflox}$ homozygous males were crossed initially with *Wnt1-Cre* hemizygous females. Cre recombinase was determined to be expressed too late in the NCC of the resultant embryos to produce a NCC phenotype (see section 5.4). They were then crossed with *Sox1-Cre* hemizygous females, predicted to produce conditional knockdown of FoxD3 in an expected ~50% of the resultant $Tg^{FoxD3shRNAflox}$ heterozygous embryos.

5.2.4. CELL CULTURE TECHNIQUES

P19 embryonal carcinomal cells were identified by western blotting and real time quantitative reverse transcription PCR (qRT-PCR) as expressing both FoxD3 and Snai1 mRNA and protein. They were thus employed in the current studies to demonstrate knockdown of these genes by shRNAs.

Standard aseptic techniques were employed for maintenance of cell cultures. 10 cm tissue culture plates were coated with gelatine (5 ml 0.1% gelatine applied to plates and aspirated after 1 h). Cell were grown in filtered medium (10 g DMEM, 1.5 g sodium bicarbonate, 10 ml antibiotic, 100 ml FCS made up to 1 L in Milli-Q water).

Cells cultures were split by removing medium, rinsing twice in 10 ml sterile magnesium and calcium free PBS and then trypsinising the cells (1 ml trypsin added to the plate and then incubated for 3 min at 37°C). 9 ml medium was added to this and cells were transferred to a 15 ml falcon and pelletted by centrifugation for 5 min at 1,000 rpm. The supernatant was removed and the cells were resuspended in 1 ml of medium and then made up to 10 ml with more medium. Cell counts were conducted on 10 µl of resuspended cells mixed with 10 µl of Trypan Blue (to distinguish the blue stained dead cells) using a haemocytometer. The resuspended cells were diluted to appropriate numbers and 1 ml of cells was mixed with 9 ml of medium on gelatine coated plates.

5.2.4.1. PLASMID TRANSFECTION INTO P19 CELLS

On the day prior to transfection, 0.5 x 10^5 cells were plated into 24 well gelatine coated plates in medium without antibiotics. Cells were transfected with plasmids containing the NR (control) and R (experimental) *shRNAflox* transgenes using Lipofectamine 200 (Invitrogen) transfection kit according to the kit's protocols. Transfection was confirmed by GFP fluorescence in cells transfected with the NR construct after 24 h.

5.2.4.2. LYSIS OF P19 CELLS

P19 cells were lysed 48 h after transfection. Radio Immuno Precipitation Assay (RIPA) lysis buffer was used to lyse cells for western blotting, to enable the release of transcription factor proteins from the nucleus. Trizol reagent (Invitrogen) was used to lyse cells to extract RNA for qRT-PCR.

5.2.5. WESTERN BLOTTING

Western blotting was used to evaluate knockdown of SNAI1 and FOXD3 in P19 cells after transfection with R constructs (in contrast to NR constructs) and to detect FOXD3 knockdown in the heads of E9.5 $Tg^{FoxD3shRNAflox}$;*Sox1-Cre*knockdown embryos (in contrast to $Tg^{FoxD3shRNAflox}$ embryos in which no cre was expressed)

5.2.5.1. PROTEIN EXTRACTION

P19 cells were lysed by washing twice with PBS and then placing the 24 well plate on ice before adding 1 ml per well of the RIPA cell lysis buffer (10 mM Tris pH 7.4, 5 mM EDTA, 150 mM NaCl, 1% sodium deoxycholate, 1% Triton X-100, 0.1% SDS, 1 mM DDT, protease inhibitors). Cell were scraped and transferred to an eppendorf before 3 pulses of sonication.

The cranial region of E9.5 stage matched embryos were snap frozen on dry ice and stored at -80°C. They were then homogenised in 1 ml of Trizol reagent by repeated pipetting and proteins extracted according to the Trizol protocol.

Bradford assays were conducted to quantify protein levels by staining with a concentration range of Coomassie Blue stain and reading the absorbance shift of the dye in a 96 well plate reader. The volume of protein sample required for a 10 µg loading was determined from a bovine serum albumin (BSA) standard curve.

5.2.5.2. PROTEIN SAMPLE PREPARATION, SEPARATION AND TRANSFER

50 µl of the protein sample (0.2 µg/µl) was combined with 50 µl of 2x Laemmli sample buffer pH 6.8 (4% SDS, 10% 2-mercaptoethanol, 20% glycerol, 0.004% bromophenol blue and 0.125 M TrisHCl), incubated at 100°C for 5 min, and then placed on ice before loading. Polyacrylamide gels were prepared according to the quantities in Table 5.1. Samples (including positive controls) and a molecular weight marker were run through the gel at 50 mA and 200 V for 1 h.

The gel was extracted from its plates, soaked in methanol for 10 min, then placed on a methanol soaked transfer membrane. This was sandwiched between six sheets of blotting paper soaked in transfer buffer and placed in a transfer plate at 400 mA and 20 V for 40 min.

Table 5.1. Preparation of Polyacrylamide Gels

	12.5% RUNNING GEL	STACKING GEL
Buffer	2.5 ml	1.25 ml
Acrylamide	2.5 ml	0.66 ml
10% SDS	0.1 ml	0.05 ml
Water	4.813 ml	3.0 ml
10% ammonium persulphate	0.075 ml	0.05 ml
TEMED	0.012 ml	0.006 ml

5.2.5.3. ANTIBODY BINDING

Membranes were blocked for 30 min in 10% milk in TBST before application of the primary antibody. The anti Snai1 primary antibody (rabbit polyclonal to SNAIL (Abcam)) or the anti-FoxD3 primary antibody (rabbit polyclonal to FOXD3 (Chemicon)) were applied at a concentration of 1:1000 in TBST for 30 min. The membrane was then washed five times in TBST for 5 min each before application of a goat anti-rabbit HRP secondary antibody at a concentration of 1:2000 in TBST for 30 min. It was again washed five times in TBST before developing.

5.2.5.4. DEVELOPING

The membrane was laid on clingfilm and chemilumiscent substrate ECL plus (2 ml solution A, 50 µl solution B) was added for 5 min. The ECL plus was tipped off and the membrane sealed in a clean piece of clingfilm and placed in a cassette for exposure of chemiluminescence to X-ray film.

5.2.5.5. STRIPPING

After developing, the antibodies were stripped from the membrane by wetting with methanol, two 10 min washes in Milli-Q, 15 min in stripping solution (Peirce), and two 5 min TBST washes. The membrane was then blocked and reprobed as before, using the anti-β-tubulin primary antibody (1:5000) and the goat anti-rabbit HRP secondary antibody (1:2000) to confirm equal protein loading.

5.2.6. REAL TIME QUANTITATIVE REVERSE TRANSCRIPTION PCR (qRT-PCR)

QRT-PCR was used to detect knockdown of *Snai1* and *FoxD3* mRNA in P19 cells after transfection with R constructs (in contrast to NR constructs). Transfected P19 cells were lysed by the addition of 200 µlTrizol reagent to each well and pipetting up and down. mRNA was extracted according to the Trizol protocol. First strand cDNA was synthesised from the mRNA using SuperScript II reverse transcriptase (Invitrogen) according to the kit protocol.

Two primers were designed for each of *FoxD3* and *Snai1* for use in qRT-PCR using an online tool (OligoPerfect from Invitrogen) (see Table 5.4). Melting curve analysis indicated that the earlier *FoxD3* primer and the *Snai1* primer bridging the first two introns did not form primer dimers.

SYBR Green qPCR supermix (Invitrogen) was used with the above primers (according to the kit's instructions) to amplify and fluorescently label *FoxD3* and *Snai1* products from the total cDNA in triplicate. Negative controls were: (i) without template and (ii) the product of the first strand cDNA synthesis without the enzyme. The results were analysed using 7500 Fast System SDS software.

5.2.7. PCR PROTOCOLS

5.2.7.1. H1-BGH PCR

Primers targeted to the H1 promoter and the BGH polyadenylation site of the *shRNAflox* transgene were identified using an online tool (Primer3) (see Table 5.4). These were used to identify the presence of the transgene in DNA samples (from bacterial cells and transgenic mice) as well as to distinguish between the non recombined transgene (amplifying a 1670 bp product) and the recombined transgene (amplifying a 360 bp product). The PCR procedure was conducted as described in Chapter 3, but using different concentrations of reagents in the mix, as follows:

2.5 µl buffer
5 µl nucleotides mix (100 mM stock)
1 µl magnesium chloride (25 mM stock)
1 µl forwards primer (10 µM stock)
1 µl reverse primer (10 µM stock)
13.3 µlMilli-Q water
0.2 µl TAQ polymerase
1 µl DNA

5.2.7.2. CRE HOTSTART PCR

Embryos resulting from crosses between $Tg^{FoxD3shRNAflox}$ and *Sox1-Cre*transgenic mice were analysed for the presence of the *Cre* sequence by the hotstart Cre PCR. Two PCR mixes were made: the DNA mix (see Table 5.4 for primers) and the Enzyme mix (Table 5.2). The DNA mix was added to 0.5 ml eppendorfs which were left open with a drop of mineral oil to prevent evaporation, inserted into the PCR machine and the program started (Table 5.3). The program was paused after denaturing the DNA at 85°C and the Enzyme mix was added to each tube before closing their lids, closing the machine and restarting the program.

Table 5.2. CreHotstart PCR Reagents

	DNA MIX	**ENZYME MIX**
Milli-Q	7.08 µl	6.4 µl
Taq polymerase buffer	1.2 µl	0.8 µl
$MgCl_2$ (25 mM)	0.72 µl	0.48 µl
Cre-A primer (25 µM)	1.0 µl	-
Cre-B primer (25 µM)	1.0 µl	-
dNTP 25 mM	-	0.16 µl
Taq polymerase 5 u/µl	-	0.16 µl (just before use)
TOTAL VOLUME	**11 µl**	**8 µl**

Table 5.3. Crehotstart PCR Program

PCR STEPS	TEMPERATURE	TIME
Denaturation	94°C	2 min
Pause	85°C	30 sec
Denaturation	94°C	30 sec
Annealing	63°C	30 sec
Extension	72°C	45 sec
Number of cycles	30x	
Extension	72°C	5 min

Table 5.4. Primers used in the Development of the *shRNAflox*Transgenic Mice

PROTOCOL	PRIMER	SEQUENCE	ANNEAL	PRODUCT
PCR	H1 forward	tcgctatgtgttctgggaaa	60°C	1670 bp / 360 bp
	BGH reverse	gcgatgcaatttcctcattt		
	Cre-A forward	accctgatcctggcaatttcggc	63°C	500 bp
	Cre-B reverse	gatgcaacgagtgatgaggttcgc		
Sequencing	eGFP forward	acatggtcctgctggagttc	60°C	677bp
	pcDNA3 reverse	tcgaggctgatcagcgggtt		
qRT-PCR	FoxD3#1forward	gaaggctggtgaagtgagg	60°C	87 bp
	FoxD3#1 reverse	gcaaaggaggtgtgagtgt		
	FoxD3#2forward	gctgggaataactttccgta	60°C	93 bp
	FoxD3#2 reverse	tcagataaaactgcgcagag		
	Snai1#1 forward	aactatagcgagctgcagga	60°C	158 bp
	Snai1#1 reverse	cttttgccactgtcctcat		
	Snai1#2 forward	tggaaaggccttctctagg	60°C	139 bp
	Snai1#2 reverse	cctggcactggtatctcttc		

5.2.8. RIBOPROBE PREPARATION AND IN SITU HYBRIDISATION

The Crabp-1 riboprobe (Table 5.5) was prepared using the techniques described in Chapter 2. The Otx2 riboprobe was received as a labelled RNA probe from J.P. Martinez-Barbera. *In situ* hybridisation was also conducted as described in Chapter 2.

Table 5.5 Antisense RNA Probe Used for *In Situ* Hybridisation

PLASMID	INSERT SIZE (bp)	INSERT SITE	LINEAR-ISE WITH	TRANSCR-IBE WITH	SOURCE
Crabp-1	700 bp	EcoRI	BamH1	T7	P. Chambon

5.2.9.FLUORESCENCE MICROSCOPY

Light microscopy and photography were conducted as described in Chapter 2. To visualise GFP expression, both in P19 cells which had been transfected with the NR construct and in Sox1-Cre;ROSA26EGFP embryos, fluorescence microscopy was performed using a Leica MZFLIII fluorescence stereomicroscope and photography was conducted using a Leica DC500 camera.

5.3. RESULTS

5.3.1. DEVELOPING THE TRANSGENIC CONSTRUCT

Five sequences designed to produce shRNAs targeted against each of *FoxD3* and *Snai1* mRNAs (termed F1-F5 and S1-S5 respectively) (see Figure 5.1) were inserted into constructs downstream of the H1 RNA pol II promoter and separated from it by a floxed stop sequence as indicated in Figure 5.2 A. These constructs were inserted into modified pcDNA3(+) vectors (now termed the 'non-recombined' constructs). Transformation into *Cre*-expressing competent cells resulted in the 'recombined' constructs which expressed the shRNA as demonstrated by PCR in Figure 5.2 B.

The non-recombined and recombined constructs were used to test the efficiency of each shRNA sequence in knocking down the products of the *FoxD3* and *Snai1* genes, both mRNA and protein. Recombined (R) and non-recombined (NR) versions of each construct were transfected into P19 cells, which express both genes of interest. By comparison with transfection of a non-recombined construct (F5NR), the level of *Snai1* mRNA was reduced to 59% by transfection with S1R and to 68% by transfection with S2R. The level of *FoxD3* mRNA was reduced to 13% by transfection with F2R and to 0% by transfection with F5R (Figure 5.2 C).

Western blot analysis identified no knockdown of the FOXD3 protein by the F2R or F5R*in vitro*, however both S1R and S2R produced near complete knockdown of SNAI1 (Figure 5.2 D). These results demonstrate poor correlation between the high level of FoxD3 mRNA knockdown and low level of protein knockdown *in vitro* which will be discussed in more detail in section 5.4.

Figure 5.2. Developing the transgenic construct for generation of the *FoxD3* knockdown mouse model.

(A) Schematic of the *shRNAflox* transgene containing: (i) an H1 polymerase III promoter (H1); (ii) floxed stop cassette (5T stop codon, thymidine kinase promoter (TK) and enhanced green fluorescent protein cDNA (eGFP)); and (iii) shRNA sequences. The transgene was inserted into a pcDNA3(+) backbone (Invitrogen) replacing the pCMV promoter of the vector.

(**B**) *Cre* mediated excision produces a recombined shRNA transgene. PCR products were produced using primers located in the H1 promoter and BGH polyadenylation signal. Non-Cre-recombined plasmid DNA (NR) containing the shRNA sequences F2, F5, S1 and S2 yielded a 1670 base pair product, while Cre-recombined plasmid DNA (R) yielded a 360 base pair product.

(**C,D**) The ability of the recombined shRNA transgene to knockdown target mRNA (*FoxD3* and *Snai1*) and proteins (SNAI1 only), demonstrated *in vitro* using whole cell lysates from P19 cells transfected with the non-recombined and recombined shRNA constructs. (C) Quantitative reverse-transcriptase PCR of RNA extracted from whole cell lysates. Knockdown of *Snai1* and *FoxD3* mRNA after transfection of cells with the recombined constructs (S1R, S2R, F2R and F5R) was quantified against levels of mRNA after transfection with a non-recombined construct (F5NR in each case). *Snai1* mRNA levels were knocked down to 59% and 68% by the S1R and S2R constructs respectively, while *FoxD3* levels were knocked down to 13% and 0% by the F2R and F5R constructs respectively. (D) Western blot analysis of whole cell lysates showing high levels of the 29 kDa SNAI1 protein evident after transfection with the non-recombined constructs (S1NR and S2NR) in contrast to the near absence of the protein after transfection with the recombined, shRNA expressing constructs (S1R and S2R).

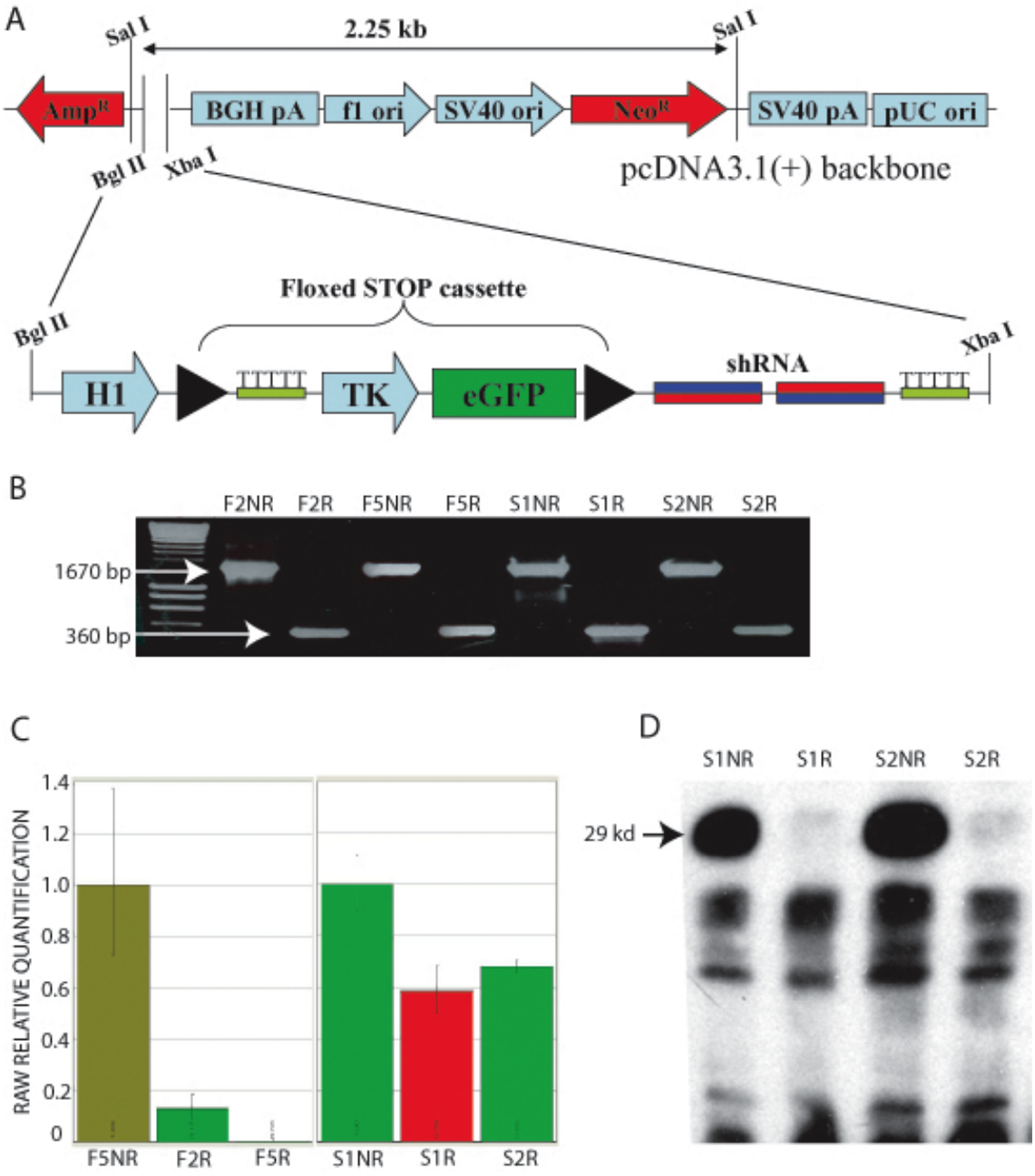
A
Sal I
2.25 kb
Sal I
Amp^R
BGH pA
f1 ori
SV40 ori
Neo^R
SV40 pA
pUC ori
pcDNA3.1(+) backbone
Bgl II
Xba I
Floxed STOP cassette
Bgl II
Xba I
H1
TK
eGFP
shRNA
B
F2NR F2R F5NR F5R S1NR S1R S2NR S2R
1670 bp
360 bp
C
RAW RELATIVE QUANTIFICATION
1.4
1.2
1.0
0.8
0.6
0.4
0.2
0
F5NR F2R F5R S1NR S1R S2R
D
S1NR S1R S2NR S2R
29 kd

5.3.2. DEVELOPING THE TRANSGENIC FOXD3 KNOCKDOWN MODEL

Based on the *in vitro* studies, the S1NR and the F5NR constructs were selected to be electroporated into ES cells which were then injected into mouse blastocysts to produce chimeras. The S1NR construct produced two chimeric males but neither transmitted the construct through the germline. Six chimeric animals were produced from the F5NR construct, of which two transmitted the $Tg^{FoxD3shRNAflox}$ allele through the germ line. Offspring of one of these chimeras was used as a founder for a colony which was backcrossed several times onto the C57BL/6 background to produce homozygous floxed FoxD3 short hairpin RNA (*FoxD3shRNAflox*) mice.

The $Tg^{FoxD3shRNAflox/FoxD3shRNAflox}$ homozygous mice were initially crossed with *Wnt1-Cre*heterozygous mice (as described in section 3.1.3). When examined at E10.5, no morphological phenotype was observed in 12 $Tg^{FoxD3shRNAflox}$ heterozygous embryos carrying the *Wnt1-Cre* transgene, compared with 15 $Tg^{FoxD3shRNAflox}$ heterozygotes that lacked the *Wnt1-Cre* transgene. It is possible that the onset of *Wnt1* expression was too late to knockdown *FoxD3* expression prior to the delamination of the cranial neural crest in these embryos. In particular, the time lag between *Cre* expression and protein knockdown (via *Cre* mediated excision of loxP sites, shRNA production and *FoxD3* mRNA targeting and degradation) has not been determined.

Sox1 is one of the earliest transcription factors to be expressed by ectodermal cells committed to the neural fate, its onset coinciding with the induction of neural ectoderm (Collignon et al., 1996; Pevny et al., 1998). The *Sox1-Cre* mouse expresses *Cre*recombinase under control of the *Sox1* promoter and, as such, is expected to express *Cre* throughout the neural plate, including the NCC from very early stages (Takashima et al., 2007). Hence, *Sox1-Cre* mediated recombination should significantly precede *Wnt1-Cre* mediated recombination during NCC development. *Cre* expression is then maintained in all progeny of *Sox1* expressing cells which can be seen throughout the neural tube and in migrating NCC (Figure 5.3 A).

$Tg^{FoxD3shRNAflox/FoxD3shRNAflox}$mice were crossed with *Sox1-Cre*mice and the resulting embryos were genotyped for the presence of the *Cre* sequence (as well as for the *FoxD3shRNAflox* construct which was expected in all embryos). A proportion of embryos containing both transgenes (the conditional FoxD3 knockdown model) demonstrated a number of distinctive phenotypes which are characterised in the following section. Substantial knockdown of FOXD3 protein in embryos containing both transgenes was confirmed by western blot analysis (Figure 5.3 B).

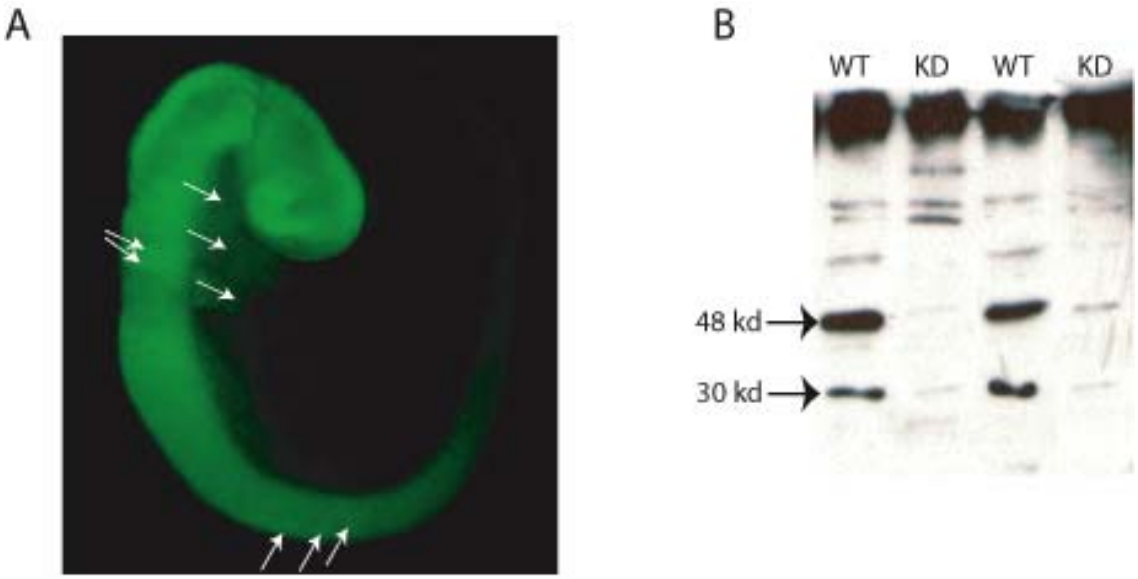

Figure 5.3. Developing the Transgenic Knockdown Model

(**A**) *Sox1-Cre;ROSA26-EGFP* mouse at E9.5. GFP fluorescence is observed in *Sox1* expressing cells and their progeny. Migratory NCC are indicated with white arrows in the facial mesenchyme, branchial arches, and in streams emanating from rhombomere 4 and migrating into the somites.

(**B**) Knockdown of FoxD3 protein demonstrated *in vivo* by western blot analysis of lysates of wild type (WT) and conditional *FoxD3* knockdown (KD) mouse embryo heads. Both the 48 and 30 kDa forms of FOXD3 protein are reduced in abundance or absent in the knockdown embryos.

5.3.3. CHARACTERISATION OF THE PHENOTYPE OF THE CONDITIONAL FOXD3 KNOCKDOWN MODEL

Knockdown of *FoxD3* in *Sox1* expressing cells produced a number of phenotypic abnormalities which were characterised by the study of E9.5 and E10.5 embryos both before and after *in situ* hybridisation for a range of probes.

The *FoxD3shRNAflox* construct was confirmed in all 25 embryos for which a definitive genotype could be obtained, consistent with the homozygous status of the backcrossed $Tg^{FoxD3shRNAflox}$colony. Moreover, the *Cre* DNA sequence was confirmed in 12 out of these 25 embryos, approximately 50% as expected after crossing the $Tg^{FoxD3shRNAflox/FoxD3shRNAflox}$line with *Sox1-Cre* mice. A further group of embryos could not be genotyped for *Cre* owing to technical difficulties but, nevertheless, phenotypic frequencies were also determined for this group of embryos. The number of conditional *FoxD3* knockdown embryos (i.e. hemizygous$Tg^{FoxD3shRNAflox}$;*Sox1-Cre*) was estimated by dividing the total number of embryos by two (given the expected 50% frequency of the *Cre*transgene). Indeed, frequencies of defects in the estimated population of conditional *FoxD3* knockdown embryos were similar to the phenotypic frequencies found within the smaller population of conditional *FoxD3* knockdown embryos confirmed by genotyping (Table 5.6). This provides supporting evidence that the findings within the genotyped population can be extrapolated to the larger ungenotyped population, increasing confidence levels in the results.

NCC were identified using probes against the NCC markers *Crabp1*(Maden et al., 1992) and *Sox9*(described in section 2.1.1) (Figure 5.4 A-F). NCC are initially specified in the neuroepithelium of both normal and *FoxD3* knockdown embryos (black arrowheads in Figure 5.4 A,B). The numbers of NCC migrating along typical pathways, such as into the branchial arches appeared slightly reduced (but far from absent) in all conditional *FoxD3* knockdown embryos examined and in 89% of those estimated from the ungenotyped population (which ranged from the 11 to 40 somite stage) (Figure 5.4 B, E-F; Figure 5.5; Table 5.6).

Morphologically a reduction in cranial flexure was observed in 2 of 3 (66%) conditional *FoxD3* knockdown embryos (confirmed by genotyping) examined at the 11 to 15 somite stage (Figure 5.4 B). In the ungenotyped population, 3 of the 14 embryos demonstrated this morphology, representing 43% of the expected (i.e. 7) conditional *FoxD3* knockdown embryos (Figure 5.5; Table 5.6).

At later stages (29 to 40 somite stages) a reduced angle of axial curvature was evident in the cephalic flexure of all 8 (100%) confirmed conditional *FoxD3* knockdown embryos (Figure 5.4 E-F, H) and in 17 out of 38 embryos in the ungenotyped population where 50% would be predicted to be cre positive, hence 89% of the predicted *FoxD3* knockdown embryos(Table 5.6). The reduction in axial curvature was quantified in 36 somite embryos after labelling with the fore- and midbrain marker *Otx2*. Embryos were oriented so that a vertical line passed through the dorsal-most point of the posterior limit of *Otx2* labelling and the dorsal point of the otic vesicle. The angle was measured between two lines originating at the highest point of the embryo and passing to the dorsal-most point of the posterior limit of *Otx2* labelling posteriorly and to the groove which is the posterior limit of the forebrain ventricles anteriorly (Figure 5.4 G, H). The angles of axial curvature at the cephalic flexure were found to differ significantly between the wild type and FoxD3 knockdown embryos (mean $^{\pm}$SEM curvature angles: 98.6°$^{\pm}$ 0.98°in WT N=5; 111.2°$^{\pm}$ 0.86° in KD N=5; $p< 0.0001$).

Abnormalities were observed in the branchial arches (BAs) of conditional *FoxD3* knockdown embryos from the 11 somite stage onwards: 50% of the confirmed (and 42% of the unconfirmed) *FoxD3* knockdown embryos demonstrated some form of BA defects (Figure 5.5; Table 5.6). These defects fell into two broad categories: (i) hypoplastic BAs were evident in earlier embryos, and also later embryos in association with reduced levels of labelled NCC. This was usually most apparent in the first BA (Figure 5.4 asterisk in B, D) although sometimes also affected the other BAs of later stage embryos (Figure 5.4 E); (ii) at later stages the mandibular and maxillary processes of the first BA also demonstrated positioning defects.

In mild instances, the maxillary process appeared stretched across the gap from the first BA to the medial nasal process (sometimes causing the mandibular process to become separated from the maxillary by a larger than usual gap as indicated with a white arrow in Figure 5.4 D). In more severe instances, there was a unilateral failure of bridging of the gap between the region adjacent to the hindbrain and the medial nasal process. This either took the form of both the mandibular and maxillary processes being attached to the region adjacent to the hindbrain (Figure 5.4 F) or both being attached to the medial nasal process (Figure 5.4 E). In the second instance, subsequent BAs were also affected, becoming hypoplastic. All instances of unilateral failure of bridging by the first BA derivatives demonstrated cranial asymmetry such that the forebrain and

midbrain were tilted to one side (Figure 5.4 E, F). This was evident in 50% of confirmed (and 32% unconfirmed) conditional *FoxD3* knockdown embryos (Table 5.6).

Exencephaly was observed in 38% of confirmed (and 32% unconfirmed) conditional *FoxD3* knockdown embryos between the 29-40 somite stages (Table 5.6). It was usually associated with failure of bridging and cranial asymmetry and extended throughout the forebrain (Figure 5.4 E, F). However, in one instance exencephaly was localised in a small area of the midbrain-forebrain boundary with no failure of bridging or cranial asymmetry. Moreover, there was one example of failure of bridging and cranial asymmetry that did not have exencephaly. There was no evidence of exencephaly at the earlier stages examined (Figure 5.5; Table 5.6).

Table 5.6. Phenotype frequencies of conditional *FoxD3* knockdown (KD) and wild type (WT) embryos, where confirmed by genotyping, and phenotype frequencies of predicted KD embryos.

PHENOTYPE (somite range, SS)	GENOTYPED				PREDICTED *	
	WT	%	KD	%	KD	%
Reduced NCC (11-40SS)	0/10	0%	9/9	100%	8/9	89%
Reduced Curvature (11-15SS)	0/3	0%	2/3	66%	3/7	43%
Reduced Curvature (29-40SS)	0/7	0%	8/8	100%	17/19	89%
BA Abnormalities (11-40SS)	0/13	0%	6/12	50%	17/40	42%
Cranial Asymmetry (29-40SS)	0/7	0%	4/8	50%	6/19	32%
Exencephaly (18-28SS)	0/3	0%	0/1	0%	0/12	0%
Exencephaly (29-40SS)	0/7	0%	3/8	38%	6/19	32%

* Prediction based on expectation that 50% of ungenotyped embryos were *Sox1-Cre*.

Total numbers of genotyped embryos = 11-15 somites: 3 WT, 3 KD; 18-28 somites: 3 WT, 1 KD; 29-40 somites: 7 WT, 8 KD.

Total numbers of ungenotyped embryos = 11-15 somites: 14; 16-17 somites: 4; 18-28 somites: 24; 29-40 somites: 38.

Figure 5.4. PHENOTYPE OF CONDITIONAL *FOXD3* KNOCKDOWN MODEL

Wild type and conditional *FoxD3* knockdown embryos were hybridised as wholemounts with probes against NCC markers *Sox9* at the 15 somite stage (A,B) and *Crabp1* at the 37 somite stage (C-F), and the fore- and midbrain marker *Otx2* at the 36 somite stage (G,H). Right and left sided views of the same two knockdown embryos are shown in E,F.

(**A,B**) *Sox9* expressing NCC are evident in the neuroepithelium (black arrowheads in A and B), however migratory NCC in the cranial mesenchyme and first branchial arch (white arrows in A) are less apparant in the conditional *FoxD3* knockdown mouse (B) in combination with hypoplasia of the first branchial arch (asterisk) and a reduction in the angle of cranial flexure.

(**C-F**) *Crapb1* expressing migratory NCC in the mandibular process (m), maxillary process (mx) and second branchial arch (2) are less evident in the conditional *FoxD3* knockdown embryos (D-F), which also demonstrate a reduction in axial curvature at the cephalic flexure and hypoplasia of the maxillary and mandibular processes and second branchial arch. (D) Mild phenotype in which the maxillary process appears separated from the (usually adjacent) mandibular process and second branchial arch (white arrow). (E,F) More severe phenotypes associated with further diminished *Crabp1* expression. In one embryo (E), both the maxillary and mandibular processes are associated with the medial nasal process (mnp) bilaterally, leaving a large gap (asterisk) between the mandibular process and the second arch. In the other embryo (F) a different, asymmetric phenotype is present in which there is mild separation of maxillary and mandibular processes on the embryo's right side (arrow), but a large gap between maxillary/mandibular/second arch and medial nasal process on the left (asterisk). Both embryos with the severe phenotype (E,F) display forebrain exencephaly (white line and ex).

(**G,H**) Angle of axial curvature at the cephalic flexure measured between two lines originating at the highest point of vertically oriented embryos and passing through the dorsal limit of the midbrain posteriorly (posterior limit of blue stain) and the groove which is the posterior limit of the forebrain ventricles anteriorly. The angle is more acute in the wild type (G) than in the conditional *FoxD3* knockdown embryo (H).

Scale bars in A-H represent 500 μm.

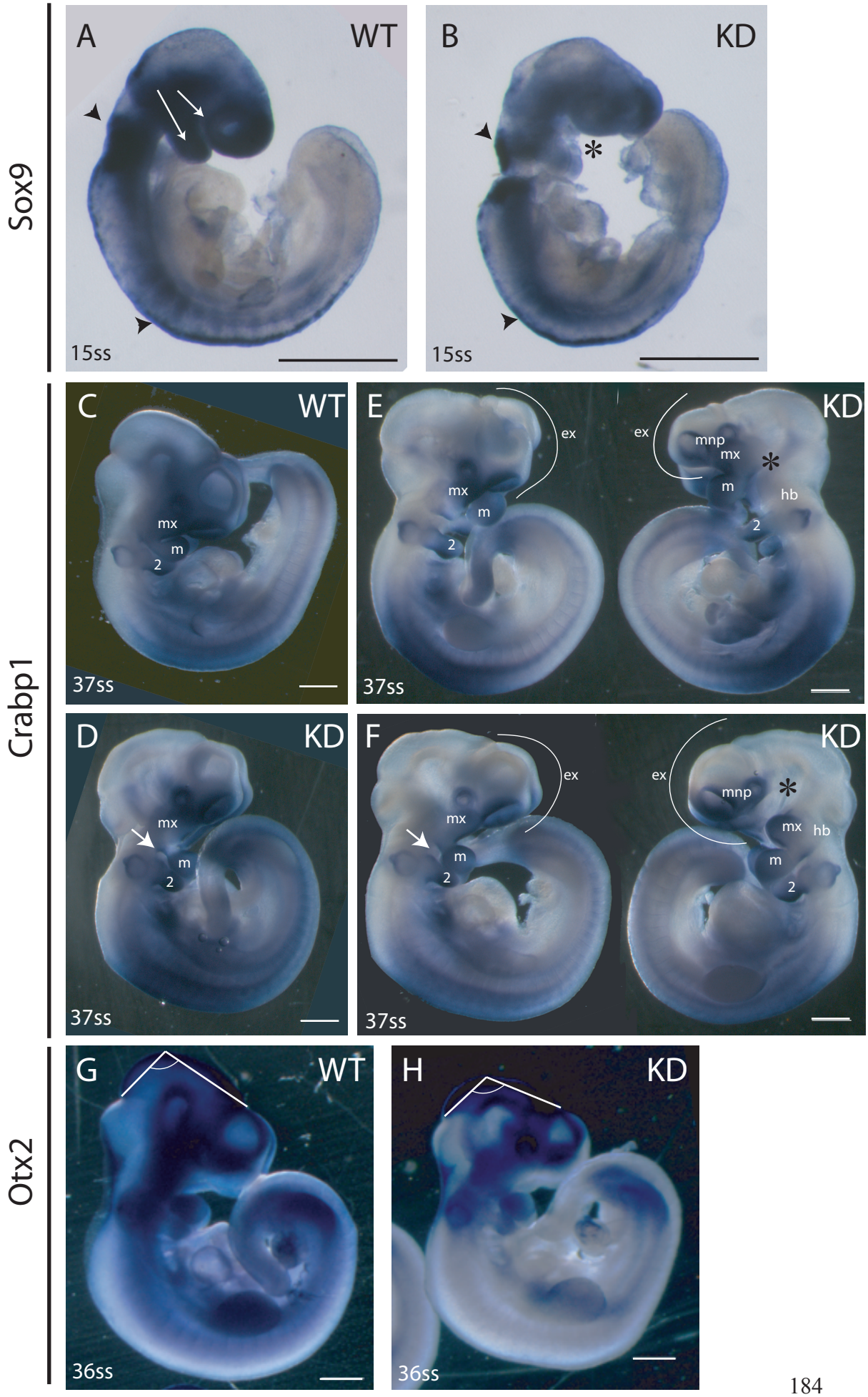
Sox9
Crabp1
Otx2
A
WT
15ss
B
KD
15ss
C
WT
mx
m
2
37ss
E
ex
mx
m
2
KD
ex
mnp
mx
m
hb
2
37ss
D
KD
mx
m
2
37ss
F
ex
mx
m
2
KD
ex
mnp
mx
hb
m
2
37ss
G
WT
36ss
H
KD
36ss

Figure 5.5.Graphical representation of phenotype frequencies of conditional *FoxD3* knockdown (KD) and wild type (WT) embryos, whereconfirmed by genotyping, and phenotype frequencies of predicted KD embryos.

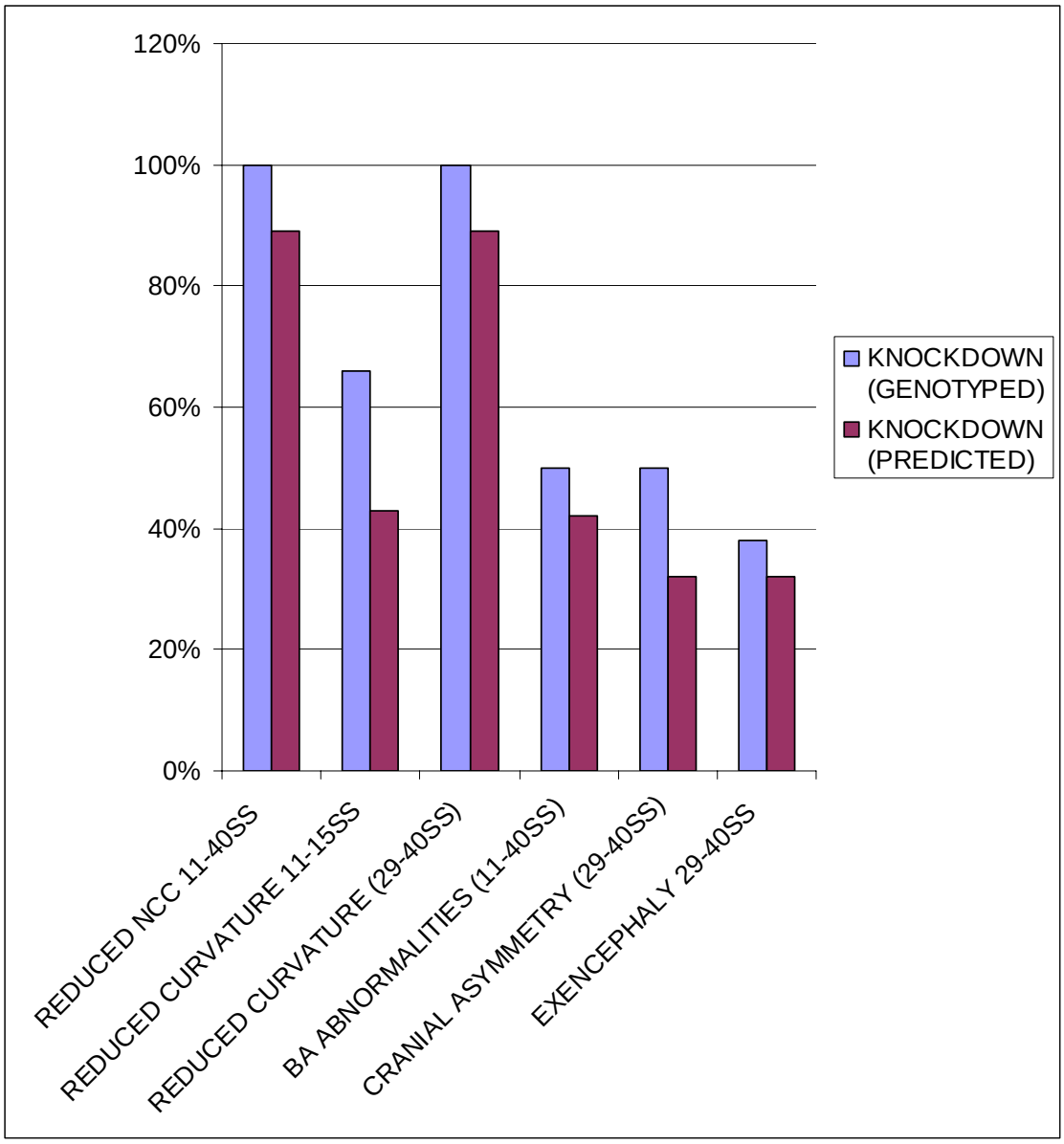

5.4. DISCUSSION

The aim of the current chapter was to establish a model in which NCC delamination could be inhibited *in vivo* in order to test the causal nature of the association made previously between inhibition of NCC delamination and failure of DLHP formation, and then to determine the subsequent neural tube phenotype. Having identified *FoxD3* and *Snai1* as factors which are implicated in the EMT of NCC, constructs conditionally expressing shRNAs were designed which efficiently knocked down the expression of each gene of interest. Although knockdown of *FoxD3* mRNA by the shRNA constructs in cell culture was proven, knockdown of the protein in cell culture could not be demonstrated. This may reflect the role identified for FoxD3 in stem cell maintenance (Liu & Labosky, 2008). Once the protein was knocked down in cells expressing the shRNA they may have failed to survive. Further experimentation would be required to demonstrate this effect.

A transgenic mouse was successfully developed which was found to efficiently knock down levels of FOXD3 protein conditionally in the NCC (thus circumventing the early embryonic lethality of the *FoxD3*$^{-/-}$mouse). Since the onset of these studies a *FoxD3* conditional knockout mouse has been described in the literature in which NCC specific deletion of *FoxD3* is driven by *Cre* expression under control of the *Wnt1* promoter (Teng et al., 2008). The phenotype described in that conditional knockout mouse replicates many of the findings described here in the conditional *FoxD3*shRNA knockdown model, validating the use of the shRNA gene knockdown approach to study the effects of gene inactivation *in vivo*. There are, however, several differences between the two models which may primarily reflect the different embryonic stages examined and the phenotypes looked for and reported, rather than differences between the two models *per se*.

In the conditional knockout model (Teng et al., 2008), a short period of *FoxD3* expression was reported, which resulted from the onset of *FoxD3* expression preceding the *Wnt1-Cre* mediated excision and recombination of floxed*FoxD3* DNA (Teng et al., 2008). This demonstrates that the time between onset of *Wnt1* expression and onset of *FoxD3* expression is not quite sufficient for the *Cre*-mediated DNA recombination to prevent *FoxD3* expression completely.

These findings are in accordance with the current observations on the conditional *FoxD3* knockdown model. In the latter, *Cre* expression and subsequent

excision and recombination of floxed DNA was followed by a number of further, time consuming steps: the RNA hairpins must be transcribed in the nucleus, exported to the cytoplasm, combine with the RISC and mediate degradation of target RNA. This extra time lag made *Wnt1-Cre* an unsuitable source of *Cre* in order to prevent *FoxD3* expression in NCC, and explains why no obvious phenotype was observed using this mouse line. Use of the *Sox1-Cre* line ensured that *Cre* was expressed earlier relative to the onset of *FoxD3* expression, so that activated RISC would be ready in the cytoplasm of prospective NCC to degrade *FoxD3*mRNA as soon as it was produced, thus minimising any FOXD3 protein produced from the outset.

Incidentally a conditional *Snai1* knockout mouse was also reported during the course of the PhD studies, but surprisingly no effect was observed on the early specification or delamination of NCC, or on the development of the cranial neural tube in this model (Murray et al., 2006; Murray and Gridley, 2006a; Murray and Gridley, 2006b). NCC specific *Snai1* knockout on a *Snai2*$^{-/-}$background did cause later NCC defects resulting in failure of mandibular development and subsequent craniofacial abnormalities (Murray et al., 2007), although NCC specification and emigration were not reported as abnormal. This suggests that, even if the *Snai1shRNA* construct had generated germ-line chimeras in the present project, there might have been little or no inhibition of NCC delamination in the resulting conditional knockdown embryos.

5.4.1. EFFECT OF CONDITIONAL FOXD3 KNOCKDOWN ON EARLY NCC

FoxD3 was first identified in embryonic stem cells (ESC) and early NCC (Labosky and Kaestner, 1998). *FoxD3*$^{-/-}$ embryos fail around the time of implantation due to a failure to maintain the progenitor pool of both embryonic and trophoblast lineages (Hanna et al., 2002; Tompers et al., 2005). This precluded the study of the effects of *FoxD3* ablation on mouse NCC, of which it is one of the earliest markers, being down regulated upon differentiation (Labosky & Kaestner, 1998; Cheung et al., 2005). Previous data in chick and *Xenopus* demonstrated that ectopic *FoxD3* expression in neuroectoderm is sufficient to induce a NCC fate and in some cases induce features of EMT, while knockdown of *FoxD3* in *Xenopus* suppresses NCC specification (Dottori et al., 2001; Kos et al., 2001; Sasai et al., 2001). In contrast NCC specification in the zebrafish has been shown to occur in the absence of *FoxD3* (Montero-Balaguer et al., 2006; Arduini et al., 2009).

The aim of the current study was to determine the effects of the inhibition of delamination of NCC from the neuroepithelium on subsequent development, particularly neural tube closure, in the cranial region. The results show that shRNA mediated knockdown of FoxD3 in mouse NCC leads to reduced numbers of NCC evident in typical migratory pathways to the branchial arches and cranial mesenchyme, a phenotype which replicates that found upon conditional knockout of *FoxD3* in NCC (Teng et al., 2008). This finding indicates that, in mammals as in other vertebrates, FoxD3 plays a role in NCC development prior to or during their early migration.

The fact that premigratory NCC are evident in the neuroepithelium and a significant proportion of NCC are evident in the migratory pathways (albeit in reduced numbers) may imply that: (i) *FoxD3* is indeed required for NCC specification and/or delamination (as in *Xenopus* and chick), but that gene knockdown was incomplete, or that (ii) *FoxD3* plays a later role in development, in maintenance of the migratory NCC. Several points are worthy of consideration. First shRNA mediated knockdown of *FoxD3* was demonstrated to be very efficient, but did not entirely eliminate FOXD3 protein in all embryos. Thus, residual protein could have been responsible for the specification and delamination of reduced numbers of NCC. It should be noted that embryos in the present study were hemizygous for the *FoxD3shRNA* construct, and it is possible that ensuring homozygosity would have increased the completeness of *FoxD3* knockdown. However, as no definitive measures of specification or delamination were undertaken (e.g. *in vitro* delamination assays or cell counts pre- and post-delamination *in vivo*), it is unclear whether persistent NCC specification/delamination, owing to 'leaky' *FoxD3* knockdown, was present in this study. Furthermore, as described above, the use of the *Wnt1-Cre* mouse in the conditional knockout model resulted in small numbers of *FoxD3* expressing NCC evident in the neuroepithelium. Thus, the conditional knockout model is also a 'leaky' model (Teng et al., 2008). A more definitive model might be provided by crossing the floxed*FoxD3* conditional knockout mouse with the *Sox1-Cre* mouse.

A formal alternative possibility that should also be considered is that the reduction in NCC evident in the migration pathways reflects a primary role for *FoxD3* in the maintenance of NCC progenitors. Studies of apoptosis, proliferation and differentiation in the *FoxD3*shRNA knockdown model would be required to assess a role in progenitor maintenance. While such work was prevented by time limitations, previous studies provide support for this role of *FoxD3* as described below.

FoxD3 expression is limited to embryonic and trophoblast stem cells of the blastocyst and later the NCC population, all tissues sharing a common trait as pluripotent progenitor cells (Labosky & Kaestner, 1998; Tompers et al., 2005). *FoxD3* expression is down regulated in these cell populations when they are induced to differentiate, whereas maintenance of expression in chick migrating NCC inhibits differentiation, implicating *FoxD3* in control of stem cell differentiation (Sutton et al., 1996; Dottori et al., 2001). Inactivation of *FoxD3* in the blastocyst and ESC lines demonstrated its importance for maintaining the progenitor pool by repressing differentiation, promoting self-renewal and maintaining survival of stem cells (Hanna et al., 2002; Liu & Labosky, 2008). Its inactivation in the NCC progenitors of the mouse (as in the zebrafish) again resulted in failure to maintain the progenitor pool (evident from an increase in apoptosis and reduction in NCC derivatives) (Lister et al., 2006; Stewart et al., 2006; Teng et al., 2008).

5.4.2. EFFECT OF NCC DEFECTS ON NEURAL TUBE MORPHOLOGY

Based on the complete penetrance of the NCC defect in the *FoxD3* conditional knockdown embryos, the expression pattern of *FoxD3* in the early NCC, and the role subsequently identified for the gene in the maintenance of the NCC progenitors, it is likely that the NCC defect described above is the primary defect in the *FoxD3shRNA* knockdown embryos. Other abnormalities observable in the knockdown embryos, including the reduction in axial curvature, hypoplasia of the branchial arches and forebrain exencephaly, are secondary.

The first morphological phenotype to become evident during the development of the *FoxD3shRNA* conditional embryos was decreased axial curvature in the cranial region, which is believed to result from failure of expansion of the cranial mesenchyme owing to defective immigration and proliferation of NCC. The loss of NCC progenitor cells in the cranial migratory pathways might affect the mesenchymal scaffolding that supports the cranial neural tube, and lead to gross axial defects. Several mouse models in which early NCC development is disturbed demonstrate a similar cranial morphology, supporting the proposed involvement of NCC in this phenotype. These include the *Tcof1* knockout mouse model and rat embryos in which microfilaments have been disrupted by inhibitors (Morriss-Kay and Tuckett, 1985; Dixon and Dixon, 2004).

The phenotype of reduced axial curvature was noted in earlier chapters of this thesis, in conjunction with diminished levels of migrating NCC in both the *Kumba* mutant and after inhibition of NCC delamination in cultured embryos. In both of these models, failure of DLHP formation and exencephaly co-existed, raising the possibility that reduction in expansion of cranial mesenchyme was a contributory factor to the midbrain exencephaly. Indeed, expansion of the cranial mesenchyme is known to play a role in neural fold elevation particularly in the midbrain and at the Closure 2 site (Solursh and Morriss, 1977).

Data in the present chapter contribute further to resolving whether it is a failure of DLHP formation or failure of mesenchymal expansion or a combination of both which limits closure of the midbrain region following disruption of NCC development. As the specification and delamination of NCC appears relatively unaffected by the knockdown of *FoxD3*, then according to the hypothesis under test, no effects would be anticipated on the formation of DLHPs in the *FoxD3shRNA* conditional embryos. The finding that Closure 2 and midbrain closure occurs normally in the knockdown model implies that the DLHPs are indeed formed. Since reduction in axial curvature (resulting here from the failure of maintenance of NCC) is still observed, this argues that diminished cranial mesenchyme expansion may not play a causative role in the development of midbrain exencephaly.

There is, however, a caveat to this conclusion. The increasing percentage of embryos displaying reduction in axial curvature at later developmental stages (Table 5.6) implies that the absence of NCC progenitors from the cranial mesenchyme may have been a relatively late phenomenon, and did not immediately follow delamination. That is, NCC may have entered the mesenchyme normally, and contributed to initial normal mesenchymal expansion that supported midbrain closure. Subsequently, NCC were not maintained, contributing to failure of further mesenchymal expansion, and so limiting axial curvature at a later stage. Clearly, these studies are not able to assess the effects of failure of mesenchymal expansion alone (dissociated from failure of DLHP formation).

Interestingly the morphological phenotype of reduced axial curvature is not observed upon knockout of *FoxD3* conditionally in the NCC (Teng et al., 2008). This might be because the morphological phenotype of the conditional knockout was mainly studied in later stage embryos, by which time the severe craniofacial abnormalities associated with NCC defects may have obscured any reduction in cranial flexure.

5.4.3. BRANCHIAL ARCH DEFECTS

Early hypoplasia of the first, and occasionally the second, BA of *FoxD3* knockdown embryos reflects the reduced numbers of contributory migratory NCC. In addition, a striking finding at E10.5 was abnormal morphological patterning of the BA region.

These morphological aberrations seem to stem from the difficulty of extending the maxillary process from the site of the first BA (adjacent to rhombomere 2) to bridge the gap to join the medial nasal process (adjacent to the forebrain). In mild cases this difficulty results in a bilateral stretching of the maxillary process away from the mandibular process which can additionally affect the subsequent branchial BA by drawing them apart. In the more severe cases, the gap may be bridged unilaterally, while the other side fails, causing the mandibular and maxiallary processes to become isolated either adjacent to the medial nasal process (drawing the contribution of NCC anteriorly and thus depriving the second and subsequent BA of NCCs) or the hindbrain (depriving the face of contributions from the first BA). These morphological abnormalities can be attributed to the hypoplasia of the first BA (due to the primary NCC defect) in combination with the increased distance from the hindbrain to forebrain caused by the reduction in midbrain axial curvature mentioned in the previous section (a secondary defect). The frequencies of defects lend weight to this order of causality – complete penetrance of the primary NCC defect leads to complete penetrance of the secondary midbrain axial curvature phenotype. These two phenotypes result in a range of branchial arch phenotypes with incomplete penetrance.

Cranial asymmetry was always displayed in association with the more severe BA morphological defect of unilateral failure of the maxillary process to extend to the medial nasal process (termed here ‘bridging). It seems likely that this was due to pulling from the side on which the maxillary process bridged the gap to join the medial nasal process successfully. The converse is, however, possible – that the cranial asymmetry (induced by unknown mechanisms) enabled the maxillary process on one side to bridge the gap and prevented it on the other side.

The exencephalic defect was generally an opening of the forebrain and was always observed in conjunction with unilateral failure of bridging and cranial asymmetry (although failure of bridging and asymmetry did not always associate with exencephaly). This implies that these defects may be related, specifically that bridging defects and cranial asymmetry can result in exencephaly. Exencephaly was never noted

in earlier embryos, and this suggests that closure occurs at earlier stages and is followed by a re-opening event. Perhaps unilateral failure of bridging by the maxillary process and subsequent asymmetry (or vice versa) exerts a lateral dragging force on the closed neural folds and causes them to reopen. Hence, this exencephalic defect cannot be attributed to failure of midbrain closure (as predicted to result from the failure of NCC delamination) and, although related to the primary NCC defect, appears to be downstream of other craniofacial defects.

The BA defects observed in the *FoxD3* knock down model are to some extent confirmed in the *FoxD3* conditional knockout model which displayed reductions in the size of the maxillary and mandibular prominences at E10.5, despite initial NCC colonisation at E9.5 (Teng et al., 2008). At E16.5 many of the NCC derived cranial bones were absent or reduced in size, resulting in cleft face and palate phenotypes with 100% penetrance at birth – the expected result of the defects noted in the current studies. No unilateral defects of the branchial aches or asymmetry of the cranial region are described in the conditional knockout model, nor is exencephaly, although one of the figures appears to display an exencephalic embryo.

The phenotype produced upon knockdown of *FoxD3* in NCC is reminiscent of the human malformations Treacher Collins syndrome (TCS), and hemifacial microsomia (HFM). HFM is characterised by facial asymmetry resulting from maxillary and/or mandibular hypoplasia and sometimes presents with facial clefting (Fan et al. 2005). It usually occurs sporadically, however familial cases have been reported (Singer et al., 1994). Candidate genes have been proposed, including *Goosecoid* and Hemifacial microsomia-associated (*Hfm*), but have not yet been confirmed in humans (Kelberman et al., 2001).

TCS otherwise known as Frontonasal Dysplasia, is characterised by craniofacial abnormalities including hypoplasia of the zygomatic bones and mandible, and cleft palate, sometimes presenting asymmetrically. *Tcof1*haploinsufficiency in the mouse results in the same severe craniofacial malformations characteristic of TCS, including reduced axial curvature and exencephaly on certain genetic backgrounds (Dixon et al., 2000). These defects are attributed to excessive NCC apoptosis in the neuroepithelium reducing the progenitor pool available for colonisation of the facial structures (Dixon et al., 2006). Loss of function mutations in the TCOF1 gene account for around 90% of TCS cases (Dixon et al., 1996), and two further genes have also been recently implicated after genetic screening of TCS patients (Dauwerse et al., 2011).

In the light of the similarities between the phenotype produced upon disruption *FoxD3* in the mouse neural crest and those of the *Tcof1*$^{+/-}$mouse model and the human syndromes described, perhaps further screening of TCS and HFM patients might uncover mutations in *FoxD3* which, as in the *mother superior* zebrafish mutation, are specific to the NCC (Montero-Balaguer et al., 2006).

5.5. CONCLUSIONS

The development of a transgenic conditional *FoxD3*shRNA knockdown model was intended as a means of inhibiting the delamination of NCC from the cranial neural tube. Thus, it was hoped to determine whether NCC delamination is necessary for cranial neural tube closure, as predicted from previous studies. The *FoxD3* knockdown model was successfully generated, producing a phenotype which concurred with that of the recently described *FoxD3* conditional knockout model. The effect on delamination of the NCC was not, however, successfully demonstrated and it seems likely that knockdown of *FoxD3* mainly affects NCC maintenance, rather than specification or delamination. Furthermore the exencephaly produced in this model is not located in the midbrain region as predicted by the hypothesis, but appears to result from a reopening event in the forebrain. As such, this model fails to significantly extend the analysis of whether cranial NCC delamination is necessary for DLHP formation and midbrain closure.

The reduction in axial curvature noted in earlier chapters, and also in the FoxD3 knockdown model, reflects a reduction in the numbers of NCC contributing to the facial mesenchyme which appears to reduce the scaffolding supporting the neural tube and securing the hindbrain and forebrain neural tube together, to sustain axial curvature at the cephalic flexure. Hence, the FoxD3 knockdown approach demonstrates a role for NCC maintenance in enabling a normal gross axial morphology of the cranial region. Furthermore unilateral failure of this scaffolding in the cranial region seems to be responsible for the reopening event in the forebrain, demonstrating an indirect role for normal NCC development in neurulation.

Further characterisation of the conditional *FoxD3* knockdown model could be conducted by examining other structures to which NCC contribute, such as the enteric nervous system, dorsal root ganglia, and cardiac outflow tract. It would also be interesting to determine the effect of the branchial arch defects on craniofacial

derivatives at later stages. The crucial studies, however, would be to define the primary defect more clearly by looking at NCC specification by counting labelled cells in sections through the cranial neural tube *in vivo* and delamination using *in vitro* delamination assays. Furthermore if the NCC are found to delaminate then apoptosis, proliferation and differentiation assays could be conducted in the early migrating NCC to determine their fate. Sections through the cranial region would confirm the presence of DLHPs and would also reveal the density of the cranial mesenchyme.

CHAPTER 6

GENERAL DISCUSSION

The findings of this thesis can be summarised as follows:

1. A detailed examination of neurulation stage mouse embryos confirmed that the midbrain is mechanically the most unfavourable region for neural tube closure along the body axis. Factors opposing closure, in mechanical terms, are: (i) the high degree of axial curvature, as a result of the cephalic flexure; (ii) the widely spaced and biconvex neural folds; (iii) the occurrence of a significant *de novo* closure event - Closure 2 - at the midbrain-forebrain boundary. From this analysis, it was inferred that high levels of mechanical force oppose the convergence of the tips of the neural folds in the midbrain.

2. Factors that appear to mitigate the risk of failed closure in the midbrain are: (i) the considerable support for elevation of the neural folds provided by expansion of the underlying cranial mesenchyme (Morriss and Solursh, 1978; Chen and Behringer, 1995; Zhao et al., 1996); (ii) formation of DLHPs in the midbrain neural plate (Morriss-Kay, 1981). Pre-closure emigration of NCC from the tips of the neural folds may be a factor enabling (or required for) midbrain closure by facilitating DLHP formation. This was the main hypothesis under test in the research. During the research, however, another possible role for NCC development emerged in the elevation of the neural folds which will be addressed further in section 6.2.

3. Two mouse mutant models known to exhibit both NCC defects and exencephaly were examined as a means of testing the hypothesis. In the *Zic2-Kumba* mutant, cranial NCC emigration defects were associated with failure of DLHP formation and subsequent development of exencephaly. In contrast, in the *Pax3-splotch* mutant a dissociation was observed between the NCC defects (which were restricted to the spinal region) and hindbrain exencephaly. DLHP formation appeared normal in these embryos. This study provided limited support for the role of NCC emigration in dorsolateral bending and closure of the midbrain, although this evidence was correlative only.

4. Chemical inhibition of matrix metalloproteases, necessary for EMT, inhibited NCC delamination and prevented DLHP formation in cultured embryos. There was limited evidence also for development of exencephaly in treated embryos, although the ultimate effect on neural tube closure could not be examined in detail, due to the technical limitations of maintaining embryos in culture for long periods. Nevertheless, this study provides the first experimental evidence in favour of a role for NCC emigration in dorsolateral bending and closure of the midbrain.

5. Knockdown of *FoxD3* at the earliest stages of mouse NCC development *in vivo* was achieved using a conditional shRNA transgenic approach. Interestingly, this appeared to have no effect on NCC specification or delamination, and Closure 2 occurred normally in knockdown embryos, implying the successful development of DLHPs (although this was not specifically studied). However, knockdown of *FoxD3* did appear to adversely affect the maintenance of the NCC progenitor pool during their migration. This was in accordance with the findings in the NCC specific conditional *FoxD3* knockout model which was developed in parallel with these studies, as well as the role identified for *FoxD3* in progenitors of the early embryo (Hanna et al., 2002; Teng et al., 2008).

These results prompt some conclusions and raise a number of questions, pointing to the need for further studies, as follows:

6.1. ROLE FOR NCC DELAMINATION IN MIDBRAIN DLHP FORMATION

The findings outlined above support the hypothesised role for NCC emigration in dorsolateral bending of the midbrain region. Previous research has indicated that dorsolateral bending is necessary for midbrain closure and the current findings associate reduced NCC emigration with failure of dorsolateral bending and failure of midbrain closure. However, they failed to exclude the contribution that NCC might make to mesenchymal expansion, elevation and closure of the midbrain which will now be discussed further.

6.2. POSSIBLE ROLE FOR NCC-DEPENDENT MESENCHYME EXPANSION IN SUPPORTING MIDBRAIN CLOSURE

A relatively novel concept that emerged from this research is the contribution that migration and proliferation of NCC adjacent to the midbrain might make to mesenchymal expansion, elevation and closure of the neural tube – failure of NCC specification or delamination or the maintenance of the early migratory NCC would all reduce the pool of progenitors available for the expansion of mesenchyme required to support elevation of the midbrain neural folds. Any model in which specification or delamination of NCC was affected would be predicted to affect midbrain closure by inhibiting DLHP formation, but would also inherently affect the role for NCC in expansion of the cranial mesenchyme and

elevation of the midbrain neural folds. This would make it difficult to separate these two NCC functions experimentally.

The effect of mesenchyme expansion on midbrain closure has been demonstrated previously in *Twist* and *Cart1* mutant mice (Chen & Behringer, 1995; Zhao et al., 1996) and has always been assumed to depend on cranial mesodermal proliferation together with expansion of extracellular matrix filled intercellular spaces (Morriss & Solursh, 1978). However, defects of NCC derivatives have in fact been identifyed in each of these models, implying that perhaps the failure of mesenchyme expansion observed in these models reflects a NCC defect (Qu et al., 1999; Bildsoe et al., 2009). The contribution of specifically NCC expansion (as opposed to expansion of the primary mesenchyme) has never been directly addressed.

The contribution of NCC to mesenchymal expansion in the midbrain region is evident in the reduction in axial curvature noted in all the models in which reduced cranial NCC migration was observed. Having said this, the conditional *FoxD3* knockdown model indicates that partial (but certainly not complete) inhibition of maintenance of migrating NCC in the cranial mesenchyme is not sufficient to prevent midbrain closure, since this occurred apparently normally in the knockdown embryos. In this model, however, failure of NCC progenitor maintenance was a relatively late occurring phenomenon, occurring after midbrain closure. It could be argued that the NCC defects emerged too late to be useful in identifying effects of NCC expansion on midbrain closure.

Further studies would thus be required to dissociate the effects on midbrain closure of the two NCC processes: 1 - the facilitation of dorsolateral bending by NCC delamination and 2 - the contribution of NCC migration and proliferation to mesenchymal expansion and elevation. For this a subtractive method would be required. First the effect of disrupting both DLHPs and mesenchymal expansion could be quantified, perhaps using a conditional mouse model in which MMPs are knocked out in the NCC. Then the effect of inhibiting mesenchymal expansion after delamination could be determined using the DTA ablation mouse crossed with a mouse in which Cre is expressed in migratory NCC, thus ablating them. Finally the effect of preventing mesenchymal expansion could then be subtracted from the effect of disrupting both DLHPs and mesenchymal expansion.

The findings of the current studies confirmed that MMPs play a role in NCC delamination. MMP-2 and -9 have been implicated previously in the EMT in metastasis (Chambers and Matrisian, 1997; Hofmann et al., 2000; Kosaka et al., 2010) and MMP-2 has been implicated in the EMT of NCC (Erickson and Isseroff, 1989; Robbins et al.,

1999; Cai and Brauer, 2002; Duong and Erickson, 2004). Knockout of MMP-2 in the mouse model leads to early onset severe experimental autoimmune encephalomyelinitis, the mouse model for multiple sclerosis (Esparza et al., 2004). There is evidence that multiple sclerosis is a neurocristopathy (Behan and Chaudhury, 2010), however the effect of the MMP-2 null mutation does not appear to have catastrophic consequences for NCC delamination. This implies that perhaps there may be some redundancy with other members of the MMP family such as MMP-9 and that a double conditional knockout of both MMP-2 and -9 would be required to inhibit the delamination of NCC.

An alternative method to distinguish the effects of the NCC contribution to mesenchymal expansion from the effects of enhancing mechanical flexibility of the dorsal neuroepithelium would be to utilise the conditional DTA ablation model with a premigratory NCC specific Cre allele. This would specifically ablate the NCC prior to their EMT, mimicking the effect of their delamination by enhancing the flexibility of the neural folds, while preventing any NCC contribution to the underlying mesenchyme.

6.3. A ROLE FOR NCC IN MAINTAINING NEURAL TUBE CLOSURE

The conditional knockdown of *FoxD3* did not affect the development of NCC at an early enough stage to investigate any role for NCC delamination (or perhaps expansion of early migrating NCC) in midbrain closure. Nevertheless, these embryos did exhibit hypoplasia of NCC derivatives in the facial structures (such as the maxillary process) and an apparent failure of the mesenchymal 'scaffolding' supporting the cephalic flexure. Interestingly, in a few embryos unilateral failure of this scaffolding seems to have exerted tension and caused reopening of the fused forebrain neural folds, leading to forebrain exencephaly.

6.4. MODEL OF MULTILEVEL REGULATION OF NEURULATION BY NCC

These considerations lead to a new model of cranial closure in the mouse embryo that has complex multilevel regulation by the development of NCC, with three distinct elements (Figure 6.1): (i) enhancement of DLHP formation by the NCC emigration; (ii) contribution of migrating and proliferating NCC to mesenchymal expansion that supports midbrain closure; (iii) development of the mesenchymal derivatives of the first branchial arch, which requires maintenance of NCC progenitors and, through scaffolding of the cranial neural tube, prevents reopening.

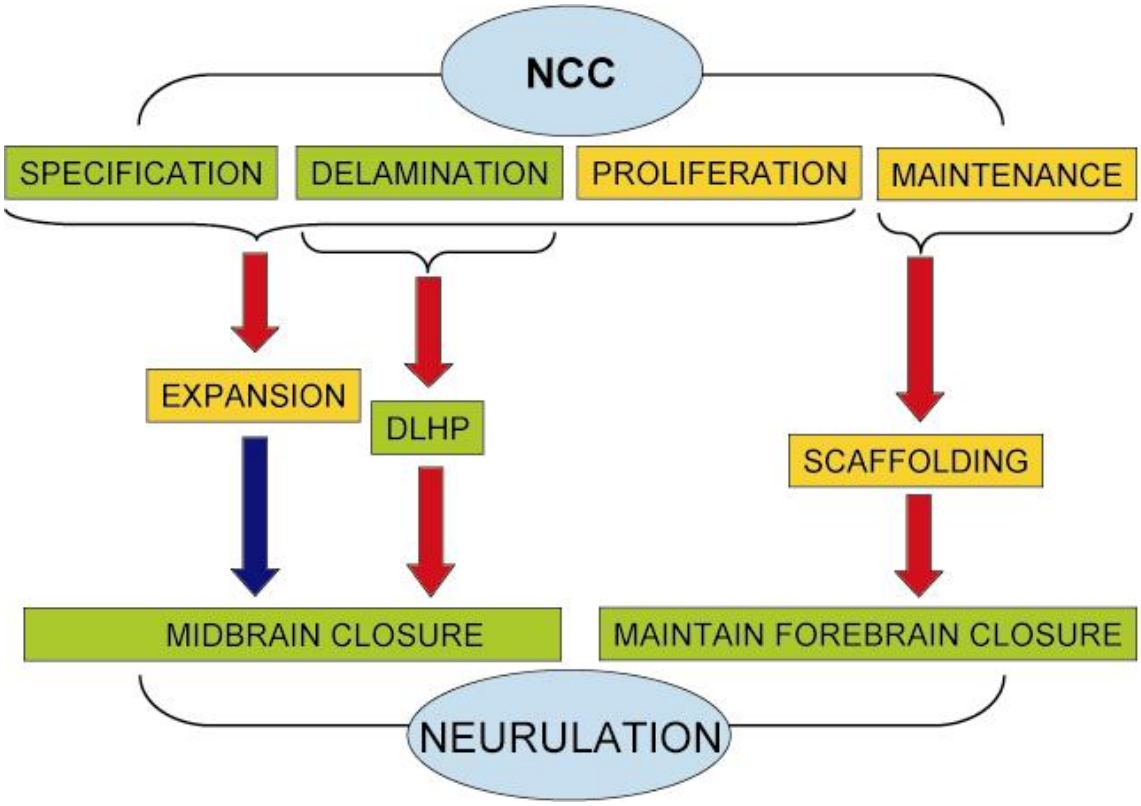

Figure 6.1. Model of the Complex Multilevel Regulation of Neurulation by NCC

The processes of NCC development exert different effects on neurulation. Red and blue arrows indicate findings of the current research and previous research respectively, and green and yellow boxes represent processes occurring within the neuroepithelium and mesenchyme respectively.

6.5. ALTERNATIVE APPROACHES TO KNOCKDOWN OF GENES REQUIRED FOR NCC DELAMINATION

Early in the work of this thesis, attempts were made to use electroporation of siRNAs directly into the neural plate as a means of reducing the expression of genes like *FoxD3* and *Snai1* in the cultured mouse embryo. While not as well developed as electroporation in the chick embryo, a number of labs have successfully used electroporation of expression vectors in mouse embryos maintained in whole embryo culture (Mellitzer et al., 2002; Calegari et al., 2002; Ybot-Gonzalez et al., 2007b).

In the present studies, electroporation of siRNAs and a GFP expression vector into the NCC of the midbrain was achieved but the migration of NCC appeared normal in both the control and experimental groups (Figure 6.2 A,D). Increasing the concentration of siRNA or the voltage at which they were electroporated in an attempt to elicit an effect adversely affected the embryo morphology in both the control and experimental groups (Figure 6.2 B,C,E,F), making it impossible to draw conclusions regarding the DLHP or other morphology of the region. Furthermore, in some instances the patterning of NCC was affected bilaterally, despite the electroporation of siRNAs being unilateral, indicating that NCC were affected by the electroporation procedure itself (Figure 6.2 E).

Irrespective of these limitations, these studies would have been constrained by the same restriction applicable to the inhibitor cultures described in Chapter 4 - the limited duration of time that embryos can be reliably cultured for.

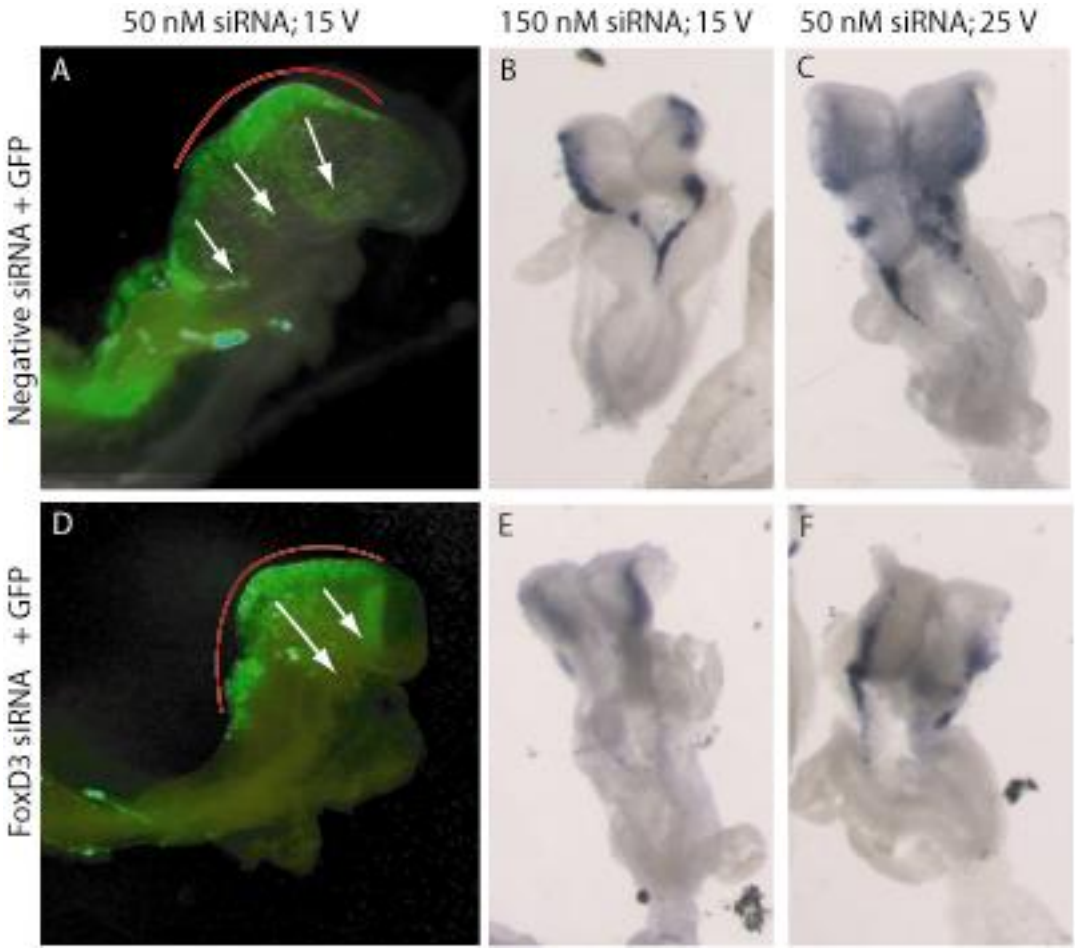

Figure 6.2. Electroporation of siRNA constructs into cultured mouse embryos
Embryos electroporated at varying voltages with 500 ng of EGFP expression vector and varying concentrations of either negative (control) siRNAs (A-C) or siRNAs directed against *FoxD3* mRNA (D-F). Green fluorescence indicates GFP expression (A,D). and blue staining indicates *FoxD3* expression (B,C,E,F).

(**A,D**) Embryos electroporated with 50 nM siRNA at 15 V showing targeting of electroporation to the midbrain NCC (red line indicating green fluorescence in the neuroepithelium in A and D). No difference was observed between the control and *FoxD3* siRNAs in the migration of NCC towards the mesenchyme of the forebrain and first branchial arch (white arrows in A and D).
(**B,E**) Embryos electroporated with 150 nM siRNA at 15 V and (**C,F**) 50 nM siRNA at 25 V showed abnormal neural tube morphology, including bending of the neural plate (B) and failure of Closure 1 (C,E,F). Note that *FoxD3* positive NCC are absent bilaterally from the embryo in E despite unilateral electroporation of siRNA.

6.6. STUDYING THE MECHANICS OF NEURAL TUBE CLOSURE

The current work has suggested that NCC delamination from the dorsal neuroepithelium of the midbrain reduces the cell density of this region, and thus enhances its mechanical flexibility. This in turn is seen as facilitating the formation of DLHPs more ventrally in the neuroepithelium by permitting an acute angle to be formed in the epithelial sheet at the junction of the neuroepithelium and the surface ectoderm, recently vacated by the NCC. Mechanical predictions of this sort are difficult, perhaps impossible, to measure solely using biological approaches, and therefore biomechanical methodology would be needed in future to examine these questions further. For example, the use of atomic force microscopy can measure the elasticity/rigidity of epithelial layers (Gaikwad et al. 2010; Tao et al. 1992) and when applied to developmental systems can provide novel insights into processes such as the role of cytoskeleton-dependent changes in cell-cortex tension governing cell sorting in zebrafish gastrulation (Krieg et al., 2008). Similarly use of other mechanical measurement methods has revealed surprisingly simple mechanical features of the *Xenopus* gastrula (von Dassow et al. 2010). Such techniques, when used in combination with the biological techniques of this thesis, could provide an ultimate test of the 'NCC delamination and closure' hypothesis.

6.7. POSSIBLE SIGNALLING MECHANISMS IN CRANIAL NEURULATION

The current research has taken a purely mechanistic approach to the study of the effect of NCC development on cranial neurulation, ignoring the possible role of signalling mechanisms in the process. For example previous work had implied that NCC were required for normal neurulation and morphogenesis in the cranial region by regulating the expression of genes such as the organising gene FGF8 (Creuzet et al., 2006).

BMP signalling is another mechanism which has been implicated in neurulation. While the work of this thesis was in progress, other members of the lab provided evidence that the absence of DLHPs in the spinal region of *Zic2-Kumba* mutants results from over-activation of BMP signalling. BMPs are necessary and sufficient to inhibit dorsolateral bending in the mouse spinal neural plate, and immunohistochemistry for Smad-1,5,8, an indicator of the strength of BMP signalling, revealed more intense expression in $Zic2^{ku/ku}$ embryos than in wild type (Ybot-Gonzalez et al., 2007a). Most

recently, the BMP antagonist dorsomorphin (Yu et al 2008) has been found in preliminary experiments to enhance spinal closure in both normal and *Zic2*$^{ku/ku}$ embryos (S. Raza, unpublished). While the role of BMPs in DLHP regulation has not yet been extended to the cranial region, it does raise the question of the relative importance of NCC emigration and BMP signalling control, in enabling midbrain DLHPs to form. These mechanisms are interlinked as BMP signalling is necessary for NCC specification. Hence the effects of each on DLHP formation would be difficult to dissociate. An interesting approach would be to combine the use of dorsomorphin and MMP-2 inhibitors in varying ratios to determine the effects on midbrain NCC and DLHP formation in both wild type and *Zic2*$^{ku/ku}$ embryos.

REFERENCES

Abdul-Aziz, N.M., Turmaine, M., Greene, N.D., & Copp, A.J. (2009). EphrinA-EphA receptor interactions in mouse spinal neurulation: implications for neural fold fusion. *Int.J Dev.Biol.* 53, 559-568.

Ahlgren, S.C., Thakur, V., & Bronner-Fraser, M. (2002). Sonic hedgehog rescues cranial neural crest from cell death induced by ethanol exposure. *Proc.Natl.Acad.Sci.USA* 99, 10476-10481.

Anderson, R.B. (2010). Matrix metalloproteinase-2 is involved in the migration and network formation of enteric neural crest-derived cells. *Int.J Dev.Biol.* 54, 63-69.

Anderson, R.B., Turner, K.N., Nikonenko, A.G., Hemperly, J., Schachner, M., & Young, H.M. (2006a). The cell adhesion molecule l1 is required for chain migration of neural crest cells in the developing mouse gut. *Gastroenterology* 130, 1221-1232.

Anderson, R.M., Stottmann, R.W., Choi, M., & Klingensmith, J. (2006b). Endogenous bone morphogenetic protein antagonists regulate mammalian neural crest generation and survival. *Dev.Dyn.* 235, 2507-2520.

Andoniadou, C.L., Signore, M., Sajedi, E., Gaston-Massuet, C., Kelberman, D., Burns, A.J., Itasaki, N., Dattani, M., & Martinez-Barbera, J.P. (2007). Lack of the murine homeobox gene Hesx1 leads to a posterior transformation of the anterior forebrain. *Development* 134, 1499-1508.

Antony, A.C. & Hansen, D.K. (2000). Hypothesis: Folate-responsive neural tube defects and neurocristopathies. *Teratology* 62, 42-50.

Arduini, B.L., Bosse, K.M., & Henion, P.D. (2009). Genetic ablation of neural crest cell diversification. *Development* 136, 1987-1994.

Aruga, J., Tohmonda, T., Homma, S., & Mikoshiba, K. (2002). Zic1 promotes the expansion of dorsal neural progenitors in spinal cord by inhibiting neuronal differentiation. *Dev.Biol.* 244, 329-341.

Asher, J.H., Jr. & Friedman, T.B. (1990). Mouse and hamster mutants as models for Waardenburg syndromes in humans. *J.Med.Genet.* 27, 618-626.

Auerbach, R. (1954). Analysis of the developmental effects of a lethal mutation in the house mouse. *J.Exp.Zool.* 127, 305-329.

Aybar, M.J. & Mayor, R. (2002). Early induction of neural crest cells: lessons learned from frog, fish and chick. *Curr.Opin.Genet.Dev.* 12, 452-458.

Aybar, M.J., Nieto, M.A., & Mayor, R. (2003). *Snail* precedes *Slug* in the genetic cascade required for the specification and migration of the *Xenopus* neural crest. *Development* 130, 483-494.

Aymé, S. & Philip, N. (1995). Possible homozygous Waardenburg syndrome in a fetus with exencephaly. *Am.J.Med.Genet.* 59, 263-265.

Baker, C.V., Bronner-Fraser, M., Le Douarin, N.M., Teillet, M.A., (1997). Early- and late-migrating cranial neural crest cell ppulations have equivalent developmental potential in vivo. *Development.* 124, 3077-87.

Baker, J.C., Beddington, R.S.P., & Harland, R.M. (1999). Wnt signaling in *Xenopus* embryos inhibits *Bmp4* expression and activates neural development. *Genes Dev.* 13, 3149-3159.

Bamforth, S.D., Braganτa, J., Eloranta, J.J., Murdoch, J.N., Marques, F.I.R., Kranc, K.R., Farza, H., Henderson, D.J., Hurst, H.C., & Bhattacharya, S. (2001). Cardiac malformations, adrenal agenesis, neural crest defects and exencephaly in mice lacking Cited2, a new Tfap2 co-activator. *Nature Genet.* 29, 469-474.

Barra, J. (1990). An X-linked recessive mutation producing cleft palate, crooked tail, and polydactyly in mice. *J.Hered.* 81, 388-392.

Bastidas, F., De Calisto, J., & Mayor, R. (2004). Identification of neural crest competence territory: Role of Wnt signaling. *Dev.Dyn.* 229, 109-117.

Beechey, C.V. & Searle, A.G. (1986). Mutations at the *Sp* locus. *Mouse News Letter* 75, 28.

Behan, P.O. & Chaudhuri, A. (2010). The sad plight of multiple sclerosis research (low on fact, high on fiction): critical data to support it being a neurocristopathy. *Inflammopharmacology*. 18, 265-90.

Bildsoe, H., Loebel, D.A., Jones, V.J., Chen, Y.T., Behringer, R.R., & Tam, P.P. (2009). Requirement for Twist1 in frontonasal and skull vault development in the mouse embryo. *Dev.Biol.* 331, 176-188.

Bockman, D.E. & Kirby, M.L. (1984). Dependence of thymus development on derivatives of the neural crest. *Science* 223, 498-500.

Brewer, S., Feng, W.G., Huang, J., Sullivan, S., & Williams, T. (2004). Wnt1-Cre-mediated deletion of AP-2α causes multiple neural crest-related defects. *Dev.Biol.* 267, 135-152.

Brewster, R., Lee, J., & Altaba, A.R.I. (1998). Gli/Zic factors pattern the neural plate by defining domains of cell differentiation. *Nature* 393, 579-583.

Brouns, M.R., Matheson, S.F., Hu, K.Q., Delalle, I., Caviness, V.S., Jr., Silver, J., Bronson, R.T., & Settleman, J. (2000). The adhesion signaling molecule p190 RhoGAP is required for morphogenetic processes in neural development. *Development* 127, 4891-4903.

Brown, S.A., Warburton, D., Brown, L.Y., Yu, C.Y., Roeder, E.R., Stengel-Rutkowski, S., Hennekam, R.C., & Muenke, M. (1998). Holoprosencephaly due to mutations in ZIC2, a homologue of Drosophila odd-paired. *Nature Genet.* 20, 180-183.

Burns, A.J. & Le Douarin, N.M. (2001). Enteric nervous system development: Analysis of the selective developmental potentialities of vagal and sacral neural crest cells using quail-chick chimeras. *Anat.Rec.* 262, 16-28.

Burns, A.J., Roberts, R.R., Bornstein, J.C., & Young, H.M. (2009). Development of the enteric nervous system and its role in intestinal motility during fetal and early postnatal stages. *Semin.Pediatr.Surg.* 18, 196-205.

Burstyn-Cohen, T. & Kalcheim, C. (2002). Association between the cell cycle and neural crest delamination through specific regulation of G1/S transition. *Dev.Cell* 3, 383-395.

Burstyn-Cohen, T., Stanleigh, J., Sela-Donenfeld, D., & Kalcheim, C. (2004). Canonical Wnt activity regulates trunk neural crest delamination linking BMP/noggin signaling with G1/S transition. *Development* 131, 5327-5339.

Cai, D.H. & Brauer, P.R. (2002). Synthetic matrix metalloproteinase inhibitor decreases early cardiac neural crest migration in chicken embryos. *Dev.Dyn.* 224, 441-449.

Calegari, F., Haubensak, W., Yang, D., Huttner, W.B., & Buchholz, F. (2002). Tissue-specific RNA interference in postimplantation mouse embryos with endoribonuclease-prepared short interfering RNA. *Proc.Natl.Acad.Sci.USA* 99, 14236-14240.

Camerer, E., Barker, A., Duong, D.N., Ganesan, R., Kataoka, H., Cornelissen, I., Darragh, M.R., Hussain, A., Zheng, Y.-W., Srnivasan, Y., Brown, C., Xu, S.-M., Regard, J.B., Lin, C.-Y., Craik, C.S., Kirchhofer, D., & Coughlin, S.R. (2010). Local protease signalling contributes to neural tube closure in the mouse embryo. *Dev.Cell* 18, 25-38.

Cano, A., Perez-Moreno, M.A., Rodrigo, I., Locascio, A., Blanco, M.J., Del Barrio, M.G., Portillo, F., & Nieto, M.A. (2000). The transcription factor snail controls epithelial-mesenchymal transitions by repressing E-cadherin expression. *Nat.Cell Biol.* 2, 76-83.

Carmona, R., González-Iriarte, M., Macías, D., Pérez-Pomares, J.M., García-Garrido, L., & Muñoz-Chápuli, R. (2000). Immunolocalization of the transcription factor Slug in the developing avian heart. *Anat.Embryol.* 201, 103-109.

Carter, M., Ulrich, S., Oofuji, Y., Williams, D.A., & Ross, M.E. (1999). *Crooked tail* (*Cd*) models human folate-responsive neural tube defects. *Hum.Mol.Genet.* 8, 2199-2204.

Carver, E.A., Jiang, R., Lan, Y., Oram, K.F., & Gridley, T. (2001). The mouse snail gene encodes a key regulator of the epithelial-mesenchymal transition. *Mol Cell Biol.* 21, 8184-8188.

Chai, Y., Jiang, X.B., Ito, Y., Bringas, P., Jr., Han, J., Rowitch, D.H., Soriano, P., McMahon, A.P., & Sucov, H.M. (2000). Fate of the mammalian cranial neural crest during tooth and mandibular morphogenesis. *Development* 127, 1671-1679.

Chambers, A.F. & Matrisian, L.M. (1997). Changing views of the role of matrix metalloproteinases in metastasis. *J Natl.Cancer Inst.* 89, 1260-1270.

Chan, W.Y., Cheung, C.S., Yung, K.M., & Copp, A.J. (2004). Cardiac neural crest of the mouse embryo: axial level of origin, migratory pathway and cell autonomy of the *splotch* (*Sp*^{2H}) mutant effect. *Development* 131, 3367-3379.

Chatkupt, S. & Johnson, W.G. (1993). Waardenburg syndrome and myelomeningocele in a family. *J.Med.Genet.* 30, 83-84.

Chen, S.Y., Charness, M.E., Wilkemeyer, M.F., & Sulik, K.K. (2005). Peptide-mediated protection from ethanol-induced neural tube defects. *Dev.Neurosci.* 27, 13-19.

Chen, Z.-F. & Behringer, R.R. (1995). *twist* is required in head mesenchyme for cranial neural tube morphogenesis. *Genes Dev.* 9, 686-699.

Cheung, M. & Briscoe, J. (2003). Neural crest development is regulated by the transcription factor Sox9. *Development* 130, 5681-5693.

Cheung, M., Chaboissier, M.C., Mynett, A., Hirst, E., Schedl, A., & Briscoe, J. (2005). The transcriptional control of trunk neural crest induction, survival, and delamination. *Dev.Cell* 8, 179-192.

Chi, C.L., Martinez, S., Wurst, W., & Martin, G.R. (2003). The isthmic organizer signal FGF8 is required for cell survival in the prospective midbrain and cerebellum. *Development* 130, 2633-2644.

Cohlan, S.Q. (1954). Congenital anomalies in the rat produced by excessive intake of vitamin A during pregnancy. *Pediatrics* 13, 556-567.

Collignon, J., Sockanathan, S., Hacker, A., Cohen-Tannoudji, M., Norris, D., Rastan, S., Stevanovic, M., Goodfellow, P.N., & Lovell-Badge, R. (1996). A comparison of the properties of *Sox-3* with *Sry* and two related genes, *Sox-1* and *Sox-2*. *Development* 122, 509-520.

Conway, S.J., Bundy, J., Chen, J.W., Dickman, E., Rogers, R., & Will, B.M. (2000). Decreased neural crest stem cell expansion is responsible for the conotruncal heart defects within the *Splotch* (*Sp^{2H}*)/*Pax3* mouse mutant. *Cardiovasc.Res.* 47, 314-328.

Conway, S.J., Henderson, D.J., Anderson, R.H., Kirby, M.L., & Copp, A.J. (1997). Development of a lethal congenital heart defect in the *splotch* (*Pax3*) mutant mouse. *Cardiovasc.Res.* 36, 163-173.

Copp, A., Cogram, P., Fleming, A., Gerrelli, D., Henderson, D., Hynes, A., Kolatsi-Joannou, M., Murdoch, J., & Ybot-Gonzalez, P. (2000). Neurulation and neural tube closure defects. *Methods Mol.Biol.* 136, 135-160.

Copp, A. J. (1994). Genetic models of mammalian neural tube defects. *In Neural Tube Defects (Ciba Foundation Symposium 181)*, G. Bock & J. Marsh, eds., Chichester: John Wiley & Sons, pp. 118-134.

Copp, A.J. (2005). Neurulation in the cranial region - normal and abnormal. *J.Anat.* 207, 623-635.

Copp, A.J. & Brook, F.A. (1989). Does lumbosacral spina bifida arise by failure of neural folding or by defective canalisation? *J.Med.Genet.* 26, 160-166.

Copp, A.J., Brook, F.A., Estibeiro, J.P., Shum, A.S.W., & Cockroft, D.L. (1990). The embryonic development of mammalian neural tube defects. *Prog.Neurobiol.* 35, 363-403.

Copp, A.J., Greene, N.D.E., & Murdoch, J.N. (2003a). Dishevelled: linking convergent extension with neural tube closure. *Trends Neurosci.* 26, 453-455.

Copp, A.J., Greene, N.D.E., & Murdoch, J.N. (2003b). The genetic basis of mammalian neurulation. *Nat.Rev.Genet.* 4, 784-793.

Correia, A.C., Costa, M., Moraes, F., Bom, J., Novoa, A., & Mallo, M. (2007). Bmp2 is required for migration but not for induction of neural crest cells in the mouse. *Dev.Dyn.* 236, 2493-2501.

Creuzet, S.E., Martinez, S., & Le Douarin, N.M. (2006). The cephalic neural crest exerts a critical effect on forebrain and midbrain development. *Proc.Natl.Acad.Sci.U.S.A* 103, 14033-14038.

Curtin, J.A., Quint, E., Tsipouri, V., Arkell, R.M., Cattanach, B., Copp, A.J., Fisher, E.M., Nolan, P.M., Steel, K.P., Brown, S.D.M., Gray, I.C., & Murdoch, J.N. (2003). Mutation of *Celsr1* disrupts planar polarity of inner ear hair cells and causes severe neural tube defects in the mouse. *Curr.Biol.* 13, 1-20.

Da-Silva, E.O., Batista, J.E., Medeiros, M.A., & Fonteles, S.M. (1993). Craniofacial anthropometric studies in Waardenburg syndrome type I. *Clin.Genet.* 44, 20-25.

Danielian, P.S., Muccino, D., Rowitch, D.H., Michael, S.K., & McMahon, A.P. (1998). Modification of gene activity in mouse embryos in utero by a tamoxifen-inducible form of Cre recombinase. *Curr.Biol.* 8, 1323-1326.

Darken, R.S., Scola, A.M., Rakeman, A.S., Das, G., Mlodzik, M., & Wilson, P.A. (2002). The planar polarity gene strabismus regulates convergent extension movements in Xenopus. *EMBO J* 21, 976-985.

Dauwerse, J.G., Dixon, J., Seland, S., Ruivenkamp, C.A., van, H.A., Hoefsloot, L.H., Peters, D.J., Boers, A.C., Daumer-Haas, C., Maiwald, R., Zweier, C., Kerr, B., Cobo, A.M., Toral, J.F., Hoogeboom, A.J., Lohmann, D.R., Hehr, U., Dixon, M.J., Breuning, M.H., & Wieczorek, D. (2011). Mutations in genes encoding subunits of RNA polymerases I and III cause Treacher Collins syndrome. *Nature Genet.* 43, 20-22.

Davidson, L.A. & Keller, R.E. (1999). Neural tube closure in *Xenopus* laevis involves medial migration, directed protrusive activity, cell intercalation and convergent extension. *Development* 126, 4547-4556.

De Calisto, J., Araya, C., Marchant, L., Riaz, C.F., & Mayor, R. (2005). Essential role of non-canonical Wnt signalling in neural crest migration. *Development* 132, 2587-2597.

Deardorff, M.A., Tan, C., Saint-Jeannet, J.P., & Klein, P.S. (2001). A role for frizzled 3 in neural crest development. *Development* 128, 3655-3663.

Del Barrio, M.G. & Nieto, M.A. (2002). Overexpression of Snail family members highlights their ability to promote chick neural crest formation. *Development* 129, 1583-1593.

Del Barrio, M.G. & Nieto, M.A. (2004). Relative expression of *Slug, RhoB,* and HNK-1 in the cranial neural crest of the early chicken embryo. *Dev.Dyn.* 229, 136-139.

Dixon, J., Brakebusch, C., Fässler, R., & Dixon, M.J. (2000). Increased levels of apoptosis in the prefusion neural folds underlie the craniofacial disorder, Treacher Collins syndrome. *Hum.Mol.Genet.* 9, 1473-1480.

Dixon, J. & Dixon, M.J. (2004). Genetic background has a major effect on the penetrance and severity of craniofacial defects in mice heterozygous for the gene encoding the nucleolar protein Treacle. *Dev.Dyn.* 229, 907-914.

Dixon, J., Edwards, S.J., Gladwin, A.J., Dixon, M.J., Loftus, S.K., Bonner, C.A., Koprivnikar, K., & Wasmuth, J.J. (1996). Positional cloning of a gene involved in the pathogenesis of Treacher Collins syndrome. *Nature Genet.* 12, 130-136.

Dixon, J., Jones, N.C., Sandell, L.L., Jayasinghe, S.M., Crane, J., Rey, J.P., Dixon, M.J., & Trainor, P.A. (2006). Tcof1/Treacle is required for neural crest cell formation and proliferation deficiencies that cause craniofacial abnormalities. *Proc.Natl.Acad.Sci.U.S.A* 103, 13403-13408.

Dottori, M., Gross, M.K., Labosky, P., & Goulding, M. (2001). The winged-helix transcription factor Foxd3 suppresses interneuron differentiation and promotes neural crest cell fate. *Development* 128, 4127-4138.

Duong, T.D. & Erickson, C.A. (2004). MMP-2 plays an essential role in producing epithelial-mesenchymal transformations in the avian embryo. *Dev.Dyn.* 229, 42-53.

Ebert, P.J., Timmer, J.R., Nakada, Y., Helms, A.W., Parab, P.B., Liu, Y., Hunsaker, T.L., & Johnson, J.E. (2003). Zic1 represses *Math1* expression via interactions with the *Math1* enhancer and modulation of *Math1* autoregulation. *Development* 130, 1949-1959.

Elms, P., Siggers, P., Napper, D., Greenfield, A., & Arkell, R. (2003). Zic2 is required for neural crest formation and hindbrain patterning during mouse development. *Dev.Biol* 264, 391-406.

Elul, T. & Keller, R. (2000). Monopolar protrusive activity: A new morphogenic cell behavior in the neural plate dependent on vertical interactions with the mesoderm in *Xenopus*. *Dev.Biol.* 224, 3-19.

Epstein, D.J., Vekemans, M., & Gros, P. (1991). splotch (Sp^{2H}), a mutation affecting development of the mouse neural tube, shows a deletion within the paired homeodomain of Pax-3. *Cell* 67, 767-774.

Epstein, D.J., Vogan, K.J., Trasler, D.G., & Gros, P. (1993). A mutation within intron 3 of the *Pax-3* gene produces aberrantly spliced mRNA transcripts in the splotch (*Sp*) mouse mutant. *Proc.Natl.Acad.Sci.USA* 90, 532-536.

Erickson, C.A. & Isseroff, R.R. (1989). Plasminogen activator activity is associated with neural crest cell motility in tissue culture. *J.Exp.Zool.* 251, 123-133.

Erickson, C.A. & Weston, J.A. (1983). AN SEM analysis of neural crest migration in the mouse. *J.Embryol.Exp.Morphol.* 74, 97-118.

Esparza, J., Kruse, M.m Lee, J., Michaud, M., & Madri, J.A. (2004). MMP-2 null mice exhibit an early onset and severe experimental autoimmune encephalomyelitis due to an increase in MMP-9 expression and activity. *FASEB. J.* 18, 1682-91.

Estibeiro, J.P., Brook, F.A., & Copp, A.J. (1993). Interaction between splotch (*Sp*) and curly tail (*ct*) mouse mutants in the embryonic development of neural tube defects. *Development* 119, 113-121.

EUROCAT Working Group (1991). Prevalence of neural tube defects in 20 regions of Europe and the impact of prenatal diagnosis, 1980-1986. *J.Epidemiol.Community Health* 45, 52-58.

Ewart, J.L., Cohen, M.F., Meyer, R.A., Huang, G.Y., Wessels, A., Gourdie, R.G., Chin, A.J., Park, S.M.J., Lazatin, B.O., Villabon, S., & Lo, C.W. (1997). Heart and neural tube defects in transgenic mice overexpressing the Cx43 gap junction gene. *Development* 124, 1281-1292.

Fleming, A. & Copp, A.J. (1998). Embryonic folate metabolism and mouse neural tube defects. *Science* 280, 2107-2109.

Fleming, A. & Copp, A.J. (2000). A genetic risk factor for mouse neural tube defects: defining the embryonic basis. *Hum.Mol.Genet.* 9, 575-581.

Franz, T. (1989). Persistent truncus arteriosus in the Splotch mutant mouse. *Anat.Embryol.* 180, 457-464.

Franz, T. (1992). Neural tube defects without neural crest defects in Splotch mice. *Teratology* 46, 599-604.

Garcia-Castro, M.I., Marcelle, C., & Bronner-Fraser, M. (2002). Ectodermal Wnt function as a neural crest inducer. *Science* 297, 848-851.

Gaston-Massuet, C., Henderson, D.J., Greene, N.D.E., & Copp, A.J. (2005). Zic4, a zinc finger transcription factor, is expressed in the developing mouse nervous system. *Dev.Dyn.* 233, 1110-1115.

Gavalas, A., Studer, M., Lumsden, A., Rijli, F.M., Krumlauf, R., & Chambon, P. (1998). *Hoxa1* and *Hoxb1* synergize in patterning the hindbrain, cranial nerves and second pharyngeal arch. *Development* 125, 1123-1136.

Geelen, J.A.G. & Langman, J. (1979). Ultrastructural observations on closure of the neural tube in the mouse. *Anat.Embryol.* 156, 73-88.

Gerrelli, D. & Copp, A.J. (1997). Failure of neural tube closure in the *loop-tail* (*Lp*) mutant mouse: analysis of the embryonic mechanism. *Dev.Brain Res.* 102, 217-224.

Golden, J.A. & Chernoff, G.F. (1993). Intermittent pattern of neural tube closure in two strains of mice. *Teratology* 47, 73-80.

Goulding, M., Sterrer, S., Fleming, J., Balling, R., Nadeau, J., Moore, K.J., Brown, S.D.M., Steel, K.P., & Gruss, P. (1993). Analysis of the *Pax-3* gene in the mouse mutant *splotch*. *Genomics* 17, 355-363.

Graham, A., Koentges, G., & Lumsden, A. (1996). Neural Crest Apoptosis and the Establishment of Craniofacial Pattern: An Honorable Death. *Mol.Cell Neurosci.* 8, 76-83.

Greene, N.D. & Copp, A.J. (2005). Mouse models of neural tube defects: investigating preventive mechanisms. *Am.J.Med.Genet.C.Semin.Med.Genet.* 135, 31-41.

Greene, N.D., Massa, V., & Copp, A.J. (2009). Understanding the causes and prevention of neural tube defects: Insights from the splotch mouse model. *Birth Defects Res.A Clin Mol.Teratol.* 85, 322-330.

Grim, M., Halata, Z., & Franz, T. (1992). Schwann cells are not required for guidance of motor nerves in the hindlimb in Splotch mutant mouse embryos. *Anat.Embryol.* 186, 311-318.

Gumbiner, B.M. (2000). Regulation of cadherin adhesive activity. *J.Cell Biol.* 148, 399-404.

Gunn, T.M., Juriloff, D.M., & Harris, M.J. (1996). Exencephaly and cleft cerebellum in SELH/Bc mouse embryos are alternative developmental consequences of the same underlying genetic defect. *Teratology* 54, 230-236.

Hall, A. (1998). Rho GTPases and the actin cytoskeleton. *Science* 279, 509-514.

Hall, A. & Nobes, C.D. (2000). Rho GTPases: molecular switches that control the organization and dynamics of the actin cytoskeleton. *Philos.Trans.R.Soc.Lond B Biol Sci.* 355, 965-970.

Hamblet, N.S., Lijam, N., Ruiz-Lozano, P., Wang, J., Yang, Y., Luo, Z., Mei, L., Chien, K.R., Sussman, D.J., & Wynshaw-Boris, A. (2002). Dishevelled 2 is essential for cardiac outflow tract development, somite segmentation and neural tube closure. *Development* 129, 5827-5838.

Hammond, S.M., Bernstein, E., Beach, D., & Hannon, G.J. (2000). An RNA-directed nuclease mediates post-transcriptional gene silencing in Drosophila cells. *Nature* 404, 293-296.

Hanna, L.A., Foreman, R.K., Tarasenko, I.A., Kessler, D.S., & Labosky, P.A. (2002). Requirement for Foxd3 in maintaining pluripotent cells of the early mouse embryo. *Genes Dev.* 16, 2650-2661.

Harris, M.J. & Juriloff, D.M. (2010). An update to the list of mouse mutants with neural tube closure defects and advances toward a complete genetic perspective of neural tube closure. *Birth Defects Res.A Clin Mol.Teratol.* 88, 653-669.

Hawley, S.H.B., Wünnenberg-Stapleton, K., Hashimoto, C., Laurent, M.N., Watabe, T., Blumberg, B.W., & Cho, K.W.Y. (1995). Disruption of BMP signals in embryonic *Xenopus* ectoderm leads to direct neural induction. *Genes Dev.* 9, 2923-2935.

Hemann, M.T., Fridman, J.S., Zilfou, J.T., Hernando, E., Paddison, P.J., Cordon-Cardo, C., Hannon, G.J., & Lowe, S.W. (2003). An epi-allelic series of p53 hypomorphs created by stable RNAi produces distinct tumor phenotypes in vivo. *Nature Genet.* 33, 396-400.

Henderson, D.J., Ybot-Gonzalez, P., & Copp, A.J. (1997). Over-expression of the chondroitin sulphate proteoglycan *versican* is associated with defective neural crest migration in the *Pax3* mutant mouse (*splotch*). *Mech.Dev.* 69, 39-51.

Henderson, D.J., Ybot-Gonzalez, P., & Copp, A.J. (2000). RhoB is expressed in migrating neural crest and endocardial cushions of the developing mouse embryo. *Mech.Dev.* 95, 211-214.

Henion, P.D. & Weston, J.A. (1997). Timing and pattern of cell fate restrictions in the neural crest lineage. *Development* 124, 4351-4359.

Hildebrand, J.D. & Soriano, P. (1999). Shroom, a PDZ domain-containing actin-binding protein, is required for neural tube morphogenesis in mice. *Cell* 99, 485-497.

Hofmann, U.B., Westphal, J.R., Waas, E.T., Becker, J.C., Ruiter, D.J., & van Muijen, G.N. (2000). Coexpression of integrin alpha(v)beta3 and matrix metalloproteinase-2 (MMP-2) coincides with MMP-2 activation: correlation with melanoma progression. *J.Invest Dermatol.* 115, 625-632.

Hol, F.A., Hamel, B.C.J., Geurds, M.P.A., Mullaart, R.A., Barr, F.G., Macina, R.A., & Mariman, E.C.M. (1995). A frameshift mutation in the gene for PAX3 in a girl with spina bifida and mild signs of Waardenburg syndrome. *J.Med.Genet.* 32, 52-56.

Holmberg, J., Clarke, D.L., & Frisén, J. (2000). Regulation of repulsion versus adhesion by different splice forms of an Eph receptor. *Nature* 408, 203-206.

Hornyak, T.J., Hayes, D.J., Chiu, L.Y., & Ziff, E.B. (2001). Transcription factors in melanocyte development: distinct roles for Pax-3 and Mitf. *Mech.Dev.* 101, 47-59.

Hoth, C.F., Milunsky, A., Lipsky, N., Sheffer, R., Clarren, S.K., & Baldwin, C.T. (1993). Mutations in the paired domain of the human PAX3 gene cause Klein-Waardenburg syndrome (WS-III) as well as Waardenburg syndrome type I (WS-I). *Am.J.Hum.Genet.* 52, 455-462.

Inoue, T., Hatayama, M., Tohmonda, T., Itohara, S., Aruga, J., & Mikoshiba, K. (2004). Mouse Zic5 deficiency results in neural tube defects and hypoplasia of cephalic neural crest derivatives. *Dev.Biol* 270, 146-162.

Inoue, Y.U., Asami, J., & Inoue, T. (2009). Genetic labeling of mouse rhombomeres by Cadherin-6::EGFP-BAC transgenesis underscores the role of cadherins in hindbrain compartmentalization. *Neurosci.Res.* 63, 2-9.

Ishibashi, M., Ang, S.-L., Shiota, K., Nakanishi, S., Kageyama, R., & Guillemot, F. (1995). Targeted disruption of mammalian *hairy* and *Enhancer of split* homolog-1 (*HES-1*) leads to up-regulation of neural helix-loop-helix factors, premature neurogenesis, and severe neural tube defects. *Genes Dev.* 9, 3136-3148.

Itaranta, P., Viiri, K., Kaartinen, V., & Vainio, S. (2009). Lumbo-sacral neural crest derivatives fate mapped with the aid of Wnt-1 promoter integrate but are not essential to kidney development. *Differentiation* 77, 199-208.

Ivanova, A., Signore, M., Caro, N., Greene, N.D.E., Copp, A.J., & Martinez-Barbera, J.P. (2005). In vivo genetic ablation by Cre-mediated expression of diphtheria toxin fragment A. *Genesis.* 43, 129-135.

Jacobson, A.G. & Tam, P.P.L. (1982). Cephalic neurulation in the mouse embryo analyzed by SEM and morphometry. *Anat.Rec.* 203, 375-396.

Jiang, R.L., Lan, Y., Norton, C.R., Sundberg, J.P., & Gridley, T. (1998). The slug gene is not essential for mesoderm or neural crest development in mice. *Dev.Biol.* 198, 277-285.

Jiang, X.B., Rowitch, D.H., Soriano, P., McMahon, A.P., & Sucov, H.M. (2000). Fate of the mammalian cardiac neural crest. *Development* 127, 1607-1616.

Joyner, A.L., Liu, A., & Millet, S. (2000). Otx2, Gbx2 and Fgf8 interact to position and maintain a mid-hindbrain organizer. *Curr.Opin.Cell Biol.* 12, 736-741.

Juriloff, D.M. & Harris, M.J. (2000). Mouse models for neural tube closure defects. *Hum.Mol.Genet.* 9, 993-1000.

Juriloff, D.M., Harris, M.J., Tom, C., & MacDonald, K.B. (1991). Normal mouse strains differ in the site of initiation of closure of the cranial neural tube. *Teratology* 44, 225-233.

Karfunkel, P. (1974). The mechanisms of neural tube formation. *Int.Rev.Cytol.* 38, 245-271.

Kelberman, D., Tyson, J., Chandler, D.C., McInerney, A.M., Slee, J., Albert, D., Aymat, A., Botma, M., Calvert, M., Goldblatt, J., Haan, E.A., Laing, N.G., Lim, J., Malcolm, S., Singer, S.L., Winter, R.M., & Bitner-Glindzicz, M. (2001). Hemifacial microsomia: progress in understanding the genetic basis of a complex malformation syndrome. *Hum.Genet.* 109, 638-645.

Keller, R. (2002). Shaping the vertebrate body plan by polarized embryonic cell movements. *Science* 298, 1950-1954.

Keller, R., Shook, D., & Skoglund, P. (2008). The forces that shape embryos: physical aspects of convergent extension by cell intercalation. *Phys.Biol.* 5, 15007.

Kibar, Z., Vogan, K.J., Groulx, N., Justice, M.J., Underhill, D.A., & Gros, P. (2001). *Ltap*, a mammalian homolog of *Drosophila Strabismus/Van Gogh*, is altered in the mouse neural tube mutant Loop-tail. *Nature Genet.* 28, 251-255.

Klootwijk, R., Franke, B., Van der Zee, C.E.E.M., De Boer, R.T., Wilms, W., Hol, F.A., & Mariman, E.C.M. (2000). A deletion encompassing *Zic3* in Bent tail, a mouse model for X-linked neural tube defects. *Hum.Mol.Genet.* 9, 1615-1622.

Knight, R.D. & Schilling, T.F. (2006). Cranial neural crest and development of the head skeleton. *Adv.Exp.Med.Biol.* 589, 120-133.

Koblar, S.A., Murphy, M., Barrett, G.L., Underhill, A., Gros, P., & Bartlett, P.F. (1999). *Pax-3* regulates neurogenesis in neural crest-derived precursor cells. *J.Neurosci.Res.* 56, 518-530.

Kohlbecker, A., Lee, A.E., & Schorle, H. (2002). Exencephaly in a subset of animals heterozygous for AP-2a mutation. *Teratology* 65, 213-218.

Kos, R., Reedy, M.V., Johnson, R.L., & Erickson, C.A. (2001). The winged-helix transcription factor FoxD3 is important for establishing the neural crest lineage and repressing melanogenesis in avian embryos. *Development* 128, 1467-1479.

Kosaka, T., Kikuchi, E., Mikami, S., Miyajima, A., Shirotake, S., Ishida, M., Okada, Y., & Oya, M. (2010). Expression of snail in upper urinary tract urothelial carcinoma: prognostic significance and implications for tumor invasion. *Clin.Cancer Res.* 16, 5814-5823.

Kotch, L.E. & Sulik, K.K. (1992). Patterns of ethanol-induced cell death in the developing nervous system of mice; Neural fold states through the time of anterior neural tube closure. *Int.J.Dev.Neurosci.* 10, 273-279.

Krieg, M., rboleda-Estudillo, Y., Puech, P.H., Kafer, J., Graner, F., Muller, D.J., & Heisenberg, C.P. (2008). Tensile forces govern germ-layer organization in zebrafish. *Nat.Cell Biol* 10, 429-436.

Krispin, S., Nitzan, E., Kassem, Y., & Kalcheim, C. (2010). Evidence for a dynamic spatiotemporal fate map and early fate restrictions of premigratory avian neural crest. *Development* 137, 585-595.

Kunath, T., Gish, G., Lickert, H., Jones, N., Pawson, T., & Rossant, J. (2003). Transgenic RNA interference in ES cell-derived embryos recapitulates a genetic null phenotype. *Nat.Biotechnol.* 21, 559-561.

Kwang, S.J., Brugger, S.M., Lazik, A., Merrill, A.E., Wu, L.Y., Liu, Y.H., Ishii, M., Sangiorgi, F.O., Rauchman, M., Sucov, H.M., Maas, R.L., & Maxson, R.E., Jr. (2002). Msx2 is an immediate downstream effector of Pax3 in the development of the murine cardiac neural crest. *Development* 129, 527-538.

LaBonne, C. & Bronner-Fraser, M. (2000). Snail-related transcriptional repressors are required in *Xenopus* for both the induction of the neural crest and its subsequent migration. *Dev.Biol.* 221, 195-205.

Labosky, P.A. & Kaestner, K.H. (1998). The winged helix transcription factor Hfh2 is expressed in neural crest and spinal cord during mouse development. *Mech.Dev.* 76, 185-190.

Lagutin, O.V., Zhu, C.Q.C., Kobayashi, D., Topczewski, J., Shimamura, K., Puelles, L., Russell, H.R.C., McKinnon, P.J., Solnica-Krezel, L., & Oliver, G. (2003). Six3 repression of Wnt signaling in the anterior neuroectoderm is essential for vertebrate forebrain development. *Genes Dev.* 17, 368-379.

Lammer, E.J., Chen, D.T., Hoar, R.M., Agnish, N.D., Benke, P.J., Braun, J.T., Curry, C.J., Fernhoff, P.M., Grix, A.W., Lott, I.T., Richard, J.M., & Sun, S.C. (1985). Retinoic acid embryopathy. *N.Engl.J.Med.* 313, 837-841.

Lang, D., Chen, F., Milewski, R., Li, J., Lu, M.M., & Epstein, J.A. (2000). Pax3 is required for enteric ganglia formation and functions with Sox10 to modulate expression of *c-ret*. *J.Clin.Invest.* 106, 963-971.

Lawson, A., Schoenwolf, G.C., England, M.A., Addai, F.K., & Ahima, R.S. (1999). Programmed cell death and the morphogenesis of the hindbrain roof plate in the chick embryo. *Anat.Embryol.* 200, 509-519.

Le Douarin, N.M. 1982. *The Neural Crest* Cambridge, Cambridge University Press.

Le Douarin, N.M. (2004). The avian embryo as a model to study the development of the neural crest: a long and still ongoing story. *Mech.Dev.* 121, 1089-102

Le Douarin, N.M. & Teillet, M.A. (1973). The migration of neural crest cells to the wall of the digestive tract in avian embryo. *J Embryol.Exp.Morphol.* 30, 31-48.

Li, J., Molkentin, J.D., & Colbert, M.C. (2001). Retinoic acid inhibits cardiac neural crest migration by blocking c-Jun N-terminal kinase activation. *Dev.Biol.* 232, 351-361.

Liem, K.F., Tremml, G., Roelink, H., & Jessell, T.M. (1995). Dorsal differentiation of neural plate cells induced by BMP-mediated signals from epidermal ectoderm. *Cell* 82, 969-979.

Lister, J.A., Cooper, C., Nguyen, K., Modrell, M., Grant, K., & Raible, D.W. (2006). Zebrafish Foxd3 is required for development of a subset of neural crest derivatives. *Dev.Biol.* 290, 92-104.

Liu, J.-P. & Jessell, T.M. (1998). A role for rhoB in the delamination of neural crest cells from the dorsal neural tube. *Development* 125, 5055-5067.

Liu, Y. & Labosky, P.A. (2008). Regulation of embryonic stem cell self-renewal and pluripotency by Foxd3. *Stem Cells* 26, 2475-2484.

Locascio, A., Manzanares, M., Blanco, M.J., & Nieto, M.A. (2002). Modularity and reshuffling of *Snail* and *Slug* expression during vertebrate evolution. *Proc.Natl.Acad.Sci.USA* 99, 16841-16846.

Lumsden, A., Sprawson, N., & Graham, A. (1991). Segmental origin and migration of neural crest cells in the hindbrain region of the chick embryo. *Development* 113, 1281-1291.

Luo, T., Lee, Y.H., Saint-Jeannet, J.P., & Sargent, T.D. (2003). Induction of neural crest in *Xenopus* by transcription factor AP2α. *Proc.Natl.Acad.Sci.USA* 100, 532-537.

MacDonald, K.B., Juriloff, D.M., & Harris, M.J. (1989). Developmental study of neural tube closure in a mouse stock with a high incidence of exencephaly. *Teratology* 39, 195-213.

Maden, M., Horton, C., Graham, A., Leonard, L., Pizzey, J., Siegenthaler, G., Lumsden, A., & Eriksson, U. (1992). Domains of cellular retinoic acid-binding protein I (CRABP I) expression in the hindbrain and neural crest of the mouse embryo. *Mech.Dev.* 37, 13-23.

Mansouri, A., Pla, P., Larue, L., & Gruss, P. (2001). *Pax3* acts cell autonomously in the neural tube and somites by controlling cell surface properties. *Development* 128, 1995-2005.

Mansouri, A., Stoykova, A., Torres, M., & Gruss, P. (1996). Dysgenesis of cephalic neural crest derivatives in *Pax7*$^{-/-}$ mutant mice. *Development* 122, 831-838.

Martinez-Barbera, J.P., Rodriguez, T.A., Greene, N.D.E., Weninger, W.J., Simeone, A., Copp, A.J., Beddington, R., & Dunwoodie, S. (2002). Folic acid prevents exencephaly in *Cited2* deficient mice. *Hum.Mol.Genet.* 11, 283-293.

Massa, V., Savery, D., Ybot-Gonzalez, P., Ferraro, E., Rongvaux, A., Cecconi, F., Flavell, R.A., Greene, N.D.E., & Copp, A.J. (2009). Apoptosis is not required for mammalian neural tube closure. *Proc.Natl.Acad.Sci.U.S.A* 106, 8233-8238.

Matsuda, M. & Keino, H. (1994). An open cephalic neural tube reproducibly induced by cytochalasin D in rat embryos *in vitro*. *Zool.Sci.* 11, 547-553.

Mayor, R. & Aybar, M.J. (2001). Induction and development of neural crest in *Xenopus laevis*. *Cell Tissue Res.* 305, 203-209.

Mayor, R., Morgan, R., & Sargent, M.G. (1995). Induction of the prospective neural crest of *Xenopus*. *Development* 121, 767-777.

McMahon, A.P., Joyner, A.L., Bradley, A., & McMahon, J.A. (1992). The midbrain-hindbrain phenotype of *Wnt-1*$^{-}$*/Wnt-1*$^{-}$ mice results from stepwise deletion of *engrailed*-expressing cells by 9.5 days postcoitum. *Cell* 69, 581-595.

Mellitzer, G., Hallonet, M., Chen, L., & Ang, S.L. (2002). Spatial and temporal 'knock down' of gene expression by electroporation of double-stranded RNA and morpholinos into early postimplantation mouse embryos. *Mech.Dev.* 118, 57-63.

Mikuma, T., Kawasaki, H., Yamamoto, Y., & Taira, K. (2004). Overexpression of Dicer enhances RNAi-mediated gene silencing by short-hairpin RNAs (shRNAs) in human cells. *Nucleic Acids Symp.Ser.(Oxf)* 191-192.

Miner, J.H., Cunningham, J., & Sanes, J.R. (1998). Roles for laminin in embryogenesis: exencephaly, syndactyly, and placentopathy in mice lacking the laminin alpha5 chain. *J.Cell Biol.* 143, 1713-1723.

Mizuseki, K., Kishi, M., Matsui, M., Nakanishi, S., & Sasai, Y. (1998). Xenopus Zic-related-1 and Sox-2, two factors induced by chordin, have distinct activities in the initiation of neural induction. *Development* 125, 579-587.

Montero-Balaguer, M., Lang, M.R., Sachdev, S.W., Knappmeyer, C., Stewart, R.A., De La Guardia, A., Hatzopoulos, A.K., & Knapik, E.W. (2006). The mother superior mutation ablates foxd3 activity in neural crest progenitor cells and depletes neural crest derivatives in zebrafish. *Dev.Dyn.* 235, 3199-3212.

Morrison-Graham, K., Schatteman, G.C., Bork, T., Bowen-Pope, D.F., & Weston, J.A. (1992). A PDGF receptor mutation in the mouse (*Patch*) perturbs the development of a non-neuronal subset of neural crest- derived cells. *Development* 115, 133-142.

Morriss, G.M. & Solursh, M. (1978). The role of primary mesenchyme in normal and abnormal morphogenesis of mammalian neural folds. *Zoon* 6, 33-38.

Morriss-Kay, G., Ruberte, E., Fukiishi, Y. (1993). Mammalian neural crest and neural crest derivatives. *Ann. Anat.* 175, 501-7.

Morriss-Kay, G. & Tuckett, F. (1985a). The role of microfilaments in cranial neurulation in rat embryos: effects of short-term exposure to cytochalasin D. *J Embryol.Exp.Morphol.* 88, 333-348.

Morriss-Kay, G.M. (1981). Growth and development of pattern in the cranial neural epithelium of rat embryos during neurulation. *J.Embryol.Exp.Morphol.* 65 (Suppl.), 225-241.

Morriss-Kay, G.M. & Tuckett, F. (1985b). The role of microfilaments in cranial neurulation in rat embryos: effects of short-term exposure to cytochalasin D. *J.Embryol.Exp.Morphol.* 88, 333-348.

Morriss-Kay, G.M. & Tuckett, F. (1989). Immunohistochemical localisation of chondroitin sulphate proteoglycans and the effects of chondroitinase ABC in 9- to 11-day rat embryos. *Development* 106, 787-798.

Murdoch, J.N., Henderson, D.J., Doudney, K., Gaston-Massuet, C., Phillips, H.M., Paternotte, C., Arkell, R., Stanier, P., & Copp, A.J. (2003). Disruption of *scribble* (*Scrb1*) causes severe neural tube defects in the *circletail* mouse. *Hum.Mol.Genet.* 12, 87-98.

Murray, S.A., Carver, E.A., & Gridley, T. (2006). Generation of a Snail1 (Snai1) conditional null allele. *Genesis.* 44, 7-11.

Murray, S.A. & Gridley, T. (2006a). Snail family genes are required for left-right asymmetry determination, but not neural crest formation, in mice. *Proc.Natl.Acad.Sci.U.S.A* 103, 10300-10304.

Murray, S.A. & Gridley, T. (2006b). Snail1 gene function during early embryo patterning in mice. *Cell Cycle* 5, 2566-2570.

Murray, S.A., Oram, K.F., & Gridley, T. (2007). Multiple functions of Snail family genes during palate development in mice. *Development* 134, 1789-1797.

Nagai, T., Aruga, J., Minowa, O., Sugimoto, T., Ohno, Y., Noda, T., & Mikoshiba, K. (2000). Zic2 regulates the kinetics of neurulation. *Proc.Natl.Acad.Sci.USA* 97, 1618-1623.

Nagai, T., Aruga, J., Takada, S.J., Günther, T., Spörle, R., Schughart, K., & Mikoshiba, K. (1997). The expression of the mouse *Zic1, Zic2* and *Zic3* gene suggests an essential role for *Zic* genes in body pattern formation. *Dev.Biol.* 182, 299-313.

Nakata, K., Koyabu, Y., Aruga, J., & Mikoshiba, K. (2000). A novel member of the *Xenopus Zic* family, *Zic5*, mediates neural crest development. *Mech.Dev.* 99, 83-91.

Nakata, K., Nagai, T., Aruga, J., & Mikoshiba, K. (1997). *Xenopus Zic3*, a primary regulator both in neural and neural crest development. *Proc.Natl.Acad.Sci.USA* 94, 11980-11985.

Nieto, M.A., Sargent, M.G., Wilkinson, D.G., & Cooke, J. (1994). Control of cell behavior during vertebrate development by *Slug*, a zinc finger gene. *Science* 264, 835-839.

Nolan, P.M., Peters, J., Strivens, M., Rogers, D., Hagan, J., Spurr, N., Gray, I.C., Vizor, L., Brooker, D., Whitehill, E., Washbourne, R., Hough, T., Greenaway, S., Hewitt, M., Liu, X.H., McCormack, S., Pickford, K., Selley, R., Wells, C., Tymowska-Lalanne, Z., Roby, P., Glenister, P., Thornton, C., & Thaung, C. (2000). A systematic, genome-wide, phenotype-driven mutagenesis programme for gene function studies in the mouse. *Nature Genet.* 25, 440-443.

Nye, J.S., Balkin, N., Lucas, H., Knepper, P.A., McLone, D.G., & Charrow, J. (1998). Myelomeningocele and Waardenburg syndrome (Type 3) in patients with interstitial deletions of 2q35 and the PAX3 gene: Possible digenic inheritance of a neural tube defect. *Am.J.Med.Genet.* 75, 401-408.

Nyholm, M.K., bdelilah-Seyfried, S., & Grinblat, Y. (2009). A novel genetic mechanism regulates dorsolateral hinge-point formation during zebrafish cranial neurulation. *J.Cell Sci.* 122, 2137-2148.

Nyholm, M.K., Wu, S.F., Dorsky, R.I., & Grinblat, Y. (2007). The zebrafish zic2a-zic5 gene pair acts downstream of canonical Wnt signaling to control cell proliferation in the developing tectum. *Development* 134, 735-746.

O'Rahilly, R. & Muller, F. (1989). Bidirectional closure of the rostral neuropore in the human embryo. *Am.J.Anat.* 184, 259-268.

O'Rahilly, R. & Müller, F. (2003). Somites, spinal ganglia, and centra - Enumeration and interrelationships in staged human embryos, and implications for neural tube defects. *Cells Tissues Organs* 173, 75-92.

O'Rahilly, R. & Muller, F. (2007). The development of the neural crest in the human. *J.Anat.* 211, 335-351.

Olmeda, D., Montes, A., Moreno-Bueno, G., Flores, J.M., Portillo, F., & Cano, A. (2008). Snai1 and Snai2 collaborate on tumor growth and metastasis properties of mouse skin carcinoma cell lines. *Oncogene* 27, 4690-4701.

Oppenheim, R.W., Flavell, R.A., Vinsant, S., Prevette, D., Kuan, C.Y., & Rakic, P. (2001). Programmed cell death of developing mammalian neurons after genetic deletion of caspases. *J.Neurosci.* 21, 4752-4760.

Padmanabhan, R. & Muawad, W.M. (1985). Exencephaly and axial skeletal dysmorphogenesis induced by acute doses of ethanol in mouse fetuses. *Drug.Alcohol.Depend.* 16, 215-227.

Paulussen, A.D., Schrander-Stumpel, C.T., Tserpelis, D.C., Spee, M.K., Stegmann, A.P., Mancini, G.M., Brooks, A.S., Collee, M., Maat-Kievit, A., Simon, M.E., van, B.Y., Stolte-Dijkstra, I., Kerstjens-Frederikse, W.S., Herkert, J.C., van Essen, A.J., Lichtenbelt, K.D., van, H.A., Kwee, M.L., Lachmeijer, A.M., Tan-Sindhunata, G.M., van Maarle, M.C., Arens, Y.H., Smeets, E.E., de Die-Smulders, C.E., Engelen, J.J., Smeets, H.J., & Herbergs, J. (2010). The unfolding clinical spectrum of holoprosencephaly due to mutations in SHH, ZIC2, SIX3 and TGIF genes. *Eur.J Hum.Genet.* 18, 999-1005.

Peeters, M. C. E., Hekking, J. W. M., Shiota, K., Drukker, J., & Van Straaten, H. W. M. Differences in axial curvature correlate with species-specific rate of neural tube closure in embryos of chick, rabbit, mouse, rat and human. Anat.Embryol. 1998.
Ref Type: In Press

Peeters, M.C.E., Hekking, J.W.M., Vainas, T., Drukker, J., & Van Straaten, H.W.M. (1997). Spatio-temporal curvature pattern of the caudal body axis for non-mutant and *curly tail* mouse embryos during the period of caudal neural tube closure. *Anat.Embryol.* 195, 259-266.

Pevny, L.H., Sockanathan, S., Placzek, M., & Lovell-Badge, R. (1998). A role for SOX1 in neural determination. *Development* 125, 1967-1978.

Pohl, B.S. & Knöchel, W. (2001). Overexpression of the transcriptional repressor FoxD3 prevents neural crest formation in *Xenopus* embryos. *Mech.Dev.* 103, 93-106.

Qu, S., Tucker, S.C., Zhao, Q., Decrombrugghe, B., & Wisdom, R. (1999). Physical and genetic interactions between Alx4 and Cart1. *Development* 126, 359-369.

Quemelo, P.R., Lourenco, C.M., & Peres, L.C. (2007). Teratogenic effect of retinoic acid in swiss mice. *Acta Cir.Bras.* 22, 451-456.

Read, A.P. & Newton, V.E. (1997). Waardenburg syndrome. *J.Med.Genet.* 34, 656-665.

Reedy, M.V., Faraco, C.D., & Erickson, C.A. (1998). The delayed entry of thoracic neural crest cells into the dorsolateral path is a consequence of the late emigration of melanogenic neural crest cells from the neural tube. *Dev.Biol.* 200, 234-246.

Robbins, J.R., McGuire, P.G., Wehrle-Haller, B., & Rogers, S.L. (1999). Diminished matrix metalloproteinase 2 (MMP-2) in ectomesenchyme- derived tissues of the *Patch* mutant mouse: Regulation of MMP-2 by PDGF and effects on mesenchymal cell migration. *Dev.Biol.* 212, 255-263.

Rowitch, D.H., Danielian, P.S., Lee, S.M.K., Echelard, Y., & McMahon, A.P. (1997). Cell interactions in patterning the mammalian midbrain. *Cold Spring Harbor Symp.Quant.Biol.* 62, 535-544.

Ruhin, B., Creuzet, S., Vincent, C., Benouaiche, L., Le Douarin, N.M., Couly, G. (2003) Patterning of the hyoid cartiladge depends upon signals arising from the ventral foregut endoderm. *Dev. Dyn.* 228, 239-46.

Sadler, T.W., Greenberg, D., Coughlin, P., & Lessard, J.L. (1982). Actin distribution patterns in the mouse neural tube during neurulation. *Science* 215, 172-174.

Sah, V.P., Attardi, L.D., Mulligan, G.J., Williams, B.O., Bronson, R.T., & Jacks, T. (1995). A subset of *p53*-deficient embryos exhibit exencephaly. *Nature Genet.* 10, 175-180.

Sanek, N.A., Taylor, A.A., Nyholm, M.K., & Grinblat, Y. (2009). Zebrafish zic2a patterns the forebrain through modulation of Hedgehog-activated gene expression. *Development* 136, 3791-3800.

Sasai, N., Mizuseki, K., & Sasai, Y. (2001). Requirement of *FoxD3*-class signaling for neural crest determination in *Xenopus*. *Development* 128, 2525-2536.

Satokata, I., Ma, L., Ohshima, H., Bei, M., Woo, I., Nishizawa, K., Maeda, T., Takano, Y., Uchiyama, M., Heaney, S., Peters, H., Tang, Z.Q., Maxson, R., & Maas, R. (2000). *Msx2* deficiency in mice causes pleiotropic defects in bone growth and ectodermal organ formation. *Nature Genet.* 24, 391-395.

Satokata, I. & Maas, R. (1994). *Msx1* deficient mice exhibit cleft palate and abnormalities of craniofacial and tooth development. *Nature Genet.* 6, 348-356.

Sauka-Spengler, T. & Bronner-Fraser, M. (2008). A gene regulatory network orchestrates neural crest formation. *Nat.Rev.Mol.Cell Biol.* 9, 557-568.

Schatteman, G.C., Morrison-Graham, K., Van Koppen, A., Weston, J.A., & Bowen-Pope, D.F. (1992). Regulation and role of PDGF receptor α-subunit expression during embryogenesis. *Development* 115, 123-131.

Schoenwolf, G.C. (1984). Histological and ultrastructural studies of secondary neurulation of mouse embryos. *Am.J.Anat.* 169, 361-374.

Schoenwolf, G.C. (1985). Shaping and bending of the avian neuroepithelium: morphometric analyses. *Dev.Biol.* 109, 127-139.

Schoenwolf, G.C. & Smith, J.L. (1990). Mechanisms of neurulation: Traditional viewpoint and recent advances. *Development* 109, 243-270.

Schorle, H., Meier, P., Buchert, M., Jaenisch, R., & Mitchell, P.J. (1996). Transcription factor AP-2 essential for cranial closure and craniofacial development. *Nature* 381, 235-238.

Schroeder, T.E. (1970). Neurulation in Xenopus laevis. An analysis and model based upon light and electron microscopy. *J. Embryol. Exp. Morphol.* 23, 427-62.

Schwarz, Q., Maden, C.H., Davidson, K., & Ruhrberg, C. (2009). Neuropilin-mediated neural crest cell guidance is essential to organise sensory neurons into segmented dorsal root ganglia. *Development* 136, 1785-1789.

Sechrist, J., Scherson, T., & Bronner-Fraser, M. (1994). Rhombomere rotation reveals that multiple mechanisms contribute to the segmental pattern of hindbrain neural crest migration. *Development* 120, 1777-1790.

Sechrist, J., Serbedzija, G.N., Scherson, T., Fraser, S.E., & Bronner-Fraser, M. (1993). Segmental migration of the hindbrain neural crest does not arise from its segmental generation. *Development* 118, 691-703.

Sefton, M., Sanchez, S., & Nieto, M.A. (1998). Conserved and divergent roles for members of the Snail family of transcription factors in the chick and mouse embryo. *Development* 125, 3111-3121.

Selleck, M.A.J. & Bronner-Fraser, M. (1995). Origins of the avian neural crest: The role of neural plate-epidermal interactions. *Development* 121, 525-538.

Serbedzija, G.N., Bronner-Fraser, M., & Fraser, S.E. (1992). Vital dye analysis of cranial neural crest cell migration in the mouse embryo. *Development* 116, 297-307.

Serbedzija, G.N., Fraser, S., & Bronner-Fraser, M. (1990). Pathways of trunk neural crest cell migration in the mouse embryo as revealed by vital dye labelling. *Development* 108, 605-612.

Serbedzija, G.N. & McMahon, A.P. (1997). Analysis of neural crest cell migration in splotch mice using a neural crest-specific LacZ reporter. *Dev.Biol.* 185, 139-147.

Shum, A.S.W. & Copp, A.J. (1996). Regional differences in morphogenesis of the neuroepithelium suggest multiple mechanisms of spinal neurulation in the mouse. *Anat.Embryol.* 194, 65-73.

Simeone, A. (2000). Positioning the isthmic organizer - where *Otx2* and *Gbx2* meet. *Trends Genet.* 16, 237-240.

Singer, S.L., Haan, E., Slee, J., & Goldblatt, J. (1994). Familial hemifacial microsomia due to autosomal dominant inheritance. Case reports. *Aust.Dent.J.* 39, 287-291.

Smart, N., Risebro, C.A., Melville, A.A., Moses, K., Schwartz, R.J., Chien, K.R., & Riley, P.R. (2007). Thymosin beta4 induces adult epicardial progenitor mobilization and neovascularization. *Nature* 445, 177-182.

Smith, J.L. & Schoenwolf, G.C. (1987). Cell cycle and neuroepithelial cell shape during bending of the chick neural plate. *Anat.Rec.* 218, 196-206.

Smith, J.L. & Schoenwolf, G.C. (1989). Notochordal induction of cell wedging in the chick neural plate and its role in neural tube formation. *J.Exp.Zool.* 250, 49-62.

Smith, J.L., Schoenwolf, G.C., & Quan, J. (1994). Quantitative analyses of neuroepithelial cell shapes during bending of the mouse neural plate. *J.Comp.Neurol.* 342, 144-151.

Solursh, M. & Morriss, G.M. (1977). Glycosaminoglycan synthesis in rat embryos during the formation of the primary mesenchyme and neural folds. *Dev.Biol.* 57, 75-86.

Soo, K., O'Rourke, M.P., Khoo, P.L., Steiner, K.A., Wong, N., Behringer, R.R., & Tam, P.P.L. (2002). Twist function is required for the morphogenesis of the cephalic neural tube and the differentiation of the cranial neural crest cells in the mouse embryo. *Dev.Biol.* 247, 251-270.

Soriano, P. (1999). Generalized lacZ expression with the ROSA26 Cre reporter strain. *Nature Genet.* 21, 70-71.

Southard-Smith, E.M., Kos, L., & Pavan, W.J. (1998). *Sox10* mutation disrupts neural crest development in *DOM* Hirschsprung mouse model. *Nature Genet.* 18, 60-64.

Spokony, R.F., Aoki, Y., Saint-Germain, N., Magner-Fink, E., & Saint-Jeannet, J.P. (2002). The transcription factor Sox9 is required for cranial neural crest development in Xenopus. *Development* 129, 421-432.

Stephenson, D.A., Mercola, M., Anderson, E., Wang, C.Y., Stiles, C.D., Bowen-Pope, D.F., & Chapman, V.M. (1991). Platelet-derived growth factor receptor alpha-subunit gene (Pdgfra) is deleted in the mouse patch (Ph) mutation. *Proc.Natl.Acad.Sci.USA* 88, 6-10.

Stern, C.D. (2002). Induction and initial patterning of the nervous system - the chick embryo enters the scene. *Curr.Opin.Genet.Dev.* 12, 447-451.

Sternlicht, M.D. & Werb, Z. (2001). How matrix metalloproteinases regulate cell behavior. *Annu.Rev.Cell Dev.Biol.* 17, 463-516.

Stevenson, R.E., Seaver, L.H., Collins, J.S., & Dean, J.H. (2004). Neural tube defects and associated anomalies in South Carolina. *Birth Defects Res.A Clin.Mol.Teratol.* 70, 554-558.

Steventon, B., Araya, C., Linker, C., Kuriyama, S., & Mayor, R. (2009). Differential requirements of BMP and Wnt signalling during gastrulation and neurulation define two steps in neural crest induction. *Development* 136, 771-779.

Stewart, R.A., Arduini, B.L., Berghmans, S., George, R.E., Kanki, J.P., Henion, P.D., & Look, A.T. (2006). Zebrafish foxd3 is selectively required for neural crest specification, migration and survival. *Dev.Biol.* 292, 174-188.

Streit, A. & Stern, C.D. (1999). Establishment and maintenance of the border of the neural plate in the chick: involvement of FGF and BMP activity. *Mech.Dev.* 82, 51-66.

Stumpo, D.J., Bock, C.B., Tuttle, J.S., & Blackshear, P.J. (1995). MARCKS deficiency in mice leads to abnormal brain development and perinatal death. *Proc.Natl.Acad.Sci.USA* 92, 944-948.

Sun, T., Jayatilake, D., Afink, G.B., Ataliotis, P., Nistér, M., Richardson, W.D., & Smith, H.K. (2000). A human YAC transgene rescues craniofacial and neural tube development in PDGFRα knockout mice and uncovers a role for PDGFRα in prenatal lung growth. *Development* 127, 4519-4529.

Sutton, J., Costa, R., Klug, M., Field, L., Xu, D.W., Largaespada, D.A., Fletcher, C.F., Jenkins, N.A., Copeland, N.G., Klemsz, M., & Hromas, R. (1996). *Genesis*, a winged helix transcriptional repressor with expression restricted to embryonic stem cells. *J.Biol.Chem.* 271, 23126-23133.

Takashima, Y., Era, T., Nakao, K., Kondo, S., Kasuga, M., Smith, A.G., & Nishikawa, S. (2007). Neuroepithelial cells supply an initial transient wave of MSC differentiation. *Cell* 129, 1377-1388.

Tallquist, M.D. & Soriano, P. (2003). Cell autonomous requirement for PDGFRα in populations of cranial and cardiac neural crest cells. *Development* 130, 507-518.

Tan, S.S. & Morriss-Kay, G.M. (1985). The development and distribution of the cranial neural crest in the rat embryo. *Cell Tissue Res.* 240, 403-416.

Taneyhill, L.A. & Bronner-Fraser, M. (2005). Dynamic alterations in gene expression after Wnt-mediated induction of avian neural crest. *Mol.Biol.Cell* 16, 5283-5293.

Tapadia, M.D., Cordero, D.R., & Helms, J.A. (2005). It's all in your head: new insights into craniofacial development and deformation. *J.Anat.* 207, 461-477.

Tassabehji, M., Read, A.P., Newton, V.E., Harris, R., Balling, R., Gruss, P., & Strachan, T. (1992). Waardenburg's syndrome patients have mutations in the human homologue of the *Pax-3* paired box gene. *Nature* 355, 635-636.

Teng, L., Mundell, N.A., Frist, A.Y., Wang, Q., & Labosky, P.A. (2008). Requirement for Foxd3 in the maintenance of neural crest progenitors. *Development* 135, 1615-1624.

Thiery, J.P. (2003). Epithelial-mesenchymal transitions in development and pathologies. *Curr.Opin.Cell Biol.* 15, 740-746.

Thiery, J.P., Acloque, H., Huang, R.Y., & Nieto, M.A. (2009). Epithelial-mesenchymal transitions in development and disease. *Cell* 139, 871-890.

Thomas, A.J. & Erickson, C.A. (2009). FOXD3 regulates the lineage switch between neural crest-derived glial cells and pigment cells by repressing MITF through a non-canonical mechanism. *Development* 136, 1849-1858.

Ting, S.B., Wilanowski, T., Auden, A., Hall, M., Voss, A.K., Thomas, T., Parekh, V., Cunningham, J.M., & Jane, S.M. (2003). Inositol- and folate-resistant neural tube defects in mice lacking the epithelial-specific factor Grhl-3. *Nature Med.* 9, 1513-1519.

Tompers, D.M., Foreman, R.K., Wang, Q.H., Kumanova, M., & Labosky, P.A. (2005). Foxd3 is required in the trophoblast progenitor cell lineage of the mouse embryo. *Dev.Biol.* 285, 126-137.

Tosney, K.W. (1982). The segregation and early migration of cranial neural crest cells in the avian embryo. *Dev.Biol.* 89, 13-24.

Trainor, P.A., Sobieszczuk, D., Wilkinson, D., & Krumlauf, R. (2002). Signalling between the hindbrain and paraxial tissues dictates neural crest migration pathways. *Development* 129, 433-442.

Tremblay, P., Kessel, M., & Gruss, P. (1995). A transgenic neuroanatomical marker identifies cranial neural crest deficiencies associated with the *Pax3* mutant *Splotch*. *Dev.Biol.* 171, 317-329.

Ueno, N. & Greene, N.D.E. (2003). Planar cell polarity genes and neural tube closure. *Birth Defects Research (Part C)* 69, 318-324.

van Straaten, H.W., Hekking, J.W., Consten, C., & Copp, A.J. (1993). Intrinsic and extrinsic factors in the mechanism of neurulation: effect of curvature of the body axis on closure of the posterior neuropore. *Development* 117, 1163-1172.

Van Straaten, H.W.M., Jansen, H.C.J.P., Peeters, M.C.E., Copp, A.J., & Hekking, J.W.M. (1996). Neural tube closure in the chick embryo is multiphasic. *Dev.Dyn.* 207, 309-318.

Van Straaten, H.W.M., Peeters, M.C.E., Hekking, J.W.M., & Van der Lende, T. (2000). Neurulation in the pig embryo. *Anat.Embryol.* 202, 75-84.

Villanueva, S., Glavic, A., Ruiz, P., & Mayor, R. (2002). Posteriorization by FGF, Wnt, and retinoic acid is required for neural crest induction. *Dev.Biol.* 241, 289-301.

Vincentz, J.W., Barnes, R.M., Rodgers, R., Firulli, B.A., Conway, S.J., & Firulli, A.B. (2008). An absence of Twist1 results in aberrant cardiac neural crest morphogenesis. *Dev.Biol.* 320, 131-139.

Waddington, C.H. (1936). The Problems of Embryology. *Br.Med.J* 2, 862-864.

Wallingford, J.B. & Harland, R.M. (2001). *Xenopus* Dishevelled signaling regulates both neural and mesodermal convergent extension: parallel forces elongating the body axis. *Development* 128, 2581-2592.

Wallingford, J.B., Rowning, B.A., Vogeli, K.M., Rothbächer, U., Fraser, S.E., & Harland, R.M. (2000). Dishevelled controls cell polarity during *Xenopus* gastrulation. *Nature* 405, 81-85.

Warr, N., Powles-Glover, N., Chappell, A., Robson, J., Norris, D., & Arkell, R.M. (2008). Zic2-associated holoprosencephaly is caused by a transient defect in the organizer region during gastrulation. *Hum.Mol.Genet.* 17, 2986-2996.

Weil, M., Jacobson, M.D., & Raff, M.C. (1997). Is programmed cell death required for neural tube closure. *Curr.Biol.* 7, 281-284.

Wilkinson, D.G., Bailes, J.A., & McMahon, A.P. (1987). Expression of the proto-oncogene int-1 is restricted to specific neural cells in the developing mouse embryo. *Cell* 50, 79-88.

Wilson, P.A. & Hemmati-Brivanlou, A. (1997). Vertebrate neural induction: Inducers, inhibitors, and a new synthesis. *Neuron* 18, 699-710.

Wilson, P.A., Lagna, G., Suzuki, A., & Hemmati-Brivanlou, A. (1997). Concentration-dependent patterning of the *Xenopus* ectoderm by BMP4 and its signal transducer *smad1*. *Development* 124, 3177-3184.

Winograd, J., Reilly, M.P., Roe, R., Lutz, J., Laughner, E., Xu, X., Hu, L., Asakura, T., Vander Kolk, C., Strandberg, J.D., & Semenza, G.L. (1997). Perinatal lethality and multiple craniofacial malformations in *MSX2* transgenic mice. *Hum.Mol.Genet.* 6, 369-379.

Wollnik, B., Tukel, T., Uyguner, O., Ghanbari, A., Kayserili, H., Emiroglu, M., & Yuksel-Apak, M. (2003). Homozygous and heterozygous inheritance of *PAX3* mutations causes different types of Waardenburg syndrome. *Am.J.Med.Genet.* 122A, 42-45.

Xu, D., Yoder, M., Sutton, J., & Hromas, R. (1998a). Forced expression of Genesis, a winged helix transcriptional repressor isolated from embryonic stem cells, blocks granulocytic differentiation of 32D myeloid cells. *Leukemia* 12, 207-212.

Xu, W., Baribault, H., & Adamson, E.D. (1998b). Vinculin knockout results in heart and brain defects during embryonic development. *Development* 125, 327-337.

Yang, J., Mani, S.A., Donaher, J.L., Ramaswamy, S., Itzykson, R.A., Come, C., Savagner, P., Gitelman, I., Richardson, A., & Weinberg, R.A. (2004). Twist, a master regulator of morphogenesis, plays an essential role in tumor metastasis. *Cell* 117, 927-939.

Ybot-Gonzalez, P. & Copp, A.J. (1999). Bending of the neural plate during mouse spinal neurulation is independent of actin microfilaments. *Dev.Dyn.* 215, 273-283.

Ybot-Gonzalez, P., Gaston-Massuet, C., Girdler, G., Klingensmith, J., Arkell, R., Greene, N.D., & Copp, A.J. (2007a). Neural plate morphogenesis during mouse neurulation is regulated by antagonism of BMP signalling. *Development* 134, 3203-3211.

Ybot-Gonzalez, P., Savery, D., Gerrelli, D., Signore, M., Mitchell, C.E., Faux, C.H., Greene, N.D.E., & Copp, A.J. (2007b). Convergent extension, planar-cell-polarity signalling and initiation of mouse neural tube closure. *Development* 134, 789-799.

Zhang, J., Hagopian-Donaldson, S., Serbedzija, G., Elsemore, J., Plehn-Dujowich, D., McMahon, A.P., Flavell, R.A., & Williams, T. (1996). Neural tube, skeletal and body wall defects in mice lacking transcription factor AP-2. *Nature* 381, 238-241.

Zhao, Q., Behringer, R.R., & De Crombrugghe, B. (1996). Prenatal folic acid treatment suppresses acrania and meroanencephaly in mice mutant for the *Cart1* homeobox gene. *Nature Genet.* 13, 275-283.

Zhong, W.M., Jiang, M.M., Schonemann, M.D., Meneses, J.J., Pedersen, R.A., Jan, L.Y., & Jan, Y.N. (2000). Mouse *numb* is an essential gene involved in cortical neurogenesis. *Proc.Natl.Acad.Sci.USA* 97, 6844-6849.